Functional analysis of siRNA mediated knockdowns of fibroblast growth factors in *Hydra vulgaris*

Dissertation

zur Erlangung des Grades eines

Doktor der Naturwissenschaften

(Dr. rer. nat.)

des Fachbereichs Biologie der Philipps-Universität Marburg

vorgelegt von

Lisa Andrea Reichart

aus Gelnhausen

Marburg, November 2020

Die vorliegende Dissertation wurde von Mai 2015 bis November 2020 am Fachbereich Biologie der Philipps-Universität Marburg unter Leitung von Prof. Dr. Monika Hassel angefertigt.

Vom Fachbereich Biologie der Philipps-Universität Marburg (Hochschulkennziffer 1180) als Dissertation angenommen am _____

Erstgutachter*in: Prof. Dr. Monika Hassel
Zweitgutachter*in: Prof. Dr. Christian Helker

Tag der Disputation: _____

Abstract

Fibroblast growth factor receptor (FGFR) signaling is crucial in animal development. Two FGFRs and one FGFR-like receptor, which lacks the intracellular domain, are known in the Cnidarian *Hydra vulgaris*. FGFRa, also known as Kringelchen, is an important factor in the developmental process of budding, as it controls the detachment of the bud. It is still unknown, which extracellular ligands are responsible for the start of the relevant signal transduction cascades in *Hydra*.

This study gives first insights into the potential functions of five FGFs previously identified in *Hydra*. Analysis of the gene and protein expression patterns of different FGFs in several *Hydra* strains suggest that FGFs may comprise evolutionary conserved, multiple functions in bud detachment, neurogenesis, migration and cell differentiation, as well as in the regeneration of head and foot structures in *Hydra*.

The electroporation of siRNAs into adult *Hydra* was used to analyze knockdown effects of FGFs and FGFRs in *Hydra*. This method was efficiently reproducing phenotypes obtained using the FGFR inhibitor SU5402 or, alternatively phosphorothioate antisense oligonucleotides or a dominant-negative FGFR mutant. Additionally, the siRNA-mediated knockdown showed a potential function of *FGFRa* in neuronal development and of *FGFc* in the differentiation of I-cells.

In summary this work provides new insights into potential functions of FGFs and FGFRs in the model organism *Hydra vulgaris* and provides a basis for further studies investigating interactions of FGFRs and FGFs in this organism.

Zusammenfassung

Die Signaltransduktion durch Fibroblastenwachstumsfaktorrezeptoren (engl. *fibroblast growth factor receptors*, FGFRs) ist wichtig für Wachstums- und Entwicklungsprozesse von Tieren. Bei dem Süßwasserpolypen *Hydra vulgaris* sind zwei FGFRs bekannt, sowie ein weiterer den FGFRs ähnlicher Rezeptor (FGFR-like) ohne intrazellulare Kinasedomäne. FGFRa, auch als Kringelchen bezeichnet, ist wegen seiner Rolle in dem Ablöseprozess der Knospe ein unabdingbarer Faktor in ihrer Entwicklung. Bisher ist allerdings unbekannt, welche extrazellulären Liganden an FGFR von *Hydra* binden und diese relevante Signaltransduktionskaskade aktivieren.

In der vorliegenden Arbeit wurden fünf zuvor identifizierte potenzielle FGFs auf ihre möglichen Funktionen in *Hydra* untersucht. Die Analyse von Gen- und Proteinexpressionsmustern unterschiedlicher FGFs in verschiedenen *Hydra* Stämmen weist auf evolutionär konservierte, vielfältige Funktionen der FGFs in der Knospenablösung, Neurogenese, Migration, Zelldifferenzierung und in der Regeneration von Kopf- und Fußstrukturen in *Hydra* hin.

Mit Hilfe der siRNA-Elektroporation wurden die Effekte eines Knockdowns von FGFs und FGFR in *Hydra* untersucht. Dabei konnten die bereits zuvor beobachteten Phänotypen, erzeugt durch pharmakologische Inhibition mit dem FGFR-Inhibitor SU5402, das Einbringen von Phosphorothioate-Antisense-Oligonukleotiden oder der Verwendung dominant-negativer FGFR Mutanten, erfolgreich reproduziert werden. Zusätzlich zeigte der siRNA Knockdown eine mögliche Funktion von *FGFRa* in der Neuronenentwicklung und von *FGFc* in der Differenzierung der I-Zellen.

Zusammenfassend gewährt diese Arbeit neue Einblicke in mögliche Funktionen verschiedener FGFs in *Hydra* und dient damit als Grundlage für weitere Untersuchungen zur Interaktion von FGFs und FGFRs diesem Organismus.

Contents

List of Abbreviations

ALP alsterpaullone.

BMP bone morphogenetic protein.

dsRNA double stranded RNAs.

ECM extracellular matrix.

FGF fibroblast growth factor.

FGFR fibroblast growth factor receptor.

FITC fluorescein isothiocyanate.

HSPGs heparan sulfate proteoglycans.

I-cells interstitial cells.

i-cells small interstitial cells.

Ig immunoglobulin.

ISH *in situ* hybridization.

MAPK mitogen-activated protein kinase.

MMP matrix metalloprotease.

RISC RNA-induced silencing complex.

RNAi RNA interfence.

Rock Rho-associated kinase.

siRNA small interfering RNA.

Wnt Wingless/Integrated.

List of Figures

List of Tables

1 Introduction

Metazoan development consists of many complex mechanisms and the underlying processes like cell division, pattern formation, morphogenesis, cell growth and differentiation have to be organized.

Controlling and fine tuning of such developmental processes includes genetic mechanisms and differential gene expression (Thisse & Thisse, 2005; Wolpert et al., 2002). Animals of all kind use similar genetic molecular machineries (Holland, 1999). Basal mechanisms seem therefore to be highly conserved amongst the animal kingdom and phylogenetically basal organisms can help to understand the evolutionary processes underlying signaling pathways in development.

One important signaling pathway in animal development is the fibroblast growth factor receptor (FGFR) signaling pathway (Thisse & Thisse, 2005). It is, e.g., involved in patterning, morphogenesis, differentiation, cell proliferation or migration. Fibroblast growth factor (FGF) signaling pathways have their origin in the last common ancestor of Eumetazoa (Babonis & Martindale, 2017; Bertrand et al., 2014; Lange et al., 2014; Matus et al., 2007; Oulion et al., 2012; Rebscher et al., 2009) and knowledge gained from the studies in animals of older phyla like the cnidarian *Hydra vulgaris* help to understand the evolutionary conservation of the FGFR signaling.

1.1 The fibroblast growth factor receptor signaling pathway

The fibroblast growth factor receptors are highly conserved throughout the animal kingdom: From trachea development in *Drosophila melanogaster* to limb bud outgrowth in vertebrates, FGFRs are important developmental factors in vertebrates and invertebrates (Kadam et al., 2009; Röttinger et al., 2008; Thisse & Thisse, 2005). Further, FGFRs are involved in mesoderm formation, tissue differentiation, angiogenesis, and wound healing. They also play a role in tumor development and metastasis (C. J. Powers et al., 2000; Sutherland et al., 1996; Thisse & Thisse, 2005). The activation of FGFRs occurs by

binding of FGF ligands (Mohammadi et al., 2005). FGFs can be found in all Eumetazoans, where they are essential during organogenesis, embryogenesis, and tissue homeostasis, as well as during migration, differentiation, cell survival, metabolism and in neural functions (Bertrand et al., 2014; Maddaluno et al., 2017; Matus et al., 2007; Ornitz & Itoh, 2015).

1.1.1 The molecular structure of FGFRs

FGFRs belong to the receptor tyrosine kinase family (Dai et al., 2019; Lee et al., 1989). In mammals, four similar FGF receptors (FGFR 1–4) were identified (Dai et al., 2019; Itoh & Ornitz, 2004). Vertebrate FGFRs comprise a characteristic structure (fig. 1.1): an extracellular ligand binding domain, consisting of three immunoglobulin-like (Ig) domains, a transmembrane domain for anchoring the receptor into the membrane and a bipartite intracellular kinase domain, which provides enzymatic activity (Mohammadi et al., 2005; Ornitz & Itoh, 2015; Thisse & Thisse, 2005). The hydrophobic signal peptide (SP) is located at the N-terminus of the receptor and is essential for the translocation into the endoplasmatic reticulum and for guidance of the receptor to the membrane (Lodish et al., 2000; Mohammadi et al., 2005).

The Ig loops of the extracellular domain (Ig I–III) are stabilized by disulfide bridges between two cysteines and are divided by short linker sequences (Ornitz & Itoh, 2015; Thisse & Thisse, 2005). Binding of FGF ligands is mediated by the Ig loops II and III (Pellegrini et al., 2000; Plotnikov et al., 2000; Schlessinger, 2000) and the ligand specificity is mediated by the alternative splicing of the Ig loop III, which can be tissue-dependent (Holzmann et al., 2012; Ornitz, 2000; C. J. Powers et al., 2000). Ig loop I and the following linker sequence are not directly involved in ligand binding (Plotnikov et al., 2000). In between Ig loop I and Ig loop II of most triploblastic animals an acidic box is located (Rebscher et al., 2009), which can link basic heparin binding sites via electrostatic interactions (Olsen et al., 2004). These interactions enable physical proximity of Ig loop I to the ligand binding site at Ig loop II and Ig loop III, which reduces the receptor's ability to bind heparin or FGF and therefore causes autoinhibition (Olsen et al., 2004; J. Xu et al., 1992). Binding of the co-factor heparin is mediated by a series of basic and hydrophobic amino acids in the Ig II domain (Pellegrini et al., 2000; Schlessinger, 2000). The intracellular part of the FGF receptors includes a bipartite highly conserved tyrosine kinase domain. The ligand binding enables the phosphorylation of six highly conserved tyrosine residues in the kinase domain, which is essential for signaling (Johnson & Williams, 1992; Mohammadi et al., 2005; Ornitz & Itoh, 2015; Rebscher et al., 2009).

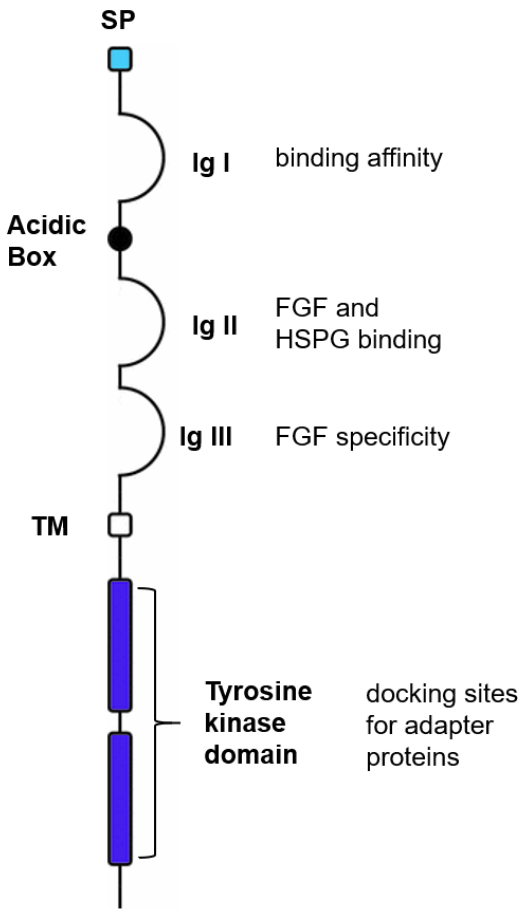

Figure 1.1: Scheme of the canonical vertebrate FGFR structure. The signal peptide (SP, light blue) is located at the N-terminus. Three extracellular immunoglobulin-like (Ig) domains (Ig I–III) are followed by a single transmembrane helix domain (TM, white box). An acidic box is located between Ig I and II (black box). The highly conserved split tyrosine kinase domain is located cytoplasmatically (dark blue). Modified after Tiong et al. (2013).

In vertebrates, the alternative receptor splicing provides several isoforms with different functions, e.g. FGFR1 and FGFR2 miss the N-terminal region of Ig loop II (Johnson et al., 1990; C. J. Powers et al., 2000). Secreted FGFRs without a membrane- and intracellular domain or membrane-bound isoforms without kinase-domain likely act as negative regulators. They are still capable of FGF binding, but the signal transduction is not possible per se (Johnson et al., 1990; Johnson & Williams, 1992; C. J. Powers et al., 2000). Additionally, a fifth FGFR receptor (FGFR5 or FGFRL1) has a similar structure and function, but is an own gene rather than a splicing variant of the other FGFRs (Dai et al., 2019; Trueb, 2011; Wiedemann & Trueb, 2000). The FGFRL1 was shown to bind different FGF ligands in varying affinities, thus regulating the pathway, e. g. in *Xenopus* embryos (Steinberg et al., 2010). In a variant of the human FGFR1, the extracellular domain undergoes proteolytic cleavage after membrane anchoring (Hanneken, 2001). The presence of C-terminal variations of FGFRs correlate with chemo tactical functions (Landgren et al., 1998).

In invertebrates, the FGFR structure basically resembles the described structure in vertebrates. A noticeable difference is the variation in Ig loop numbers. The *Drosophila melanogaster* Breathless and the *Tribolium castaneum* FGFR contain five Ig loops, while the *Drosophila* Heartless and the *Dugesia japonica* FGFR2 contain only two (Ogawa et al., 2002; Sharma et al., 2015; Shishido et al., 1993). FGF receptors of *Caenorhabditis elegans* (EGL-15), *Strongylocentrotus purpuratus*, *Halocynthia roretzi*, *Platynereis dumerilii* and *Dugesia japonica* (DjFGFR1) developed three Ig loops (DeVore et al., 1995; Goodman et al., 2003; Kamei et al., 2000; McCoon et al., 1996; Ogawa et al., 2002). The acidic box is missing in all invertebrates (Cebrià et al., 2002; Rebscher et al., 2009).

1.1.2 FGFs as ligands for the FGFR signaling

The evolutionary origin of the FGFs is hypothesized in in a gene that codes for a protein with an FGF-like domain (FGFL), which appeared in the last common ancestor of choanoflagellates and metazoans (Bertrand et al., 2014). The first bona fide FGF emerged in the ancestor of Eumetazoans after the duplication of a FGFL gene. Since then, the FGF family diversified and today the FGF family comprises 22 members in humans (Itoh et al., 2015) (fig. 1.2).

Vertebrate FGFs were first discovered as a mitogen causing cultured fibroblasts to proliferate (Armelin & Sato, 1973; Gospodarowicz, 1974), and nowadays different FGFs are known with diverse functions, e.g. during tissue repair and regeneration as in the limb regeneration in axolotls (Beenken & Mohammadi, 2009; Dorey & Amaya, 2010; Itoh

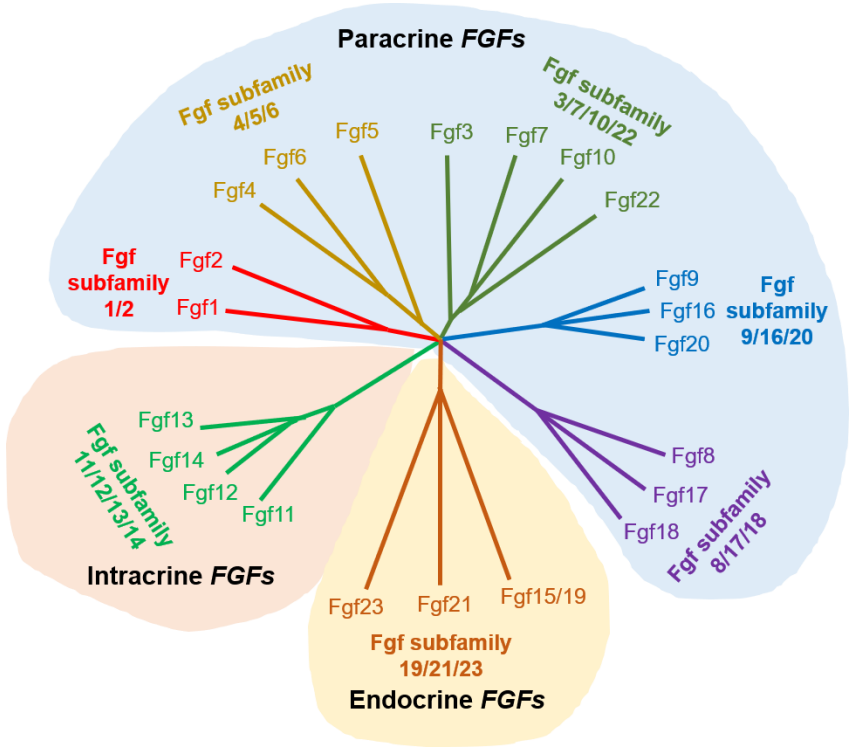

Figure 1.2: FGF families. Arrangement of the 22 vertebrate FGFs into seven subfamilies. Modified after Ornitz and Itoh (2015).

& Ornitz, 2011; Maddaluno et al., 2017; Makanae et al., 2014; Mullen et al., 1996; Yun et al., 2010). They are involved in early central nervous system (CNS) development, neurulation, brain patterning and anterior-posterior patterning of the early neural plate (Hébert, 2011). Functions of FGFs in cell migration were shown inter alia during migration of mesencephalic neural crest cells (Kubota & Ito, 2000; Yun et al., 2010). Pyramus and Thisbe in *Drosophila* as well as Egl-17 in *C. elegans* are important factors during cell and tissue migration as well as of heart and muscle development (Burdine et al., 1997; Stathopoulos et al., 2004). The FGF ligand Branchless controls neurogenesis and tracheal morphogenesis in *Drosophila* (Muha & Müller, 2013; Sutherland et al., 1996). FGFs can also act dosage-dependent to accomplish different functions: In the *Drosophila* mesoderm development, low amounts of FGF promote cell migration towards an FGF source, whereas high FGF concentrations lead to cell adhesion (Bae et al., 2012).

FGFs are approximately 150 to 300 amino acids long (Basilico & Moscatelli, 1992; Mohammadi et al., 2005). The protein sizes vary between 17 kDa to 34 kDa in vertebrates (Ornitz & Itoh, 2001). Invertebrate FGFs show more variability regarding their size: *Drosophila* FGFs range between 82 kDa and 86 kDa, whereas FGFs of *Ciona intestinalis*

with 21 to 31 kDa share a similar size with vertebrate FGFs (Satou et al., 2002; Stathopoulos et al., 2004; Sutherland et al., 1996). The main differences are in the length of the N- and C-terminal structures (Popovici et al., 2005).

All FGF members share a conserved sequence of approximately 120 amino acids with 16 % to 65 % sequence identity, also known as the core region (Ornitz & Itoh, 2001). This core region is important for the interaction with FGFRs and adopts a conserved β-trefoil fold consisting of 12 antiparallel β-strands (Beenken & Mohammadi, 2009; Mohammadi et al., 2005; Zhu et al., 1990). The trefoil coil is flanked by amino- and carboxy-terminal regions that vary in length and sequence between FGFs, thus mediating different functions for different FGFs (Belov & Mohammadi, 2013). Core regions of vertebrates and invertebrates principally differ from each other, but core regions between different human FGFs show more differences to each other than core regions of FGFs between different species (Coulier et al., 1997). Thus, the classification of FGFs is based on their core sequences according to human FGFs (Itoh et al., 2015) (fig. 1.2). The first characterized FGFs were acidic FGF (aFGF, now FGF1) and basic FGF (bFGF, now FGF2) (Abraham, Mergia, et al., 1986; Abraham, Whang, et al., 1986; Gospodarowicz & Moran, 1975). Today, the human FGF family comprises up to 22 distinct polypeptides which are subdivided into seven or eight groups, depending on the autonomy of FGF3 as an own distinct group (Itoh & Ornitz, 2011; Itoh et al., 2015; Ornitz & Itoh, 2001; Oulion et al., 2012; Popovici et al., 2005).

Most FGFs are paracrine growth factors, which are secreted and interact with FGFRs (Ornitz & Itoh, 2015). They show a high affinity of binding to the FGF receptors, but also bind heparin or heparan sulfate proteoglycans (HSPGs) as co-receptors (Belov & Mohammadi, 2013; Lin, 2004). The binding sites for HSPGs reside in the FGF core region (Ornitz, 2000). The affinity to bind HSPGs of the extracellular matrix (ECM) modulates the diffusion range of FGFs (Beenken & Mohammadi, 2009; Bökel & Brand, 2013; Itoh & Ornitz, 2011). Groups of paracrine FGFs are FGF1/2, FGF4/5/6, FGF3/7/10/22, FGF8/17/18/24 and FGF9/16/20. Endocrine FGFs are summarized in the group FGF15/19/21/23. These FGFs lost their ability to bind to HSPGs due to an atypical β-trefoil fold, and can therefore function within a higher range (Beenken & Mohammadi, 2009, 2012; Goetz et al., 2007; Itoh & Ornitz, 2011; Itoh et al., 2015). The FGF family FGF11/12/13/14 acts in an intracrine manner and does not bind to FGFRs, possibly serving as a co-factor for other molecules (Goldfarb, 2005; Itoh & Ornitz, 2011; Ornitz & Itoh, 2015). The intracrine FGFs in vertebrates can activate voltage-gated Na^+-channels (Nav) in neurons (Itoh & Ornitz, 2011; Lou et al., 2005) which are important for controlling the excitability of neuronal

cells and can regulate processes like locomotion and cognition (Marban et al., 1998). In vertebrate FGFs 2–10 and 16–23 a signal peptide (SP) is located N-terminally which is lacking in FGF1 (acidic) and FGF2 (basic) as well as in the FGFs 11–14 (Itoh & Ornitz, 2011; Ornitz & Itoh, 2001; Oulion et al., 2012; Zhang et al., 2012).

1.1.3 The activation of the FGFRs and their downstream pathways

The activation of the FGFR signaling pathways is triggered by the interaction of FGF with FGFR (Mohammadi et al., 2005). The binding of the FGF to the co-factor HS/HSPG, which is mediated by the Ig loop II, leads to conformational changes, thus stabilizing receptor homodimers and can be modified by alternative splicing (Beenken & Mohammadi, 2009; Holzmann et al., 2012; Ibrahimi et al., 2005; Ornitz, 2000; Ornitz & Itoh, 2015; C. J. Powers et al., 2000; Schlessinger, 2000). The receptor dimerization transphosphorylates tyrosine residues in the intracellular domain (Furdui et al., 2006). The receptor transphosphorylation generates docking sites for intracellular binding proteins (Lemmon & Schlessinger, 2010), e.g. the docking proteins FGF receptor substrate 2 (Frs2, vertebrate specific) (Gotoh, 2008) or in the fly, of downstream-of-FGFR (Dof, also known as stumps or heartbroken, *Drosophila*-specific) (Vincent et al., 1998). Tyrosin phosphorylation, furthermore, activates enzymes with Src homology 2/3 -binding sites (SH2- or SH3) (Mohammadi et al., 1991). The binding of the docking proteins generates secondary binding sites for adapter proteins like growth factor receptor-bound protein 2 (Grb2) (Lowenstein et al., 1992), son of sevenless (SOS) (Eswarakumar et al., 2005), CRK and CRKL (Birge et al., 2009) as well as Src homology region 2 domain-containing phosphatase-2 (Shp2/ corkscrew (Csw) in *Drosphila*) (Eswarakumar et al., 2005; Gotoh, 2008; Hadari et al., 1998; Lax et al., 2002). The FGFR downstream pathway of the phospholipase c gamma (PLCγ) is directly activated by binding of PLC at transphosphorylated sites of the FGFRs (Mohammadi et al., 1991; Thisse & Thisse, 2005).

The activation of the FGF receptors starts several downstream pathways depending on the cellular context. Those downstream pathways include signaling via PLC/PI/PKC, RAS/mitogen-activated protein (MAP)-kinase, Rho/Rock and PI3-kinase (fig. 1.3). Other signaling targets are p38, JNK or pathways via signal transducers and activators of transcription (STAT) (Boilly et al., 2000; Brewer et al., 2016; Lemmon & Schlessinger, 2010; Ornitz & Itoh, 2015). Crosstalk with other signaling pathways are common. As an example, FGFR also acts downstream of the Wingless/Integrated (Wnt) signaling pathway

in regenerating tissues of *Xenopus* and zebrafish (Maddaluno et al., 2017). During retinal regeneration, Notch acts as downstream regulator of FGF8 (Wan & Goldman, 2017). Interactions of FGFR and bone morphogenetic protein (BMP) signaling are common during development, e.g. in axis formation and tissue specification (Schliermann & Nickel, 2018). Thus, depending on the activated downstream regulators, FGFR signaling controls multiple cellular processes like (collective) cell migration, cell proliferation, morphogenesis or cell differentiation (Boilly et al., 2000).

1.1.4 The role of FGFs during regeneration and wound healing

Repair and regeneration involve a large variety of growth factors, cytokines, and differentiation factors (Werner & Grose, 2003). FGFs are known for their importance in many biological processes, e.g. differentiation, proliferation and migration (Ornitz & Itoh, 2015) and different FGFs were found to be crucial factors in a variety of regenerating tissues in invertebrates and vertebrates (Maddaluno et al., 2017). The function of FGFs in repair is often mediated by paracrine FGFs with a low diffusion gradient.

In mammals, the wound healing and regeneration of tissues is often imperfect and leads to the formation of scars. Other animals, like *Hydra* and planarians, are capable to regrow completely from small body fragments or, like frog, fish and salamander, to regrow specific body parts (Tanaka & Reddien, 2011). The regeneration of limbs is accompanied by blastema formation. Blastema formation in amphibians can be induced by exogenous application of BMPs combined with FGF2 and FGF8 which allows for regeneration rather than normal wound healing processes (Makanae et al., 2014). The same combination promotes tail regeneration in axolotls (Makanae et al., 2016). Furthermore, FGF8 was identified as a key player in axolotl limb regeneration, as it induces the proliferation of blastema cells after the limb amputation (Nacu et al., 2016). Other FGFs are also important during limb regeneration processes: FGF10 stimulates the limb regeneration in *Xenopus* limb stumps (Yokoyama et al., 2001), the application of FGF4 results in stump tissue outgrowth in chicken limbs (Kostakopoulou et al., 1996) and FGF2 plays a role in mouse digit regeneration (Takeo et al., 2013). FGF20 was found to regulate the early stages of zebrafish fin regeneration (Whitehead et al., 2005). Additionally, FGFs have a conserved role during the regeneration of neural tissues, which has been shown for planarians (Cebrià et al., 2002). FGF2 is a key regulator in repair and protection of ischemic, metabolic and traumatic brain injuries in mammals (Alzheimer & Werner, 2003) and an overexpression of FGF2 in mice showed faster nerve cell regeneration (Jungnickel et al., 2006). During the healing of skin wounds, FGF2 and

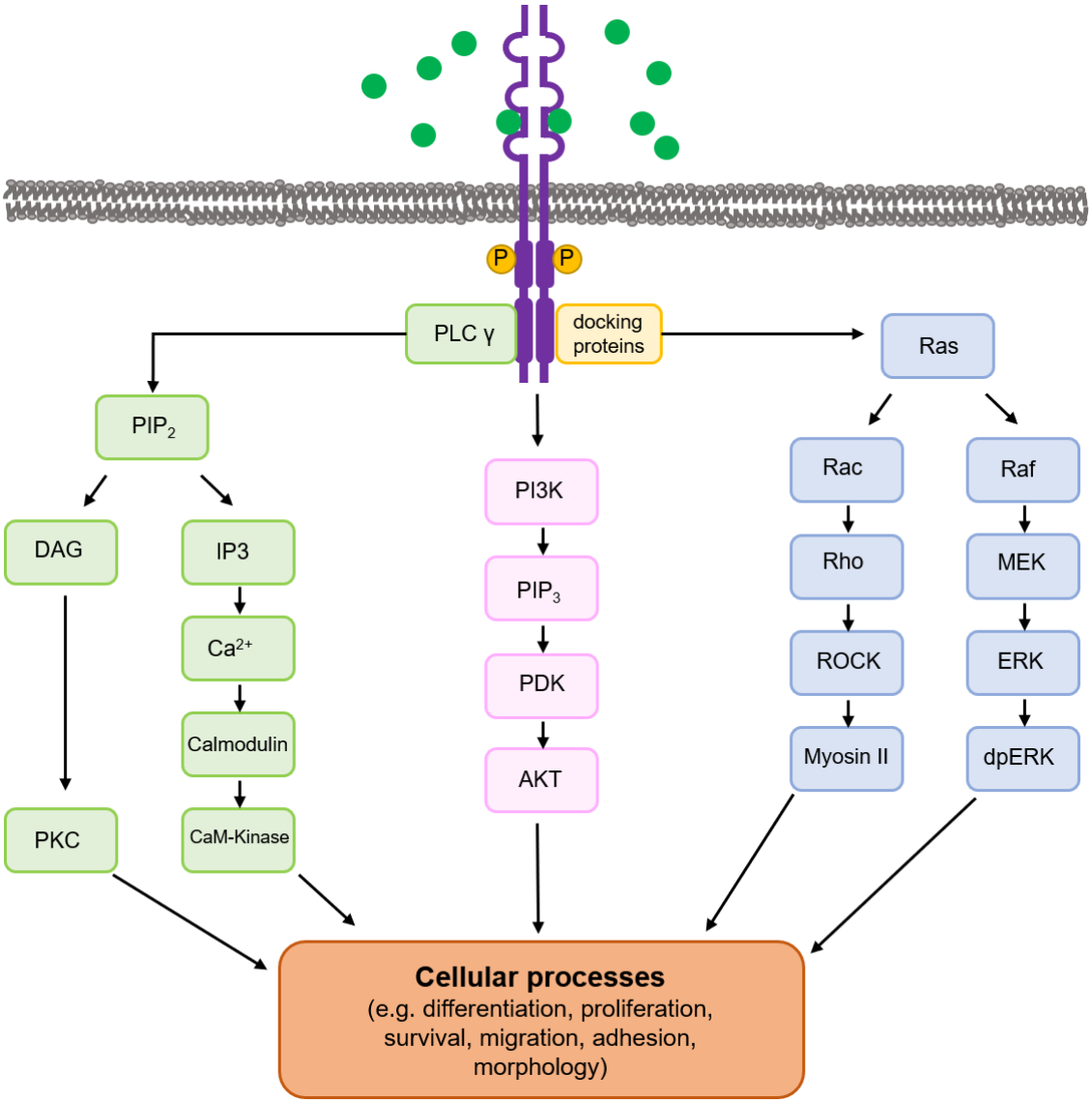

Figure 1.3: Simplified scheme of FGFR signaling pathways. After binding of FGF ligands (green circles) to the receptors, the transphosphorylated kinase domains recruits docking proteins (yellow). These activate downstream pathways e.g. via PI3K (pink pathway) or Ras (blue pathways). PLCγ is directly activated by the receptors and activates DAG and IP3 pathways (green pathways). FGFR pathways therewith regulate multiple cellular processes (orange). Modified after Hallinan et al. (2016) and Teven et al. (2014).

FGF7 have shown to be crucial factors (Nunes et al., 2016; Werner & Grose, 2003). In addition to the insights gained in various studies, FGFs can also be utilized for application to human wounds to induce regeneration, where several materials and substrates are developed to limit the FGFs diffusion range to allow local application (Yun et al., 2010).

1.2 The model organism *Hydra vulgaris*

FGFR signaling is a multifunctional pathway during animal development. The studies in old phyla like Cnidaria help investigating the evolutionary aspect of FGFR signaling. The following section introduces the Cnidarian *Hydra vulgaris* as a model organism and depicts its characteristic features.

1.2.1 Characteristics of *Hydra*

The freshwater polyp *Hydra* belongs to the ancestral phylum Cnidaria which diverged early from the rest of the animals and is a sister group to Bilateria (Technau et al., 2012). Despite its simple morphology *Hydra* uses the same complex genetic machineries as vertebrates (Galliot, 2012; Steele, 2002). Its simple radial symmetric body plan is divided into a head with mouth opening, hypostome and tentacles, a tubular body column, and a foot with a basal disc and a foot pore (fig. 1.4; Meinhardt (2002)). *Hydra* consists of two epithelial layers, the outer ectoderm, and the inner endoderm which are separated by a cell-free mesogloea, an extracellular matrix (ECM) (Sarras et al., 1991; Sarras, 2012). Cells of ecto- and endoderm synthesize this layer and are anchored in the mesogloea (Shimizu et al., 2008). Small pores in the mesogloea are used to allow cell-cell interactions of ecto- and endodermal cells (Sarras, 2012). Epithelial cells in *Hydra* function as epitheliomuscle cells, combining muscular functions in the basal cell part with epithelial functions in the apical domain (Leclère & Röttinger, 2017). With the help of the epitheliomuscle cells, *Hydra* contracts and elongates its body: basal contractile myonemes in the ectoderm run longitudinal across the body while endodermal myonemes occur in a circular orientation (Aufschnaiter et al., 2017).

The *Hydra* polyp is potentially immortal, and has a high regeneration capacity due to its three distinct stem cell lines (fig. 1.4) (Galliot, 2012): Ectodermal stem cells give rise to cells of the outer epithelial layer (ectoderm). Endodermal stem cells develop into epithelial cells in the gastrodermis (or endoderm). A third stem cell lineage, the interstitial stem cell lineage, consists of multipotent stem cells, the interstitial cells (I-

cells) which give rise to all non-epithelial cells in the animal and are located between the ectodermal cells (Bosch et al., 2009; Bosch & David, 1986; David, 2012; David & Murphy, 1977; Hobmayer et al., 2012). These cells differentiate into neuronal cells, gland cells, mucous cells and nematocytes. Epithelial cells divide every three to four days, whereas small interstitial cells have a shorter life span of only 1.5 days (David & Campbell, 1972; Martínez & Bridge, 2012). An overview of several *Hydra* cell types is given in figure 1.5.

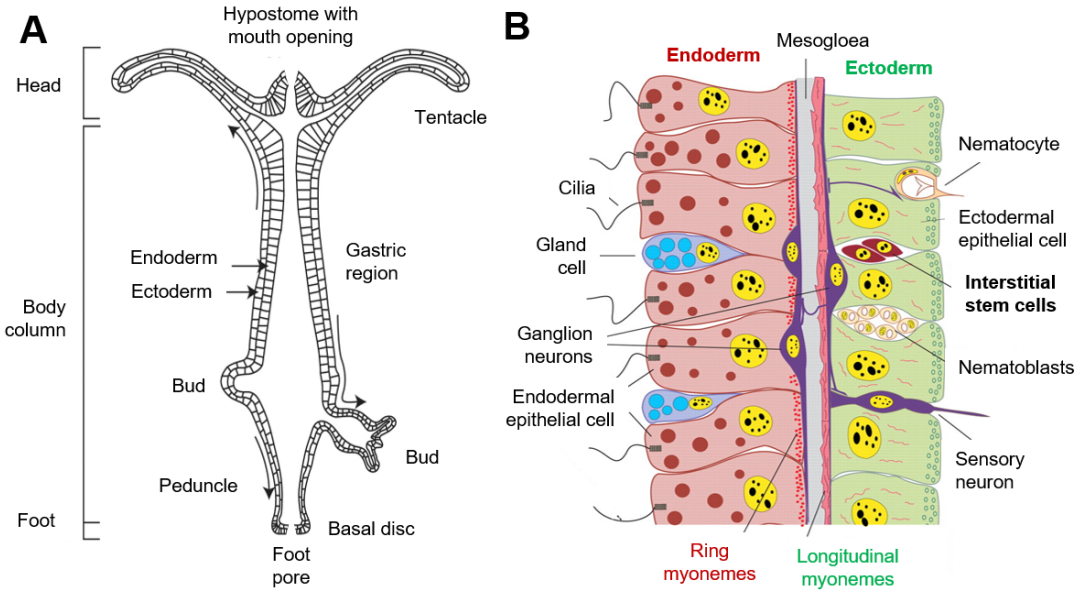

Figure 1.4: Scheme of the *Hydra* body plan. (A) Longitudinal cross section of *Hydra*. The basic structure consists of head, body column and foot. The polyp is built by two epithelial layers, the ecto- and endoderm. An early and a late bud are depicted on the left and right site of the polyp, respectively. The arrows indicate directions of tissue movement. Modified after Bode (2009). (B) Scheme of the *Hydra* cell types. Ectodermal stem cells (green) and endodermal stem cells (red) are unipotent stem cells. Interstitial stem cells are multipotent stem cells. Modified after (Technau et al., 2012).

Cells and tissue in the adult *Hydra* are constantly moving, either actively or passively, caused by a constant shift between production and elimination of cells (Bosch et al., 2009). Endo- and ectodermal epithelial cells in the body column permanently undergo mitosis (Burnett, 1966; Dübel et al., 1987) and are shifted, according to the current view, mostly passive as a tissue complex towards the extremities like tentacles and basal disc, where cells terminally transdifferentiate and are lost (Bode, 2011; Bosch et al., 2009). About 80 % of cells in well-fed polyps are exported as a tissue sheet and used to form buds (Bode, 1996). Small interstitial cells (i-cells) migrate actively to their destination and even the usually immobile stem cells (I-cells) possess the ability to repopulate i-cell

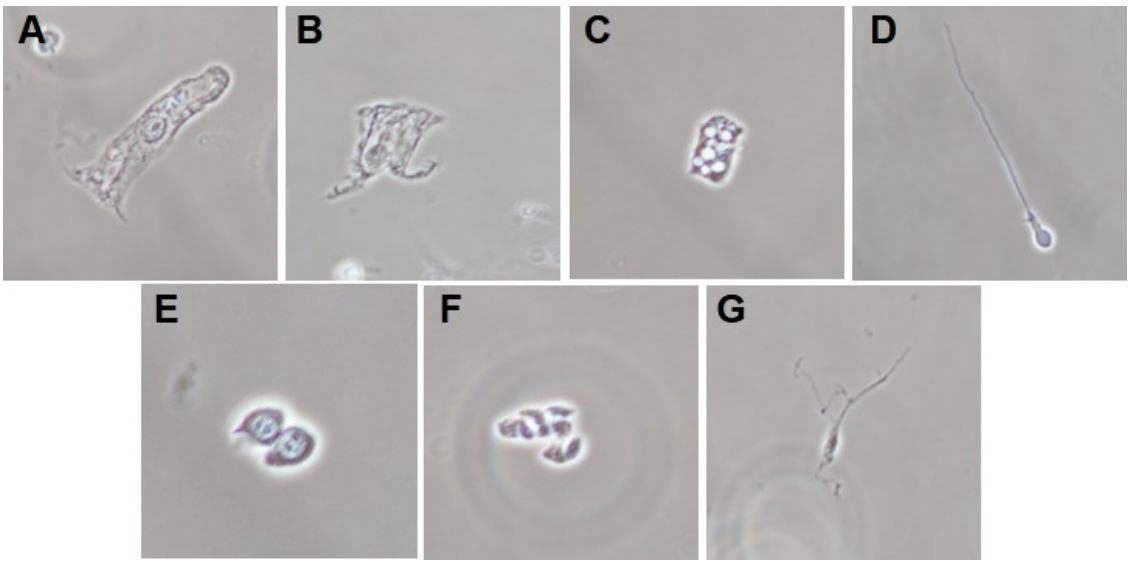

Figure 1.5: Cell types of a *Hydra*. (A–G) Several *Hydra* cell types as obtained by a single cell preparation (maceration, according to David 1973) are shown. (A) Endodermal epithelial muscle cell. (B) Ectodermal epithelial muscle cell. (C) Gland cell. (D) Example of a nematocyst: Discharged stenotele (penetrant nematocyst). (E) A pair of I-cells (stem cells). (F) Nest of nematoblasts. (G) Neuron.

free tissue (Boehm & Bosch, 2012; Bosch et al., 2009; Campbell, 1967; David, 2012; David & Murphy, 1977; Martínez & Bridge, 2012).

Cells differentiate in various zones along the polyp body. One active differentiation zone is at the tentacle base, where ectodermal epitheliomuscle cells transdifferentiate into battery cells and integrate nematocytes which migrated actively as nematoblasts from the body column to the tentacles (Aufschnaiter et al., 2011; Boehm & Bosch, 2012; David, 2012; Hobmayer & David, 1989). The *Hydra* ectoderm is coated with a glycocalyx, a cuticle like protective layer composed of glycosaminoglycans and secreted by the ectodermal cells (Böttger et al., 2012; Holstein et al., 2010; Schröder & Bosch, 2016). Glandulomuscular cells in the basal disc help *Hydra* to attach to the substrate (Burnett, 1966; Davis, 1973; Lentz, 1966).

1.2.2 The reproduction of *Hydra*

Hydra propagates sexually and asexually, where the asexual reproduction by budding is the characteristic way to reproduce. A bud evaginates laterally in the mid body region and grows to a complete polyp within four days. Then, it detaches from the parent as an autonomous individual (Otto & Campbell, 1977). The budding process is divided into three phases and subdivided into 10 different budding stages (fig. 1.6, Otto and Campbell

(1977)). Different signaling pathways (e.g. Wnt, FGFR and Notch) are involved in the budding process (Münder et al., 2010; Philipp et al., 2009; Prexl et al., 2011; Steele, 2002).

In the initiation phase (budding stages 1 to 3), canonical and non-canonical Wnt signaling control the evagination of endo- and ectodermal tissue (Hobmayer et al., 2000; Philipp et al., 2009). During the elongation phase (budding stages 3 to 6), the bud grows (elongates) and new tentacles start to form, while a massive tissue movement towards the bud occurs and cell division is increased (Bode, 1996). The differentiation of the head and development of the tentacles are under control of canonical Wnt signaling (Hobmayer et al., 2000). The last budding phase is the detachment phase (stages 7 to 10) which is characterized by the separation of the bud and the adult polyp. The formation of the boundary between parent and bud is thereby under control of FGFR and Notch signaling (Hasse et al., 2014; Münder et al., 2010; Sudhop et al., 2004). The bud constricts towards the parent and from stage 8 onwards the constriction site narrows (Holz et al., 2017). Concomitant with the constriction of the bud, F-actin starts to accumulate at the boundary between bud and parent and shortly before the detachment, the typical circularly and longitudinally oriented F-actin fibers rearrange in parent and bud. As the cells in the bud and at the bud base change their shape during the budding and detachment process, the actin cytoskeleton needs to reorganize which is achieved by targeting at least two downstream FGFR pathways (Hasse et al., 2014; Holz et al., 2020; Holz et al., 2017). The last step is the final detachment of the bud. Contracting sphincter or constrictor muscles in the basal disc thereby allow the segregation of the bud and the adult (Takahashi et al., 1997).

Sexual reproduction in *Hydra* can be induced by a temperature or hunger stress stimulus (V. Martin et al., 1997) and is crucial for generating transgenic animals (Juliano et al., 2014; Klimovich et al., 2019; Wittlieb et al., 2006). *Hydra vulgaris* AEP, the only strain to generate transgenic animals, is either male or female (fig. 1.7), while other *Hydra* strains are hermaphroditic (Kaliszewicz & Lipińska, 2013; V. Martin et al., 1997). Females usually produce a single egg and males several testes (V. Martin et al., 1997). During the testis development, the ectoderm thickens, and interstitial cells (i-cells) migrate into the evaginated tissue. In the testis, i-cells develop further into immature and mature sperm cells which are released to the surrounding environment through a pore in the testes. Eggs differentiate as well from a cluster of i-cells and lay on a cushion of ectodermal cells forming a pouch (V. Martin et al., 1997; Tannreuther, 1908). Mature eggs break through the ectodermal layer and are to be fertilized within about two hours. After gastrulation,

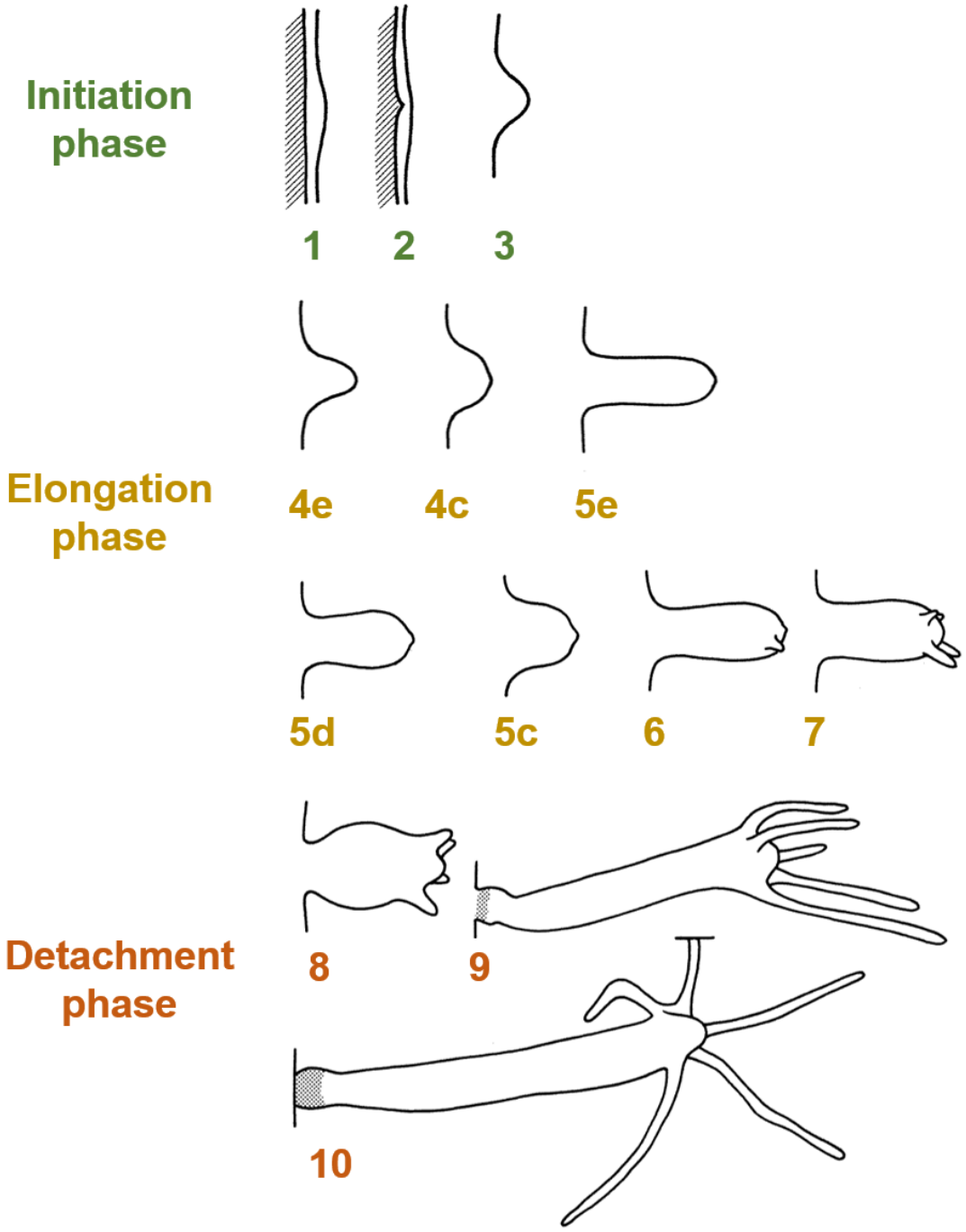

Figure 1.6: Budding scheme of *Hydra*. The budding process in *Hydra* is divided into three phases with 10 stages. Initiation phase (green): Ectoderm and endoderm thicken, and the bud starts to evaginate. Elongation phase (yellow): The bud further grows and elongates. First tentacle buds start to grow. Detachment phase (orange): A constriction forms at the border between the bud and its adult polyp. The bud develops the basal disc. Final detachment and separation of bud and adult occurs. Modified after Otto and Campbell (1977).

the egg develops an impermeable shell-like structure called cuticle, that protects the embryo until hatching. Hatching takes place 2 to 24 weeks later (V. Martin et al., 1997).

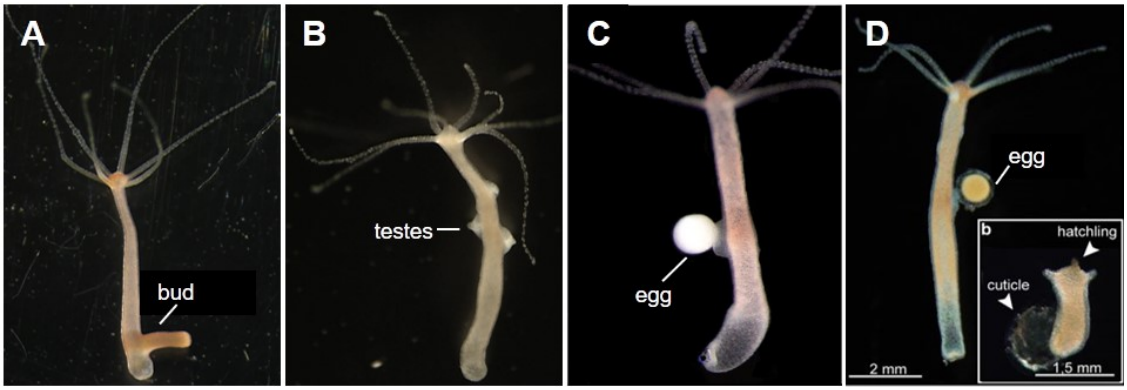

Figure 1.7: Asexual and sexual propagation in *Hydra vulgaris* AEP. (A) Asexually propagating *Hydra* with a stage 5 bud. The bud is elongated, but no tentacles formed yet. (B–D) Sexually propagating *Hydra*. (B) Male *Hydra* with three developed testes above the budding zone. (C–D) Female *Hydra* with one developed egg, each. (C) The egg is presented on its pouch and is ready for fertilization. Modified after Fraune et al. (2010). (D) Mature egg after formation of the protective cuticle. (Db) A freshly hatched *Hydra*. Modified after Franzenburg et al. (2013).

1.2.3 Regeneration in *Hydra*

Hydra possesses a remarkable regeneration ability which makes it a model organism eligible for regeneration processes (Bosch, 2007; Galliot, 2012). The underlying mechanism of wound healing in *Hydra* is called morphallaxis (Bosch, 2007). Morphallaxis, in comparison to epimorphosis, involves regeneration by the re-organization of existing tissue into new structures without blastema formation and in absence of cellular proliferation, which in *Hydra* lasts for at least 12 hours after the sectioning (Agata et al., 2007; Holstein et al., 1991). Several studies showed that all necessary genes for regeneration must be activated in the epithelial cells, making them the main components in *Hydra* regeneration and that the endoderm initiates the wound healing process (Bibb & Campbell, 1972; Marcum & Campbell, 1978; Sugiyama & Fujisawa, 1978). The reorganization at the wound into a lumen with ectodermal cells on the outside and endodermal cells in the inside within the first 12 hours is possibly driven by differential cell adhesion between both epithelial layers (Gierer et al., 1972; Technau & Holstein, 1992). Another important role in the *Hydra* regeneration plays the mesogloea, as it anchors the epithelial cells which promotes their survival (Bosch, 2007). At the start of the regeneration, the mesogloea is immediately retracted and must rebuilt subsequently to separate both

epithelial cell layers (Shimizu-Nishikawa et al., 2003). It was shown, that morphallaxis depends on a high activity of matrix metalloproteases (MMPs) which are key regulators for degradation and remodelling of the mesogloea (Bosch, 2007; Leontovich et al., 2000; Sarras et al., 2002; Shimizu-Nishikawa et al., 2003).

An easy way to investigate the regeneration in *Hydra* is by mid-gastric bisection, which leaves the polyp in two halves that both fully regenerate after about four days (Vogg et al., 2019). In this process the tissue pieces keep their positional information and apical regenerative ends develop into a head, and basal regenerative ends into a foot (Cummings & Bode, 1984; MacWilliams, 1983; Wolpert et al., 1974). The head organizer is important during the head regeneration and establishes within 18–30 h (Sato et al., 1990) with the first head and tentacle structures emerging after 48–72 h (Technau & Holstein, 1992). The foot regeneration is complete about 56 hours after bisection (Vogg et al., 2019).

Besides the high regeneration capacity of *Hydra* after sectioning, it can also develop into full-grown polyps after the dissociation into single cells (Gierer et al., 1972; Noda, 1971; Technau et al., 2000; Technau & Holstein, 1992). During the first 12 hours of reaggregation, cell sorting processes lead to the segregation and reformation of ecto- and endoderm. It is thereby noticeable, that the cells of ecto- and endoderm are sorted according to their original body layer rather than their origin along the apical-basal axis in the polyp (Technau & Holstein, 1992).

Different *Hydra* halves can be combined on a needle (a process called transplantation) and within two hours both individual body halves are regenerated and joined into one *Hydra* polyp (MacWilliams, 1983; Murate et al., 1997; Shimizu, 2012; Shimizu & Sawada, 1987). The transplantation was shown as a useful tool to investigate i-cell migration (Fujisawa et al., 1990). Transplanted tissue can induce either head or foot structures depending from where the tissue was taken (Berking, 2003) and the transplantation of head tissue parts can induce a secondary axis as the head acts as an organizer (Broun & Bode, 2002; Kadu et al., 2012; MacWilliams, 1983).

Several signaling pathways were shown to be involved in regeneration processes in *Hydra*: The head regeneration for instance requires canonical Wnt signaling (Bode, 2003; Hobmayer et al., 2000) and Notch signaling is necessary for *Wnt3a* expression in the head organizer of the regenerating head (Münder et al., 2013). VEGF has been shown to function during regeneration (Krishnapati & Ghaskadbi, 2013) and a BMP5-8 homologue was identified to be involved in tentacle formation and foot patterning during the regeneration in *Hydra* (Reinhardt et al., 2004). Further, the head regeneration

is associated with an increase in PKC activity (Hassel et al., 1998; Müller, 1989) and it was shown that MAPK-pathways are also necessary for the formation of the head organizer (Arvizu et al., 2006; Tischer et al., 2013). While the *FGFRa* gene (Sudhop, 2006) and at least one *Hydra* FGF (Lange et al., 2014) are upregulated during the regeneration process in *Hydra*, little is known about the general role of the FGFR signaling during the regeneration in *Hydra*.

1.2.4 The *Hydra* nerve net and neurogenesis

Interstitial stem cells (I-cells) of the body column differentiate into several specialized cell types (Bosch et al., 2009; Bosch & David, 1986; David, 2012; David & Murphy, 1977; Hobmayer et al., 2012). 60 % of I-cells renew themselves, 40 % undergo differentiation into e.g. nematoblasts/nematocytes or neuroblasts/neurons (David, 2012). Nerve cell precursors in the body column stay in the G2-phase and await further signals for their terminal differentiation into ganglion or sensory cells. As i-cells in head and foot only differentiate into neurons, the density of neurons in these regions is higher than in the rest of the body (David & Gierer, 1974). Neurons make about 3 % of total cells in *Hydra* with up to 9.9 % in *Hydra vulgaris* Zürich strain (formerly *Hydra attenuata*) (David, 1973; Hassel & Berking, 1988). Nerve cells position themselves between epitheliomuscle cells of both layers (Galliot et al., 2009). Sensory neuron cells are thereby located within the ectodermal layer, whereas ganglionic neurons are found in both epithelial layers.

Hydra is probably one of the simplest animals in terms of nerve net formation, although it has mainly tree individual, biochemically distinct, nerve nets, which are all organized in a diffuse way (Cristino et al., 2007; Dupre & Yuste, 2017). These nerve nets are divided into functional groups depending on the reaction they provoke in the animal (Dupre & Yuste, 2017). One nerve net (rhythmic potential circuits 1, RP1) is localized in the ectoderm and is used during the reaction to a light stimulus. Rhythmic potential 2 (RP2) has an endodermal origin and is relevant for radial contractions. The third nerve net is the contraction burst network (CB). CB is situated in the ectoderm and regulates longitudinal contractions. A fourth network is restricted to the region just only located below the tentacle and is referred to as sub tentacle network (STN). It is used for "nodding" of the head. The differentiation of nerve cells is regulated by at least one neuro peptide, Hym355, which is secreted by the nerve cell itself (Takahashi et al., 2000) and epitheliopeptides of the LPW-family which are secreted by epithelia muscle cells which inhibits the differentiation of neurons (Takahashi et al., 2009). Both peptides

are thought to regulate themselves antagonistically in a positive feedback-loop (Bosch & Fujisawa, 2001; Koizumi, 2002).

A lifelong reproduction of neurons is balanced by the loss of neurons at the extremities (Bode et al., 1988). Neuron precursors migrate to the terminal destination, where they differentiate into neurons. Treatment with hydroxyurea (HU) for several days depletes I-cells and, and after a couple of weeks also neurons in *Hydra*, creating a so-called nerve-free *Hydra* (Bode, 1983; Sacks & Davis, 1979). After cross-transplantation of animals with removed nerve cells and untreated animals, stem cells of untreated *Hydra* can re-populate nerve-free *Hydra* and therewith renew the interstitial stem cell lineage (Bosch et al., 2009; Koizumi, 2002).

1.3 The FGFR signaling in *Hydra*

Although *Hydra* seems to be a simple organism, its development is controlled by different signaling pathways which also can be found in bilaterian animals. The FGF receptors have their origin in the common ancestor of Placozoa, Cnidaria, and Bilateria (Rebscher et al., 2009) and FGFs in the ancestor of Eumetazoans (Bertrand et al., 2014). The FGFR signaling was shown to have essential roles in the Cnidarians *Nematostella vectensis* and *Hydra vulgaris*: In *Nematostella*, it is required for the development of the apical organ in the larvae, in gastrulation and neurogenesis (Matus et al., 2007; Rentzsch et al., 2008) and in *Hydra* the FGFR signaling was found to be critical for the detachment of the vegetative bud (Hasse et al., 2014; Holz et al., 2017; Sudhop et al., 2004).

In *Hydra*, two canonical FGFRs and one FGFR-like1 molecules are known (Rudolf et al., 2013; Sudhop et al., 2004; Suryawanshi et al., 2020). At least one of the two canonical receptors, FGFRa (Kringelchen), is crucial for the detachment of the bud by controlling boundary formation and tissue constriction in the late stages of the bud (Hasse et al., 2014; Holz et al., 2017; Sudhop et al., 2004). For the other receptors, FGFRb (Rudolf et al., 2013; Suryawanshi et al., 2020) and FGFR-like1, less is known so far. FGFR-like1 is supposed to function as a decoy receptor (Lange, 2016). The described FGFR structure in vertebrates differs in the *Hydra* FGFRa, as the acidic box is rather an acidic region than clustered and the Ig loop III is not clamped by cysteines but by two hydrophobic amino acids (Sudhop et al., 2004).

The *Hydra* docking apparatus is hypothesized as quite complex (Suryawanshi et al., 2020). The transcription patterns of the vertebrate specific docking protein Frs2 as well as the *Drosophila*-specific docking protein Dof were not correlated with that of the

FGFRs and it remains unclear, whether the *Hydra* FGFR signaling requires either of those docking proteins. Nevertheless, the downstream components Grb2, Crkl, Sos and Shp2/Csw are all upregulated, just like the two canonical FGFRs, at the late bud base suggesting their requirement for the downstream signaling cascade of FGFR.

Former work has identified potential FGFR ligands in *Hydra* (referred to as FGFa, FGFc, FGFe and FGFf) which were categorized into the known FGF groups or identified as close relatives (Lange et al., 2014). Proposed functions of FGFs in *Hydra* include roles in cell guidance and/or differentiation, as the gene expression was located at boundaries and terminal structures, e.g. at the tentacle bases and tentacle tips. The tentacle base just like the bud base is a zone of actively migrating interstitial cells and additionally a zone of terminal differentiation of nemato- and neuroblasts as well as epitheliomuscle cells (Aufschnaiter et al., 2011; Boehm & Bosch, 2012; David, 2012). Other groups reported FGF expression in the ectoderm of the budding region, concluding a possible role in interstitial stem cell maintenance (Krishnapati & Ghaskadbi, 2013). Although many components of the FGFR signaling in *Hydra* are known, the precise functions and interactions have yet to be described, especially the role and function of different FGFs during budding and regeneration of *Hydra*.

1.4 RNA interference as a tool for gene analysis

To get insight into the functions of a specific gene it is a common strategy to silence the gene, mRNA, or protein. Several techniques are used to induce the knockdown of a gene of interest. An efficient RNA-induced mechanism of silencing a gene by degrading its mRNA is the RNA interfence (RNAi). RNAi is a mechanism of naturally occurring post-transcriptional gene silencing (PTGS) and is a biological response to dsRNA viruses (Agrawal et al., 2003; Hannon, 2002). PTSG occurs in many species in the plant and animal kingdoms and is involved in biological processes regarding the protection against transposons and viruses (Agrawal et al., 2003; Cogoni & Macino, 2000). RNAi is based on virus-induced gene silencing (VIGS) in plants, where it plays an important role in pathogen resistance (Baulcombe, 1999; Hamilton & Baulcombe, 1999). The gene transcription is unaffected, and the gene silencing is mediated by translational inhibition and degradation of a specific mRNA (Siomi & Siomi, 2009). Endogenous RNAi triggers include foreign DNA or dsRNA (from viruses or transposons) and pre-microRNA (miRNA). The RNAi pathway is found in many eukaryotes but was first described in *Caenorhabditis elegans* (Fire et al., 1998; Hannon, 2002). The gene specific

RNAi mechanism offers manifold applications: Given its easy application, efficiency and specificity, RNAi is used as a common experimental tool for gene silencing (Agrawal et al., 2003). Furthermore, RNAi has potential applications as a therapeutic reagent because it can downregulate expression patterns of mutant genes in diseased cells.

1.4.1 The RNAi pathway

Basically, the RNAi mechanism is based on two processes, each involving ribonuclease enzyme activity (fig. 1.8). Introduction of trigger RNA (dsRNA of any kind or miRNA primary transcript) causes the RNA-induced silencing complex (RISC), the assembly of a nuclease complex that marks homologous mRNA for degradation (Hannon, 2002). In the first step, the RNAi pathway is started by the activation of Dicer and Drosha, members of the RNase III ribonuclease family (Bernstein et al., 2001; Siomi & Siomi, 2009). Drosha prepares miRNA for further processing in the RNAi pathway and Dicer specifically cleaves dsRNA into the small interfering RNA (siRNA) – small fragments of approximately 22 nucleotides (Bernstein et al., 2001; Siomi & Siomi, 2009; Vermeulen et al., 2005; Zamore et al., 2000). In the next step, the siRNA strands are separated into single stranded RNA (ssRNA), the so-called passenger and the guide strands where the passenger strand is degraded (Gregory et al., 2005) and the guide strand incorporates into the RISC and guides the complex towards the target mRNA (Kobayashi & Tomari, 2016; Siomi & Siomi, 2009). RNase H enzymes of the Argonaute protein family act as catalytic units of the RISC and induce cleavage of the target mRNA strand complementary to the loaded ssRNA (Kupferschmidt, 2013; Pratt & MacRae, 2009). The RNAi signal can be amplified by RNA-dependent RNA polymerase (RdRp) that converts a few exogenously encountered siRNAs into an abundant internal siRNA pool (Pak et al., 2012). A recycling of siRNAs is mediated by the destabilization of the RISC, creating a re-accessibility of the bound siRNA (Li & Rana, 2012). Exogenous triggers of the RNAi mechanism are mediated either by chemically synthesized siRNA or vector-based small hairpin RNA (shRNA) (Rao et al., 2009). Gene silencing efficiency induced by siRNA duplexes depends on parameters like length, secondary structure, sugar backbone and sequence specificity (Agrawal et al., 2003; Elbashir et al., 2001). Introduction of shRNAs can be accomplished exogenously or by transcription from RNA polymerase III promotors on a plasmid construct in vivo (after genome integration), permitting a stable and heritable gene knockdown (Miyagishi & Taira, 2002; Paddison et al., 2002; Yu et al., 2002). Opposing to siRNAs, shRNAs are synthesized in the cell nucleus and are further processed for incorporation into the cytoplasmic RISC (Cullen, 2005; Rao et al., 2009).

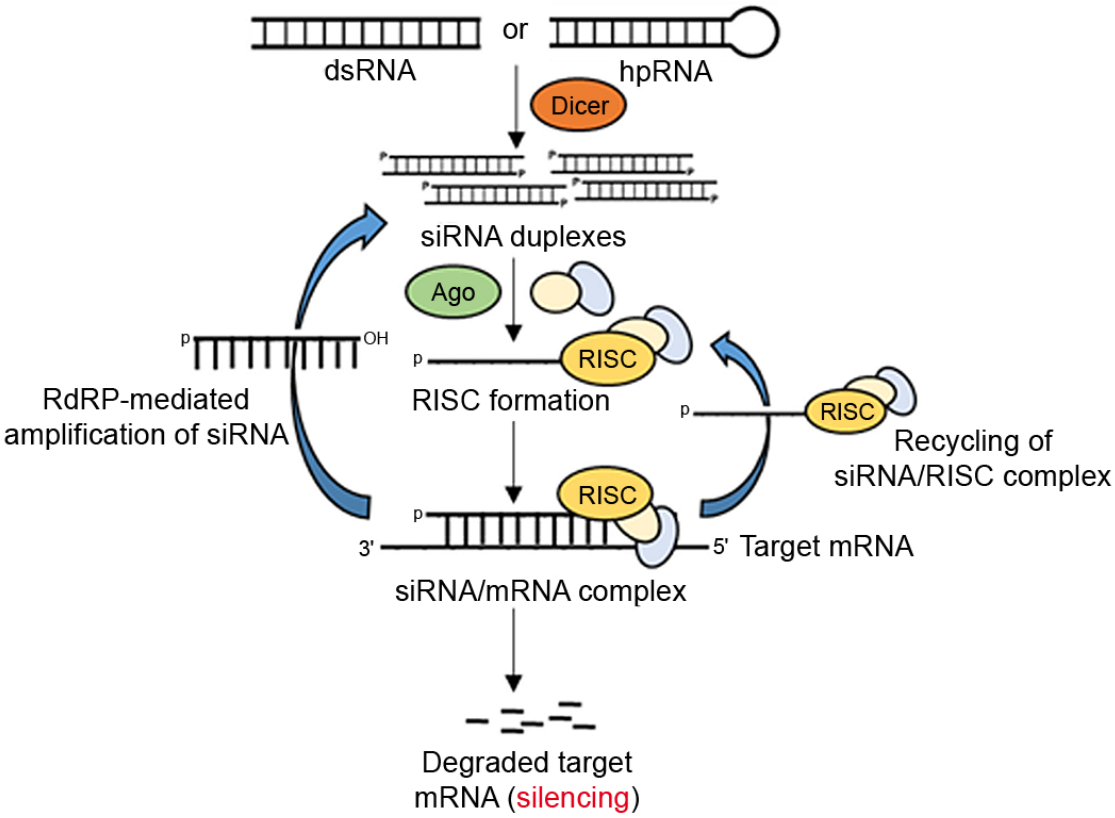

Figure 1.8: Basic scheme of the RNAi pathway. Double stranded RNAs (dsRNA) or hairpin RNAs (hpRNA) trigger the RNAi mechanism. Dicer (orange) processes the triggers into small hairpin RNAs (siRNA) of a specific length. siRNA initiates the formation of the RNA-induced silencing complex (RISC) which then binds the complementary target mRNA, thus resulting in the degradation of the mRNA and silencing the gene. Components of the pathway can be recycled (right side) or siRNA duplexes multiplied by RNA-dependent RNA polymerase (RdRp). (Majumdar et al., 2017).

1.4.2 RNAi in *Hydra*

Mechanisms of PTSG type were described in *Hydra* (Cogoni & Macino, 2000). Components of the RNAi mechanism are partially present in *Hydra* like the host-encoded RdRp which is used for the amplification of siRNAs from viral sequences. One homologue of the systemic *RNAi defective 1 (SID-1)* gene from *C. elegans* was detected (Obbard et al., 2009), which is thought to act as a passive channel for siRNAs from cell-to-cell (Feinberg & Hunter, 2003; Shih & Hunter, 2011). In *Hydra* two Dicer proteins were identified which are important for recognition and processing of dsRNA (Obbard et al., 2009). Furthermore, RNAi effects triggered by siRNA have been demonstrated in *Hydra* and the electroporation of transgenic *Hydra* with siRNA specific for GFP successfully silenced GFP in the various cell lineages carrying the transgene (Lohmann et al., 1999; Lommel et al., 2017). RNAi-mediated silencing of the transcription factor Forkhead-box protein O3 (FoxO) using shRNA vector constructs gave insight into aging and homeostasis of the metaorganism *Hydra* (Boehm et al., 2012; Mortzfeld et al., 2018).

1.5 Aim of the project

Our group identified several FGFs in *Hydra* (Lange et al., 2014) that were grouped in or near the known FGF families (fig. A.1). Despite not yet being characterized in detail, results from first transcription studies suggest potential functions in cell migration and/or differentiation. The main goal of this project was to further investigate and elucidate functions of different *Hydra* FGFs.

1. Transcriptional patterns are interesting to analyze to learn about a proteins potential function. Therefore, the potential functions of FGFs during the budding process in *Hydra* were investigated by analyzing the transcription of the FGFs *FGFa*, *FGFb*, *FGFc*, *FGFe* and *FGFf* in single *in situ* hybridization. As previous studies investigated the transcription only in *Hydra vulgaris* AEP, which phylogenetically differs from *Hydra vulgaris* Zürich and *Hydra magnipapillata* wt105 (Martínez et al., 2010; Schwentner & Bosch, 2015), the previous transcriptional data was extended and FGFs also investigated in different *Hydra* strains to identify interspecies FGF functions.

2. Previous studies found, that both FGFRs in *Hydra* are upregulated at the late bud base during the detachment of the bud (Sudhop et al., 2004; Suryawanshi et al., 2020). To analyze whether both FGF receptors are upregulated in the same cell

populations, a double ISH was performed. Further double *in situ* analysis should answer the question whether *FGFb* and *FGFf* are also co-transcribed with the receptors to further identify potential FGF ligands for both receptors.

3. The transcriptional analysis gives a good first impression of a protein's putative functions. However, only a specific antibody is able to localize the protein and gives more information. A *Hydra*-specific antibody for FGFf was further analyzed in budding animals to investigate the potential function of FGFf.

4. FGFf was found to be a FGF8 homologue (Lange et al., 2014). As FGF8 is also an important factor during regenerative processes in vertebrates, the analysis of the FGFf transcript and protein patterns during the regeneration of head and foot in bisected *Hydra* polyps should answer the question, whether FGFf is important for the *Hydra* regeneration. This allows conclusions regarding the evolutionary conservation of this FGF during regeneration.

5. To further identify the functions of FGFRs and FGFs in the bud detachment of *Hydra*, the effects of a siRNA mediated knockdown by square-pule electroporation were investigated. Further, the siRNA mediated knockdown was used to identify which FGFRs and FGFs have potential functions in cell proliferation and cell differentiation by analyzing macerated *Hydra* tissues.

2 Results

This chapter summarizes the results of experiments investigating potential functions of FGFs and FGFRs in *Hydra*. The transcriptional patterns obtained by single and double *in situ* hybridization will give first insights into potential functions of FGFs during the budding process. Additionally, the protein distribution of FGFf, a FGF8 homologue (Lange et al., 2014), was investigated during the budding process to compare transcriptional and protein patterns, thereby gaining more understanding into the potential function(s) of FGFf in *Hydra*. As FGF8 is also an important factor during regeneration, the transcriptional and protein expression of FGFf was further analysed during the head and foot regeneration in *Hydra*. A siRNA mediated knockdown for FGFRs and FGFs was investigated regarding the effect on the bud detachment, on the transcriptional level and during cell differentiation.

2.1 Analysis of the FGF transcript distribution in *Hydra*

FGFs play important roles during different developmental processes like differentiation, migration proliferation and regeneration (Ornitz & Itoh, 2015). To get a first insight into potential functions of FGFs in *Hydra*, the previous transcriptional analysis data (Lange et al., 2014) was repeated and extended.

2.1.1 The *FGFa* gene was expressed ectodermally in the peduncle

FGFa was identified to be a member of the intracrine working FGF 11–14 group (Lange et al., 2014). In *Hydra vulgaris* AEP the transcription of *FGFa* showed a weak ubiquitous pattern in the whole body (fig. 2.1). In tissue overlays at the tentacle base (fig. 2.1 A, B) and the bud base (fig. 2.1 E) this ubiquitous expression appeared like a transcriptional pattern. The *FGFa* transcription was instead only upregulated ectodermally in the peduncle of the adult polyp (fig. 2.1 A–F) and during the detachment phase in the tissue that will become

the peduncle in the bud (fig. 2.1 F). In *Hydra vulgaris* Zürich, these patterns were similar and an example for the transcription in the bud's peduncle during the detachment phase is given (fig. 2.1 G).

The *FGFa* transcription in the peduncle was found in all investigated *Hydra* strains. Whether a transcriptional upregulation in tentacles and at the bud base is due to tissue overlay must be further investigated.

2.1.2 *FGFb* was transcribed endodermally in the tentacles, buds and around the foot pore

FGFb was categorized into the FGF1/2 group (Lange, 2016), but the transcriptional pattern was yet not investigated. In adult *Hydra vulgaris* AEP, the *FGFb* transcript was detected endodermally in the tentacles (fig. 2.2 C') and in cells surrounding the foot pore (fig. 2.2 H"'). The sense probe did not yield a signal (fig. 2.2 A). In the early budding stages 1–2, *FGFb* was not upregulated in the thickened ectoderm (fig. 2.2 C). Beginning with budding stage 3, the *FGFb* transcript was upregulated endodermally in the emerging bud tip (fig. 2.2 D, E). In addition, the *FGFb* transcription was upregulated also ectodermally in the bud tip (fig. 2.2 D, D'). In the further elongation phase of the budding process *FGFb* was not transcribed in the bud tissue (not shown). The *FGFb* transcription was again upregulated when adult structures started to form: In evaginating tentacles of the bud *FGFb* was upregulated endodermally (fig. 2.2 F, G). During the detachment phase, *FGFb* was upregulated in endodermal cells surrounding the foot pore of the bud therewith resembling the adult pattern (fig. 2.2 H–H"). After the detachment of the bud, small patches of *FGFb*-positive tissue persisted in the adult polyp (fig. 2.2 H, H').

The adult transcription pattern of *FGFb* in the tentacle endoderm and the endodermal cells around the foot pore was also found in animals of the *Hydra vulgaris* Zürich strain (fig. 2.3). In developing testes, the *FGFb* transcription was not upregulated (fig. 2.3 A). In the early budding process (stages 1–4) the *FGFb* transcript was not upregulated (not shown). In budding stage 5 the *FGFb* transcription was upregulated endodermally in a ring of cells at the bud base and in patches of cells within the prospective tentacle region prior to the formation of tentacles (fig. 2.3 B). In contrast, early sprouting tentacles showed no or only a very weak *FGFb* expression (fig. 2.3 C) which increased once the tentacles started to elongate, particularly in the tentacle tips (fig. 2.3 D, D'). In the early forming foot of the bud, *FGFb* was upregulated endodermally (fig. 2.3 E, E'). After the detachment, the *FGFb* transcript was again upregulated in the endodermal cells that

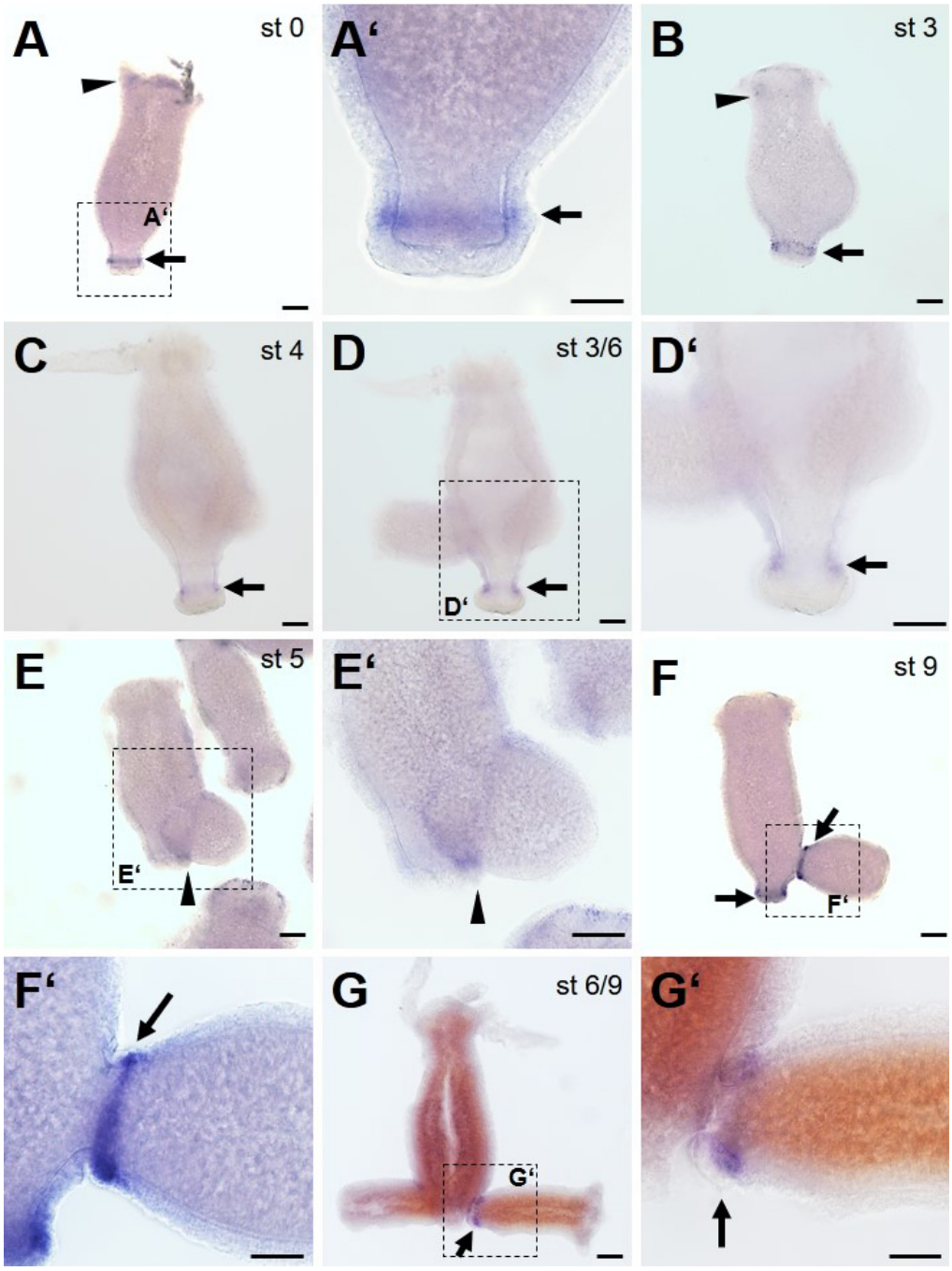

Figure 2.1: Transcription of *FGFa* in *Hydra vulgaris*. (A–F) Different budding stages of *Hydra* AEP. (G) *Hydra vulgaris* Zürich. A weak ubiquitous staining in the whole tissue was detectable in all stages. (A–F) *FGFa* was upregulated ectodermally in the peduncle. (A) In budless animals *FGFa* was transcribed at the peduncle above the foot in ectodermal cells. (B–D) *FGFa* was not upregulated during the evagination and elongation phase. (F, G) During the detachment phase *FGFa* was transcribed ectodermally in the bud's peduncle. Black arrows: expression in the peduncle. Black arrowheads: tissue overlay. Scale bars: (A–G, D', E') 100 µm (A', F', G') 50 µm.

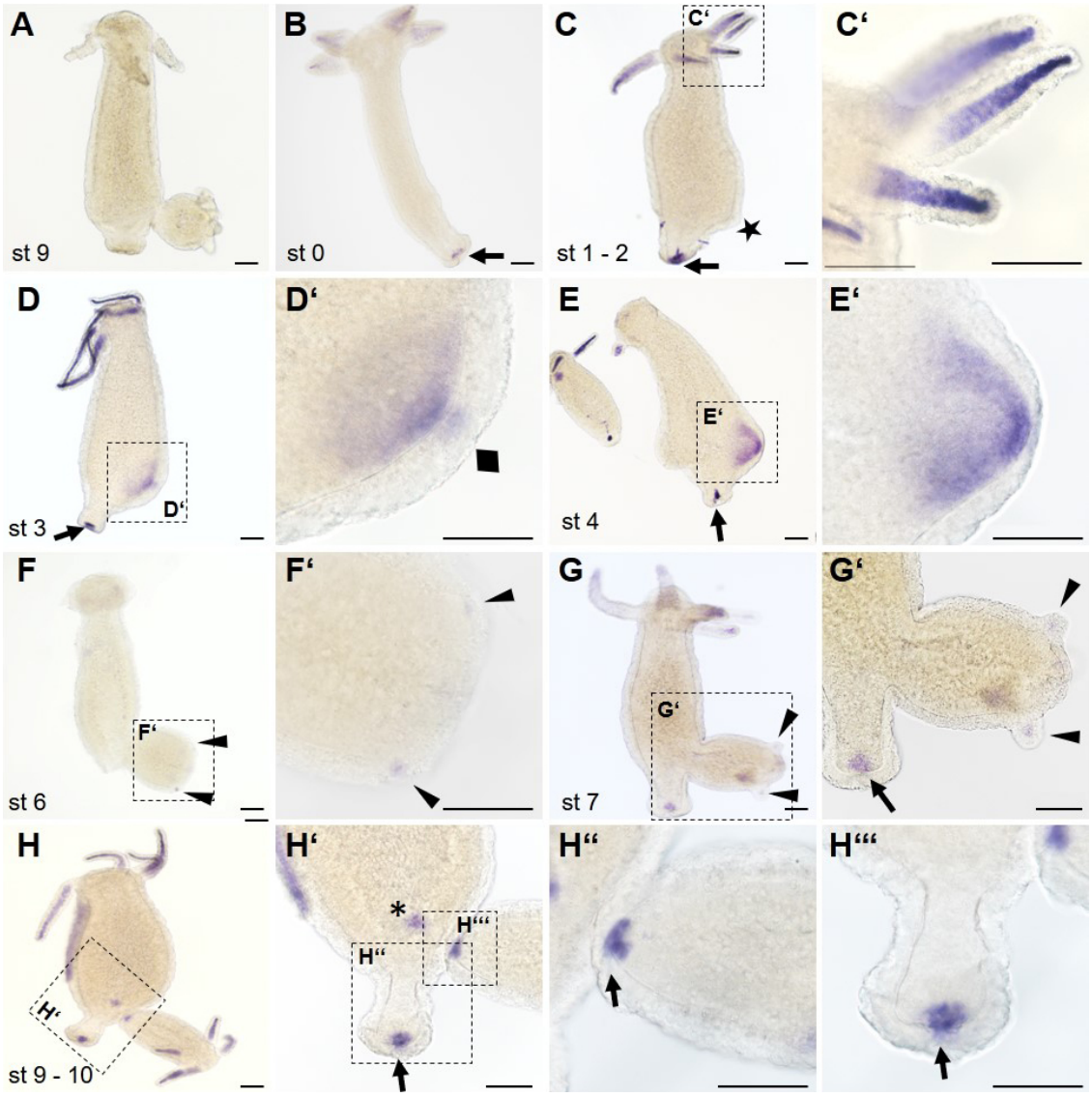

Figure 2.2: Transcription of *FGFb* in *Hydra vulgaris*. (A) *in situ* hybridization with the sense probe yielded no signal. (B) In non-budding animals *FGFb* was transcribed in tentacles and cells surrounding the foot pore (black arrow). This staining was detectable independent of the budding stage. (C) In stages 1-2 *FGFb* was not transcribed in the bud placode (black star) (C') Magnification of (C) shows the endodermal location in the tentacles. (D, E, stage 3-4) During the evagination phase, *FGFb* was upregulated endodermally at the bud tip. (D') *FGFb* was also transcribed ectodermally in the bud tip (black diamond) (F, G, stage 6-7) Beginning with tentacle evagination, *FGFb* was transcribed in the developing tentacles (black arrowheads). Animal in (F) is missing tentacles and foot. (H, H") In the detachment phase after formation of the bud's foot *FGFb* was upregulated in cells around the foot pore. (H') Small patches of *FGFb*-positive cells remained after bud detachment in the adult polyp (black asterisk). (H"') Endodermal transcription of *FGFb* in cells around the foot pore. Scale bars 100 µm.

surround the foot pore (fig. 2.3 F'). Therewith the adult pattern of *FGFb* was reached. A ring of ectodermal *FGFb*-positive cells persisted in the adult polyp after the detachment of the bud (fig. 2.3 F, F').

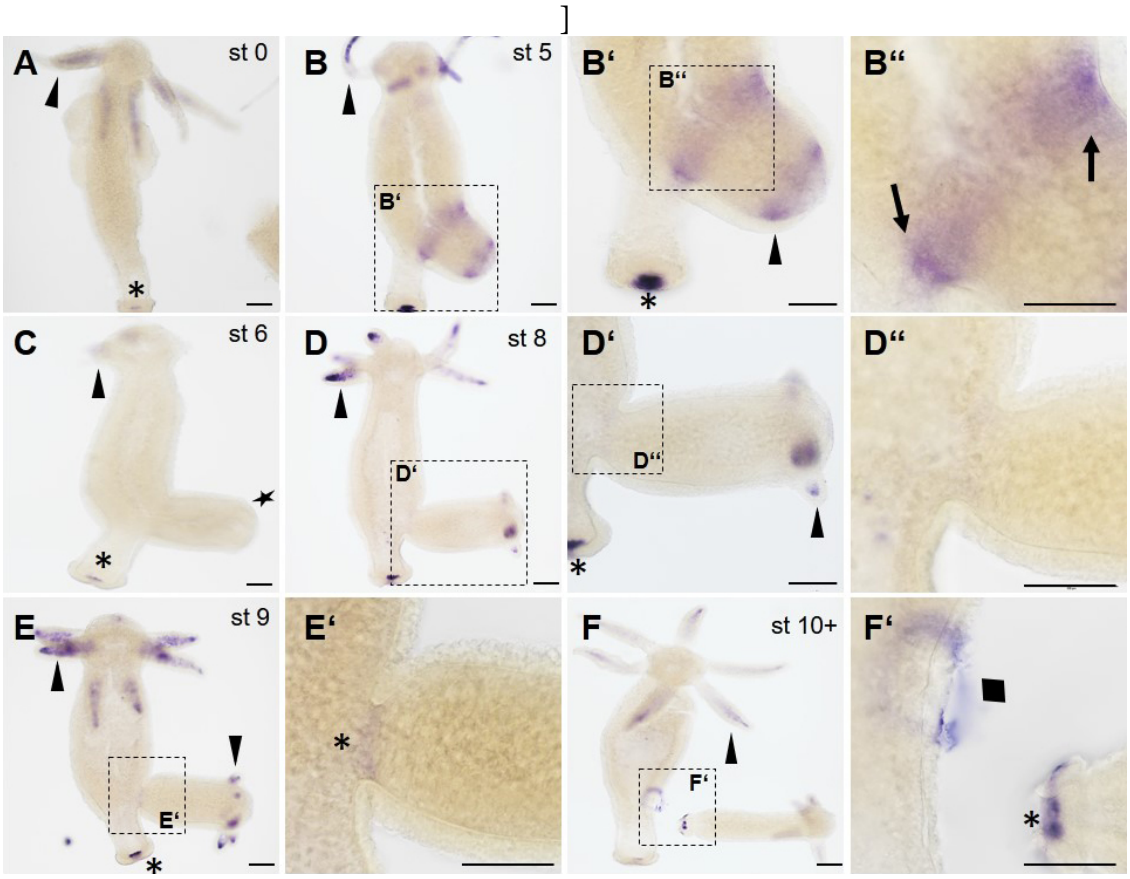

Figure 2.3: Transcription of *FGFb* in *Hydra vulgaris* Zürich. (A) Non-budding animal that transcribed *FGFb* in tentacles (black arrowhead) and foot (black asterisk), only. No *FGFb* was detected in developing testes. (B) In stage 5, *FGFb* was upregulated in an endodermal ring at the bud base (black arrows) and in patches within the prospective tentacle zone. (C) In early tentacle buds *FGFb* was not upregulated (black star). (D) During early tentacle evagination *FGFb* was transcribed in tentacle buds. (E) *FGFb* transcription was upregulated in the elongating tentacles and during foot formation in the bud. (H) After detachment, *FGFb* persisted as a ring of cells in the parent polyp (black diamond) and in the foot endoderm of the bud. Scale bars 100 µm.

The *FGFb* transcription was further analysed in animals of the *Hydra magnipapillata* wt105 strain (fig. 2.4). The endodermal transcription of *FGFb* in the tentacles and around the foot pore was upregulated during all budding stages. During the early budding stages (stage 1–3), *FGFb* was not transcribed (fig. 2.4 B). During further development of the bud, *FGFb* was upregulated at its tip in stage 4 and 5 (fig. 2.4 C', E'). *FGFb* transcription was upregulated in newly forming tentacles of the bud, but not the bud base (fig. 2.4 D, E).

In the late detachment phase, *FGFb* transcription was upregulated again in the foot endoderm of the bud in endodermal cells surrounding the foot pore (fig. 2.4 E, E”).

]

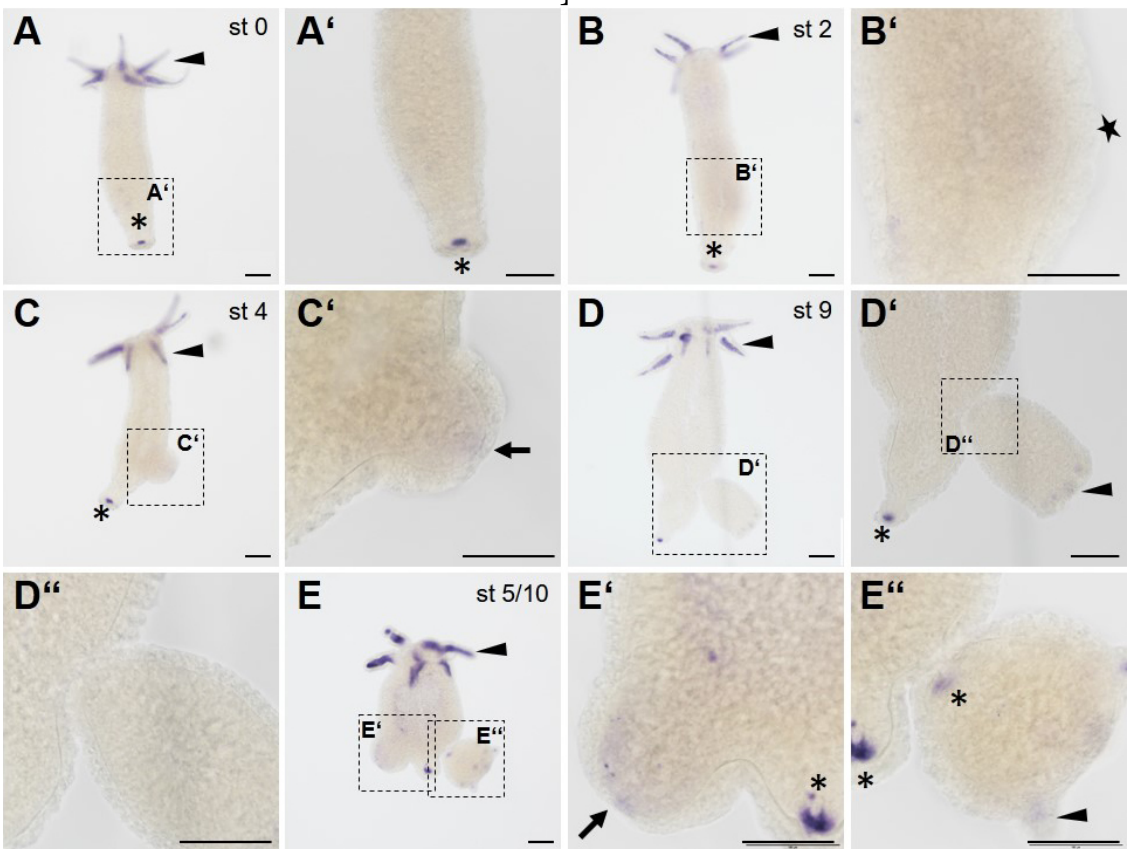

Figure 2.4: Transcription of *FGFb* in *Hydra magnipapillata* wt105. (A) Non-budding animals transcribed *FGFb* in tentacle endoderm (black arrowhead) and endodermal cells around the foot pore (black asterisk). (B) In early budding *FGFb* was not transcribed (black star). (C, C’, E’) During the elongation phase, *FGFb* was upregulated weakly at the endodermal tip of the bud (black arrow). (D) *FGFb* transcription was upregulated during the development of the new tentacles (black arrowhead). (D”) *FGFb* transcription was not upregulated at the bud base (E) Prior to detachment *FGFb* was upregulated in endodermal cells surrounding the foot pore in the bud. Scale bars 100 µm.

The endodermal *FGFb* transcription in tentacles and endodermal cells around the foot pore was found in *Hydra* of all observed strains, proposing a conserved function throughout different *Hydra* strains in these tissues. The additional *FGFb* upregulation during the early evagination phase in the *Hydra vulgaris* AEP strain and the upregulation at the bud base during the elongation phase in *Hydra vulgaris* Zürich must be further investigated.

2.1.3 The *FGFc* gene was expressed in a half-ring below the tentacle base and in the basal disc

FGFc is a member of the FGF1/2 family (Lange et al., 2014), and its gene expression pattern in selected bud stages of *Hydra vulgaris* AEP is shown in figure 2.5. In adult polyps and late bud stages, the *FGFc* transcription was upregulated ectodermally in a half-ring immediately below the tentacle base and in ectodermal cells in the basal disc (fig. 2.5 A-C). The transcription of *FGFc* was detected weakly along the whole body and found to be upregulated in the lower budding zone of the parent and in the basal disc endoderm of the animals (fig. 2.5 C). During budding, *FGFc* was first detected in the developing tentacle buds (stage 5 - 6) (fig. 2.5 A, B). During the detachment phase, the adult *FGFc* pattern (below the tentacles and in the basal disc) was detectable also in the bud (fig. 2.5 C). A weak *FGFc* transcription was upregulated at the apical rim of further developed testes (fig. 2.5 B).

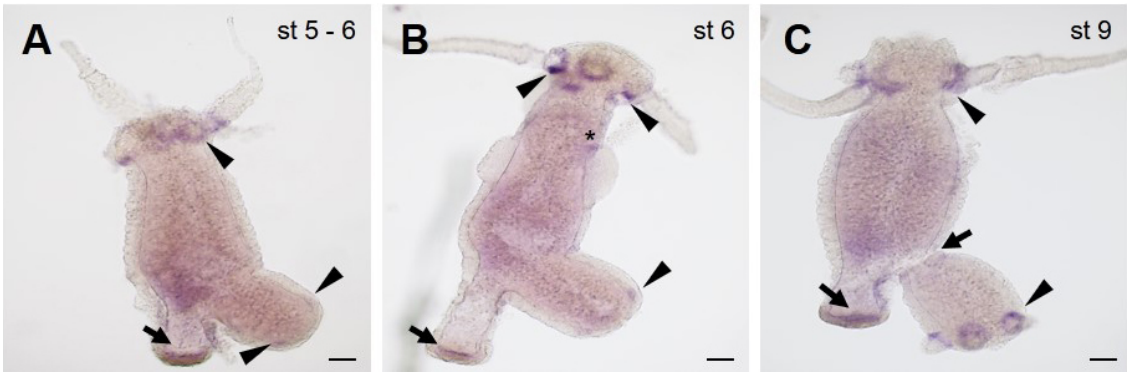

Figure 2.5: Transcription of *FGFc* in *Hydra vulgaris* AEP. (A–C) Half-ring transcription of *FGFc* below the tentacle base (black arrowhead) and weak expression in the basal disc (black arrow). (A) In early bud development, *FGFc* was not transcribed above the parent's level in the bud. (B–C) *FGFc* transcription started with the evagination of the bud tentacles (black arrowhead). (B) During testis development *FGFc* was upregulated at the upper testes-base (black asterisk). (C) During the detachment phase *FGFc* transcription was upregulated in the developing basal disc of the bud (black arrows). Scale bars 100 µm.

2.1.4 *FGFe* was transcribed in the peduncle and at the mouth opening

FGFe is a member of the FGF1/2 family (Lange et al., 2014), and its gene expression pattern in *Hydra vulgaris* AEP is shown in figure 2.6. Animals showed a ubiquitous transcription of *FGFe* along the body axis (fig. 2.6 A). The *FGFe* mRNA was upregulated

ectodermally in the peduncle (fig. 2.6 A - D). During the elongation phase of budding, from stage 4 onwards, *FGFe* transcription was upregulated at the mouth opening at the tip of the bud (fig. 2.6 C, C', D, D"). During the detachment phase of budding, *FGFe* was transcribed ectodermally at the bud base (fig. 2.6 D, D', D"') in cells of the prospective peduncle. The *FGFe* transcription was shown to be mainly upregulated in the peduncle of adult polyps and in the bud. Other *Hydra* strains were not investigated.

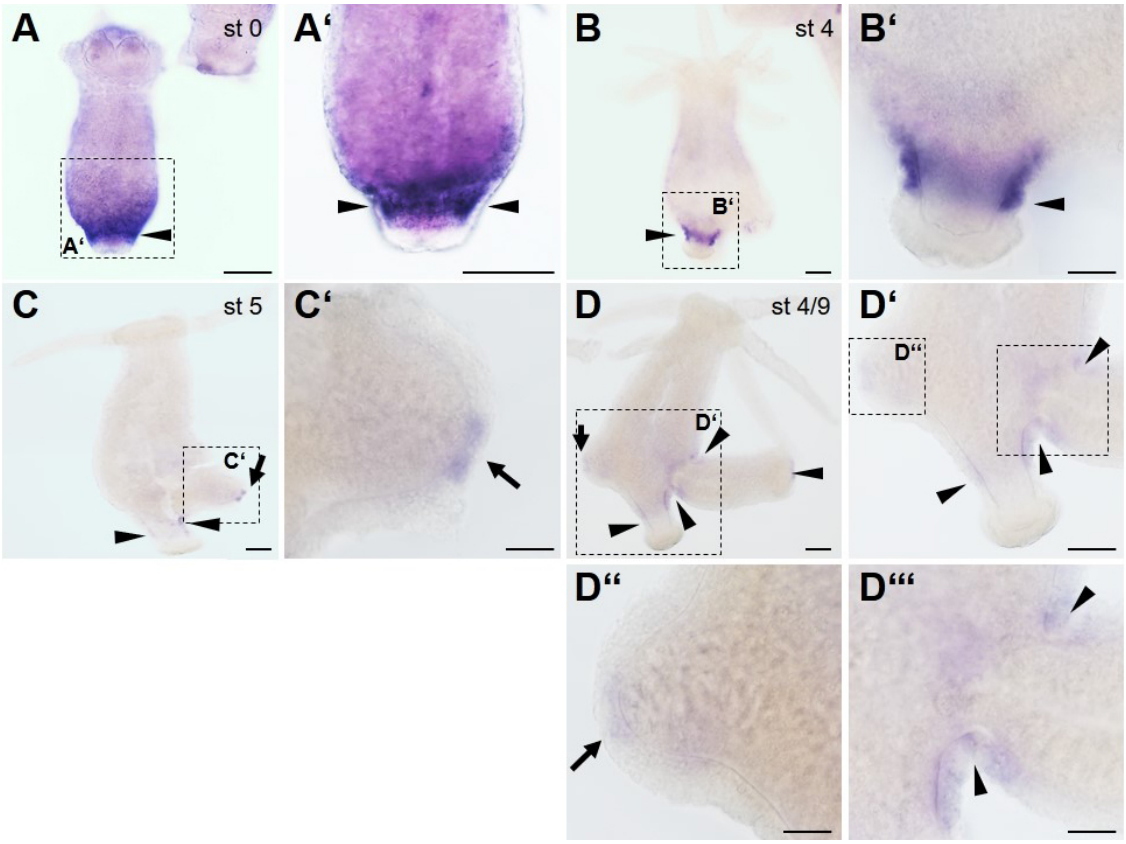

Figure 2.6: Transcription of *FGFe* in *Hydra vulgaris* AEP. (A–D) *FGFe* was upregulated ectodermally in the peduncle (black arrowhead). (C, D) During budding, the *FGFe* transcription was first located at the bud tip in the forming mouth (black arrow). (D) In further developed buds, *FGFe* was localized ectodermally at the bud's prospective peduncle. Scale bars: (A - D, D') 100 µm, (A', B', C', D", D"') 50 µm.

2.1.5 *FGFf* was transcribed dynamically during budding

The dynamic expression pattern of *FGFf* in the transition zone of body-bud and body-tentacle tissue and at all body termini has already been published (Lange et al., 2014). As a basis for further detailed investigations, its analysis was repeated here. Like for the

other FGFs, the *FGFf* gene expression was monitored in different *Hydra* strains with a focus on the budding process.

During the early evagination phase (stage 2) the *FGFf* transcription was upregulated in a few ectodermal cells in the developing bud of *Hydra vulgaris* AEP (fig. 2.7 A). In stage 3 an intense transcription at the bud's tip was detected endodermally with an additional intense zone in the prospective bud mouth ectoderm (fig. 2.7 B, B'). In stage 4, *FGFf* was upregulated in the zone of prospective tentacle evagination and the bud's mouth (fig. 2.7 C, C'). The transcriptional upregulation of *FGFf* in the evaginating tentacles and the bud mouth was also detectable in budding stage 5 (fig. 2.7 D, D", E, E"). The five evenly spaced patches of *FGFf* gene expression indicate clearly distinguishable tentacle buds (fig. 2.7 E, E'). Beginning in stage 5, *FGFf* was additionally upregulated at the bud base, first endodermally (fig. 2.7 D, D') and later ectodermally (fig. 2.7 F, G). In the late detachment phase (stage 9–10), the *FGFf* transcription had narrowed down to the peduncle region and resembled the adult circular peduncle expression pattern (fig. 2.7 F, G', G"). The adult *FGFf* transcription in the tentacle tip was endodermal (fig. 2.7 D"'). The *FGFf* transcription was upregulated at the testes base of male *Hydra* polyps (fig. 2.7 H, H'). At the same time, the transcription in foot, mouth and tentacle tips was downregulated.

The expression pattern of *FGFf* in the *Hydra vulgaris* Zürich strain resembled mostly the expression pattern described for the *Hydra vulgaris* AEP strain (fig. 2.8). Overall, the detected transcription was more intense and often found in more cells. During all budding stages, the *FGFf* gene was upregulated endodermally in the peduncle and in the tentacle tips (fig. 2.8 A–N). In the early bud evagination at stage 1, the *FGFf* gene expression was not upregulated in the bud (fig. 2.8 A). In stage 2, *FGFf* was upregulated in the endodermal bud placode (fig. 2.8 B). With the emerging bud in stage 3, the *FGFf* transcript was upregulated endodermally in the whole bud tissue with strong ectodermal accumulation as a cap at the tip (fig. 2.8 C, C'). During further evagination steps, this throughout bud-expression and the strong expression in the tip persisted (fig. 2.8 C–E). Beginning in stage 6 with formation of the tentacle buds, the *FGFf* gene expression in the bud tissue faded (fig. 2.8 F). Simultaneously, the *FGFf* transcription in the prospective tentacle buds was upregulated ectodermally (fig. 2.8 D–G). With further tentacle outgrowth, the expression shifted towards the tentacle base first (fig. 2.8 I–L), until it was only visible in the tentacle tip endoderm (fig. 2.8 M, N). From stage 6 onwards *FGFf* was first upregulated endodermally circular at the bud base (fig. 2.8 G, G'). With further elongation of the bud, the *FGFf* transcription in a ring at the bud base was switched to an ectodermal expression (fig. 2.8 H–M). This ectodermal

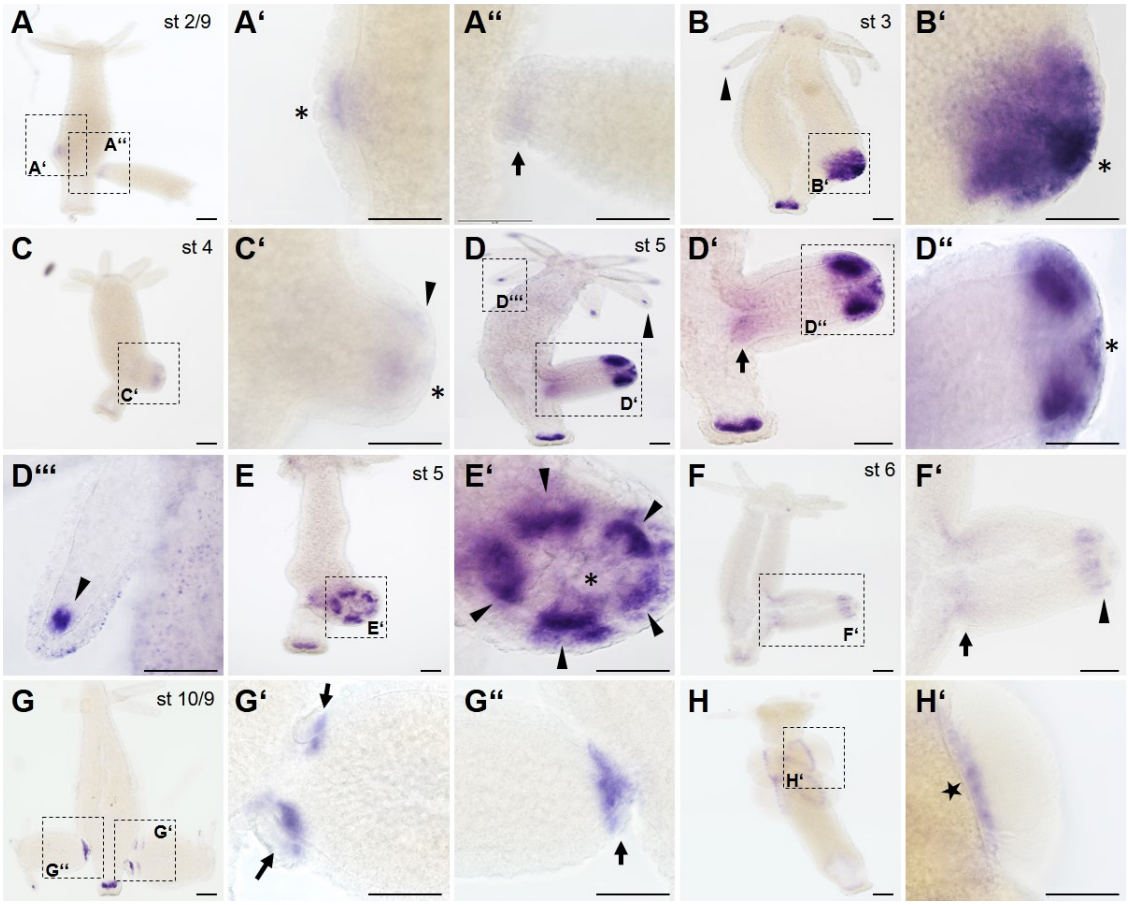

Figure 2.7: Transcription of *FGFf* in *Hydra vulgaris* AEP. (A–G) *FGFf* was upregulated in tentacle tips, foot and hypostome. Animals were from different experimental setups and thus the staining intensity varies. (A) In stage 1-2 *FGFf* was upregulated in the developing bud placode (black asterisk). (B) In stage 3 a strong accumulation of the *FGFf* gene in the bud tip ectoderm and endoderm was detectable. (C - E) Prior to tentacle evagination and during early tentacle elongation *FGFf* was upregulated in the zone of tentacle evagination and bud mouth. (D”’) Close-up of the endodermal *FGFf* transcription in the tentacle tip. (D, F) Beginning in budding stage 5, *FGFf* transcription was upregulated endodermally at the bud base. (G) FGFf was upregulated in the ectoderm at the prospective peduncle of the bud during the detachment phase. (H) Male *Hydra* polyp with developed testes. *FGFf* was transcribed at the base of the testes. Scale bars 100 µm.

circular gene expression pattern intensified during the bud elongation until the start of the constriction formation during the detachment phase (fig. 2.8 M). In stage 9, the *FGFf* transcript persisted only in a few ectodermal cells at the bud's basal disc (fig. 2.8 M, N). Concomitant, the *FGFf* transcript was also upregulated endodermally in the bud's peduncle (fig. 2.8 N, N'), herewith resembling the endodermal gene expression pattern in the adult peduncle (fig. 2.8 A–N).

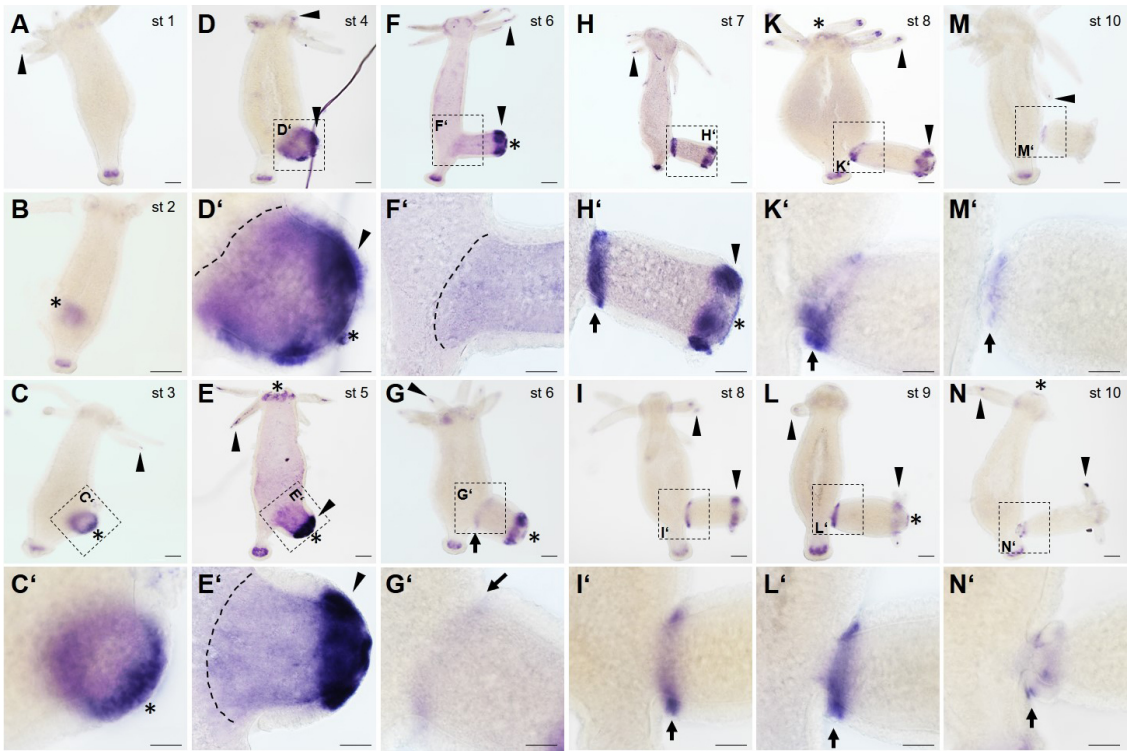

Figure 2.8: Transcription of the *FGFf* in *Hydra vulgaris* Zürich. During all budding stages, the *FGFf* gene was expressed endodermally in the tentacle tips (black arrowheads) and in the peduncle. (A) No transcription was found in stage 1 buds. (B) In early evaginating buds *FGFf* was transcribed endodermally (black asterisk). (C–F) *FGFf* was transcribed in the whole bud endoderm. (C–E) *FGFf* accumulated as an ectodermal cap at the bud tip (black asterisk). (D–H) The ectodermal cap resolved and *FGFf* was transcribed strongly in the prospective tentacle buds (black arrowheads). (G) The *FGFf* transcript was upregulated endodermally at the bud base (black arrow). (I–L) *FGFf* was transcribed ectodermally at the tentacle base (black arrow). (M, N) Endodermal upregulation of *FGFf* in the tentacle tip of the bud. (G–L) In the bud base, *FGFf* was upregulated in an ectodermal ring at the bud base. (M, N) Prior to detachment, the *FGFf* transcript localized in the bud's peduncle and basal disc (black arrows). Scale bars 50 µm.

The *FGFf* gene expression in *Hydra magnipapillata* wt105 was monitored in adult tentacle tips, mouth opening and peduncle (fig. 2.9 A–E). In early bud stages (stage 1–2) the *FGFf* transcript was localized in a patch of cells in the ectoderm of the budding zone (fig. 2.9 D, E). In further development of the bud, the *FGFf* expression intensified first at

the tip of the bud in stage 2 (fig. 2.9 D, D') and then in the whole bud in stage 3 (fig. 2.9 A, A'). With ongoing bud development, the *FGFf* gene expression zone became restricted to the zone of tentacle development, and the expression later switched to the tentacle tips only (fig. 2.9 B–E). During these budding stages, the *FGFf* transcription was also upregulated at the developing bud's mouth opening (fig. 2.8 A', B', E'). In the detachment phase the *FGFf* transcription was upregulated ectodermally at the bud base (fig. 2.9 D, D", E, E', E"). The transcription at the bud base became stronger with further outgrowth of the bud and reached the maximum shortly before detachment. *FGFf* therewith was transcribed in an ectodermal ring at the site of the bud (fig. 2.9 H).

The main transcriptional patterns of *FGFf* were comparable in the investigated *Hydra* strains, concluding a conserved function for *FGFf* in *Hydra*. Variations were especially in the intensity of the transcriptional upregulation.

Spatiotemporal expression patterns of genes provide insights into possible functions during morphogenesis. Three of the five FGFs were investigated in different *Hydra* strains. The specific gene expression patterns stayed generally the same in the different strains. No obvious changes in the typical transcription patterns occurred, but only in their intensity, suggesting that the FGF sequences are conserved at least in all observed *Hydra* strains. This leads to the assumption that they possibly comprise the same functions in different *Hydra* strains. The gene expression analysis of the five different FGFs in *Hydra* is summarized in fig. 2.10. The typical transcription pattern of each FGF during the initiation phase, the elongation phase, and the detachment phase are schematically shown. After the analyzation of the single FGF transcriptional patterns, *FGFb* and *FGFf* were further analyzed in a double-ISH to answer the question, if they are transcribed in the same cells as one of the *Hydra* FGFRs or not.

2.1.6 *FGFRa* and *FGFRb* were co-localized from stage 4 onward in cells of the bud base

Both known FGFRs in *Hydra* are found at the late bud base. A double-ISH was performed to analyze whether *FGFRa* and *FGFRb* are transcribed in the same or different cell populations (fig. 2.11). During elongation phase of the bud the transcriptional upregulation of *FGFRa* and *FGFRb* was detected (fig. 2.11 A, A'). Both transcripts were upregulated in a ring of single, scattered ectodermal cells at the bud base. During the detachment phase, the transcription of *FGFRa* (fig. 2.11 C, C') and *FGFRb* (fig. 2.11 D, D') is upregulated in an ectodermal ring at the bud base. In the double-ISH this ring of *FGFRa* and

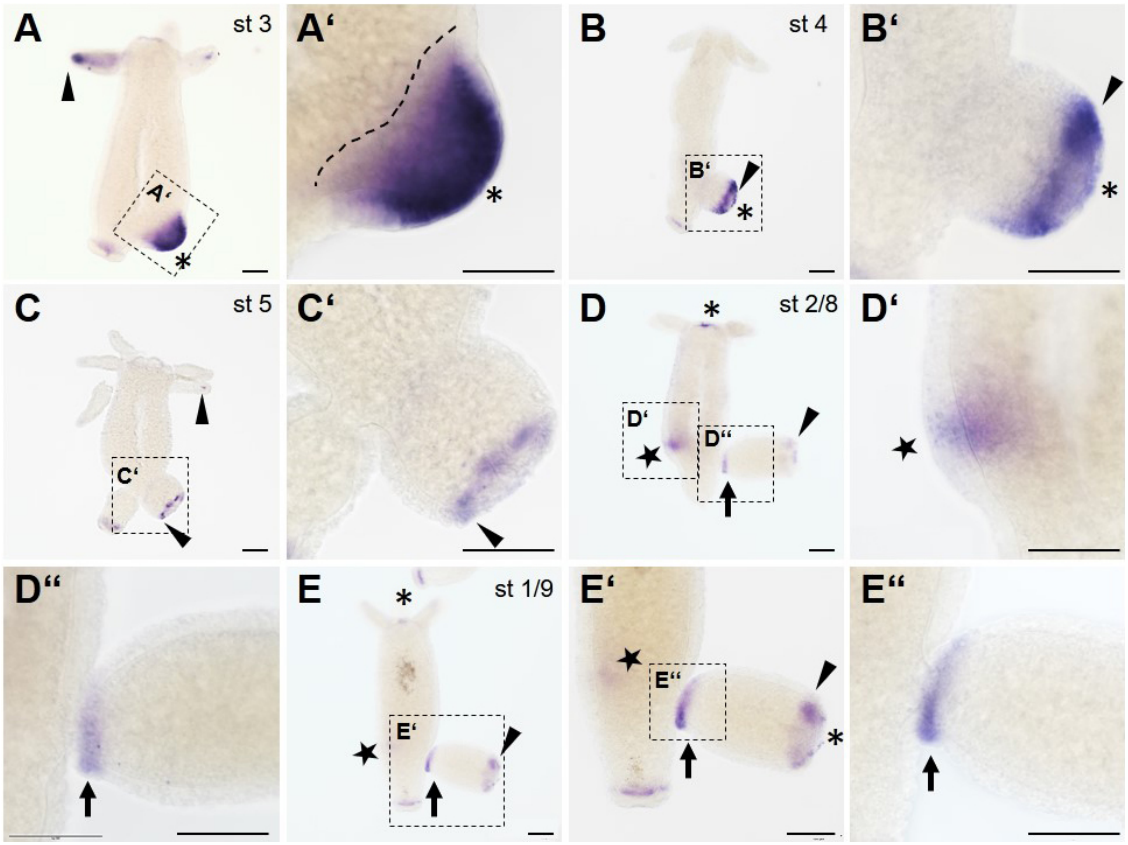

Figure 2.9: Transcription of *FGFf* in *Hydra magnipapillata* wt105. (A–E) The *FGFf* transcript was found in tentacle tips (black arrowheads), peduncle, and mouth opening (black asterisk). (A) In stage 3, *FGFf* was upregulated endodermally in the bud and ectodermally in the bud's tip (black asterisk). (B) In stage 4 *FGFf* was transcribed in the zone of prospective tentacle evagination an in the bud's mouth. (C) In stage 5 *FGFf* was upregulated endodermally in evaginating tentacles. (D, E) During the detachment phase, the *FGFf* gene was transcribed in an ectodermal ring at the bud base (black arrows). Additionally, the transcription at the tentacle buds was still detectable and switched to an adult transcription pattern in fully developed tentacles. (D, D') In stage 2, an ectodermal and endodermal *FGFf* gene expression was observed in the bud placode (black star). (E, E') In the early budding stage 1, *FGFf* transcription was already detectable in a few ectodermal cells in the budding zone (black star). Scale bars 100 µm.

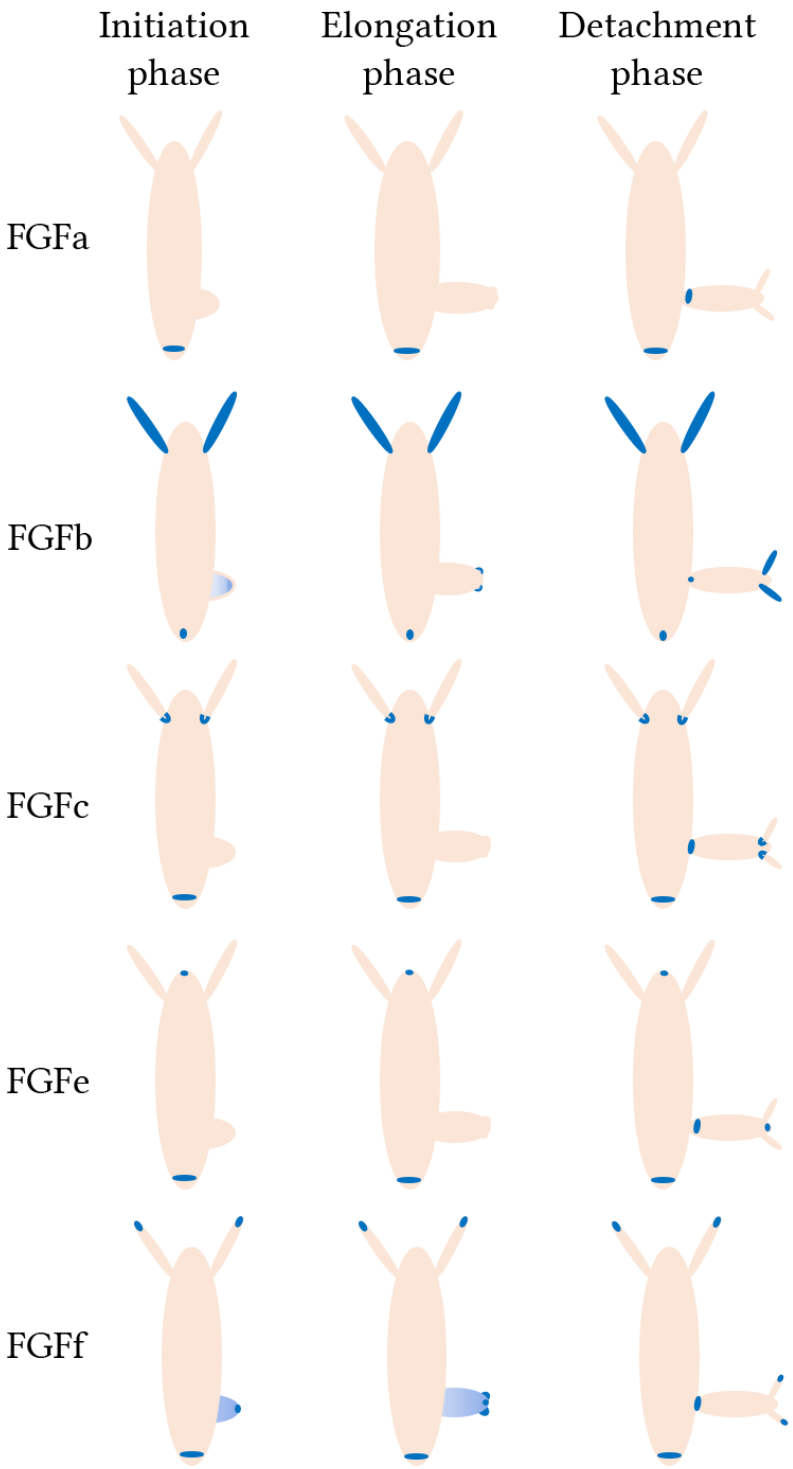

Figure 2.10: Scheme of FGF transcription patterns in *Hydra*. The characteristically *in situ* hybridization transcription patterns for the five different FGFs described above in initiation, elongation and detachment phase are schematically summarized.

FGFRb-positive cells had substantially contracted concomitant with the normal tissue constriction (fig. 2.11 B, B'). Both genes remained co-expressed as indicated by the violet color.

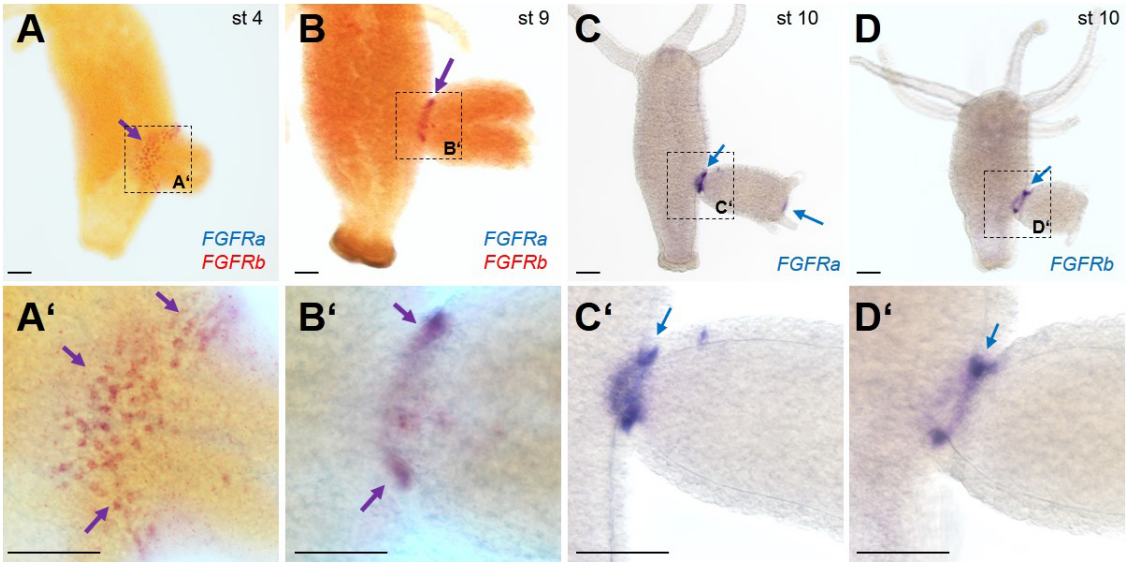

Figure 2.11: *FGFRb* and *FGFRa* transcripts in a double-ISH. (A) During elongation of the bud, *FGFRa* and *FGFRb* were co-localized in ectodermal cells at the bud base (violet arrows). (B) In the detachment phase, both, *FGFRa* and *FGFRb* formed a ring at the bud base. Co-transcription is indicated by violet color. (C) During detachment phase the *FGFRa* and (D) *FGFRb* transcripts were upregulated in an ectodermal ring at the bud base (blue arrows). Scale bars 100 µm.

2.1.7 *FGFb* and *FGFf* transcripts were excluded from cells carrying *FGFR* transcripts

FGFb and *FGFf* both belong to paracrine FGF groups (Lange, 2016) and paracrine FGFs function locally trough activation of neighboring cells via a process called diffusion (Itoh et al., 2016). The diffusion area of paracrine FGFs is regulated by HSPGs and the receptors. Assuming that FGFb and/or FGFf interact with one of the *Hydra* FGFRs their diffusion areas are potentially restricted as first indicated by the transcriptional patterns. To answer the question, whether *FGFb* or *FGFf* transcripts are co-localized with either of the FGFRs a double-ISH was performed.

At first, the spatiotemporal transcription pattern of *FGFb* was compared to that of *FGFRa* during the bud detachment phase (fig. 2.12 A–C). *FGFRa* is typically transcribed in an ectodermal ring of cells at the bud base (Sudhop et al., 2004), a pattern that was well reproduced here (fig. 2.12 A, A'). This expression pattern accompanies constriction until

the bud detaches. The ring of cells, therefore, contracts with further bud development (fig. 2.12 B, B'). The *FGFRa* transcript persisted even following bud detachment in the parent for 1 - 2 hours in a small ring of cells (fig. 2.12 C, C'). The *FGFb* transcription was upregulated at the bud base in endodermal cells of the prospective peduncle in the same cells as *FGFRa* (fig. 2.12 A, A'). During further bud development, *FGFb*, in contrast to *FGFRa*, was transcribed in endodermal cells surrounding the bud's foot pore; *FGFRa* on the other hand was expressed in cells of the adult polyp (fig. 2.12 B'). After the bud's detachment, *FGFb* was upregulated in cells that persisted in the adult polyp (fig. 2.12 C').

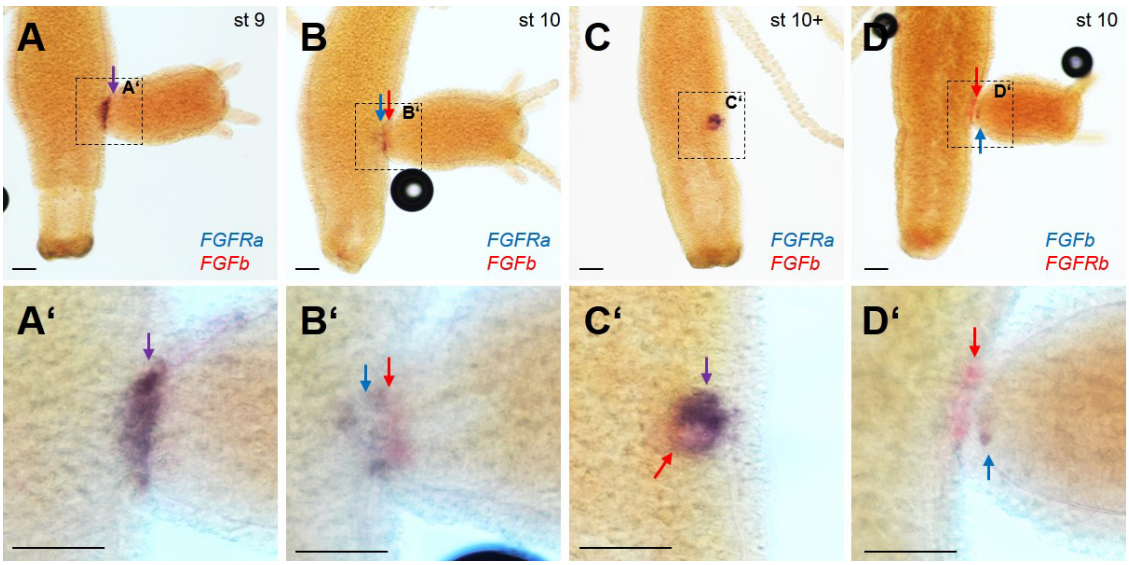

Figure 2.12: *FGFRb* and *FGFRa* transcripts in comparison to *FGFb* in a double-ISH. (A–C) Comparison of *FGFRa* and *FGFb* transcripts. (D) Comparison of *FGFRb* and *FGFb* transcripts. (A, B) *FGFRa* was upregulated in an ectodermal ring of cells close to the bud base. (A) *FGFb* was upregulated in the same cells as *FGFRa* (violet arrow). (B) *FGFb* was upregulated in endodermal cells around the foot pore in the bud (red arrow), whereas *FGFRa* was transcribed in the adult tissue (blue arrow). (C) After detachment, a small *FGFRa*-positive ring of cells persisted in the adult polyp (red arrow). *FGFb* is partially co-transcribed with *FGFRa* (violet arrow). (D) *FGFRb* persisted in the adult polyp during detachment (red arrow), *FGFb* in cells surrounding the foot pore of the bud (blue arrow). Co-transcription is indicated by violet color. Scale bars 100 µm.

The analysis of the gene expression pattern of *FGFRb* and *FGFb* showed that in the detachment phase, the *FGFb* transcription was upregulated in endodermal cells surrounding the foot pore of the bud (fig. 2.12 D'). The *FGFRb* transcription on the other hand was upregulated in ectodermal cells of the adult polyp immediately adjacent to the bud's basal disc. No co-expression of the *FGFb* and the *FGFRb* gene was detectable. This is comparable to the pattern in fig. 2.12 B'.

The analysis of a potential *FGFRa* and *FGFf* co-expression failed to show cells transcribing both, the receptor and the *FGFf* (fig. 2.13 A - C). As always, *FGFRa* positive cells were localized in the adult polyp whereas *FGFf* positive cells were located in the bud tissue (fig. 2.13 A', B', C'). Again, in the detaching bud both expression patterns could be described as an ectodermal ring at the bud base (fig. 2.13 A–C). After the formation of the bud's basal disc, *FGFRa* was detected in a small patch of ectodermal cells in the adult polyp (fig. 2.13 C). In this stage, *FGFf* was clearly located in the endoderm of the bud's peduncle.

Comparing *FGFRb* and *FGFf* gene expression patterns, no co-localization was found (fig. 2.13 D - F). During the elongation phase of the budding process, the *FGFf* transcript was upregulated at the bud's tip in developing mouth end tentacle tissue as described in single ISH (fig. 2.13, D'). In this budding stage, *FGFRb* transcription was upregulated in an ectodermal ring at the bud base (fig. 2.13 D'). Prior to the formation of the bud's basal disc, the *FGFRb* and *FGFf* transcription were upregulated ectodermally in a ring at the bud base with no co-transcription (fig. 2.13, E. E'). After the formation of the bud's basal disc the *FGFf* transcription was upregulated in the endoderm of the peduncle whereas the *FGFRb* transcription pattern persisted in ectodermal cells at the tissue bridge connecting both polyps (fig. 2.13 F, F').

2.2 Analysis of the FGFf protein distribution in *Hydra*

Transcript patterns are interesting to analyze to learn about a protein's potential function. However, only a specific antibody is able to localize the protein in the tissue. A specific antibody against the *Hydra* FGFf was tested on a western blot for several *Hydra* strains (fig. 2.14). To further identify the cells expressing the FGFf protein, the antibody was used for immunodetection in different budding stages in whole animals. The protein pattern after pharmacological inhibition of FGFR with SU5402 was further investigated.

2.2.1 A *Hydra*-specific antibody detects FGFf in different *Hydra* strains

To test the constructed FGFf antibody in different *Hydra* strains, a western blot analysis was performed. Previous work already investigated the binding of the two polyclonal peptide-antibodies for FGFf, but only in the *Hydra vulgaris* AEP strain (Lange, 2016). Due to an animal shortage in the AEP strain during my studies, this western blot analysis

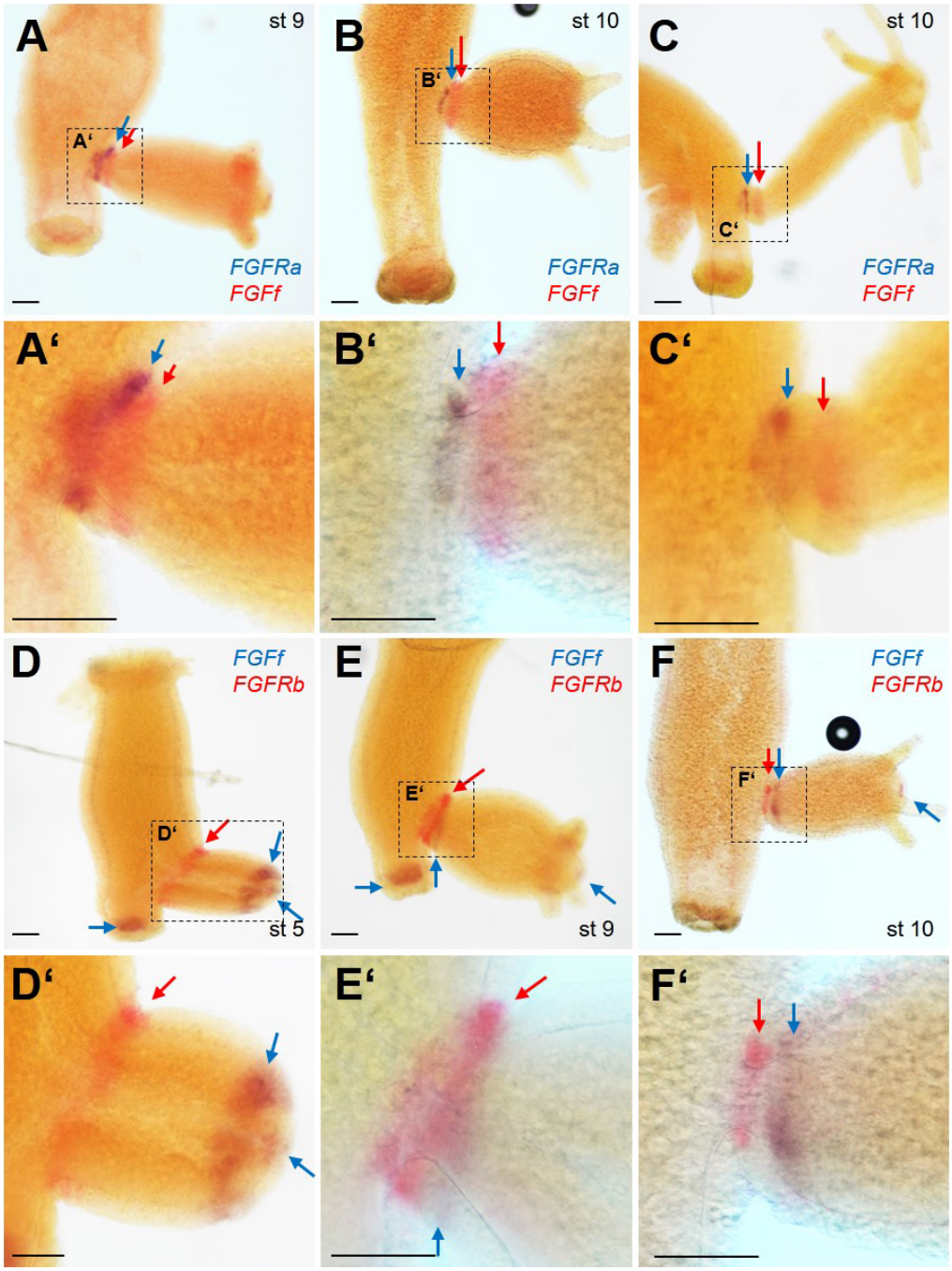

Figure 2.13: *FGFRb* and *FGFRa* transcripts in comparison to *FGFf* in a double-ISH. (A, B) *FGFRa* and *FGFf* were upregulated in ectodermal rings at the bud base. (C) *FGFf* was transcribed in the endoderm of the bud's peduncle. The *FGFRa* transcription persisted at the site of the adult polyp. (D - F) The *FGFRb* transcription was upregulated in an ectodermal ring of cells at the bud base. (A) *FGFf* was transcribed in evaginating tentacle buds (E) *FGFf* was upregulated in ectodermal cells at the bud base. (F) *FGFf* was transcribed in the endoderm of the bud's peduncle. The *FGFRb* transcription persisted at the site of the adult polyp. Co-transcription is indicated by violet color. Scale bars 100 µm.

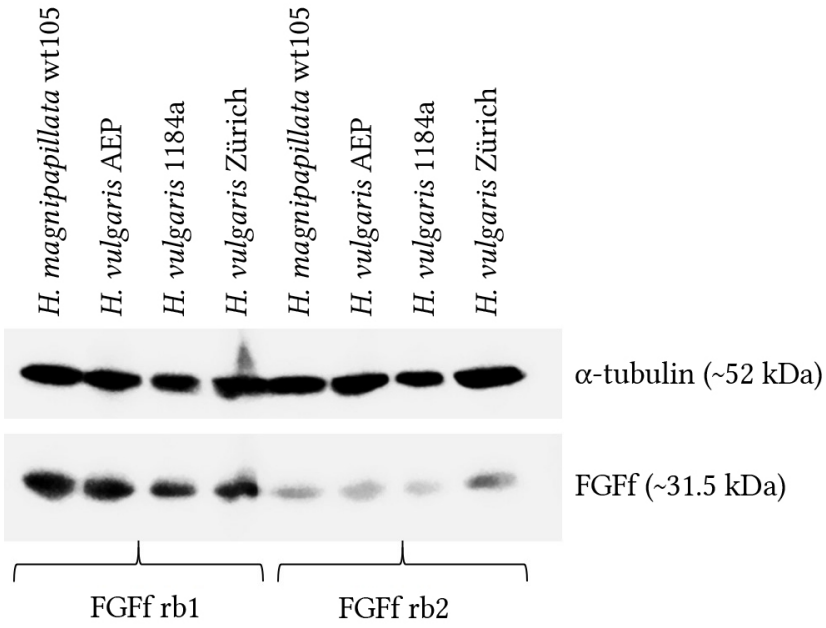

Figure 2.14: Western blot analysis of custom-made, affinity-purified polyclonal antibodies against *Hydra* FGFf peptides. Different *Hydra* strains are indicated on top. Upper row showed protein levels of α-tubulin as internal loading control. Lower row showed the protein bands detected with α-FGFf of rabbit 1 (left) and rabbit 2 (right). Both antibodies detected the FGFf protein in all investigated *Hydra* strains.

was repeated in addition with the *Hydra vulgaris* Zürich, *Hydra vulgaris* 1184a and *Hydra magnipapillata* wt105 strain, to identify whether the antibodies are able to bind the FGFf protein independent of the *Hydra* strain. As an internal loading control in the western blot, an α-tubulin antibody was used, which was detected at the expected 52 kDa (fig. 2.14). FGFf rb1 (polyclonal antibody from rabbit 1, 1:500) and FGFf rb2 (polyclonal antibody from rabbit 2, 1:500) were both able to detect the FGFf protein in all *Hydra* strains in the expected size of 31.5 kDa (fig. 2.14). Quantification of the FGFf antibodies revealed no obvious differences between the analyzed *Hydra* strains (table A.1). Interestingly, in all strains the FGFf rb2 antibody did detect less FGFf protein compared to the FGFf rb1 (about 25–50 % of rb1 intensity, table S1), but the difference was lowest in *Hydra vulgaris* Zürich. As a result of that, further experiments were performed using the FGFf antibody FGFf produced in rb1.

2.2.2 FGFf showed a dynamic pattern during bud development

A previous study gave first insights into the FGFf protein distribution in *Hydra vulgaris* AEP (Lange, 2016). Due to a shortage in AEP animals, the FGFf protein distribution during the budding process in this study was investigated using the *Hydra vulgaris* Zürich strain. When investigating animals that were potentially starting to form a bud (bud stage 0–1), the FGFf protein was upregulated in a patch of ectodermal cells in the budding zone (fig. 2.15 A, B). In the early budding stages 3 and 4, the FGFf protein was upregulated at the tip of the bud (fig. 2.15 C - E) and in single cells throughout the bud tissue (fig. 2.15 D, E). Beginning with budding stage 5, the FGFf protein was localized in the zone of the prospective tentacle evagination (fig. 2.15 F, G) with an accumulation in the putative evaginating tentacle buds. With further elongation of the tentacles the FGFf protein staining intensified and was detectable in the whole tentacle tissue (fig. 2.15 H–J). The FGFf protein distribution in the bud's tissue during the elongation phase was further examined in figure 2.16. During the elongation phase of the bud, the FGFf protein was expressed partially in single cells and patches in the bud (fig. 2.15 H, J) or evenly distributed in the whole bud tissue (fig. 2.15 G). With the beginning constriction at the bud base, a narrow ectodermal expression of FGFf established in a ring of cells right at the bud base (fig. 2.15 K). This ectodermal protein expression at the bud base was further examined in figure 2.17. Shortly before the final detachment, FGFf was expressed only at the foot structures of the bud, including basal disc and peduncle (fig. 2.15 L). During the whole budding process, the FGFf protein was detected in patches at the body column (fig. 2.15, D, E, I, J), but also in single cells throughout the body (fig. 2.15, H).

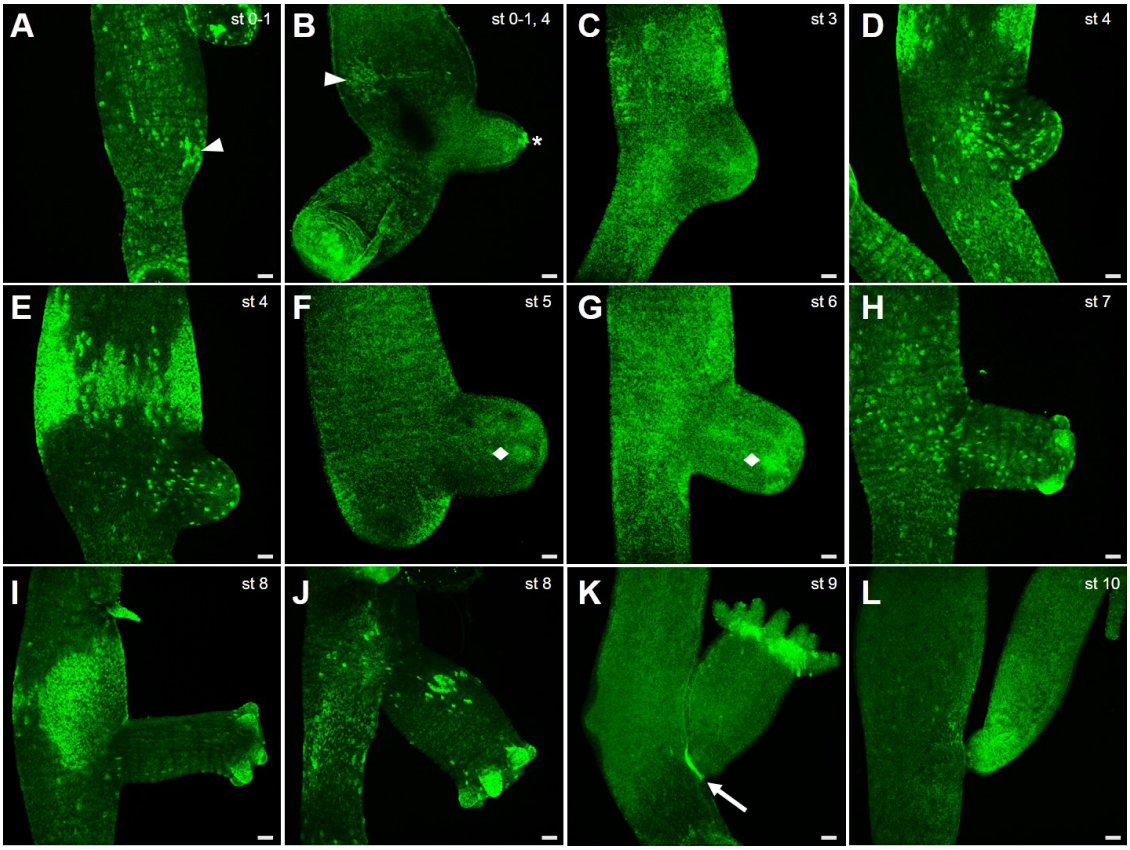

Figure 2.15: Immunodetection of the FGFf protein during budding. FGFf was upregulated in the body column during all budding stages. Patches or single cells were detectable in the whole body. (A, B) A small patch of cells was FGFf positive in the budding zone (white arrowheads). (B - E) During early evagination FGFf positive cells were distributed in the newly developing bud. (B) In stage 4 an accumulation of the FGFf protein in the bud tip was detected (white asterisk). (F, G) The FGFf protein was expressed in newly forming tentacles (white diamonds). (H–K) The staining in the tentacles intensified with further outgrowth. (K, L) During the detachment phase FGFf accumulated ectodermally at the bud base and persisted in the foot of the bud. (E, I) Patches of strong FGFf expression were detectable in some animals. Images were taken as cLSM stack and processed as maximal projection. Scale bars 100 µm.

The distribution of the FGFf protein in the elongating bud tissue was further investigated (fig. 2.16). With beginning of the tentacle evagination in stage 4 and 5, FGFf expression was strongly upregulated in the prospective tentacle buds (fig. 2.16 A). Also, during the further evagination and elongation of the tentacles, the FGFf protein was localized in the tentacle tissue (fig. 2.16 C–E). During the elongation of the bud, the FGFf protein was expressed strongly in the bud tissue, whereas the staining in the adult polyp remained weak (fig. 2.16 B–F). During the detachment phase, the intense expression of the FGFf protein in the bud persisted. Additionally, the expression increased ectodermally at the bud's prospective basal disc (fig. 2.16 E, F).

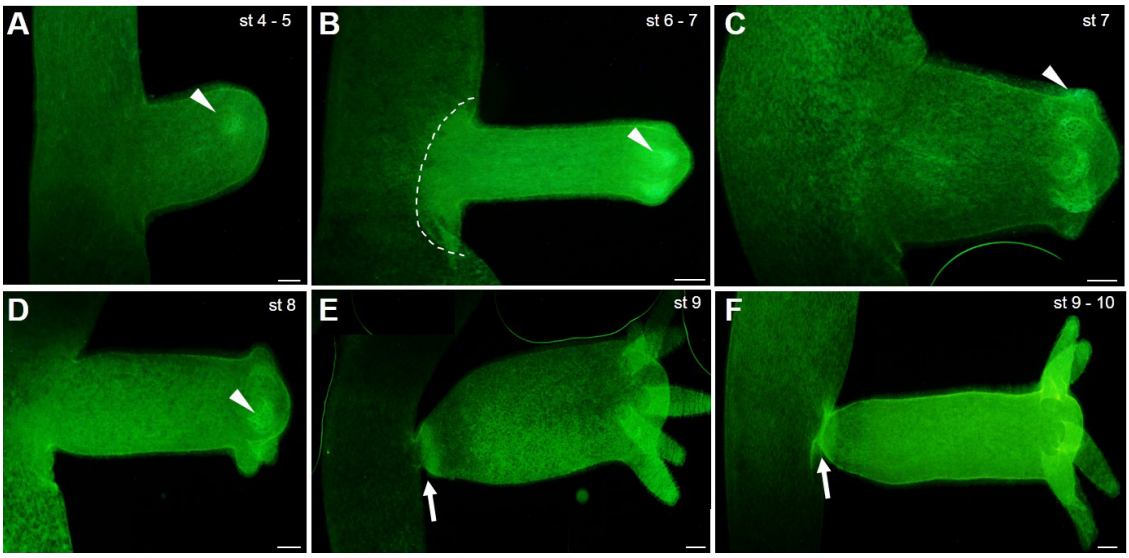

Figure 2.16: Immunodetection of FGFf during budding. (A) FGFf was expressed in tentacle buds (white arrowhead). (B - F) FGFf was strongly expressed in the bud tissue, but not as strong as in the adult polyp. (B–F) Accumulation of FGFf in the bud's tentacle. (E, F) The FGFf protein was expressed at the bud base prior to the detachment of the bud (white arrow). Scale bar 100 µm.

2.2.3 FGFf accumulated ectodermally at the bud base

The expression of FGFf at the late bud base was further investigated using a confocal laser scan microscope (cLSM) (fig. 2.17). Single layers of a cLSM stack showed the distribution of the FGFf protein in the detachment zone.

In early evaginating buds (stage 2–3), the FGFf protein expression was not yet upregulated (fig. 2.17 A). In the detachment phase, the FGFf protein accumulated in cells at the bud base (fig. 2.17 A). At a closer look, this expression at the bud base was localized in single rows of ectodermal cells in the adult polyp, in the tissue bridge connecting both

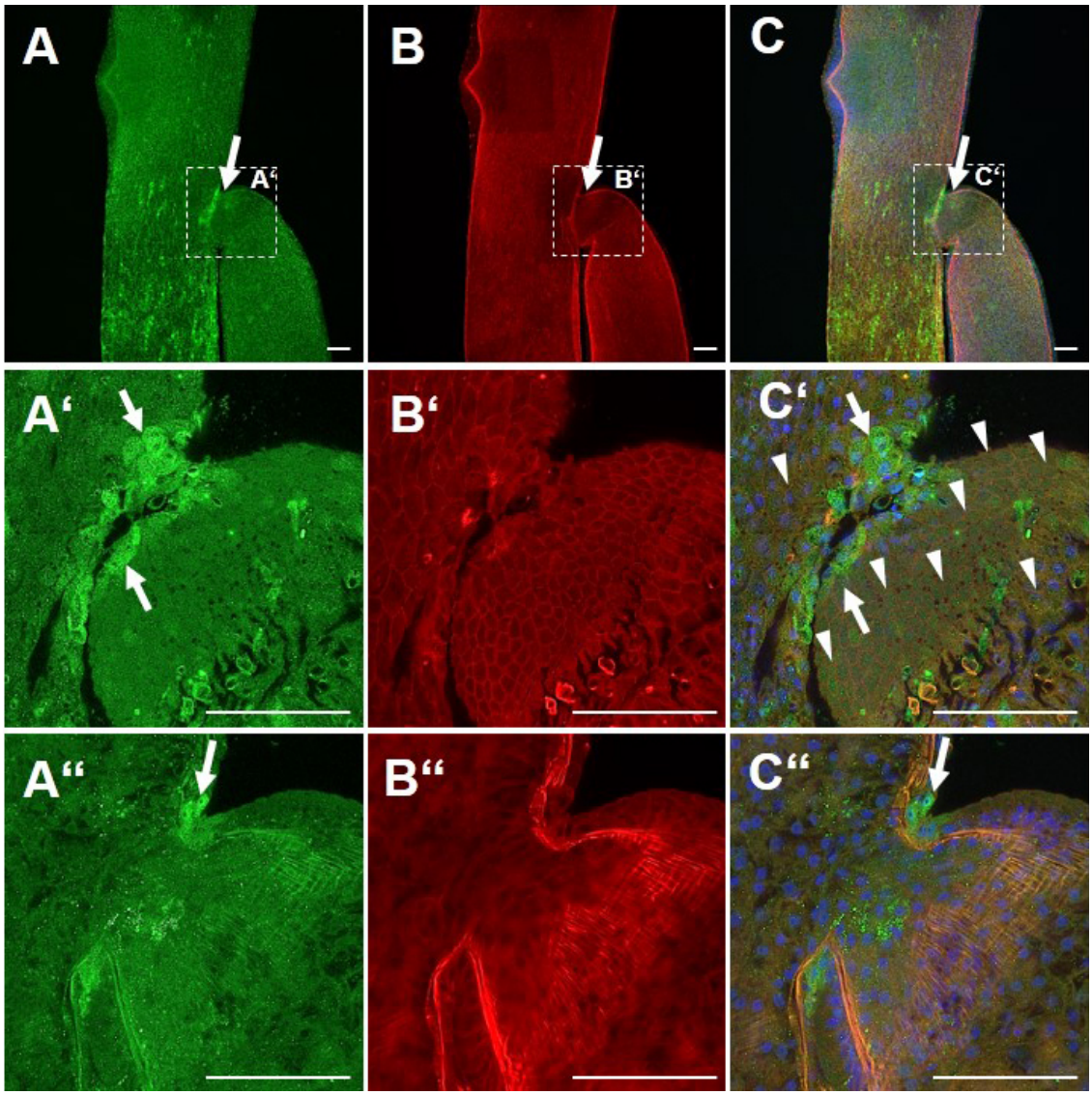

Figure 2.17: Immunodetection of FGFf during the detachment phase. (A–C) Overview of the budding zone. (A'–C') and (A"–C") Magnification of (A–C) show details of the late bud base in single layers. (A) On the left an early bud started to evaginate. On the right a bud during the detachment phase was shown. The FGFf protein accumulated at the bud base. (B - B") Phalloidin visualized actin fibers in the body. (C) Merge of A, B and DAPI channel. (A') FGFf was expressed in a few ectodermal cells in adult polyp and bud. Cells were aligned as single rows. (C') Merge of A', B' and DAPI. The localization of the FGFf protein at cell membranes in the bud's foot is indicated (white arrowheads). (A") The FGFf protein was upregulated in the ectoderm at the bud base. (C") Merge of A", B" and DAPI. Images were taken as a cLSM stack and processed at maximal projection. White arrows indicate FGFf expression at the bud base. Scale bars 100 µm.

animals as well as in a single ectodermal cell row of the bud's basal disc (fig. 2.17 A'). The FGFf protein was not detected in the endoderm and was restricted to the ectoderm (fig. 2.17, A"). Phalloidin marked the cell membranes and actin fibers along the body axis (fig. 2.17 B, B', B"). The FGFf protein expression was also found co-located to cell membranes in the bud's basal disc structures (fig. 2.17 C') indicating a potential interaction with membrane-bound FGFRs.

2.2.4 FGFf was not accumulated at the bud base after the treatment with SU5402

Treatment of *Hydra* in budding stage 3 with the FGFR-specific inhibitor SU5402 (Mohammadi et al., 1997) leads to a non-detaching bud; a Y- shaped animal composed of parent and bud results (Sudhop et al., 2004). To answer the question whether an inhibition of FGFR affects the FGFf protein distribution, SU5402-treated animals showing the specific phenotype were used for an immunodetection with an FGFf antibody (fig. 2.18). In the detachment/budding zone phalloidin did not accumulate as described (Holz et al., 2017) but instead the myonemal actin fibers arranged in a triangle at the junction between both animals (fig. 2.18 C). An FGFf protein accumulation was also not detectable (fig. 2.18 B). Instead, a protein distribution, correlated with the location of the actin fibers, was detected (fig. 2.18 D).

2.2.5 The *FGFf* gene was transcribed dynamically during regeneration

FGFs, especially FGF8, are shown to be an important regulator during wound healing and regeneration (Maddaluno et al., 2017). As *FGFf* was categorized into the FGF 8/17/18/24 group (Lange et al., 2014), its role during the regeneration process in *Hydra* was further investigated.

Animals of the *Hydra vulgaris* Zürich strain were bisected, and the transcription pattern of *FGFf* monitored until the regeneration was complete (fig. 2.19). During the foot regeneration, the *FGFf* transcription in the mouth and tentacles was unaffected. In the time of wound opening, the *FGFf* transcription was not upregulated (until 3 hours after bisection) (fig. 2.19 A–C). Starting with the wound closure (about 4–8 h after bisection), the *FGFf* transcription was upregulated in ecto- and endodermal cells at the wound edge (fig. 2.19 D–F) and later at the regenerated cap (fig. 2.19 G–L). Starting with the formation and differentiation of the foot (about 24 h after bisection) (fig. 2.19 M),

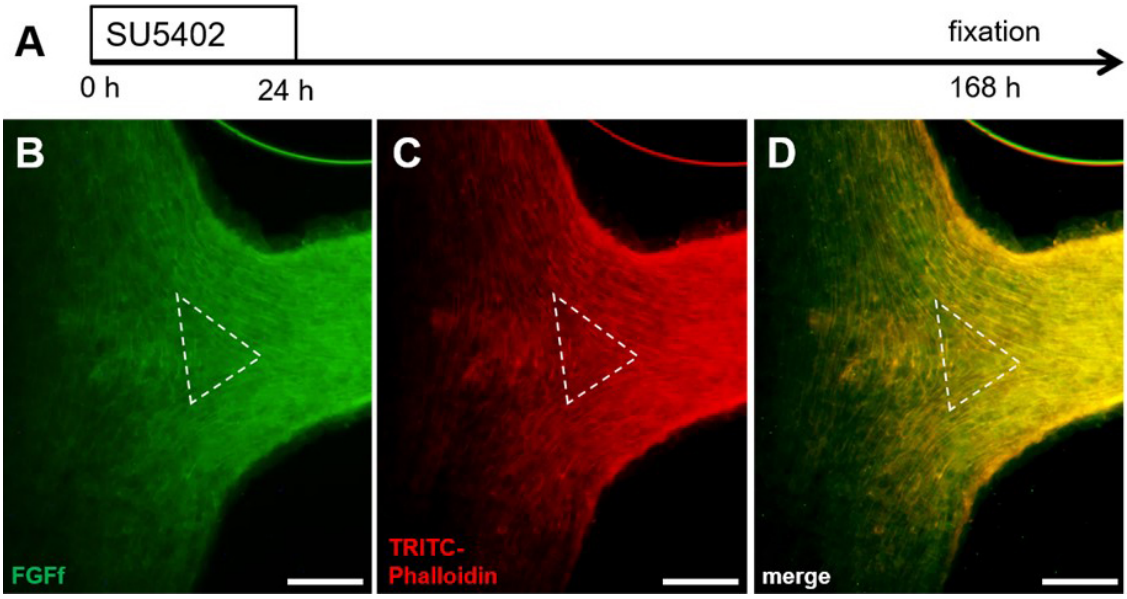

Figure 2.18: Immunodetection of FGFf in budding polyps treated with the FGFR-inhibitor SU5402. (A) Scheme of the treatment with SU5402. Animals were treated with 10 µM SU5402 for 24 hours. Fixation occurred seven days after the beginning of the treatment, when the branched phenotype was fully differentiated. (B) FGFf protein detection. The protein was not accumulated at the bud base. (C) Actin fibers stained by Phalloidin. Actin fibers were arranged in a triangle (white dotted lines). (D) Overlay of (C) & (D). Scale bars 100 µm.

the *FGFf* gene expression ceased and shifted towards an endodermal gene expression in the peduncle, therewith resembling the expression pattern of a non-regenerated normal foot (fig. 2.19 N–P).

During the head regeneration, the *FGFf* transcription in the foot was not affected by the head regeneration (fig. 2.20). The *FGFf* gene expression started at two hours after bisection and remained at first in ecto- and endodermal cells of the apical cap at the wound edges (fig. 2.20 B–D). Starting with wound closure (five hours after bisection), ectodermal and endodermal *FGFf* transcribing cells covered the closed, regenerating stump (fig. 2.20 E–L). Noticeable is that beginning with six hours post bisection, the *FGFf* transcription was located mainly endodermally (fig. 2.20 F). Additional ectodermal upregulation of *FGFf* 12 h and 14 h after bisection was found in the otherwise endodermal *FGFf* transcribing cap (fig. 2.20 I, J). In the time between 24 h and 48 h after bisection no consistent transcription pattern was found although 20 animals per time point were analyzed. In most cases (n=13/20), the transcriptional patches indicating sprouting tentacles at 36 h and 48 h were not found and the *FGFf* transcription was upregulated at the regenerating cap (fig. 2.20 N, O). With the onset of tentacle development, which surprisingly was monitored at about 24 h post sectioning (n=14/20) and before the

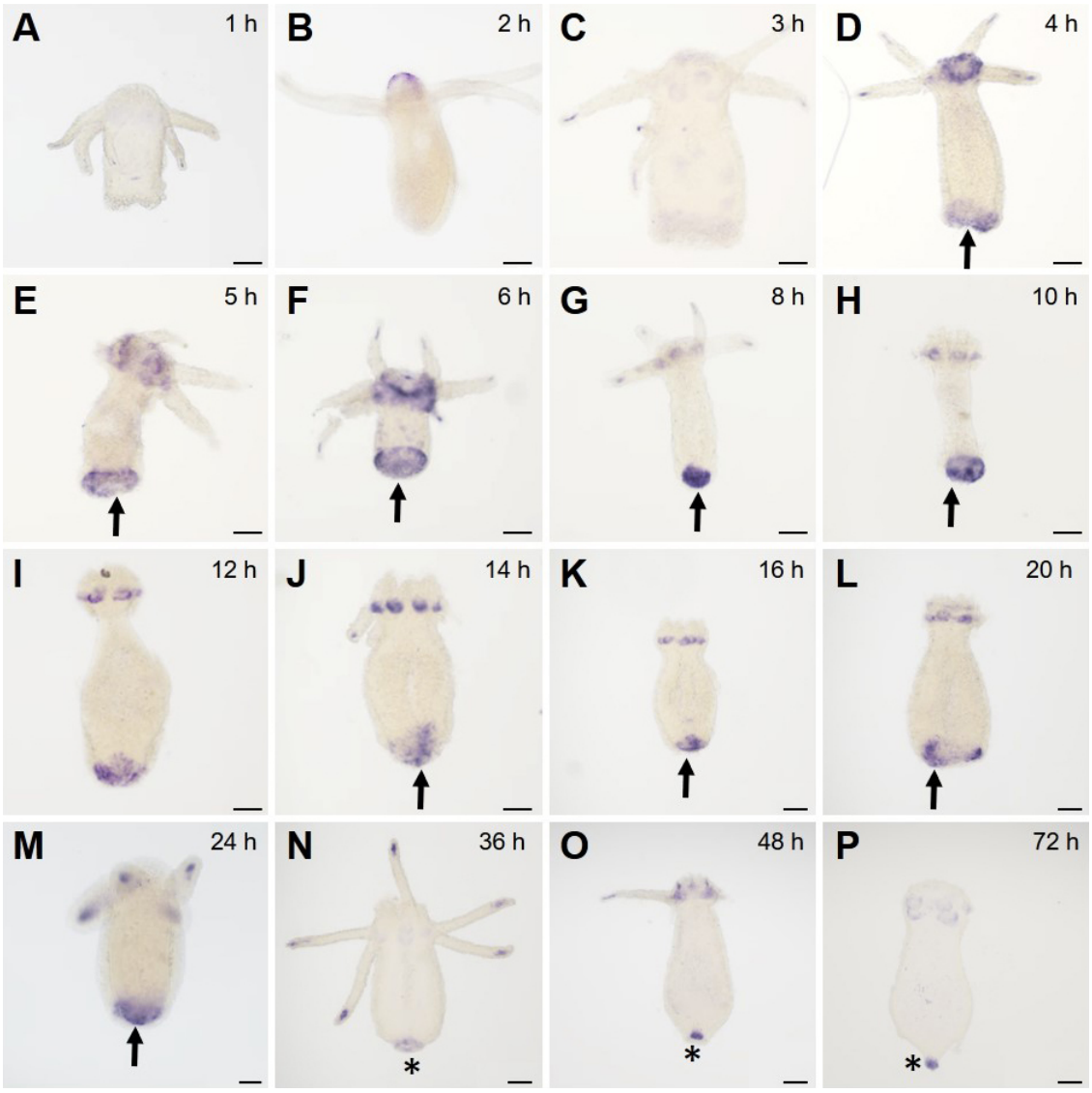

Figure 2.19: Transcription of *FGFf* during foot regeneration. (A–P) The *FGFf* gene expression at different points of time after bisection. (D - F) Upregulation of the *FGFf* transcript during foot regeneration started four hours after bisection (black arrows). (F–M) The *FGFf* transcription was upregulated in a cap-like pattern after wound closure and prior to differentiation of a new foot. (N) With formation of a new foot the typical endodermal *FGFf* transcription was restored (black asterisks). Scale bar 100 µm.

FGFf transcription was again only noticeable in the regenerating cap, the *FGFf* gene expression was upregulated in ecto- and endodermal patches in the prospective tentacle forming zones (fig. 2.20 M). In fully regenerated animals, the typical endodermal *FGFf* transcription pattern in the tentacle tips was restored (fig. 2.20 P).

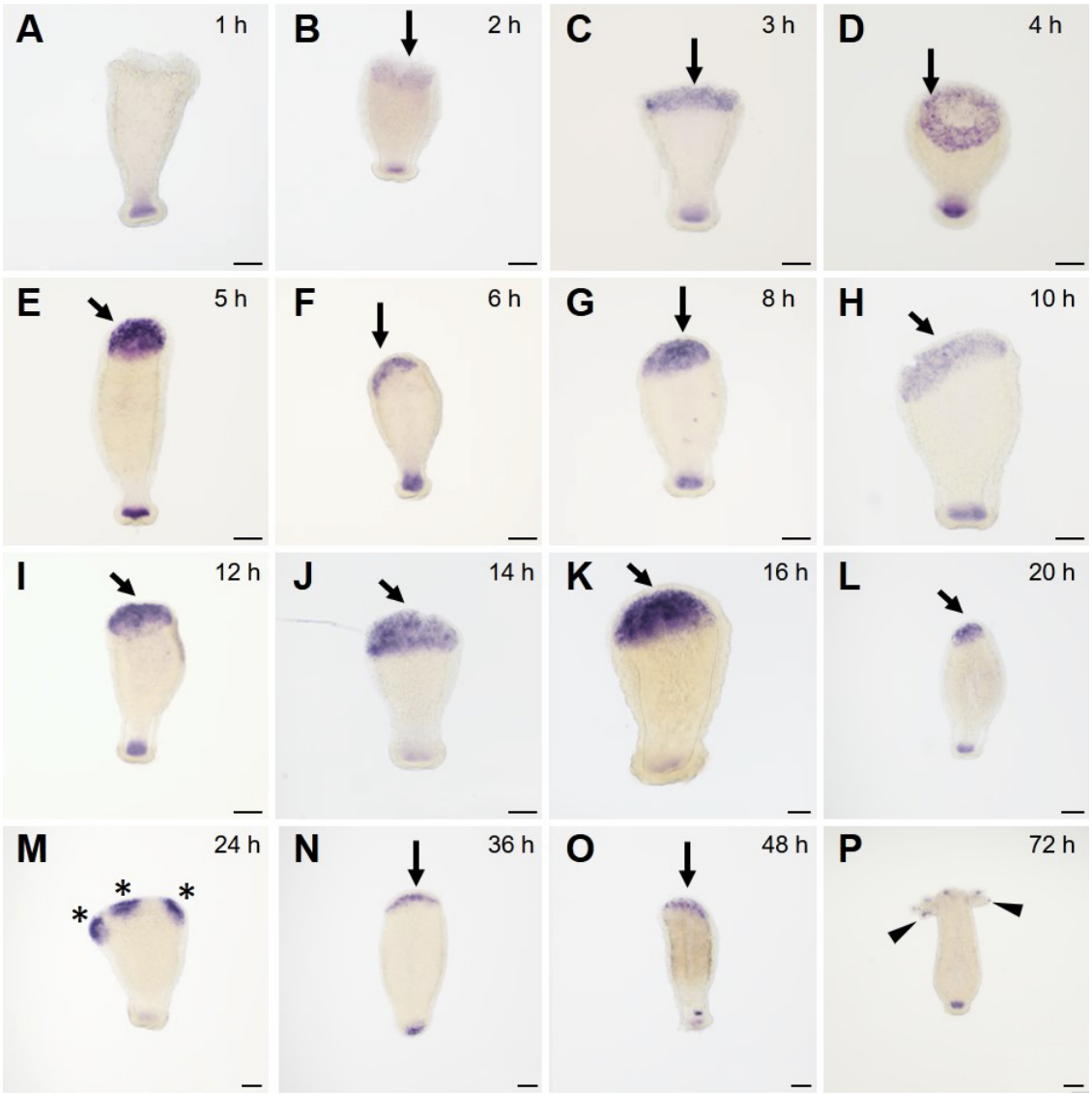

Figure 2.20: Transcription of *FGFf* during head regeneration. (A–P) The *FGFf* gene expression at different points of time after bisection. (B) Upregulation of the *FGFf* transcription during head regeneration started two hours after bisection (black arrows). (E–L) A cap-like transcription of *FGFf* was detected following to wound closure and before tentacle evagination. (M) *FGFf* was upregulated in regions of newly developing tentacles (black asterisks). (N, O) The *FGFf* transcript was upregulated in the cap. (P) After 72 h the animals were fully regenerated and tentacles tips transcribed *FGFf* endodermally (black arrowheads). Scale bars 100 µm.

2.2.6 The FGFf protein was expressed dynamically during regeneration

In ISH experiments an upregulation of the *FGFf* transcription at different time points during head and foot regeneration in *Hydra vulgaris* Zürich was detectable. To test whether the protein expression of FGFf confirmed these observations, a FGFf immunodetection was performed on regenerating bisected *Hydra vulgaris* Zürich animals.

During the regeneration of the foot structures, the FGFf protein pattern in the tentacles was not affected (fig. 2.21). Shortly after the sectioning, FGFf was not upregulated (fig. 2.21 C). After two hours, a short-term upregulation was detected at the wound (fig. 2.21 D), which ceased until six hours after the bisection (fig. 2.21 E–G). Then, the FGFf protein reappeared at the now closed wound site and persisted during further regeneration (fig. 2.21 E–H). After 16 h, the protein expression zone extended towards the head (fig. 2.21 L–N). Shortly before the differentiation of the basal disc, the FGFf expression ceased again (fig. 2.21 O, P). With the beginning of basal disc formation, the FGFf protein expression patterns resembled those of an uncut animal (fig. 2.21 Q–T). After 72 hours, the foot structure was fully regenerated (fig. 2.21 T).

During the regeneration of head structures, the FGFf protein expression in the foot remained unaffected (fig. 2.22). Within two hours after bisection, the FGFf protein was upregulated at the cut surface until eight hours of regeneration (fig. 2.22 C–H). Subsequently the expression pattern extended towards the foot (fig. 2.22 I–L). Prior to the tentacle evagination, the FGFf protein expression decreased (fig. 2.22 M, N). Beginning 27 hours post sectioning, the FGFf protein was upregulated in putative tentacle buds (fig. 2.22 O–Q). In evaginating and elongating tentacles, the FGFf expression pattern started to resemble the uncut phenotype of mature tentacles (fig. 2.22 R–T). After 72 hours, the head and tentacle structures were fully regenerated (fig. 2.22 T).

The FGFf transcription and protein were both dynamically upregulated during the regeneration process of head and foot structures.

2.3 A siRNA mediated knockdown of FGFs and FGFRs in *Hydra*

Exogenous delivery of synthetic siRNA into the cytoplasm of *Hydra* cells has been shown to generate transient knockdown effects, as the siRNA is not stably integrated into the genome (Lommel et al., 2017). According to these authors, the knockdown

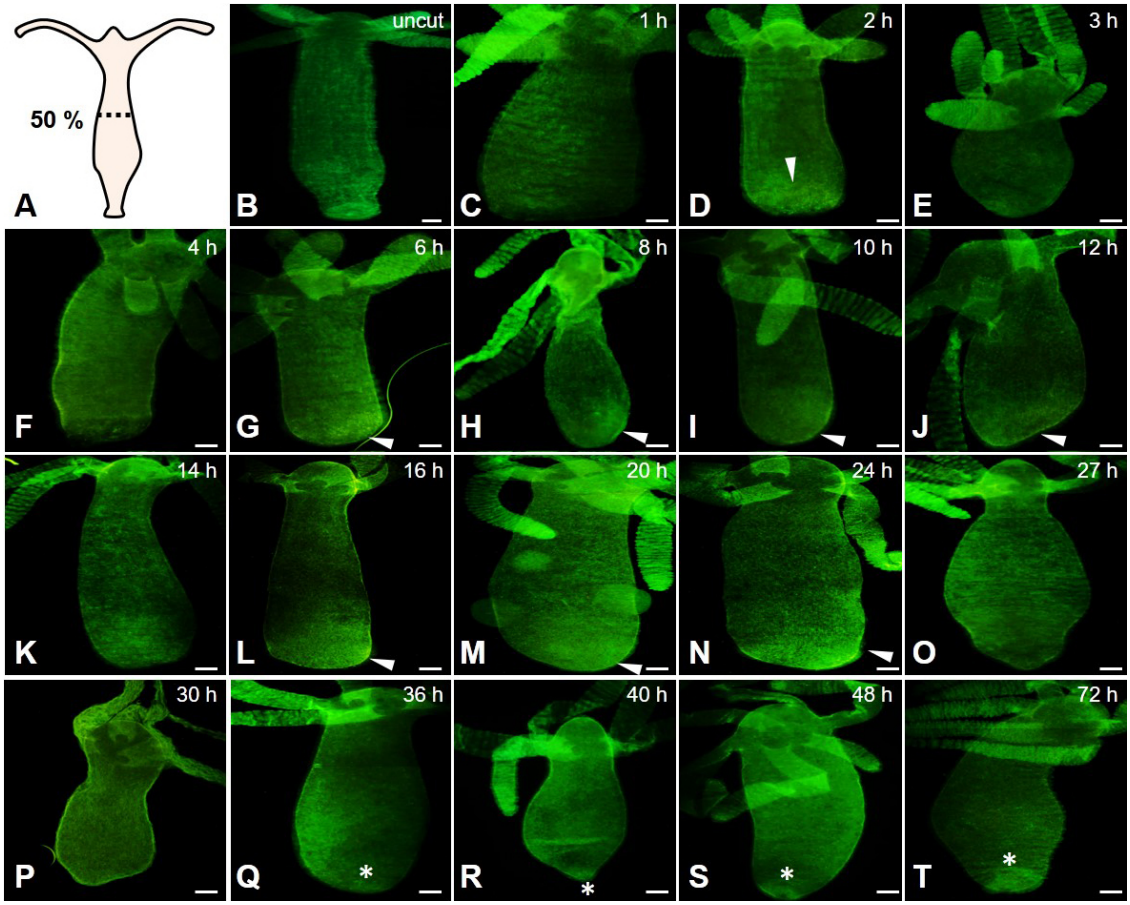

Figure 2.21: Immunodetection of FGFf during the foot regeneration. (A) Scheme depicting the site of bisection. (B) Uncut, budless animal. FGFf was expressed mainly in tentacles and basal disc with a weak overall staining in the body column. (C–T) FGFf expression at different points of time after bisection. The staining in the tentacles was detectable during all regeneration steps. (T) After 72 hours animals were fully regenerated and the FGFf expression was restored. Scale bars 100 µm.

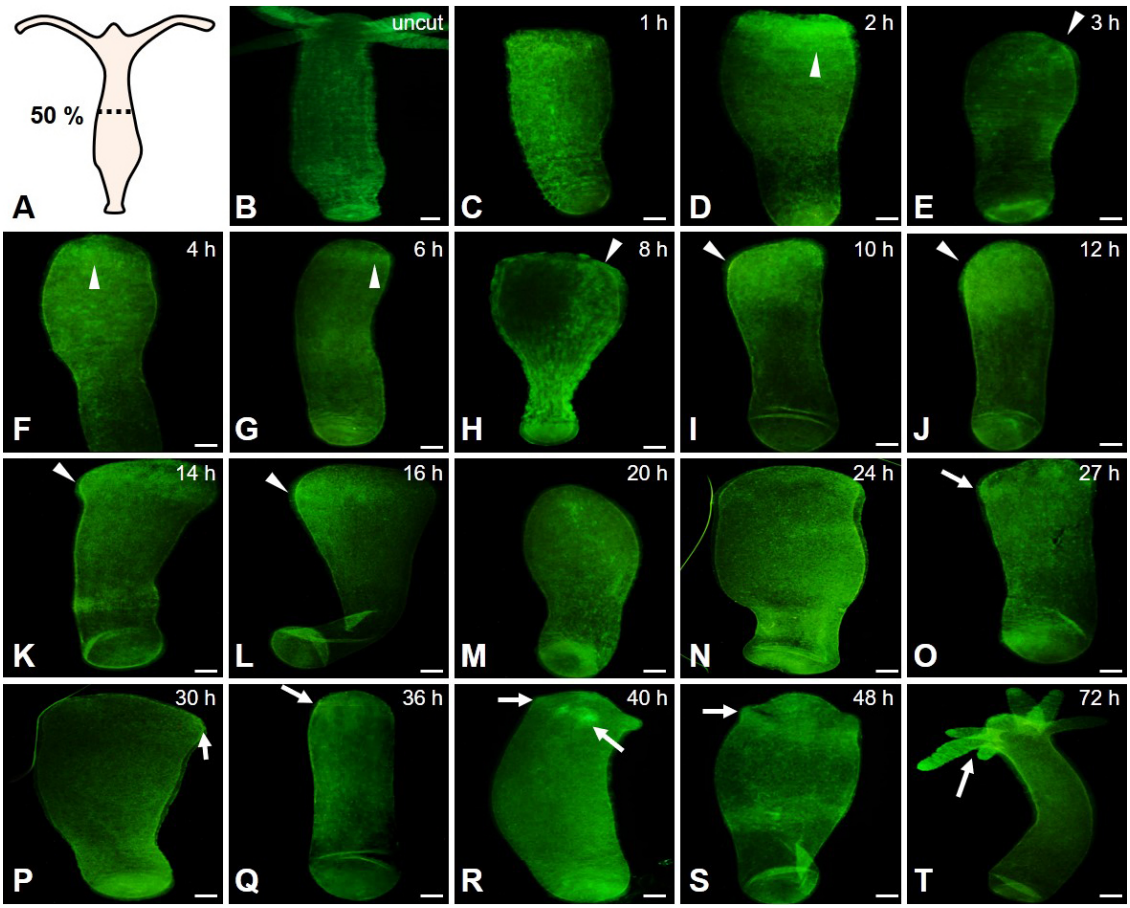

Figure 2.22: Immunodetection of FGFf during the head regeneration. (A) Scheme depicting the site of bisection. (B) Uncut, budless animal. FGFf was upregulated mainly in tentacles and foot region with a weak overall staining in the body column. (C–T) FGFf expression at different points of time after bisection. The FGFf staining of the uncut animal in the foot region was detectable during all regeneration steps. (T) After 72 hours animals were fully regenerated and the FGFf expression restored. Scale bar 100 µm.

effect of electroporated siRNA peaks at six days after the treatment and is stable for about 14 days. If not stated otherwise, siRNA experiments were hence designed to use the potential peak at six days after the electroporation. As an overall observation, electroporated animals seemed morphological intact and vital after the treatment and they died only rarely (lethality rate about 3 %). A knockdown of FGFs and FGFRs in *Hydra* was investigated by the introduction of specific siRNA-duplexes. As a positive control, *FGFRa* sequences previously used successfully as phosphorothioate antisense oligonucleotides for FGFR downregulation (Sudhop et al., 2004) were used to design siRNAs. As a negative control *pGL2 luciferase* (firefly) (Elbashir et al., 2001) was chosen which was also used as negative control in other *Hydra* studies (Ambrosone et al., 2012). As further negative controls animals electroporated without siRNA in sterile water (H_2O+) or animals without electroporation which had undergone all changes from *Hydra* medium to sterile water, to recovery medium and back to *Hydra* medium (H_2O-) were used.

2.3.1 The electroporation of FITC-Dextran was effective in all tested *Hydra* strains

The experimental setup for electroporation of siRNAs was tested by electroporating a FITC-Dextran solution into adult *Hydra*. The three non-transgenic lines *Hydra vulgaris* AEP, *Hydra vulgaris* Zürich and *Hydra magnipapillata* wt105 were tested in parallel to monitor potential strain-specific responses to electroporation. Electroporation of FITC-Dextran solution was effective in all three *Hydra* strains (fig. 2.23) and 24 hours after the pulse, a fluorescent signal was detected. Fluorescence was, however, distributed unevenly as described by Böttger et al. (2002): Some animals showed it unilateral along the body axis (fig. 2.23 B, C; F–H; J, K), some additionally at terminal structures like hypostome, tentacle and foot (fig. 2.23 B, C, F, J - L) and others in a patchy variant (fig. 2.23 D, L). Control animals showed no fluorescence signal (fig. 2.23 A, E, I). First animals started to lose the fluorescent signal 48 hours after the electroporation (not shown). In these animals the signal was restricted to a few cells in the body. 120 hours after the treatment, the fluorescence signal throughout all observed animals weakened (fig. 2.23 D, H, L), and a small number of animals (10 %) already had lost the fluorescent signal (not shown). 14 days after electroporation, most animals (93 %) had lost the fluorescent signal (not shown). The electroporation with FITC-Dextran was an effective

pre-test for the electroporation of siRNAs and showed that the setup is appropriate to introduce small particles into the adult *Hydra*.

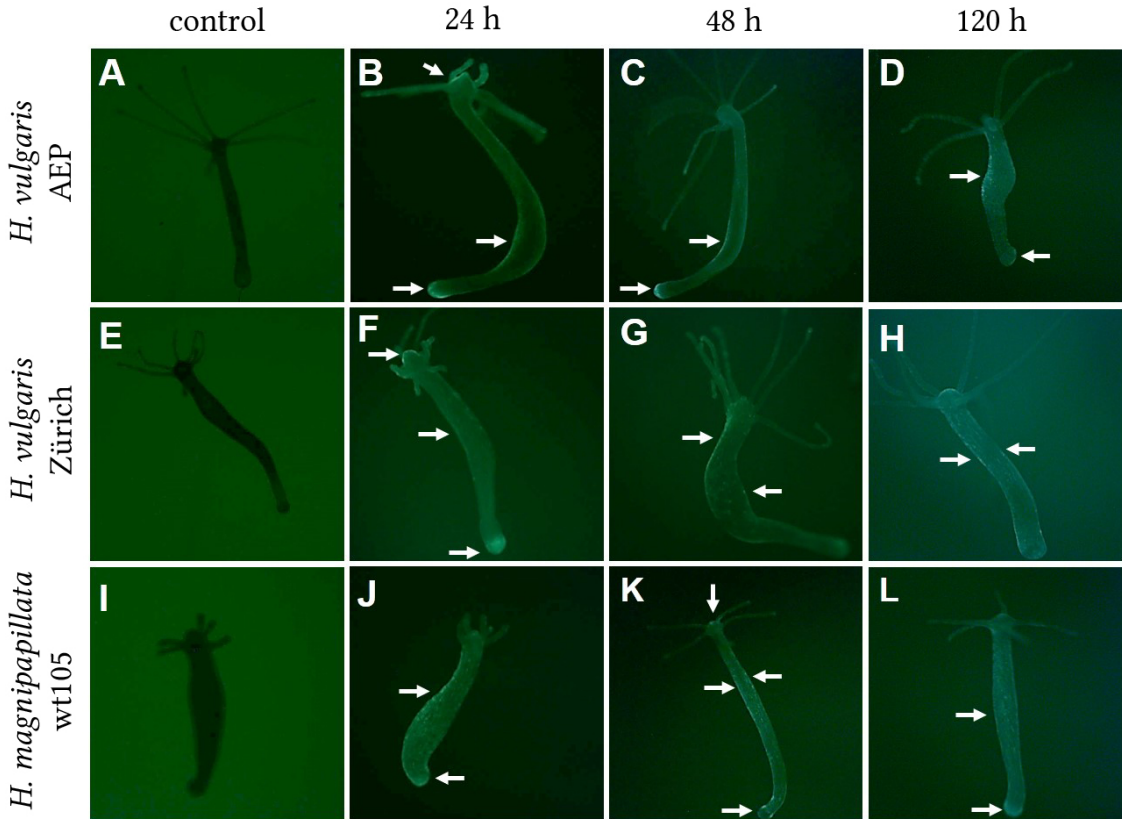

Figure 2.23: Electroporation of FITC-Dextran resulted in transiently fluorescent *Hydra*. (A, E, I) Non-electroporated animals from the investigated *Hydra* strains showed no detectable fluorescence. (B, F, J) 24 hours after the electroporation polyps were fluorescent (n=30/30). The fluorescence was distributed unilateral or in patches of cells. (C, G, K) Fluorescence was still detectable after 48 hours (n=29/30). (D, H, L) 120 hours after electroporation most animals still showed fluorescence, while occasionally the fluorescent signal had been lost (n=27/30). White arrows mark fluorescent cells. Scale bars 100 µm.

2.3.2 The siRNA mediated *FGFRa* knockdown induced a phenotype similar to the SU5402 inhibitor

To obtain a first glimpse of the effectivity of the siRNA approach in *Hydra*, two different *FGFRa* siRNAs were electroporated in animals with a bud in stage 3. As it is known that a treatment with SU5402 in this stage leads to a non-detaching bud phenotype (Sudhop et al., 2004), the detachment rate of the buds was monitored every 24 hours for one week.

The used siRNAs match the sequence of phosphorothioate antisense oligonucleotides against *FGFRa* (Sudhop et al., 2004) which reproduced the effect of a SU5402-treatment.

Electroporation of both *FGFRa* siRNAs resulted in a non-detaching phenotype when electroporated at bud stage 3 (fig. 2.24; not shown). This effect was observed in all three *Hydra* strains (*Hydra magnipapillata* wt105, *Hydra vulgaris* Zürich and AEP). The non-detaching bud stayed connected by a tissue bridge with the adult polyp and failed to develop a foot (fig. 2.24 B, D). Electroporation with the control siRNA *pGL2* did not interfere with the detachment (fig. 2.24 A, C). Electroporation of later budding stages failed to prohibit the detachment (not shown). The experimental setup was able to successfully introduce *FGFRa* siRNA into *Hydra*. Phenotypic effects from either inhibition with SU5402 or phosphorothioate antisense oligonucleotides (Sudhop et al., 2004) could be reproduced.

2.3.3 The *FGFRa* knockdown led to decreased detachment rates

To quantify how many buds did not detach after the siRNA electroporation, animals of the *Hydra vulgaris* Zürich strain were electroporated at bud stage 3 and animals with attached buds were counted. In addition to the described siRNAs for *FGFRa*, two siRNAs for FGFf were investigated. The percentage of non-detached buds is given in table A.2 and visualized as a bar graph (fig. 2.25).

As expected, 24 hours after the electroporation, all buds were still attached to their parents (fig. 2.25). First differences were observed 48 hours after the electroporation. Animals electroporated with either *pGL2* or *siFGFRa_1* did not lose their buds, whereas in other experimental groups the buds already started to detach (fig. 2.25). Most buds were lost in *siFGFRa_2* and *siFGFf_2* electroporated animals. After 120 hours, most buds in all experimental groups were detached. Only 26.6 % of buds remained attached in the *siFGFf_1* group. The *siFGFf* knockdowns neither delayed nor prevented the bud detachment. 144 hours after the electroporation, most buds were detached in the *pGL2* control group (9.3 %). Both *siFGFRa* groups on the other hand had most buds still attached to their parent (53.5 % for *FGFRa_1* and 31.4 % for *FGFRa_2*). After 172 hours, most buds had detached in *pGL2*, *siFGFf_1* and *siFGFf_2* groups. The percentages of attached buds were $<$15 % (*pGL2* = 4.7 %, *siFGFf_1* = 6.3 %, *siFGFf_2* = 11.4 %). Following the *siFGFRa_1* and *siFGFRa_2* electroporation, 48.8 % and 31.4 % of the buds, respectively, persisted firmly attached to the parental polyp. These buds showed the typical branching (Y-shape) phenotype described before.

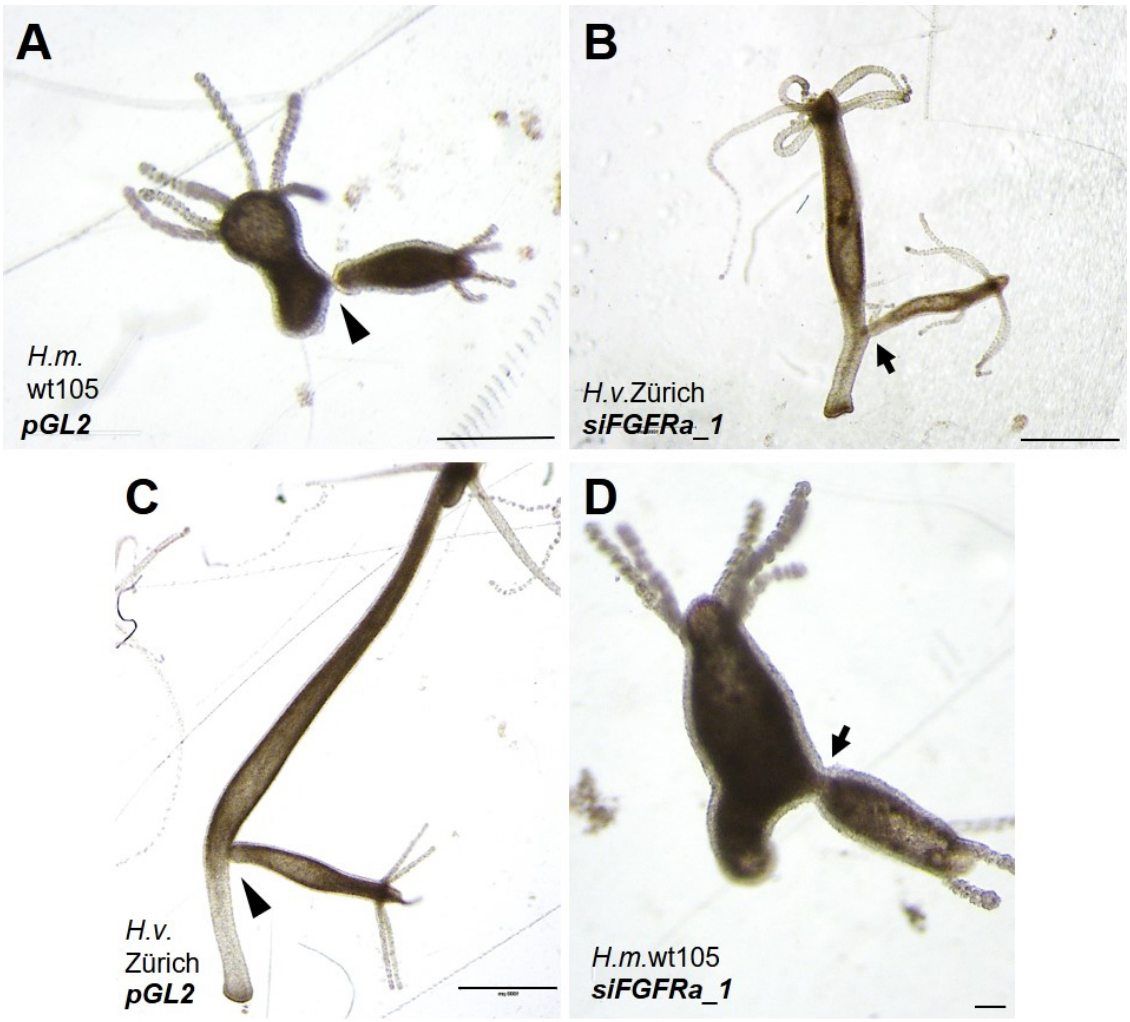

Figure 2.24: Phenotype analysis after siRNA mediated knockdown. (A, D) *Hydra magnipapillata* wt105 strain. (B, C) *Hydra vulgaris* Zürich strain. (A, C) In the *pGL2* negative control the bud stayed connected by a tiny tissue bridge (black arrowheads). (B, D) *siFGFRa_1* resulted in a SU5402 specific phenotype with non-detaching buds connected to the parent by a broad tissue bridge (black arrows). Scale bars: (A) 500 µm, (B, C) 1000 µm (D) Scale bar 100 µm.

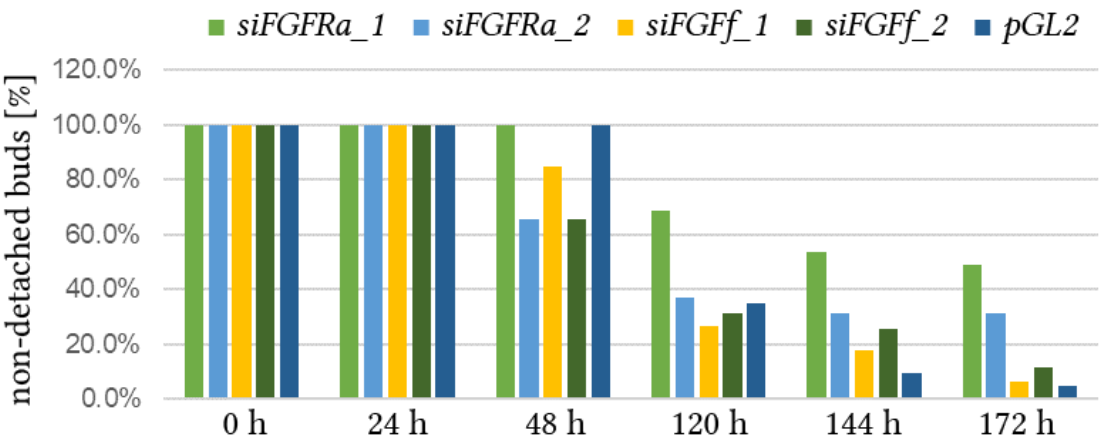

Figure 2.25: Detachment rates after siRNA electroporation in *Hydra vulgaris* Zürich. *Hydra* were collected and treated at bud stage 3. Animals with buds still attached (non-detached) were counted at the indicated points of time. *siFGFRa_1* (n=86), *siFGFRa_2* (n= 35), *siFGFf_1* (n=79), *siFGFf_2* (n= 35), *pGL2* (n= 86).

2.3.4 Statistical analysis of the siRNA detachment rates

A statistical analysis of the phenotypical observation after the siRNA electroporation was performed. The raw data is provided in table A.3. For the statistical analyzation the data of *siFGFRa_2* and *siFGFf_2* had to be discarded, because there were to few observations (n=1). Some statistical data were calculated and is provided in table 2.1. The data was further visualized with a box plot (fig. 2.26). In the *siFGFRa_1* and *pGL2* groups the same amount of attached buds was found in the first 48 hours. Because of other sample sizes, the *siFGFf_1* group had more sttached buds than the other groups. As expected, in animals of the *pGL2* control more buds were detached compared to the *siFGFRa_1* group starting 120 hours after the electroporation. This is consistent with the observation of the SU5402-typical branching (Y-shape) phenotype in *siFGFRa_1*, but not in *pGL2* animals. Similar to *pGL2*, animals electroporated with *siFGFf_1* did start to lose their buds beginning 120 h after the electroporation.

Besides *siFGFf_1* not being normally distributed at t=48 h and t=172 h an ANOVA was performed. The ANOVA revealed that the treatment as well as the time of observation had a significant effect (table 2.2). A Tukey test for both variables was performed to test where the significances occured. The Tukey test showed, that *siFGFRa_1* was the only significant treatment (table 2.3) which is again in agreement with the morphological observations. When comparing the observation time, it was clear that each point of observation between 0 h and 48 h did significantly differ from each observation point between 120 h and 172 h (table 2.4). In contrast, there were no significant effects

Table 2.1: Statistical overview of the bud detachment after siRNA treatment. The mean, standard deviation (sd) and standard error (se) for each observation point and each siRNA treatment and the p-values obtained by the Shapiro-Wilk test are shown.

treatment	time	n	mean	sd	se	Shapiro [p]
siFGFf_1	0 h	3	26.3	8.08	4.67	.726
siFGFf_1	24 h	3	26.3	8.08	4.67	.726
siFGFf_1	48 h	3	22.3	3.06	1.76	.637
siFGFf_1	120 h	3	7	6.24	3.61	.463
siFGFf_1	144 h	3	4.67	6.43	3.71	.298
siFGFf_1	172 h	3	1.67	2.89	1.67	$<$.001
pGL2	0 h	4	21.5	4.80	2.40	.420
pGL2	24 h	4	21.5	4.80	2.40	.420
pGL2	48 h	4	21.5	4.80	2.40	.420
pGL2	120 h	4	7.5	5.07	2.53	.507
pGL2	144 h	4	2.0	0.82	0.41	.683
pGL2	172 h	4	1.0	0.82	0.41	.683
siFGFRa_1	0 h	4	21.5	4.80	2.40	.420
siFGFRa_1	24 h	4	21.5	4.80	2.40	.420
siFGFRa_1	48 h	4	21.5	4.80	2.40	.420
siFGFRa_1	120 h	4	14.8	4.27	2.14	.970
siFGFRa_1	144 h	4	11.5	4.51	2.26	.230
siFGFRa_1	172 h	4	11.5	4.51	2.26	.230

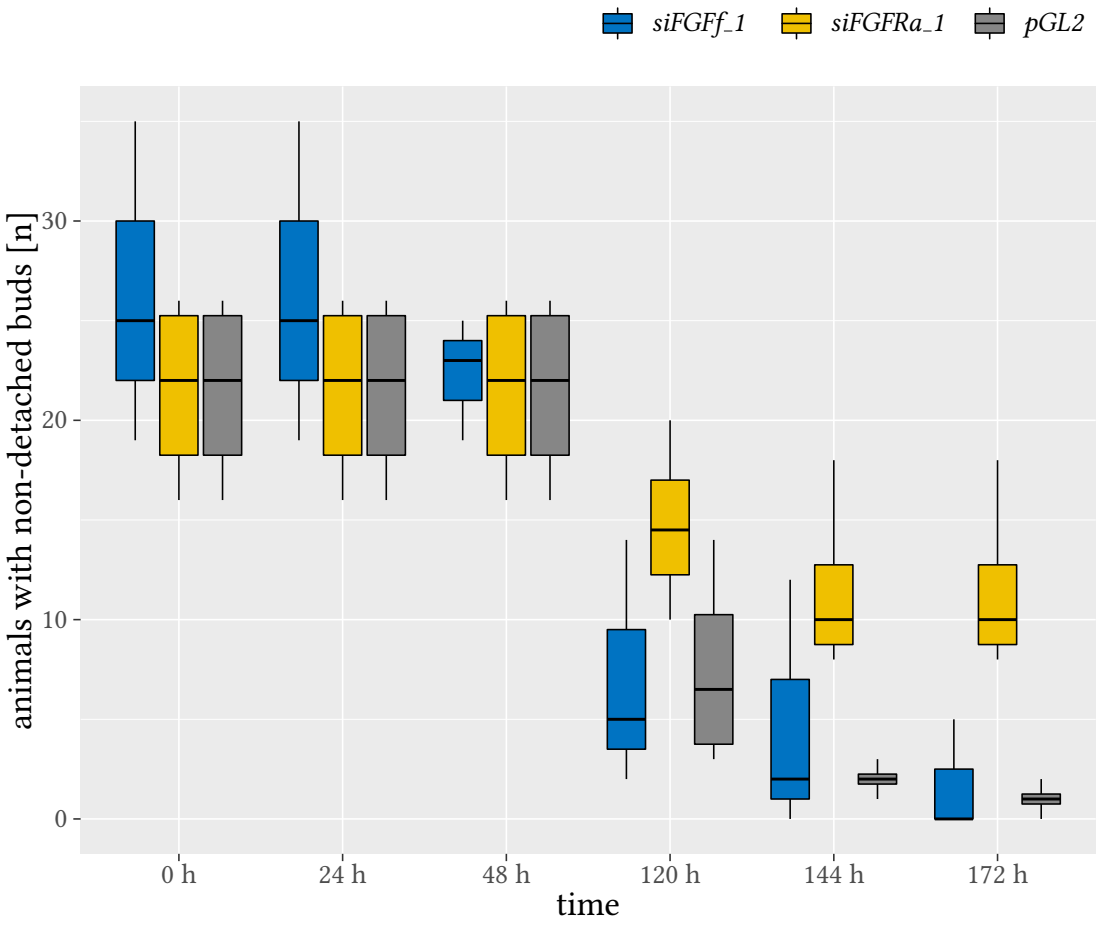

Figure 2.26: Box plot of bud detachment after siRNA electroporation. The amount of animals with an attached bud after the siRNA electroporation was visualized in box plots for each siRNA treatment and each observation point.

comparing observation points within the first 48 h or within the groups from 120 h onwards. This suggests, that theoretically two observation points, one within the first 48 h and another beginning 120 h after the electroporation, are sufficient to obtain significant results. Nevertheless, these statistical results have to be seen cautiously because of the low sample sizes.

Table 2.2: ANOVA of the detachment rates after siRNA treatments. Significant effects regarding the bud detachment were calculated. The p-values indicate that treatment and time have significant effects.

	sum sq	df	f value	p
treatment	247.6	2	5.262	.009
time	4069.0	5	34.597	<.001
treatment:time	454.5	10	1.932	.064
residuals	1129.1	48		

Table 2.3: Tukey's HSD for siRNA treatments. The significant effects between each treatment were calculated.

comparison	p
pGL2-FGFf_1	.314
siFGFRa_1-FGFf_1	.284
siFGFRa_1-pGL2	.006

2.3.5 The siRNA treatment influenced the transcription patterns

To investigate whether a siRNA mediated knockdown affects the previously described gene transcription patterns, animals were fixed six days after siRNA electroporation, regardless of their budding stage, and further processed for ISH. Six days after the electroporation the budding stage of the animals varied, even if all were electroporated in bud stage 3. Thus, in the following section not all animals show the most typical bud stage, which should be considered when making comparisons. Due to a shortage of experimental animals, some animals were used in double ISHs to investigate two probes at once.

The *FGFRa* transcription was analyzed in untreated animals as a control for the whole experimental setup (fig. 2.27 A). The *FGFRa* gene distribution was unaltered in all controls

Table 2.4: Tukey's HSD for the time after siRNA treatment. The significant effects of different observation times were calculated.

comparison	p
24h-0h	1.000
48 h-0h	.995
120h-0h	<.001
144h-0h	<.001
172h-0h	<.001
48h-24h	.995
120h-24h	<.001
144h-24h	<.001
172h-24h	<.001
120h-48 h	<.001
144h-48 h	<.001
172h-48 h	<.001
144h-120h	.447
172h-120h	.171
172h-144h	.992

and detected, e.g. in a small ring after the detachment of the bud or in a ring at the earlier bud base (fig. 2.27 B - E). In some cases, the expression level seemed more intense than previously shown, but the pattern itself remained unchanged (fig. 2.27 D).

The sequence of *siFGFRa_1* is identical with that of the *FGFRa* and the *FGFRb* genes, while *siFGFRa_2* does not match the *FGFRb* gene (fig. A.2, A.3). Therefore, the transcriptional gene expression of *FGFRa* and *FGFRb* were both investigated after electroporation with the two siRNAs. After the treatment with *siFGFRa_1* , the *FGFRa* transcription pattern was unaltered in 41 % of the animals (fig. 2.27 F) and detectable as the typical ring at the late bud base. Animals with non-detached buds failed to show *FGFRa* transcripts (fig. 2.27 G). In 30 % of the observed animals the transcription pattern of *FGFRa* was modified (fig. 2.27 H). The ring of expression had become patchy and ectopic cells outside the ring were visible. In contrast, the double staining showed that *FGFb*, as a second probe in some samples, was not affected by the *FGFRa_1* knockdown (fig. 2.27 G, H).

Inhibition with the *siFGFRa_2* siRNA did not change the *FGFRa* transcription pattern in 44 % of the animals (fig. 2.27 I). As well, the distribution of *FGFRb* was unaffected by treatment with *siFGFRa_1* (fig. 2.27 J) (54 %) or *siFGFRa_2* siRNA (fig. 2.27 K) (100 %).

A potential knockdown effect of *siFGFRa_1* siRNA was also analyzed in *Hydra vulgaris* Zürich (fig. 2.28). Here, the characteristic *FGFRa* transcription pattern was impaired. The *FGFRa* transcription was upregulated ectodermally at the bud base in all described stages. In bud stage 5, the *FGFRa* transcription was upregulated at the bud tip in the prospective mouth opening (fig. 2.28 A, A'). Simultaneously, the *FGFRa* transcription was upregulated in a broad, partially scattered ectodermal ring at the bud base (fig. 2.28 A–A"). Prior to detachment, the *FGFRa* gene expression was less patchy (fig. 2.28 B, C). Before the formation of the bud's foot, the *FGFRa* transcription was upregulated in ectodermal cells of the parent tissue in the budding zone (fig. 2.28 B–B"). At the same time, a weak endodermal *FGFRa* transcription was found in the bud base in the prospective peduncle of the bud (fig. 2.28 B'). After the formation of the bud's basal disc, *FGFRa* was strongly upregulated in the basal disc endoderm (fig. 2.28, C'). Additionally, both parent and bud, showed a weak endodermal expression of *FGFRa* in the peduncle. The *FGFRa* transcription pattern in untreated animals of the *Hydra vulgaris* Zürich strain is shown in figure A.4.

The knockdown of *FGFRa* did not lead to a loss of the *FGFRa* transcription. Instead, the transcription was either unaltered or scattered. In addition, the *FGFRa* knockdown had no impact on the transcription of *FGFRb*.

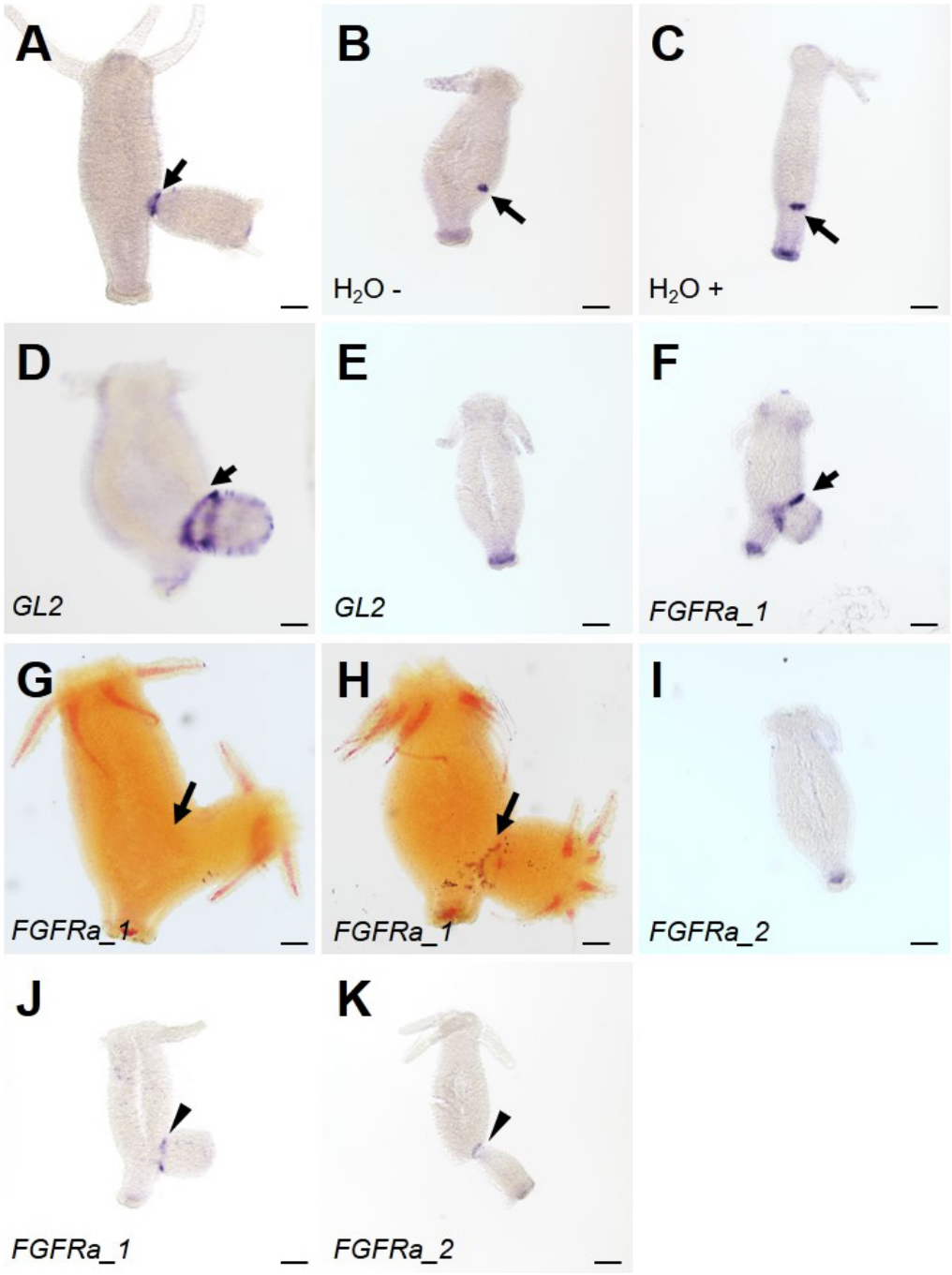

Figure 2.27: Transcription of *FGFRa* and *FGFRb* after *siFGFRa* electroporation in *Hydra vulgaris* AEP. (A–I) Analysis of the *FGFRa* transcription. (J, K) Analysis of the *FGFRb* transcription. (A) Untreated control animal. (B, C) Water controls. (D, E) *pGL2* control. (F) The *siFGFRa_1* knockdown did not alter the typical *FGFRa* transcription pattern (41 %). (G, H) The *FGFRa* pattern is modified by *siFGFRa_1* (30 %). (I) *siFGFRa_2* siRNA did not alter the expression pattern (31 %). (J) *siFGFRa_1* and (K) *siFGFRa_2* did not affect the *FGFRb* transcription (54 %/ 100 %). Scale bars 100 µm.

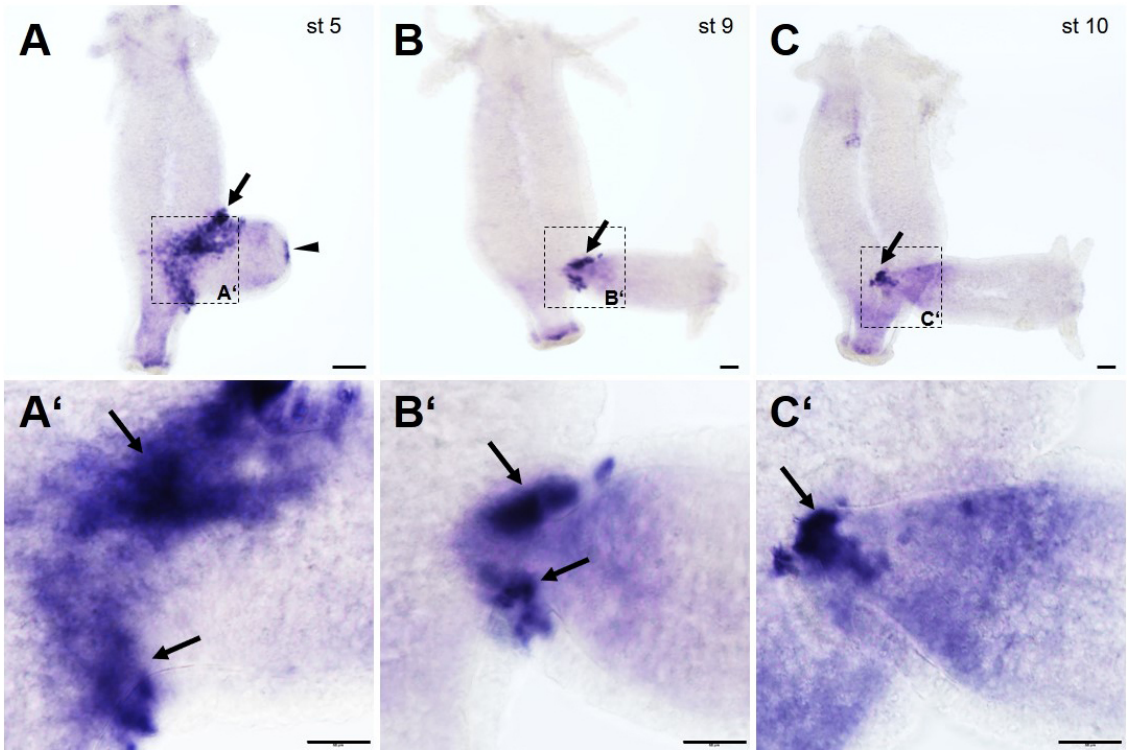

Figure 2.28: Transcription of *FGFRa* after *siFGFRa_1* electroporation in *Hydra vulgaris* Zürich. (A) In bud stage 5, *FGFRa* was transcribed at the bud tip. Additionally, a broad ring of *FGFRa* transcribing, and partially scattered, cells appeared at the bud base. (B) *FGFRa* was transcribed ectodermally in the parental and in bud tissue of and close to the bud base. The peduncle of the developing bud transcribed *FGFRa* endodermally. (C) Parental and bud peduncle with increased endodermal *FGFRa* transcription. Strong *FGFRa* signal in scattered cells of the bud basal disc endoderm. (A'–C') Magnifications of (A–C). Scale bar 100 µm.

To test the effect of a knockdown for *FGFRb*, the second FGFR in *Hydra*, specific siRNAs were designed and tested to identify potential differences between both receptors. Both *siFGFRb* knockdowns were further described using probes for *FGFRa* and *FGFRb*. Untreated animals were used as control for the experimental setup in which the *FGFRb* transcription was, as expected, upregulated in an ectodermal ring at the bud base (fig. 2.29 A). The transcriptional pattern of *FGFRb* was unaltered by either of the controls (fig. 2.29 B–D). After a knockdown with *siFGFRb_1* , the *FGFRb* transcription was upregulated in a restricted endodermal area in the peduncle (fig. 2.29 E). The electroporation with the *siFGFRb_2* resulted in characteristic *FGFRb* transcription pattern at the late bud base (fig. 2.29 F). After the detachment, a half-ring of *FGFRb*-positive cells persisted in the adult polyp and in the bud's basal disc.

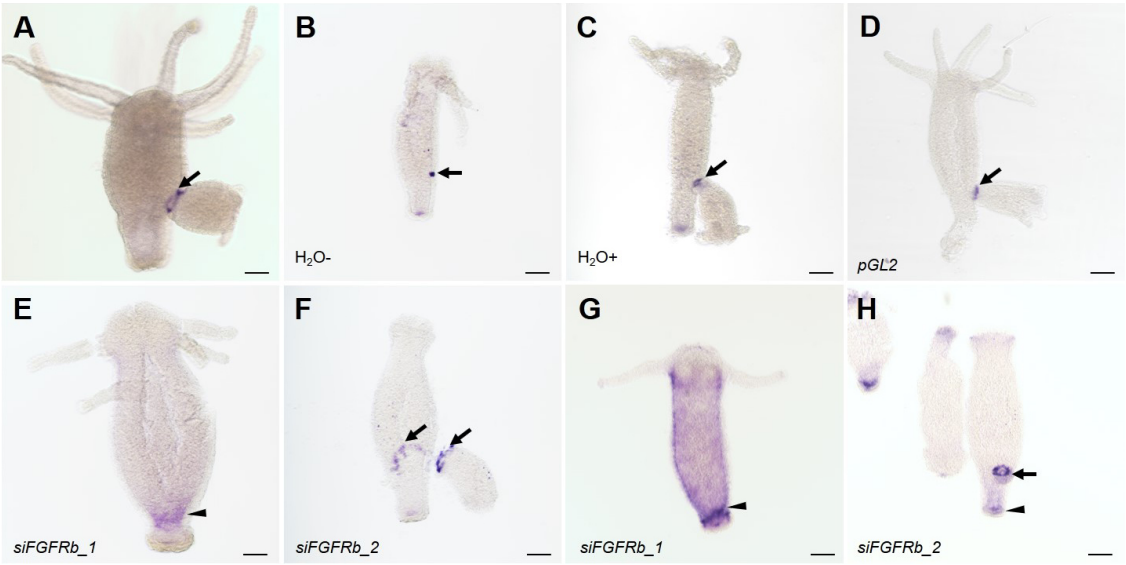

Figure 2.29: Transcription of *FGFRa* and *FGFRb* after *siFGFRb* electroporation in *Hydra vulgaris* AEP. (A–F) Analysis of the *FGFRb* gene expression. (G, H) Analysis of the *FGFRa* gene expression. (A) In untreated control animals and (B–D) other controls the *FGFRb* transcription was characteristically upregulated at the bud base (black arrows). (E) *FGFRb* was upregulated only in the peduncle (57 %) (black arrowhead). (F) The *siFGFRb_2* did not affect the expression pattern (25 %). (G) *siFGFRb_1* altered the *FGFRa* transcription (100 %). (H) The *siFGFRb_2* knockdown showed typical *FGFRa* transcription (85 %). Scale bars 100 µm.

The *FGFRa* transcription was influenced after the electroporation with *siFGFRb_1* (fig. 2.29 G). The transcript was distributed in the endoderm of the body column. Only the tentacles, the hypostome and the basal disc were devoid of an *FGFRa* signal. Additionally, the *FGFRa* transcription seemed upregulated in the peduncle. The transcription of *FGFRa*

after the *siFGFRb_2* knockdown resembled the characteristic pattern (fig. 2.29 H) with *FGFRa* being transcribed in a ring in the adult polyp after bud detachment.

The *FGFRb* knockdown either left the transcription unaffected or had only a mild influence regarding the transcriptional pattern of *FGFRb*. The *FGFRa* transcription was influenced partially by a *FGFRb* knockdown.

After investigating the knockdown effects of both *Hydra* FGF receptors, it was further tested, what effects siRNAs do have on the FGFs. At first, the transcriptional expression of *FGFb* was investigated after the electroporation with *FGFb*-specific siRNAs (fig. A.5).

In control animals the *FGFb* transcription was upregulated in the endoderm of the tentacles and in endodermal cells surrounding the foot pore (fig. 2.30 A–D). A knockdown of *FGFb* with either siRNA specific for *FGFb* diminished the gene expression described before (fig. 2.30 E, F), indicating that important sequences were inhibited with the designed siRNAs.

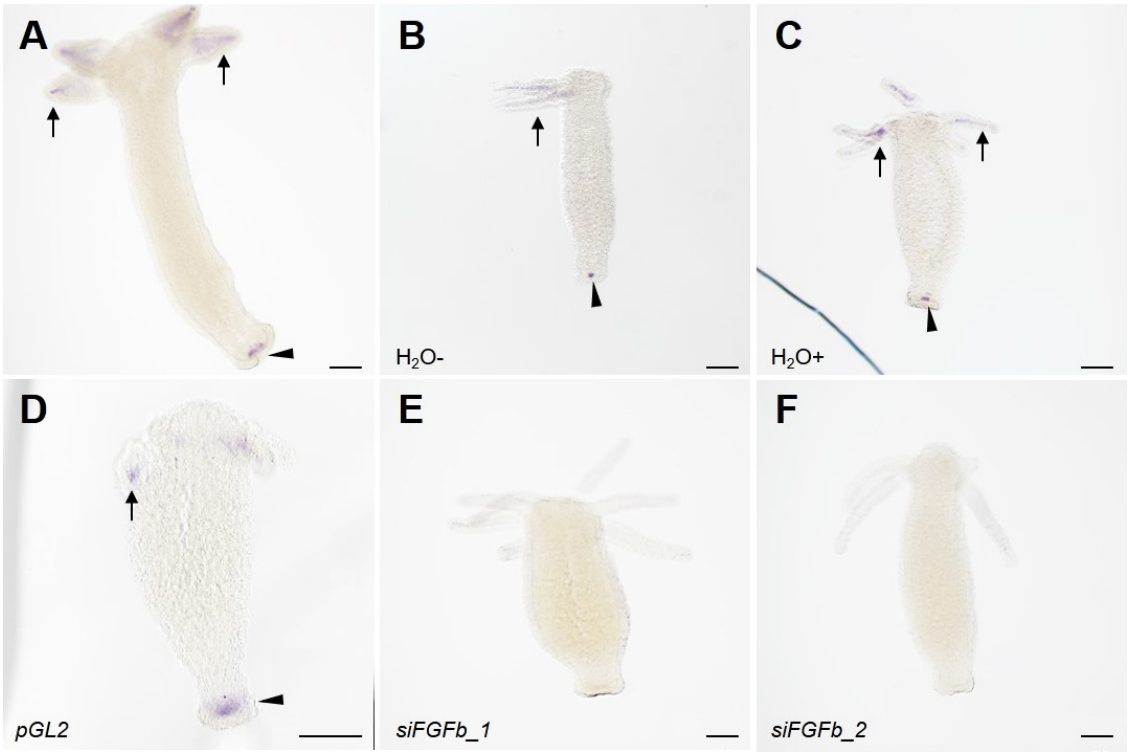

Figure 2.30: Analysis of *FGFb* siRNA in *Hydra vulgaris* AEP. (A) The untreated control animals and (B–D) other control groups showed the typical *FGFb* transcription pattern in tentacles (black arrows) and cells surrounding the foot pore (black arrowheads). (E) *siFGFb_1* or (F) *siFGFb_2* knockdown diminished the *FGFb* transcription (63 %/ 67 %). Scale bars 100 µm.

In another experiment the designed *FGFc* siRNAs (fig. A.6) were analyzed (fig. 2.31). Untreated animals showed a characteristically *FGFc* transcription at peduncle, bud base

and in a half-ring below the tentacle base (fig. 2.31, A). All further control groups displayed the same transcriptional pattern (fig. 2.31, B–D). The knockdown of *siFGFc_1* led to a loss of the *FGFc* transcription (fig. 2.31 E). In the *siFGFc_2* knockdown the *FGFc* transcript in the peduncle was diminished (fig. 2.31 F). Simultaneously, the *FGFc* transcription at the tentacle base was reduced, but still existent. These results indicate that the chosen *FGFc* siRNA sequences are partially able to downregulate *FGFc*. This experiment was performed by Lars Kneifert, M.Sc.

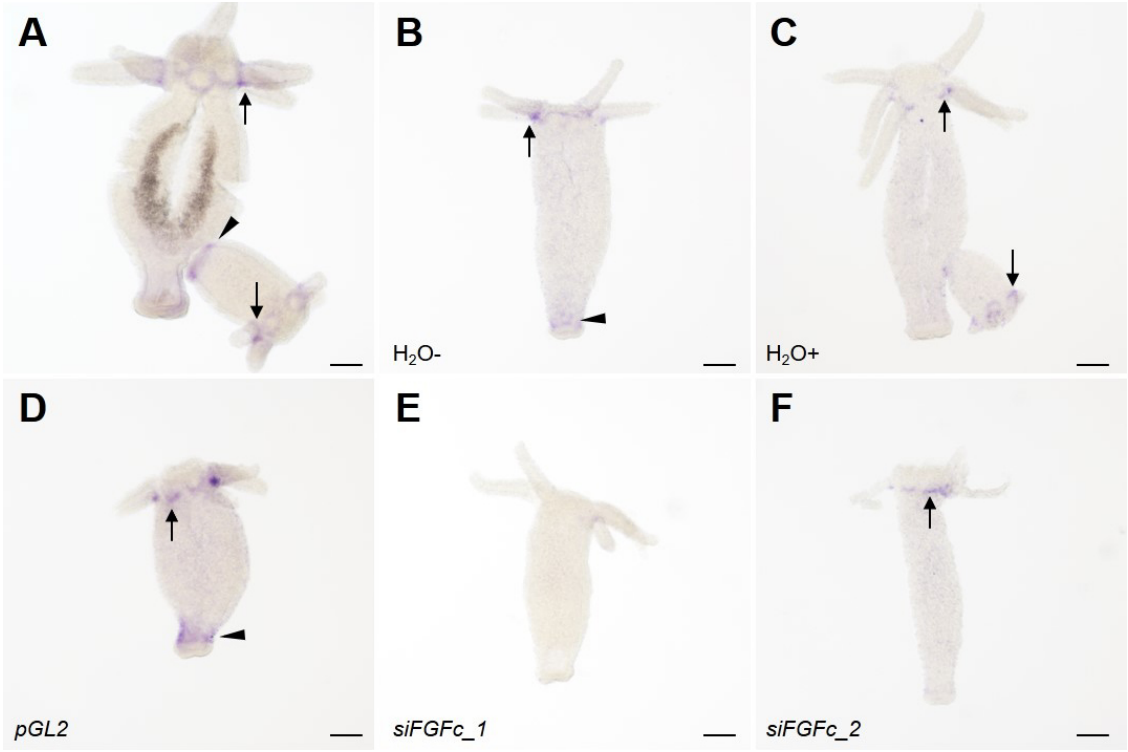

Figure 2.31: Analysis of *FGFc* siRNA in *Hydra vulgaris* AEP. (A) The untreated control animals and (B–D) other control groups showed the characteristic *FGFc* transcription below the tentacles (black arrows) and in the peduncle (black arrowheads). (E) *siFGFc_1* knockdown diminished the *FGFc* expression. (F) *siFGFc_2* knockdown partially reduced the *FGFc* gene expression. Scale bars 100 µm. ISH experiments and images for *FGFc* were performed by Lars Kneifert, M.Sc.

The *FGFf* transcription was analyzed after the knockdown of *siFGFf_1* or *siFGFf_2* (fig. 2.32) (fig. A.7). Untreated control animals (fig. 2.32, A), water controls (fig. 2.32, B, C) and *pGL2* knockdown (fig. 2.32, D) all showed no differences to the previously described transcription pattern for *FGFf*. The knockdown with *siFGFf_1* had no clear outcome: In 25 % of the animals, the pattern was unaltered compared to untreated animals (fig. 2.32 E). A partial transcriptional downregulation in the tentacles or basal disc occurred in 45 %

of the animals (not shown). As a third outcome the *FGFf* transcript was completely lost, which happened in 30 % of the animals. The same variety in the downregulation of the *FGFf* transcription was monitored with the *siFGFf_2* siRNA: In 12 % the *FGFf* transcription was unaltered (fig. 2.32 G). This knockdown also led to partial loss of the *FGFf* gene expression either in tentacles or foot region (29 %; not shown). In most cases (59 %), the *siFGFf_2* knockdown caused a total downregulation of the *FGFf* transcription (fig. 2.32 H), indicating that the chosen siRNA sequence seems important for the *FGFf* transcription.

2.3.6 The siRNA mediated knockdown of *FGFf* was not detected at the protein level

To test whether a siRNA knockdown is detectable at the protein level, animals treated with siRNA for *pGL2*, *siFGFRa_1* and *siFGFf_1* were subject to a western blot. Samples were taken seven days after the siRNA electroporation. Both α-tubulin (as internal loading control) and FGFf rb1 antibodies were detected in the expected sizes (fig. 2.33). As control, animals which were not electroporated with siRNA were used. In the control and the *siFGFf_1* group, the FGFf protein was detected in comparable amounts (table A.4). After the knockdown with *siFGFRa_1* more FGFf protein was detected. The amounts of detected FGFf protein were, compared to the control, only slightly elevated after the *pGL2* electroporation. The effect on the protein levels of FGFRa and FGFRb could not be investigated due to the lack of reliable antibodies against these *Hydra* proteins. Due to a shortage on animals, the analysis of the protein level changes was not monitored by immunodetection with whole mounts.

2.3.7 The siRNA mediated knockdowns partially influenced the cell type numbers

Since FGFs are known to be important factors for cell proliferation and differentiation in different organisms and tissues (Ornitz & Itoh, 2015), and the siRNA knockdown failed to cause substantial alterations of polyp morphology, an analysis of the cell type numbers was carried out using tissue macerates of animals six days after the electroporation. The percentage of cell types was defined in relation to the total cell count (fig. 2.34). Detailed numbers can be found in table A.5. Cell counts for the *FGFc* knockdowns were performed by Lars Kneifert, M.Sc.

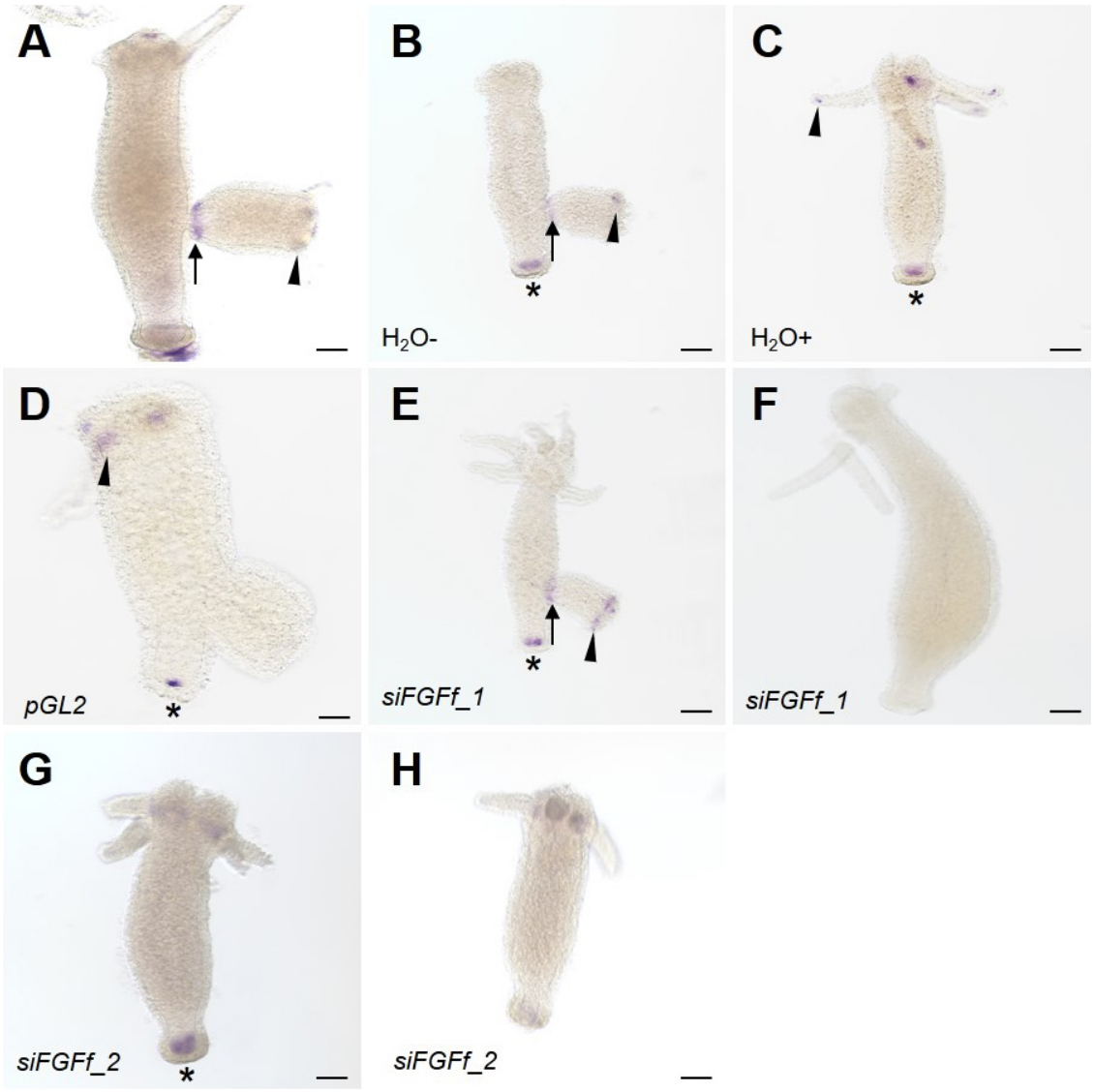

Figure 2.32: Analysis of *FGFf* siRNA in *Hydra vulgaris* AEP. (A) Untreated control animals and (B–D) other control groups transcribed the characteristic *FGFf* pattern in tentacles (black arrowheads), bud base (black arrows) and in the peduncle (black asterisk). (E, F) *siFGFf_1* knockdown. (E) No knockdown effect (25 %). (F) Partial decrease of *FGFf* transcription (45 %). (G) Complete loss of *FGFf* transcription (30 %). (G, H) *siFGFf_2*. (G) Typical *FGFf* transcription (12 %). (H) Complete downregulation of *FGFf* transcription (59 %). Scale bars 100 µm.

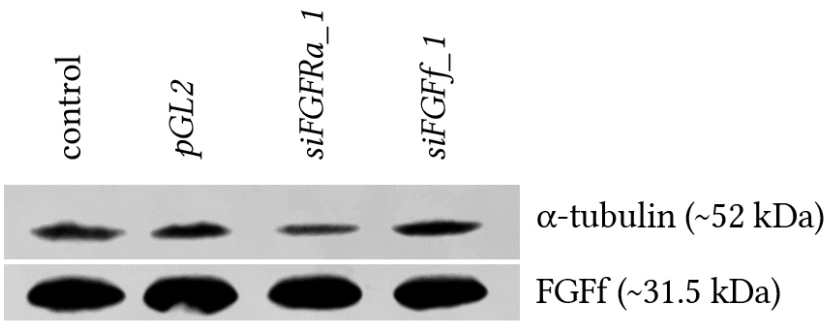

Figure 2.33: Analysis of the FGFf protein levels after siRNA knockdown. *Hydra vulgaris* Zürich strain was electroporated with siRNA and animals were analysed on a western blot seven days after the electroporation.

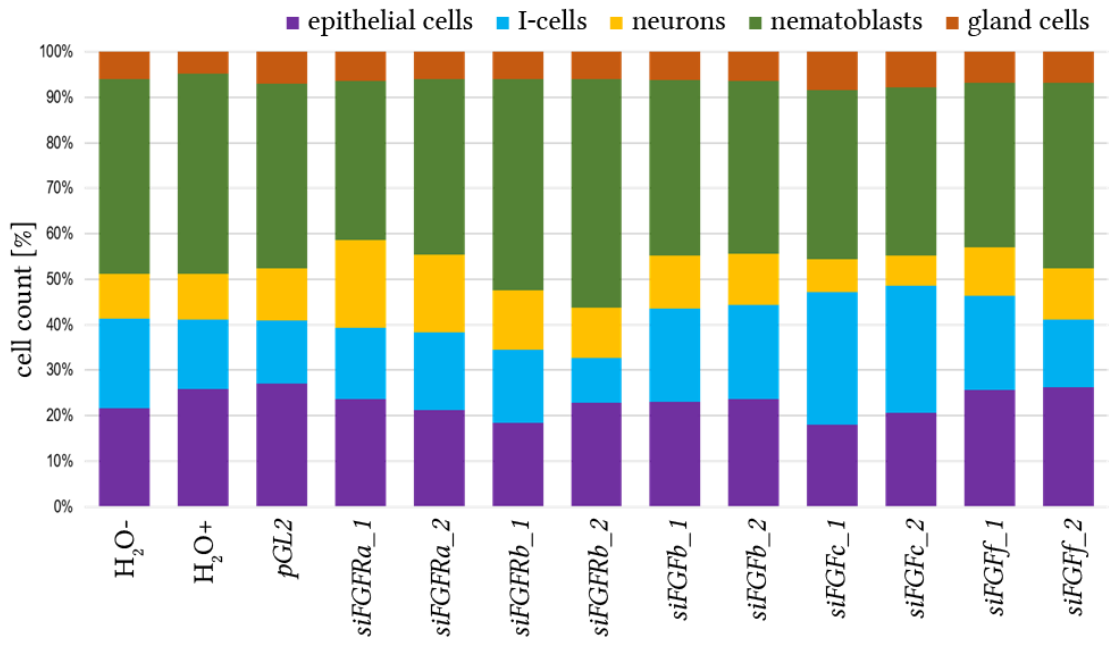

Figure 2.34: Percental distribution of cell types in *Hydra* after siRNA knockdown. Cell types were defined in proportion to the total number of cells. Total cell counts: H_2O- (n=3820); H_2O+ (n=4097); *pGL2* (n =4917); *siFGFRa_1* (n=5899); *siFGFRa_2* (n=4176); *siFGFRb_1* (n=5565); *siFGFRb_2* (n=4006); *siFGFb_1* (n=4564); *siFGFb_2* (n=4772); *siFGFc_1* (n=2210); *siFGFc_2* (n=2367); *siFGFf_1* (n=5690); *siFGFf_2* (n=5041). Epithelial cells include ecto-and endodermal epithelial cells.

As the three control groups were inconsistent when comparing the cell type numbers, the further comparison for the siRNAs was made using the H_2O- group as control. Nevertheless, the range in the control groups is given for each cell type and the most noticeable siRNA effects highlighted. The total list is provided in table A.5.

The epithelial cells in the control group varied between 21.6 % (H_2O-) and 27 % (*pGL2*). The *siFGFRb_1* (19.5 %) as well as the *siFGFc_1* (18 %) siRNA showed mildly reduced epithelial cells compared to the H_2O- control. On the other hand, both siRNAs for *FGFf* led to elevated epithelial cell levels (25.6 % and 26.2 %).

The number of I-cells in the control groups was between 13.9 % (*pGL2*) and 19.8 % (H_2O-). Noticeable is the reduction of I-cells in the *siFGFRb_2* group (8.9 %). Both siRNAs for *FGFc* instead led to elevated I-cell levels (29.3 % and 27.9 %).

The neurons in the control groups varied between 9.8 % (H_2O-) and 11.4 % (*pGL2*). The siRNAs *siFGFRa_2* and *siFGFRb_1* both led to a substantial increase of neurons in the counted samples (17 % and 13.8 %). Again, the siRNAs for *FGFc* were influenced and the neuron numbers decreased to 7.2 % and 6.6 %.

The nematoblast numbers in the control groups were determined between 40.8 % (*pGL2*) and 44.1 % (H_2O+). Noticeable was the high elevation of nematoblasts in the *siFGFRb_1* siRNA with 49.2 %. Compared to the H_2O- control group, both *FGFc* siRNAs (37.1 % and 37 %) as well as the *siFGFf_2* (36.2 %) siRNA led to reduced nematoblast levels in the counted samples.

The amount of gland cells varied between 4.8 % (H_2O+) and 7 % (*pGL2*) in the control groups. The numbers were mostly unaffected after the siRNA electroporation, except in the *FGFc* siRNAs, where the numbers were elevated up to 8.5 % (*siFGFc_1*).

In a next step, the different cell types were correlated to the number of epithelial cells as reference (table 2.5), as the epithelial cells are the cells in which the other cells are embedded and they build the basic *Hydra* structure (David & Campbell, 1972).

When setting the I-cells in comparison to the epithelial cells, the three investigated control groups were not consistent. In the H_2O- group more I-cells were found per epithelial cell compared to both other control groups, which indicates that the I-cells are potentially influenced by the electroporation process itself. Compared to the H_2O- group, the I-cell to epithelial cell ratios were reduced in the *siFGFRa_1*, *siFGFRb_2* and *siFGFf_2* groups to a level similar to the other control groups. The ratios were elevated in both *siFGFc* groups. Comparing neurons to epithelial cells, the control groups were consistent. Nevertheless, in the *siFGFRa_1*, *siFGFRa_2* and *siFGFRb_1* electroporation, elevated levels of neurons were found per epithelial cell. Simultaneously, the neurons in

Table 2.5: Cell proportions after the siRNA knockdown. I-cells, neurons and single nematoblasts were set in relation to the number of epithelial cells. Epithelial cell count is set as 100 %. Outliers are indicated in bold.

	I-cells : epithelial cell	neurons : epithelial cell	nematoblasts : epithelial cell
H2O-	0.92 : 1	0.45 : 1	1.98 : 1
H2O+	0.59 : 1	0.38 : 1	1.70 : 1
pGL2	0.51 : 1	0.42 : 1	1.51 : 1
siFGFRa_1	**0.67 : 1**	**0.82 : 1**	1.48 : 1
siFGFRa_2	0.80 : 1	**0.80 : 1**	1.81 : 1
siFGFRb_1	0.88 : 1	**0.71 : 1**	**2.53 : 1**
siFGFRb_2	**0.43 : 1**	0.48 : 1	**2.20 : 1**
siFGFb_1	0.89 : 1	0.50 : 1	1.68 : 1
siFGFb_2	0.88 : 1	0.47 : 1	1.61 : 1
siFGFc_1	**1.63 : 1**	**0.40 : 1**	2.07 : 1
siFGFc_2	**1.35 : 1**	**0.32 : 1**	1.79 : 1
siFGFf_1	0.81 : 1	0.42 : 1	1.41 : 1
siFGFf_2	**0.57 : 1**	0.43 : 1	1.56 : 1

both *FGFc* siRNAs were mildly reduced. This indicated that at *FGFRa* and *FGFc* might be important during the neurogenesis in *Hydra*. The comparison of nematoblasts and epithelial cells again showed differences between the control groups with the H_2O-group having more nematoblasts per epithelial cell compared to the other control groups. Despite the differences in the control groups, the nematoblast to epithelial cell ratios in the *siFGFRb* groups were highly elevated, indicating that *FGFRb* might be important for the nematoblast differentiation.

2.3.8 Statistical analysis of the siRNA maceration

The cells obtained after the maceration for each cell type and siRNA treatment were counted (table A.7) and statistically analysed. The arithmetic mean (mean), standard deviation (sd) and standard error (se) for the cell counts in each treatment group are listed in table A.9, and visualized by a box plot (fig. 2.35). For a first decision which statistical test to perform, the distribution of each cell type was investigated with a Shapiro-Wilk test and visualized with a density plot (fig. 2.36). Interestingly, only the nematoblasts showed a normal distribution, whereas in all other cell types the distribution was positively skewed. Hence, the values of all other cell types were normalized by log transformation for further statistical testing. Gland cells were unable to be normalized by a log transformation, but despite the lacking normal distribution of the gland cells and the ineffectiveness of the log transformation, the untransformed variable was used for further testing. Literature seems to agree, that ANOVAs are generally robust, even when failing to meet its assumptions (Blanca et al., 2017; Glass et al., 1972; Harwell et al., 1992; Lix et al., 1996; Schmider et al., 2010). Nevertheless caution is advised reviewing its results in this special case.

The ANOVA showed that the siRNA treatments had significant effects on all cell types except the nematoblasts (table 2.6). After the calculation of any significant influences, the Tukey's Honest Significant Difference (HSD) was used to determine where these effects occured (Tukey, 1977) and a full list of its results is provided in table A.11. Significant findings in relation to the H_2O+, H_2O- and *pGL2* control groups are reported in table 2.7. Interestingly, compared to all three control groups, the *siFGFRa_1* siRNA showed significant differences in the neurons and both *FGFc* siRNAs significances regarding the I-cells. Other siRNA treatments were either not statistically significant or the significance was not found in all three controls. Nevertheless, the whole statistical analysis must be seen cautiously, as the sample sizes are low. For a more valid statistic further experiments with higher sample sizes are needed.

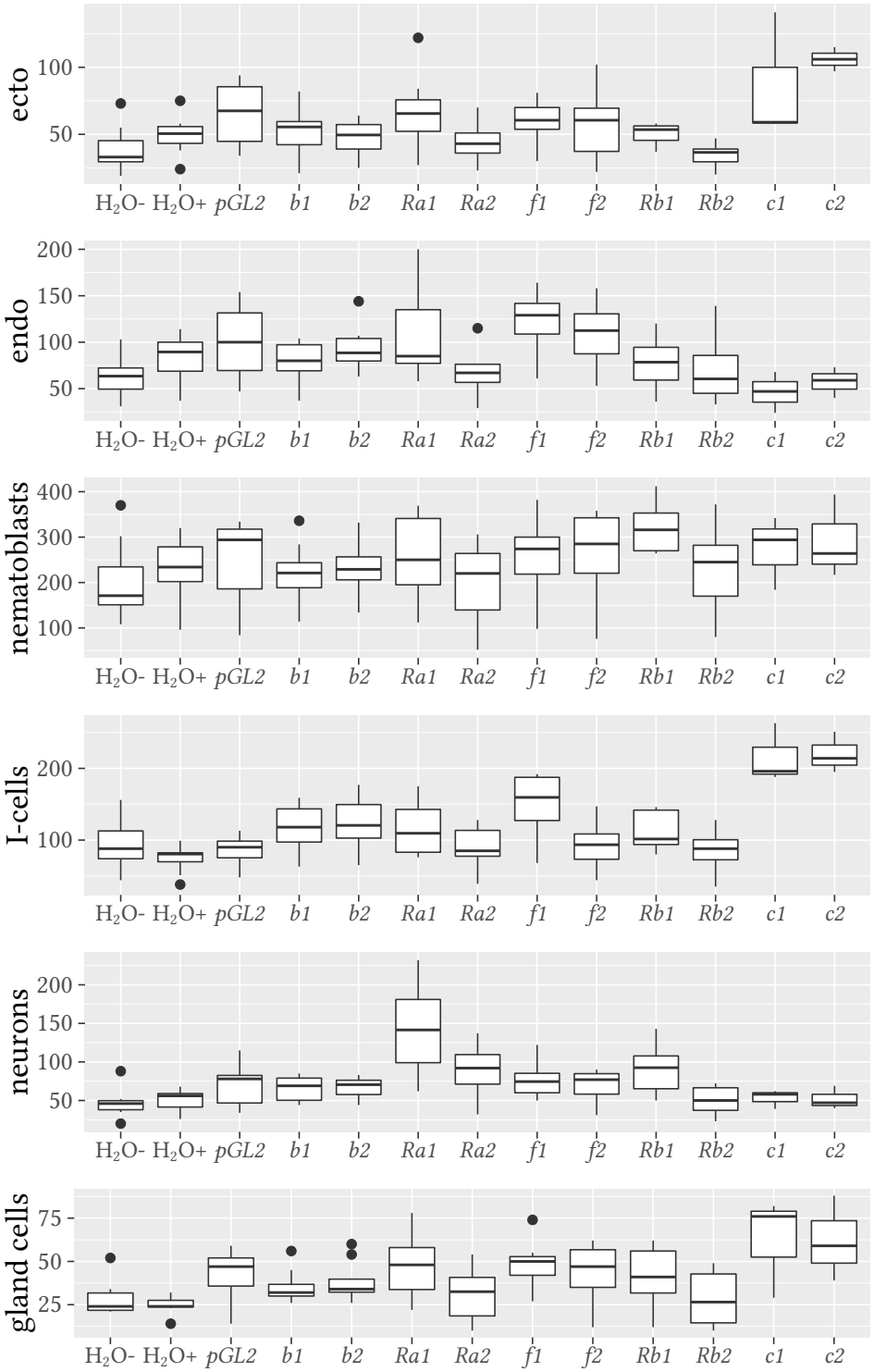

Figure 2.35: Box plots of siRNA macerations. The box plots for each siRNA treatment are shown and sorted by cell type.

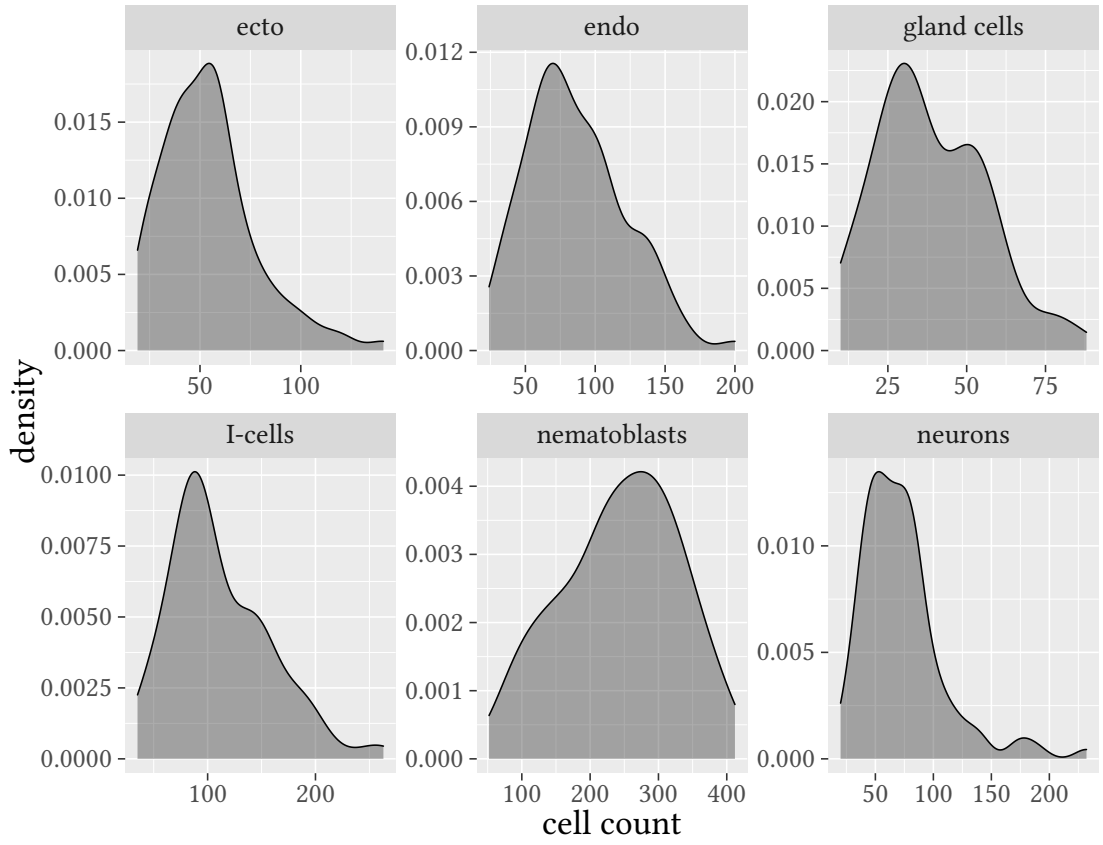

Figure 2.36: Density plots for the various cell types after siRNA treatment. The density plots show the distribution of each cell type. With the exception of the nematoblasts all plots are positively skewed. Nematoblasts seems to be normally distributed.

Table 2.6: Maceration cell count statistics. Values gained after different steps in the statistical testing are listed. Gland cell values were unable to be normalized by the log transformation but were used as untransformed variable in further testing.

sample	Shapiro [p]	Shapiro after log-Trans [p]	Levene [p]	ANOVA [p]
ecto	<.001	.368	.783	.001
endo	.029	.263	.956	.001
nematoblasts	.147	not needed	.935	.315
I-cells	<.001	.327	.954	<.001
neurons	<.001	.861	.854	<.001
gland cells	.018	.010	.259	.001

Table 2.7: Excerpt of Tukey's HSD. The statistical significant values of siRNA treatments in the macerates compared to the three control groups are depicted and p-values indicated.

cell type	treatment	H_2O- [p]	H_2O+ [p]	*pGL2* [p]
ecto	*siFGFc_2*	.004	.104	.684
endo	*siFGFf_1*	.037	.670	.989
I-cells	*siFGFc_1*	.018	<.001	.008
	siFGFc_2	.012	<.001	.006
	siFGFf_1	.340	.017	.170
neurons	*siFGFRa_1*	<.001	<.001	.017
	siFGFRb_1	.025	.139	.955
gland cells	*siFGFc_1*	.080	.027	.800
	siFGFc_2	.087	.030	.818

3 Discussion

The FGFR signaling pathway is important for many developmental processes in animals and its role during evolution can be further investigated by using phylogenetically old organisms like *Hydra vulgaris*. The simplicity of the *Hydra* body plan with its only two monolayered epithelia allows an easy characterization of gene expression. Different FGFs and FGFRs were discovered in *Hydra vulgaris* (Lange et al., 2014; Rudolf et al., 2013; Sudhop et al., 2004). The aim of this project was to get more insight in potential functions of FGFs in *Hydra*. One part of the project was the further investigation of FGF transcription and, partially, protein expression patterns during budding and regeneration in different *Hydra* strains. Another part of the project focused on siRNA-mediated knockdown of FGFs and FGFRs to understand how FGFs operate in *Hydra*.

3.1 The function of FGFa remains unclear

According to Lange et al. (2014) *FGFa* was grouped into the FGF group 11-14, which is known as an intracrine FGF group (Ornitz & Itoh, 2015). Although it is still unclear, whether *FGFa* really belongs into this FGF group or is just grouped nearby, the intracrine FGFs are known to act via voltage-gated Na^+-channels (Nav) in neurons (Itoh & Ornitz, 2011; Lou et al., 2005). Those channels control the excitability of neuronal cells and therewith regulate locomotion and cognition (Marban et al., 1998). Provided that *FGFa* is indeed an intracrine FGF, it could activate Navs, consequently functioning in locomotion/contraction of the polyp. Contraction in *Hydra* is regulated by longitudinal myonemes in the ectoderm, which results in body shortening, and circular myonemes in the endoderm, which mediate body elongation (Aufschnaiter et al., 2017). Ultrastructural analysis suggests that the muscle contraction in *Hydra* is stimulated by neurons using large vesicles which probably contain neuropeptides (Gründer & Assmann, 2015). It was shown, that neuropeptides like Hym-176, which are expressed by neurons in the peduncle region of *Hydra*, induce ectodermal muscle contractions (Yum et al., 1998) and that *Hydra* RFamide neurotransmitters (which belong to the FMRFamides (Espinoza

et al., 2000)) are co-expressed with Hym-176 in neuronal populations in the peduncle (Hansen et al., 2000). Further, FMRFamide were shown to activate Na^+-channels in snails (Cottrell et al., 1990; Lingueglia et al., 1995), but also in *Hydra* RFamide activated Na^+-channels were found (Golubovic et al., 2007). Unfortunately, the Na^+-channels in *Hydra* are located at the tentacle base but not the peduncle. As the *FGFa* transcription was found in the peduncle rather than at the tentacle base and the presented work did not identify *FGFa*-positive neurons, the activation of Navs by *FGFa* in *Hydra* seems unlikely. Further, intracrine FGFs do not activate FGFRs (Goldfarb, 2005; Itoh & Ornitz, 2011; Ornitz & Itoh, 2015), hence the function of *FGFa* in *Hydra* remains unknown.

3.2 FGFb may promote bud detachment and cell differentiation

The FGF1/2 subfamily is comprised of FGF1 and FGF2 (Ornitz & Itoh, 2015). In vertebrates, both FGFs were shown to function as proliferative factors, during cell migration, in neuronal differentiation, in the promotion of angiogenesis as well as in the regulation of the cell cycle, survival and apoptosis (Ornitz & Itoh, 2015; Yun et al., 2010). *FGFb* was categorized into the paracrine FGF1/2 group (Lange, 2016; Lange et al., 2014) but not further investigated yet. The present study suggests, that *FGFb* may hold several functions in *Hydra*, which will be elucidated in detail in the following section.

The gene expression of a *Hydra* matrix metalloprotease (HMMP) was found in the endoderm of tentacles and in cells surrounding the aboral pore similar to the described pattern of *FGFb* (Shimizu et al., 2007). HMMP is known to degrade the ECM at the aboral pore but is also of importance during the foot regeneration and the maintenance of basal disc cells in *Hydra* (Leontovich et al., 2000; Shimizu et al., 2007). The similar transcriptional patterns suggest that *FGFb* and *HMMP* may interact with each other. An example for such interaction was found in the *Drosophila* air sac primordium (ASP), where the matrix metalloprotease Mmp2 was induced by FGF in the ASP tip cells (Guha et al., 2009; N. Powers & Srivastava, 2018; Wang et al., 2010). It was shown that Mmp2 is important for the degradation and remodelling of the ECM surrounding the ASP (N. Powers & Srivastava, 2018). The remodelling of the mesogloea is also important during the detachment of the *Hydra* bud. A second *Hydra* matrix metalloprotease, *MMP-A3*, with 52 % sequence identity to *HMMP* was found, that is thought to promote the morphogenesis at the constriction site during the detachment (Münder et al., 2010). It was further hypothesized that MMP-A3 degrades ECM components leading to a

mesogloea remodelling and thus enables the detachment of the bud. The same study found out, that *MMP-A3* was co-expressed with *FGFRa* in the late detachment phase. The transcription patterns of *FGFb* and *FGFRa* were also either overlapping or in close proximity, indicating a potential interaction by a locally acting paracrine FGF (Bökel & Brand, 2013; Ornitz & Itoh, 2015). Although *FGFb* and *FGFRa* are transcribed in different epithelial layers, the interaction is still possible through pores in the mesogloea (Shimizu et al., 2008). Concluding these findings, *FGFb* may regulate the detachment of the bud by activating the FGFR signaling pathway and by interacting with metalloproteases involved in the reorganization of the mesogloea. Whether *FGFb* interacts also with *FGFRb* remains unclear and needs further investigation. Also, whether a knockdown of *FGFb* influences the morphology of the bud, e.g. leads to a Y-phenotype like the inhibition of FGFR, needs further examination.

The tentacles as well as the foot in *Hydra* contain terminally differentiated cells (David, 1973; Galliot et al., 2009). *FGFb* was also upregulated in the tentacle endoderm, indicating a potential role as cell attractant and differentiation signal. In *Hydra vulgaris* Ind-Pune a *HyFGF-1* gene was found with a *FGFb*-like expression (Turwankar & Ghaskadbi, 2019). The authors described *HyFGF-1* as a paracrine FGF with high sequence identity to *FGF-1* in chicken and in *Nematostella vectensis*. The authors concluded an expression similarity between *HyFGF-1* and *FGFf* in *Hydra vulgaris* AEP and therefore a role of *HyFGF-1* in nematocyte and neuron differentiation and the migration towards terminal structures (Lange et al., 2014). Contrary to this observation, *FGFb* and *FGFf* show very distinct transcription patterns in the present study. The knockdown of *FGFb* with either siRNA duplex led to a complete suppression of the gene expression, but no significant effects after macerate analysis were found. Nevertheless, taking into consideration that *FGFb* may interact with HMMP, the mesogloea remodelling could also promote cell migration as shown in *Drosophila*, where the ECM reorganization by Mmp2 is also hypothesized to facilitate the cell migration towards the FGF source in the ASP tip (N. Powers & Srivastava, 2018). Additionally, the FGF in the ASP tip is needed for the initiation of processes that regulate cell proliferation and survival. In *Hydra*, epithelial cells as well as nematoblasts migrate towards the tentacles, where they need to transdifferentiate into battery cells and nematocytes (Aufschnaiter et al., 2011; Boehm & Bosch, 2012; David, 2012; Hobmayer & David, 1989). One function of *FGFb* in the tentacle may be the promotion of the migration by being an attractant source as hypothesized for other FGFs (Lange et al., 2014; Turwankar & Ghaskadbi, 2019), thereby potentially interacting with metalloproteases to facilitate the migration. Another role of *FGFb* may

be as a differentiation factor for migrating cells arriving in the tentacles. Both potential functions have to be further investigated. FGFs of the FGF1/2 family are also known for their function in many regenerating processes in other organisms (Maddaluno et al., 2017), therefore a potential function for *FGFb* may also be in the regeneration of *Hydra*. As the *Hydra* regeneration is dependent on cell differentiation as well as the reorganization of the mesogloea (Agata et al., 2007; Bosch, 2007; Shimizu, 2012), this would be in accordance to the other suggested functions for *FGFb*. Nevertheless, the potential influence of *FGFb* in the *Hydra* regeneration needs to be further investigated. Both potential function in migration and regeneration may also explain the upregulation of *FGFb* in the early bud development, as the evagination and elongation of a bud is based on mass tissue movement and assumed to be a morphallactic process (Campbell, 1967; Clarkson & Wolpert, 1967; Holstein et al., 1991; Otto & Campbell, 1977).

3.3 FGFc may promote I-cell renewal and neuronal differentiation

FGFc was categorized into the FGF1/2 group (Lange et al., 2014). Krishnapati and Ghaskadbi (2013) isolated an FGF from the *Hydra vulgaris* Ind-Pune strain for which they concluded a function related to the maintenance of stem cells. FGF2 (also known as bFGF) was described to maintain stem cells in their undifferentiated state in mouse and human stem cells, partially by inducing proliferation (Gritti et al., 1996; Lotz et al., 2013; Mossahebi-Mohammadi et al., 2020). Therefore, it is proposedly needed for the self-renewal of stem cells. This is in accordance with the idea, that the found FGF in *Hydra* is needed for the self-renewal of I-cells in the body column. Although the gene expression patterns of the described *FGF* from Krishnapati and Ghaskadbi (2013) and *FGFc* show great differences, own analysis showed a high protein sequence identity between both FGFs (fig. A.8). Therefore, similar functions of *FGF* and *FGFc* can be considered.

The proliferative function of FGF2 was also found in the context of neural development. It promotes the proliferation of neural stem cells and is expressed in neural precursor cells throughout development (Dono et al., 1998; Vaccarino et al., 1999). FGF2 is also involved in the early brain development and knockout mice show less neural progenitor cells and severe defects in the cerebral cortex after a FGF2 knockout (Raballo et al., 2000). The *siFGFc* knockdown in *Hydra* led to a neuron decrease with a simultaneous, statistically significant, upregulation of I-cells which would fit the described functions

of FGF2. According to that, the potential functions of *FGFc* would be the maintenance and proliferation of the I-cells in the body column and the promotion of differentiation, especially neurons, in the lower tentacle. Hypothesizing that *FGFc* is important for the differentiation of I-cells, effects that may occur in animals with less nematocysts or neurons should be observed after the knockdown. These should include the ability to prey and feed, the ability to attach to the ground and the overall morphology. To confirm that *FGFc* is important for the proliferation of i-cells, its expression should be investigated in marked proliferating cells (e.g. after 5-ethynyl-2'-deoxyuridine (EdU)-treatment).

The transcription of *FGFc* at the lower tentacle base and in the peduncle indicates an additional function as attractant source for migrating cells. For example, nematoblasts migrate towards the tentacles and where they need to differentiate further into mature nematocysts and mature nerve cells (Galliot et al., 2009). The role of *FGFc* during the migration of i-cells needs further investigation, e.g. by creating transplants.

3.4 FGFe may function in the bud induction

According to Lange et al. (2014) *FGFe* was grouped into or near the FGF1/2 group. Although no double-ISH was performed, the transcription patterns of *FGFe* and *FGFRa* (Sudhop et al., 2004) are similar in the ectodermal bud tip at budding stage 4 and 5. As the *FGFe* transcription is localized in the ectoderm and *FGFRa* in the endoderm, a direct interaction is unlikely. Nevertheless, a connection between both epithelial layers is possible and the possibility that diffusible molecules like FGFs migrate through the mesogloea pores (Shimizu et al., 2008) is given. Interestingly, also *HyWnt2* is upregulated in the ectodermal bud tip in stage 4, but not in later stages or in the adult mouth structure (Lengfeld et al., 2009). Another *Wnt* gene, *HyWnt3*, was upregulated ectodermally, but also endodermally, in the bud tip in stage 4 and 5 and in the adult polyp. Both Wnt genes were shown to be part of the head organizer during bud formation. The similarity to the *FGFe* transcription pattern suggests, that *FGFe* may interact with the Wnt signalling pathway in the early evagination steps of the bud development. Like hypothesized for *HyWnt2*, one function for *FGFe* may be in the induction of the bud. Presumed that *FGFe* and *Wnt* signalling interact, the role of *FGFe* during regeneration is probably interesting, as the head organizer is also active during head regeneration (Lengfeld et al., 2009) and should be further investigated. The inhibition of the FGFR additionally leads to a delay in head regeneration (Turwankar & Ghaskadbi, 2019), therefore the knockdown of *FGFe* may enhance the investigation during the regeneration. The *FGFe* transcription in the

developing mouth further indicates a role for *FGFe* in the establishment of the mouth opening. In agreement with the ectodermal transcription of *FGFe* in the developing mouth are the findings, that the ectodermal layer in the adult *Hydra* mouth opens before the endodermal layer (Carter et al., 2016).

The function of *FGFe* in the peduncle remains unclear and is possibly redundant to the other *Hydra* FGFs, which are expressed in this body region.

3.5 FGFf may provide many functions in the *Hydra* development

The *Hydra* FGFf was categorized into the paracrine FGF 8/17/18/24 group (Lange et al., 2014). Especially FGF8 is known for many functions during animal development, but predominantly for its functions during vertebrate limb regeneration and development (G. R. Martin, 1998; Shimizu-Nishikawa et al., 2003). Additionally, FGF8 is a critical factor in creating the mid-hindbrain boundary and in somitogenesis (Harada et al., 2016; Naiche et al., 2011). In *Drosophila*, FGF8-homologues are required in mesoderm development and for proper trachea development (Klingseisen et al., 2009; Sutherland et al., 1996). Furthermore, FGF8 was also shown as an important factor in cell migration (Reim et al., 2012; Sun et al., 1999).

3.5.1 FGFf may promote the boundary formation during the bud detachment

Results from the double-ISH with both FGFRs revealed, that *FGFf* is transcribed in close proximity, but not overlapping to either FGFR, thus indicating a potential interaction by a locally acting paracrine FGF (Bökel & Brand, 2013; Ornitz & Itoh, 2015). The potential interaction of FGFf and FGFR may be important in the detachment of the bud, an idea that is further supported by the absence of the FGFf protein or the *FGFf* transcription (Lange, 2016) after the FGFR inhibition with SU5402. A strong accumulation of the FGFf protein in the basal disc of the detaching bud indicates its potential involvement during the bud detachment. In contrast, the siRNA knockdown of *FGFf* showed no significant influence on the detachment rates and did not lead to the formation of Y-animals. This suggests that FGFf may depend on signaling from FGFR but is not necessarily needed for the FGFR activation. Other potential interaction partners of FGFf may be Wnt genes, as an interaction of FGF and Wnt was shown in other contexts. In the mid-hindbrain boundary

(MHB) morphogenesis in zebrafish it was shown that the interaction of Wnt and FGF affects cell proliferation and cell adhesion (Gibbs et al., 2017). Dyer et al. (2014) proposed a negative feedback-loop controlled by Wnt1 that is crucial for the FGF8 activity and further, that Wnt regulates the FGF and Sprouty expression in the neurogenesis of the mid-hindbrain. Other studies have shown that FGF and Wnt signaling can both inhibit GSK-3β, an important component in the Wnt signaling pathway (Dailey et al., 2005). Both signaling pathways are also involved in promoting intracellular calcium levels, thus balancing cytoskeletal organization and cell adhesion (Gibbs et al., 2017). The calcium signals influence the cell shape in the MHB in a myosin-dependent way (Gutzman et al., 2015; Sahu et al., 2017). Further, cytoskeletal reorganization and concomitant cell shape changes are essential for proper boundary formation, as it provides local stiffness and therefore cell stabilization during boundary and constriction formation (Gibbs et al., 2017). In the lateral line formation of zebrafish, the formation of rosettes was promoted by FGFR-Ras-MAPK mediated signaling and localization of Rho-associated kinase (Rock) to promote constriction (Harding & Nechiporuk, 2012).

The formation of boundaries is also important in *Hydra*, e.g. in the bud detachment where the establishment of a morphological boundary in the detaching bud (Böttger & Hassel, 2012) was found to be under control of Notch and FGFRa (Münder et al., 2010). Further, cell shape changes and cytoskeletal reorganization under the control of a FGFR-Rho-Rock-Myosin II pathway are essential for the detachment of the bud (Holz et al., 2017) and additionally, the expression of phosphorylated Myosin-light chain (pMLC), which is important for the generation of contractile forces, was found in the ectoderm of the late *Hydra* bud base (Holz et al., 2020; Holz et al., 2017; Watanabe et al., 2007). As in the vertebrate MHB, Wnt genes, in this case *Wnt8*, are upregulated at the late *Hydra* bud base (Philipp et al., 2009), indicating a possible interaction with FGFR and Rho-Rock-Myosin II signaling. In addition, the FGFR inhibitor Sprouty (Tsang & Dawid, 2004) is expressed in cells at the late *Hydra* bud base (fig. 3.1; Suryawanshi (2017)). Taking the information of the Wnt and FGF interaction during the MHB formation into account, the following hypothesis regarding the function of *FGFf* in the *Hydra* bud detachment is suggested: An interaction of Wnt8 and FGFf initiates the activation of FGFR signaling cascades at the bud base, e.g. the Ras-Rock-Myosin II pathway that promotes cell shape changes and therewith the bud constriction. An additional activation of the Ras-MAPK-pathway leads to the transcription of *sprouty*, which was found to be involved in the cytoskeletal rearrangement in humans and to create a feedback-loop that restricts the FGFR signaling (Lim et al., 2002). As in *Drosophila*, Sprouty would therewith

regulate the proper formation and reorganization of the actin fibers (Miyoshi et al., 2004). Summarized, all elements that are necessary for the signal transduction through an FGF/FGFR-Ras-Rock-Myosin II pathway are transcribed in overlapping domains at the late bud base. In this scenario, FGFf would only play an intermediate role to deliver Wnt8 signals to the FGFRs, thus promoting further processes leading to the detachment of the bud. The further investigation of potential effects of *sprouty* and *wnt8* knockdowns would help to understand the regulation and role of FGFf during the bud detachment.

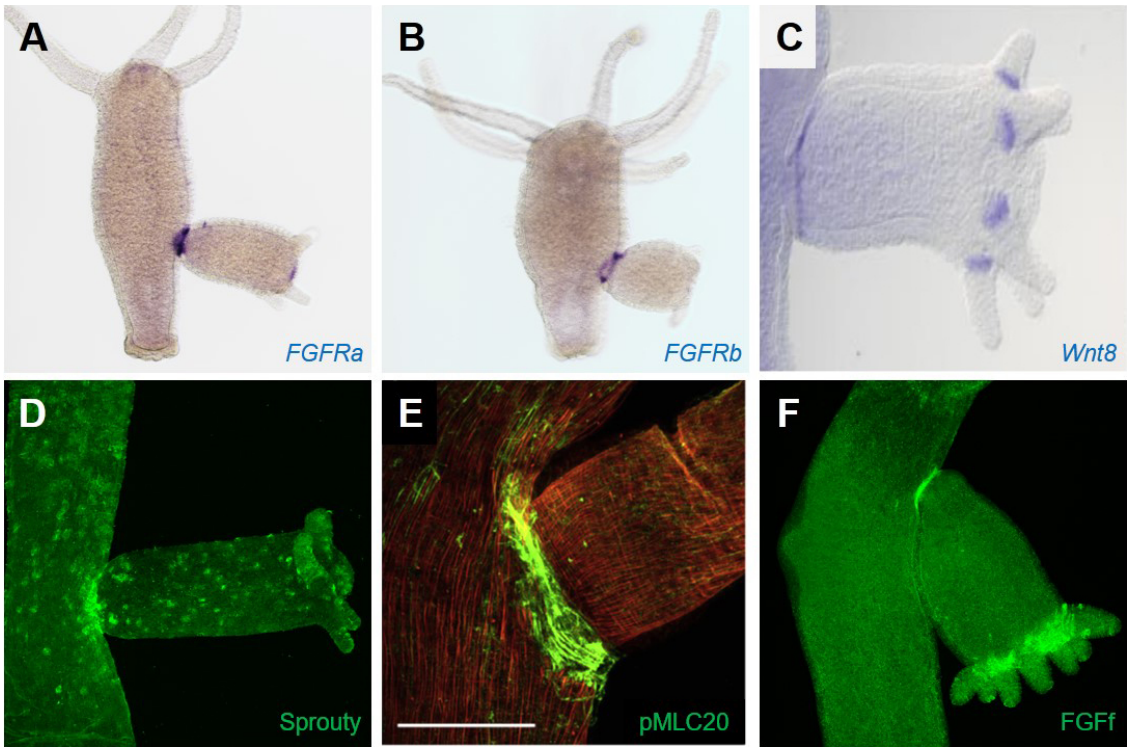

Figure 3.1: Overview of genes involved in the bud detachment. (A–C) The gene expression detected with ISH. (D–F) The protein expression detected via immunodetection. (A) The *FGFRa* transcription in a ring at the late bud base. (B) The *FGFRb* transcription in a ring at the late bud base. (C) The *Wnt8* transcription in a small ring at the late bud base. (E) Sprouty protein accumulates at the late bud base. (E) pMLC20 detects the phosphorylated myosin late chain at the late bud base prior to constriction formation. (F) FGFf is upregulated at the late bud base. (C) Modified after Philipp et al. (2009). (E) Modified after Holz et al. (2020).

3.5.2 FGFf may act in the regeneration of *Hydra*

FGF8 was shown to be important during the limb regeneration in axolotl (Nacu et al., 2016) and *Xenopus* (Shimizu-Nishikawa et al., 2003), so *FGFf*, which belongs into the same FGF family may play a role in the *Hydra* regeneration.

As a first response in the *Hydra* head regeneration, the cells in the head regenerating tips perform apoptosis (Galliot, 2013). Thereby, about 50 % of the cells undergo cell death, whereas in the foot regenerating tips less and delayed cell death occurred. Cell death responses are hereby restricted to i-cells and their derivates. The *FGFf* transcription during the head regeneration sometimes was "patchy", which may be linked to the cells undergoing apoptosis. FGFR signaling cascades were shown to be involved in cell survival and apoptosis (Ornitz & Itoh, 2015). In the mouse forebrain development, it was shown that the cell survival is influenced depending on the FGF8 dosage (Storm et al., 2003): Either no or high amounts of FGF8 increased apoptosis, whereas low FGF8 amounts decreased apoptosis. It was concluded that a high FGF8 concentration activates negative regulators of the FGFR pathway and therefore induce apoptosis. In this case the negative regulator Sprouty was hypothesized to antagonize FGFR signaling as a reaction to high FGF8 concentrations (Storm et al., 2003; Tsang & Dawid, 2004). In *Drosophila*, Sprouty was shown to inhibit cell-survival pathways (Bergmann et al., 1998). During *Hydra* regeneration, the *Sprouty* transcription was not upregulated (Suryawanshi, 2017), which makes a dosage-dependent negative feedback of the FGFR signaling mediated by Sprouty and induced by FGFf implausible. Nevertheless, the involvement of *FGFf* in cell apoptosis may be further investigated by a TUNEL assay (Gavrieli et al., 1992).

Endodermal epithelial cells located at the regenerating head tip express signaling molecules and transcription factors involved in the formation of the head organizer, which is regulated by components of the Wnt signaling pathway (Bode, 2012; Broun et al., 2005). Additionally, endodermal cells digest the apoptotic bodies and show a strong modification in their cell shape, cell connections and apico-basal polarity (Galliot, 2013). Consistent with this, the FGFf gene and protein expression were both upregulated in the endoderm during the first hours of the head regeneration. The transcription of *FGFf* and *FGFRa* during the head regeneration thereby is quite similar (Sudhop, 2006), indicating a potential interaction. For *FGFRa*, a co-expression in tissue that is important for the head organizer was thereby hypothesized. Inhibition with alsterpaullone (ALP), a GSK-3β inhibitor and therefore Wnt pathway activator, leads to the formation of ectopic head and tentacle structures in the *Hydra* body (Broun et al., 2005) and after an ALP treatment, the FGFf protein was expressed at the base of newly forming tentacles (fig. A.9). The transcription of *FGFf* was also upregulated in ectopic tentacles (Lange, 2016), thus indicating a potential interaction of FGFf and Wnt. Furthermore, the regeneration process is induced by injuring the animal, therefore the observed upregulations of the FGFf protein level could also be a consequence of a general gene upregulation cascade

after injury. For *FGFRa* it was shown that it is not upregulated after injury (Sudhop, 2006) indicating that FGF signaling in regeneration is not a response to wound healing but rather specific for the regeneration itself. If the upregulation of FGFf is also not an injury response needs to be further investigated.

3.5.3 FGFf may be involved in the bud and tentacle evagination

Early vertebrate limb development is indicated by a thickening of the lateral plate mesoderm (LPM) that further forms the limb buds. The LPM expresses FGF10 which can stimulate Wnt proteins in the surface ectoderm to build FGF8 (Kawakami et al., 2001; Ohuchi et al., 1997). Upon the onset of the FGF8 protein expression the surface ectoderm forms into the apical ectodermal ridge (AER). FGF8 and FGF10 further create a positive feedback loop, propagated by FGFR2, thereby activating the synthesis of one another (Ohuchi et al., 1997; X. Xu et al., 1998). The AER is important for the sustained outgrowth and development of limbs (Rabinowitz & Vokes, 2012; Zwilling, 1956) and the correct axis formation thereby is promoted by an interaction of FGF, Wnt and BMP signaling pathways (Rabinowitz & Vokes, 2012).

FGFf as a FGF8 homologue may have similar functions in promoting the *Hydra* bud development. The FGFf expression pattern indicates a role as potential bud induction factor. FGFf thereby may act as an attractant source where epithelial and interstitial cells need to move forward to, thus promoting the cell recruitment in the newly forming bud. This theory is supported by the finding of single FGFf positive cells in the developing bud, possibly indicating actively migrating cells. A *Hydra* head organizer under control of the Wnt signaling pathway is localized in the developing bud tip (Bode, 2012; Broun et al., 2005) and the FGFf expression in this area may indicate interactions with the Wnt signaling pathway in the establishment of head structures. Resembling the functions of Wnt during vertebrate limb induction, FGFf may be under control of the Wnt signaling to promote bud evagination. The *FGFRa* transcription was also upregulated in the developing bud tips (Sudhop et al., 2004) and a possible interaction with other FGFs (e.g. FGFb) could result in a feedback loop similar to the FGF10/FGF8/FGFR2 mechanism in vertebrate limb formation (X. Xu et al., 1998). A similar function for FGFf may be hypothesized for the evaginating tentacle buds. Assuming that the bud development in *Hydra* can be compared to limb development in vertebrates, the persisting FGFf expression in the elongating bud tissue may maintain the further outgrowth as found in the establishment of a secondary axis in vertebrates (Rabinowitz & Vokes, 2012; Zwilling,

1956). The interaction of different signaling pathways in *Hydra* budding therefore needs further investigation, as well as FGFf as a potential cell attractant and bud inducer.

3.5.4 FGFf may be a potential migration factor

FGF8 was shown as an important factor during cell migration (Reim et al., 2012; Sun et al., 1999) and different studies showed the importance for FGF signaling in collective cell migration, e.g. in the nephric duct (ND) of chicken (Attia et al., 2015) or in the zebrafish lateral line primordium (LLP) (Lecaudey et al., 2008). In *Drosophila* a dual function of FGFs was found (Bae et al., 2012): In low FGF concentrations, FGF promotes cell migration towards sources with high FGF concentration. When cells reach the FGF source, they start to adhere and differentiate, which is why migration then is stalled. In *Hydra*, a similar function was proposed for FGFf (Lange, 2016). Depending on where FGFf is expressed, it may promote either migration or adhesion and differentiation. Under normal conditions, nematoblasts migrate to terminal structures like tentacle, hypostome and foot where they transdifferentiate (Aufschnaiter et al., 2011; Boehm & Bosch, 2012; David, 2012; Hobmayer & David, 1989). Cells therefore need guidance for their migration and on the other hand a source to move towards to. The FGFf protein was found to be upregulated in patches of cells along the body, suggesting that these patches include nematoblast nests, a high FGFf concentration in the nest may promote the adhesion of the cells in the nematoblast group to one another. Consequently, FGFf would be expressed in a migrating cell collective, as nematoblasts are shown to migrate in groups (David, 2012). Simultaneously, the *FGFf* transcription was upregulated in tentacle base, tentacle tips and foot, where it may function as a source and a differentiation signal for incoming nematoblasts. Other FGFs might as well serve as attractants (e.g. *FGFc* or *FGFb*). This promotes the idea that FGFs create a long reach morphogenic gradient (Balasubramanian & Zhang, 2016; Thotakura et al., 2019; Vemaraju et al., 2012) with low concentrations also in *Hydra* to promote i-cell migration. Once migrating i-cells reach their destination, the interaction of FGFR and FGFs leads to activation of downstream signaling cascades, thus promoting differentiation. Since siRNA mediated knockdown of *FGFf* did not reveal significant effects in the macerates, the potential function of FGFf as a differentiation factor needs further investigation. Pilot experiments led to first insights on the influence of FGFf during the i-cell migration (fig. A.11). The knockdown of *FGFf* by siRNA delayed the migration towards head and foot, indicating that FGFf may has a function during the migration. Migration was also stopped or delayed after an inhibition of *FGFRa* by either siRNA (fig. A.11) or local injection of SU5402 (fig. A.10). As

both experiments were so far only performed once, a further investigation may reveal interesting functions of the FGFR signalling during collective cell migration. In addition, it remains unclear which FGFR is essential for the observed migration effect, as SU5402 and *siFGFRa_1* do not distinguish between FGFRa and FGFRb.

3.6 The *FGFRa* siRNA experiments solidifies its role during the bud detachment and suggests a function during neurogenesis

Previous studies showed the importance of FGFRa during the bud detachment (Hasse et al., 2014; Münder et al., 2010; Sudhop et al., 2004). The inhibition of *FGFRa* results in a non-detaching bud (Sudhop et al., 2004), a phenotype that was well reproduced with the siRNA electroporation. Statistical analysis revealed that *siFGFRa_1* had a significant effect on the detachment of the bud, that is that less buds detached compared to the control group. The analysis via ISH further showed, that in animals that establish this phenotype, the *FGFRa* transcription at the bud base is, as expected, not upregulated. Nevertheless, the siRNA mediated knockdown is not always complete and results in a Y-animal. Instead, the transcription of *FGFRa* after the *siFGFRa_1* was, especially in animals of the *Hydra vulgaris* Zürich strain, often scattered. *FGFRa* is initially transcribed as a broad ring at the bud base, which narrows with progressing bud development (Münder et al., 2010; Sudhop et al., 2004). It was shown that the *FGFRa* transcription was disturbed by treatment with the presenilin inhibitor DAPT, concluding that Notch regulates *FGFRa* and the sharpening of its expression (Münder et al., 2010). The scattered transcription pattern after the *siFGFRa_1* knockdown is comparable to the one after DAPT treatment. Although Notch was shown to regulate *FGFRa* expression in *Hydra*, other cases are known where FGFRs regulate Notch: In the mouse presomitic mesoderm (PSM), which controls cell maturation and is involved in the positioning of segmental boundaries, FGF signaling was shown to act upstream of Notch in the regulation of the segmentation clock (Wahl et al., 2007). As bud detachment in *Hydra* is also a process requiring the formation of boundaries, a similar mechanism is probably involved. FGFRa could inhibit Notch which may lead to the scattered transcription pattern at the bud base. This possibility could be further tested by interaction studies of FGFRa and Notch in *Hydra*.

Another finding of the siRNA studies is that a knockdown of *siFGFRa_1* led to a significant increase of neurons. This coincides with results from previous inhibition

experiments with SU5402 (Nathalie Stei, L3-student, not shown). Studies investigating the cortical development in the CNS in mice found that FGFR regulates the cellular decision between neurogenesis and stem cell renewal by acting through Notch (Rash et al., 2011). A loss of FGFR was found to increase neuronal differentiation from progenitor cells. Notch inhibition was also found to promote neurogenesis during embryogenesis in the cnidarian *Nematostella vectensis*, but not in *Hydra* (Rentzsch et al., 2017). The FGFR signaling pathway was also shown to regulate neuronal induction in amphibians, fish and birds by antagonizing the bone morphogenetic protein (BMP) signaling, whereas in the ascidian sea squirt FGFs rather than BMP inhibitors were mainly inducing neuronal cell fates (Guillemot & Zimmer, 2011; Rentzsch et al., 2017; Stern, 2005). This information can be implied to *Hydra*: The knockdown of *FGFRa* may simultaneously lead to a knockdown of Notch, which in turn regulates the *FGFRa* transcription. This hypothesized feedback loop should be investigated. In addition, the potential interaction of the BMP-signaling pathway and FGFR signaling in *Hydra* should be tested, as this may help to understand the role of FGFR during neuronal differentiation.

3.7 Conclusion and Outlook

This study aimed to gather more information of potential functions of FGFs in *Hydra vulgaris*. Transcriptional and protein analysis, as well as siRNA mediated knockdowns, revealed that some FGFs in *Hydra* are very dynamical expressed and may have overlapping functions. The proper regeneration of *Hydra* may involve at least *FGFb*, *FGFe* and *FGFf*. The i-cell differentiation pathway may be under control of FGFR and *FGFc*. *FGFc* seems to be important for maintaining the self-renewal of I-cell stem cells and their further differentiation, whereas *FGFRa* is supposedly important for neurogenesis in *Hydra*. The migration of small i-cells in *Hydra* seems to be controlled by *FGFRa* and *FGFf*. *FGFf* may function as a chemoattractant source and may promote adhesion in migrating cell collectives. Once the migrating cells reach the FGF source, different FGFs (e.g. *FGFb*, *FGFc*, *FGFf*) may induce the cell differentiation. Bud induction and maintenance may be regulated by *FGFe* and *FGFf* in interaction with the Wnt signaling pathway. *FGFf* may thereby function as a migration and differentiation source, thus creating a concentration gradient. The same principle may apply in tentacle evagination. The detachment of the *Hydra* bud is a highly dynamical process, involving at least one FGFR and several FGFs. *FGFb* may promote mesogloea (ECM) remodeling and *FGFf* may be activated by *Wnt8* to further activate FGFR. The FGFR activation may activate at least two downstream

pathways to further regulate its own signaling: The activation of the Ras-MAPK pathway would activate *Sprouty*, the negative regulator of FGFR signaling. As a second pathway the Rho-Rock-Myosin II pathway would be activated by FGFR to promote cell shape changes important for the constriction formation at the bud base. Sprouty is in addition may regulate this pathway, thus promoting the constriction formation.

Although the described FGFs seem to regulate processes in *Hydra* in a very complex and dynamic way, the proposed functions are mainly derived from transcriptional analysis. To confirm the suggested functions, further functional investigations are necessary. The siRNA electroporation allows a knockdown analysis in an organism that is otherwise genetically difficult to assess. A further stable knockdown e.g. by creating inducible shRNA vectors may give more insight into functions of FGFs and FGFRs in *Hydra*, as the observation is possible over a longer period. Further experiments should include regeneration and migration analysis in normal and knockdown conditions for all described FGFs and FGFRs in *Hydra*. Proliferation and apoptosis could be investigated by using EdU or TUNEL (Gavrieli et al., 1992) assays. Interactional studies with other signaling pathways, e.g. Notch, Wnt and BMP signaling pathways, should be considered to test the suggested pathway interactions. In addition, interactional studies like Yeast-Two-Hybrid (Fields & Song, 1989) may detect which FGFs activate which FGFRs in *Hydra*. The influence of proposed interaction partners like Sprouty should be further investigated by creating *sprouty* knockdowns with subsequent analysis in budding and migration. Expressional studies with ectopically applied *Hydra* FGF proteins may be efficient to test whether FGFs act as cell attractants and whether they are able to induce the bud evagination.

4 Methods

4.1 Model organism

In this study naturally occurring and transgenic lines of the freshwater polyp *Hydra vulgaris* were used as listed in table 4.1.

4.1.1 Cultivation of *Hydra*

All *Hydra* strains were kept at 18 °C in *Hydra* medium with a day and night cycle of 18 hours light and six hours darkness. *Hydra* medium was prepared as described in Klimovich et al. (2019). Polyps were fed 4 times per week with fresh *Artemia salina* and a change of the medium occurred six hours after feeding. The medium was exchanged daily and after feeding. Additionally, once per week, animal dishes were scraped out and cleaned with hot water, VE-water, and *Hydra* medium.

4.1.2 Artificial seawater and *Artemia salina* preparation

Artificial sea water for cultivation of *Artemia salina* was prepared by dissolving 1 kg of sea salt in 30 l of deionized water which was air ventilated overnight at 18 °C. The pH-value was adjusted to 8–8.5 with addition of 5–10 g sodiumbicarbonate. The desired salt concentration of 1.023–1.026 was measured using an araeometer. Half a teaspoon of *A. salina* cysts was added to 1 l of artificial sea water and incubated at 18 °C. Hatching occurred within 60–72 hours. *Artemia* nauplii were, after washing in tap water and exchanging to *Hydra* medium, fed to *Hydra* cultures within 24 h.

Table 4.1: List of *Hydra* strains.

name	alias	details	source
Hydra vulgaris AEP	AEP	Used for generating transgenic animals, as it can produce males and females.	Martin et al., 1997 (cited in Wittlieb et al. (2006)).
Hydra vulgaris Zürich	Zürich	Alternative name: *Hydra attenuata*.	Tardent (1966)
Hydra vulgaris 1184a	Pincher	Can propagate by constricting in the body column instead of forming buds ("pinching" phenotype).	Rob Steele and Robert Campbell
Hydra magnipapillata wt105	wt105	Genome sequenced in the *Hydra* genome project (Chapman et al., 2010).	Originated in a swamp in Mishima, Japan.
Hydra vulgaris AEP Act::GFP $^{\text{endoderm}}$/ Act::RFP $^{\text{ectoderm}}$	endoGFP/ ectoRFP	GFP-positive endodermal cells and RFP-positive ectodermal cells.	Glauber et al. (2015)
Hydra vulgaris AEP Act::GFP $^{\text{ectoderm}}$/ Act::RFP $^{\text{endoderm}}$	endoRFP/ ectoGFP	GFP-positive ectodermal cells and RFP-positive endodermal cells.	Glauber et al. (2015)
Hydra vulgaris AEP Act::GFP $^{\text{interstitial}}$	Icy	GFP-positive small i-cells and derivates in the whole body.	Khalturin et al. (2007)

4.2 *Hydra* methods

4.2.1 Fixation of *Hydra*

Animals were starved out at least 24 hours before fixation. *Hydra* were collected in 1.5 ml Eppendorf reaction tubes and incubated exposed to light for one minute in 2 % urethane to relax animals and especially their tentacles After that, the medium was replaced with 4 % paraformaldehyde (PFA). Samples were incubated at 4 °C overnight using a shaker at 50 rpm. Subsequently, animals were either directly further processed (e.g. for immunodetection) or stored in 100 % methanol (MeOH) at -20 °C (e.g. for *in situ* hybridization (ISH)).

4.2.2 Regeneration series of *Hydra*

For regeneration series, 24 hours starved out, bud-less polyps were bisected with a syringe and both parts were separately cultivated at 18 °C. During the regeneration process, animals were not fed. Fixation took place at specific time points, further indicated as hours after bisection. Fixated halves were then further used for immunodetection or ISH, while keeping the upper and lower halves separated.

4.2.3 Maceration of *Hydra* tissue

Maceration was performed using a modified protocol from Mundie (1926). Three animals were transferred into a 1.5 ml Eppendorf-reaction tube. The medium was removed, and 100 µl maceration solution was added. Samples were incubated for 20 minutes at RT in darkness. Tubes were rolled between hands approximately six to eight times until a turbid solution formed. Cells were fixated by adding 10 µl 37 % formaldehyde and incubating of 10 minutes at RT in the darkness. One drop of Tween80 was added on a poly-L-lysine coated microscope slide to reduce surface tension. Maceration solution was gently mixed and 30 µl of it added into the drop and spread into a rectangle of about 1×2 cm. Sample drying was performed for one hour at 37 °C. For evaluation cells were embedded in 90 % glycerol in *Hydra* medium and checked with phase contrast on a microscope.

4.2.4 Transplantation of *Hydra*

Transplantation of *Hydra* tissue allows e.g. the observation of cell migration. 24 hours unfed *Hydra* were cut in half and upper and lower body halves of different animals were put together with the cutting sides facing each other. Transplantation site of 50 % body length was chosen for better reproducibility. Transplants were prepared on a small insect needle which was stabilized in paraffin in a petri dish covered with *Hydra* medium. Both tissue parts were stabilized with small parts of silicone tubes. Transplants were removed from the needle after incubation at 18 °C for two to three hours, and then put into petri dishes filled with *Hydra* medium. Animals were fed starting the day after transplantation.

4.2.5 Microinjection of adult *Hydra*

Injection was performed using the Eppendorf FemtoJet with the following settings: pi 350 hPa (injection pressure), pc 50 hPa (compensation pressure), ti one second (injection time). As injection needles Eppendorf Femtotips Microinjection Capillary Tips were used. Additionally, self-made injection needles, which were pulled from borosilicate glass capillaries (0.58×1.00×80 mm) using following conditions were used: Magnet Sub: 27.2 (14.9-61.5); Magnet Main: 80 (48.2-103.1); Heater: 80.6 (30.2-700.7); Carriage: 6 (0-10). To modify cell migration in *Hydra* transplants with Icy-animals, local injection with the pharmacological FGFR- inhibitor SU5402 was performed. Transplants of transgenic foot with a non-transgenic head were injected shortly below the transplantation site at one side of the animal. This allowed an internal migration control on the other side of the animal body. Injection had to occur between ecto- and endodermal cells into the mesoglea. For better recognition of the injection site, the fluorescent cell tracker dye DiI was used. Animals were injected several times over a time period of four hours and then kept overnight at 18 °C in the darkness to prevent bleaching of the fluorescence.

4.2.6 Pharmacological inhibition in *Hydra*

24 hours starved out *Hydra* were collected into 6-well plates for pharmacological inhibition. Animals were not fed until end of treatment. The pharmacological inhibition of FGFR was achieved with the inhibitor SU5402 (Mohammadi et al., 1997). Incubation was carried out as described in Hasse et al. (2014). A treatment with alsterpaullone, a GSK-3β inhibitor and therefore Wnt pathway activator, was performed according to Broun et al. (2005).

4.2.7 Electroporation of adult *Hydra*

Animals were collected in a petri dish or Eppendorf reaction tube and washed twice with sterile MilliQ-H_2O. Animals were transferred into an electroporation cuvette (4 mm cuvette, Peqlab) and the medium was changed to electroporation medium (autoclaved MilliQ-H_2O plus substances to electroporate, e.g. siRNA). The cuvette was placed into the electroporation apparatus (square-pulser "Easyject Plus Electroporator" (Equibio)) and animals were electroporated using the following parameters: 300 V, 100 µF, 30 ms. After electroporation, animals were washed shortly with recovery medium and then transferred into a fresh petri dish containing recovery medium. *Hydra* were kept on ice until all animals were electroporated. Animals were kept in recovery medium overnight at 18 °C. The next day, medium was stepwise exchanged to *Hydra* medium and washed several times during the day. Evaluation mostly took place at six days past electroporation according to Lommel et al. (2017). FITC-Dextran was used as a control for electroporation setup (25 mg/ml in sterile water). FITC-Dextran electroporated animals were held in darkness to prevent bleaching of the fluorescence.

4.2.8 siRNA mediated knockdown in *Hydra*

For the siRNA-mediated knockdown approach custom made RP-HPLC siRNA-duplexes were designed and ordered at Kaneka Eurogentec. The siRNAs were electroporated in a final concentration of 3 µM in a total volume of 100 µl as described before. If not indicated otherwise, animals were further processed six days after electroporation. The used siRNA-Duplexes are listed in table 5.1.

4.3 DNA methods

4.3.1 Polymerase Chain reaction (PCR)

For amplification of desired DNA fragments PCR was used (Mullis et al., 1986). PCR reactions and programs in the thermocycler were adjusted according to the polymerase and primers used.

4.3.2 Insert PCR

The insert PCR was performed to linearize the plasmid DNA for probe synthesis. For that, a standard PCR mixture was made. Plasmid DNA (diluted 1:1000 in sterile H_2O)

was used as a template. All components were pipetted on ice and Taq polymerase was added last. PCR reaction was performed in a thermo cycler with program described in table 4.2. To verify positive reactions and to determine the amount of DNA, an agarose gel was poured. PCR products were further stored at -20 °C and used for experiments.

Table 4.2: Insert PCR program. A standard PCR program for the probe synthesis is provided.

step	temperature	time
1. Denturation	96 °C	1 min
2. Annealing	50 °C	1 min
3. Elongation	72 °C	2 min
4. Repeat	go to step 1, repeat 30×	
5. Final elongation	72 °C	10 min
6. Cool down	4 °C	30 min

4.3.3 Agarose gel electrophoresis

Standard agarose gel electrophoresis was used for separation of DNA and RNA fragments. A 1 % gel in 1× TAE was prepared and ran at 120 V for 30 min. Samples were mixed with 6× DNA loading dye. A DNA ladder as a molecular-weight size marker was loaded on a gel. The gel was stained after running in 3× gel red in TAE for 30 min. Gel images were taken using an UV-light and a gel-imager. Desired DNA fragments were purified with the NEB Monarch Kit.

4.3.4 DNA restriction digest

Restriction digest with site-specific endonucleases was performed according to manufacturer's instructions (Thermo Fisher Scientific). For double-digests the best suited buffer for both enzymes was chosen by the help of the manufacturer's "DoubleDigest calculator" tool (Thermo Fisher Scientific). Digested DNA was purified after agarose gel electrophoresis with the NEB Monarch Kit.

4.3.5 DNA ligation

Standard DNA ligation was performed according to manufacturer's protocol (T4 DNA ligase, Thermo Fisher Scientific) at 4 °C overnight. Ligation with commercial cloning

vectors (pGEM®-T easy and CloneJET™ PCR-cloning Kit) were carried out according to manufacturer's instructions. The total amount of DNA was 50–100 ng and the molar ration of vector DNA to insert DNA was 1:3.

4.3.6 Chemical transformation of *E. coli*

Chemically competent bacteria (Sambrook & Russell, 2006) were thawed on ice. A maximum of 10 % ligation mixture or 100 ng of plasmid DNA were added to the bacteria and incubated on ice for 30 min. A heat-shock was performed for 42 s in a 42 °C water bath (Froger & Hall, 2007). Immediately after the heat-shock, samples were put on ice for approximately 2 min. 250 µl of prewarmed (37 °C) LB medium (without antibiotics) was added to the suspension and samples were incubated at 37 °C, 250 rpm for 40–60 min. 150–300 µl of bacteria suspension were plated on pre-warmed LB-plates containing required antibiotics. Colonies were grown overnight at 37 °C. Selected colonies were further grown as a liquid culture, before extracting the plasmid.

4.3.7 Plasmid DNA preparation

For mini-preparation (5 ml) or midi-cultures (50 ml) LB-liquid cultures were inoculated with one colony containing required antibiotics. Incubation occurred at 37 °C and 250 rpm overnight. Preparation of Plasmid DNA was performed using the (NucleoSpin Plasmid, Macherey-Nagel) or (Plasmid midi Kit, Qiagen) according to manufacturer's protocol. Concentration of Plasmid DNA was quantified using a NanoDrop ND1000 apparatus (Thermo Fisher Scientific). Plasmid DNA was stored at -20 °C.

4.3.8 DNA-sequence analysis

Plasmids and PCR-products were sequenced using sanger sequencing (commercial service provided by Microsynth Seqlab). Samples were prepared according to manufacturer's instructions.

4.4 RNA methods

4.4.1 *In vitro* transcription of labelled RNA/ probe synthesis

To synthesize labelled RNA probes for *in situ* hybridization the following protocol was used. Linearized DNA from the insert PCR was diluted 1:100 depending on the construct

either with primers T3/T7 or SP6/T7 and filled into an Eppendorf reaction tube. At RT, DEPC-H_2O and 10× digoxigenin labelling mix was added. Transcription buffer was preheated to 37 °C and added. The RNA polymerase was added directly from -20 °C (T7 or SP6 for antisense probes and T7 or T3 for sense probes, depending on the used vector). All was mixed and shortly centrifuged, before incubating in a water bath at 37 °C for 3 h. Then, 1.25 µl 4 M LiCl and 38 µl 100 % EtOH (both directly from -20 °C) were added for precipitation and the mixture was incubated at -80 °C for at least 30 min. Next, the samples were centrifuged at 4 °C for 30 min. Then, the pellet was washed with 50 µl 70 % EtOH in DEPC-H_2O (from 20 °C) and again centrifuged at 4 °C for 15 min. Pellet was air-dried and resuspended in 50 µl DEPC-H_2O. Aliquots were stored at -20 °C.

4.4.2 Dot Blot

The Dot Blot method was used for measuring the quantity of RNA in synthesized RNA probes for *in situ* hybridization. Probes were diluted in DEPC-H_2O 1:10, 1:50, 1:100, 1:500. For each dilution (and pure probe), 1 µl was pipetted on a Hybond-N+ membrane. Crosslinking occurred either by applying UV light for 3 min or baking the membrane at 80 °C for an hour. After that, the membrane was blocked at RT in blocking solution for at least 30 min. Then, blocking solution was removed and an incubation of the membrane in an antibody solution followed for 30 min. Thereafter, the membrane was washed 2× in washing buffer for 15 min each, then equilibrated in staining buffer for 5 min. Staining solution was added and incubated in darkness for up to 30 min. When dots were clearly visible, the staining reaction was stopped using tap water and finally the membrane was air-dried.

4.4.3 Northern Blot

The Northern Blot method was used for measuring the quality of synthesized RNA probes for *in situ* hybridization.

First, buffer tank, gel tray and gel comb were decontaminated in 0.1 M NaOH for at least 1 h and then washed with VE-H_2O and DEPC-H_2O. Running buffer and gel were both prepared under the fume hood. For the buffer, 10× MOPS, 37 % formaldehyde and DEPC-H_2O were mixed and put in the buffer tank. For the gel, DEPC-H_2O and agarose were heated until the agarose melted. Then, after cooling down to 60 °C, 10× MOPS and 37 % formaldehyde were added and mixed, poured into a gel tray prepared with a comb and left for polymerization for about 30 min. Probes (diluted 1:10, were prepared adding

DEPC-H_2O, 10× MOPS, formaldehyde and formamide. Prepared RNA probes were then heated at 55 °C for 15 min and then shortly put on ice. Then, 2 µl 10× RNA load was added to each sample and the total amount was loaded onto the gel. RNA marker was prepared by heating it up to 70 °C for 10 min, putting it shortly on ice and followed by a short centrifugation step. Gel run was performed under the fume hood at 40 mA for about two to three hours.

Then, the gel was blotted onto a Hybond-N+ membrane using the following assembly scheme: 6 Whatman paper and a membrane in the size of the gel were prepared, as well as one Whatman paper three times as big. The membrane was activated with DEPC-H_2O and Whatman paper soaked in transfer buffer. The transfer chamber was filled with transfer buffer and a plateau was placed in the middle with the long Whatman paper on top. Three Whatman papers were laid on top of the long one and air bubbles rolled out using a Pasteur pipette. Agarose gel was shortly rinsed with DEPC-H_2O, then put head-down on top of the Whatman paper. The activated membrane was added next and thereafter three Whatman paper, again removing all air bubbles with a pasteur pipette. Absorbent paper, a glass plate and a half-filled bottle were put on top to weight it down. The chamber was sealed up with cling wrap and blot transfer was performed at RT overnight.

The next day, agarose gel pockets were marked on the back of the membrane and one corner of the membrane was cut off to bookmark the orientation. Membrane was washed for 3 min in 3× SSC, then crosslinked using either UV light for 3 min or baking the membrane at 80 °C for one hour. After that, the marker lane was separated from the rest of the membrane, incubated in marker staining solution for 10 min, then washed with H_2O until bands appeared. The rest of the membrane was shortly washed with washing buffer, then blocked in blocking solution at RT for 1 h. After washing it shortly with washing buffer it was incubated in antibody solution for at least 30 min. Next, the membrane was washed in washing buffer for 30 min before equilibrating in NTM for 3 min and incubating in membrane staining solution until bands appeared. Staining reaction was stopped by rinsing the membrane with H_2O.

4.4.4 Antibody pre-absorption for ISH

Hydra which were treated in a normal *in situ* hybridization procedure until the antibody step were used for pre-absorption of the anti-digoxigenin-AP or anti-fluorescein-AP antibody. An antibody pre-dilution of 1:400 in blocking solution was added to the animals and incubated at 4 °C and 50 rpm overnight. The next day, blocking solution

was added to a final antibody concentration of 1:2000. For a better preservation 0.01 % sodium azide was added to the final antibody solution and it was stored at 4 °C.

4.4.5 *in situ* hybridization (ISH)

Levels of mRNA in the animals were detected using the technique of *in situ* hybridization. The following protocol was modified after Grens et al. (1996) and Hansen et al. (2000). Unless indicated otherwise all steps were performed at RT and rocking at 50 rpm.

As described above animals were fixed and stored in 100 % MeOH for at least 24 hours. This removed tissue color which reduced background color. First, the medium was replaced with 100 % EtOH until the animals are white (approximately for 5–30 min). After that, the tissues were rehydrated using mixtures of 75 % EtOH and 25 % 1× PBTw, 50 % EtOH and 50 % 1× PBTw, 25 % EtOH and 75 %1× PBTw, for 5 minutes each and then with 100 % 1× PBTw at last for 3×5 min. Next, proteinase K treatment (end concentration 10 µg/ml in 1× PBTw) followed to allow better penetration of the tissue from the RNA probe. This solution was incubated for 15 min for Hydra vulgaris AEP and for 10 min for all other strains. The reaction was stopped by adding 10 µl of a glycine stock (end concentration 4 mg/ml), which was incubated for 10 min. After washing with 1× PBTw for 2×5 min, samples were washed in 0.1 M triethanolamine (TEA) for 5 min, then in a solution of 1 ml TEA and 2.5 µl acetic anhydride for 2×5 min. Animals were washed in 1× PBTw for 2×5 min and then re-fixated in 4 % PFA for 20 min. The fixation solution was washed off by using 5×5 min 1× PBTw. To remove endogenous alkaline phosphatases the animals were incubated at 85 °C in a solution of 1× PBTw and 5 mM EDTA for 10+min. Samples were cooled down to RT before adding freshly prepared hybridization solution and kept at 55 °C for at least 2 h. After 2 h of prehybridization, samples could be stored at -20 °C, but have had to be incubated at 55 °C for 2 h with fresh solution before the next steps. Next, the hybridization solution was added. Therefore, the probe of interest was used in a concentration tested as optimal before in Northern Blot or Dot Blot. The probe first was heated at 100 °C for 1 min. Then hybridization solution was added. After this, the mix was used as a hybridization solution and incubated at 55 °C rocking in a water bath overnight up to three days. Probe solutions were stored in fresh Eppendorf reaction tubes and kept again at -20 °C. Next, samples were washed with a mixture of prewarmed reduced hybridization solution and 50 % 2× SSC at 55 °C for 2×15 min. After that, a solution of preheated 2× SSC and 0.1 % CHAPS was used for washing for 2×30 min. Thereafter the samples were washed with maleic acid buffer (MAB) for 2×10 min. Then the samples were treated in MAB-B for 1 h and after that the

blocking was applied for at 4 °C at least 2 h. Preabsorbed antibody was kept overnight at 4 °C. The next day, washing was performed with MAB for 5, 10, 30 and 5×60 min followed with a last MAB step o/n at 4 °C. Then, samples were incubated in NTMT for 2×5 min and in a solution of NTMT and tetramisole (end concentration 1 mM) for 5 min. After this, the mixture was and switched to a 24 well-plate. Staining solution was added, and staining reaction was performed in the dark. The staining reaction was first checked with a binocular at RT every 5 minutes and later, for slow developing probes at 37 °C. When the color reaction has reached the desired intensity, the staining reaction was stopped by a short washing with NTMT and a washing with 70 % EtOH for 5 minutes and 100 % EtOH with 2×10 min. Samples were embedded using Euparal. After putting on the coverslip, a brass weight was put on top o/n to flatten samples which allows for better detection of the staining during imaging.

For double ISH, a dig-labelled and a fluorescein-labelled probe were incubated in parallel during hybridization steps. As both antibodies (anti-dig and anti-fluo) were coupled to alkaline phosphatase, the staining reactions had to be performed sequentially. The NBT/BCIP reaction was performed first, as the resulting blue staining is more stable during further steps than the staining with FastRed. After reaching the desired color intensity in the first staining reaction, the further steps differed from the protocol above: The staining reaction was stopped by incubation in 100 % EtOH for 30 min. Then, a 10 min incubation step with a solution of 100 mM Glycin-HCl (pH 2.2) and 0.1 % Tween20 followed. Samples were rinsed shortly for 5 times with MAB, then 2 MAB steps with 10 min each followed. Thereafter, an incubation step with MAB-B for 60 min and blocking in blocking solution at 4 °C for at least 2 h followed. Preabsorbed anti-fluorescein antibody was incubated at 4 °C overnight. The next day, the antibody solution was recovered, and samples were washed in MAB at RT (5, 10, 30 and 5×60 min). Preparations for the second staining were made by incubation in NTMT for 2×5 min and in a mixture of 1 ml NTMT and 1 µl tetramisole for 5 min. For the staining solution, FastRed tablets were prepared according to manufacturer's instructions. Staining was performed in the dark and regularly checked. After reaching the desired staining intensity, staining reaction was stopped by washing 2× for 10 min in a mixture PBS and 50 mM EDTA (pH 8). For a better refraction index the samples were kept in the solution at 4 °C overnight). Samples were mounted in a mixture of PBS, 80 % Glycerin and 50 mM EDTA.

4.5 Protein methods

4.5.1 Protein electrophoresis (SDS-PAGE) and western blot

For detection of FGFf protein levels in *Hydra* SDS-polyacrylamide gel electrophoresis (SDS-PAGE) and western blot was performed (Laemmli, 1970). This allowed the analysis and comparison of sizes in denatured proteins. For detection of FGFf 12.5 % polyacrylamide gels were prepared (Sambrook & Russell, 2006). *Hydra* samples were prepared as followed: Per sample, six unfed *Hydra* were centrifuged at 13000 rpm for 3 min to collect animals at the bottom of the reaction tube. The medium was removed, and 25 µl of 2× sample buffer added. The samples were heated at 95 °C for 5 min and suspended in the sample buffer followed by 10 min of heating. After the heat step the samples were kept on ice or stored at -20 °C until usage. A volume of 10 µl protein sample and 5 µl protein marker were loaded on the SDS-polyacrylamide gels. Gels were inserted into the gel run apparatus. Tanks were filled with 1× Laemmli buffer and the rest of the chamber filled to the minimum mark. Combs were pulled out and each pouch rinsed with 1× Laemmli buffer. The gel was run with 200 V for two to three hours, until the sample running front almost reached the end of the gel.

SDS-PAGE separated proteins in the gel were transferred by semi-dry western blotting onto a polyvinylidene fluoride (PVDF) membrane. The transfer- "bed" was prepared with 6× Whatman paper, which was soaked in Bjerrum transfer buffer (Bjerrum & Schäfer-Nielsen, 1986). The gel was equilibrated in transfer buffer for 10 min and then put front down on top of the prepared Whatman paper. Membrane was equilibrated in 100 % MeOH for 10 min, then in transfer buffer for 5 min, then laid on top of the gel. The remaining 6 Whatman papers were soaked in transfer buffer and laid upon the membrane. Supernatant transfer buffer surrounding the setup was removed and the apparatus was closed. The current was set to 1.5 mA per cm2 with the anode at the bottom and the cathode at the top. A small bottle was put on top to weight it down and the western blot did run for approximately 1.5 h.

After the semi-dry western blot, the membrane was further processed to detect the now bound proteins. First, during the dismantling of the setup, the pouches were marked on the membrane. Further, the membrane was washed in washing buffer for 2× for 10 min each. Blocking of unspecific binding sites was performed at RT for at least 2 h or at 4 °C overnight in blocking solution. For the antibody incubation 0.2–0.5 ml/cm2 antibody solution (α-FGFf (rabbit) 1:500 in blocking solution; α- alpha-tubulin (mouse) 1:5000) was used. 5 ml antibody solution was used for a whole membrane. It was

incubated overnight at 4 °C. Subsequently, 6×10 min washing steps in washing buffer were performed, then secondary antibody incubation at RT for 2 h (α-rabbit HRP 1:20000; α-mouse HRP 1:10000; in blocking buffer). Then, samples were washed in washing buffer for 6×10 min Membrane was then washed in VE-H_2O for 2×5 min. For detection of the antibodies, ECL-solution was put in the membrane and the chemiluminescent signal was detected using the LI-COR Odyssey Fc System. Quantification of the blot was made using Fiji.

4.5.2 Immunodetection

Protein levels in the animal were detected using specific antibodies. If not indicated otherwise, incubation was performed at RT and 50 rpm. For the immunodetection *Hydra* were fixed as described above. After fixation, the polyps were washed in 1× PBTx for 4×15 minutes. Thereafter, unspecific binding sites were blocked by incubation for 6–8 hours at room temperature in blocking solution. Primary antibody was diluted in blocking solution and incubated at 4 °C overnight and 50 rpm. The next day, samples were washed with 1× PBTx for 4×15 minutes, following incubation of secondary antibody (diluted in blocking solution) for 2–4 hours. Beginning with secondary antibody incubation, samples were kept in darkness to prevent bleaching of the fluorophores. Secondary antibody was washed off using 1× PBTx for 4–6× for 10 minutes. For additional DAPI staining, DAPI solution was diluted 1:10000 in washing buffer and incubated in one of the washing steps following secondary antibody incubation. For additional Phalloidin staining, Phalloidin-TRITC was diluted 1:500 in washing buffer and incubated for 1 h in a washing step after secondary antibody incubation. In both cases, 2–3 additional washing steps following the incubation were made. At last, samples were washed 1× PBS 2–3 times for 10 min and either stored at 4 °C until the next day or embedded immediately using RotiMount FluorCare.

4.6 Statistical analysis

To determine the significance of the siRNA treatments, an analysis of variance (ANOVA) was performed (Fisher, 1918; Kaufmann & Schering, 2014). To perform an ANOVA the following requirements must be met (Kaufmann & Schering, 2014):

- Independent samples: Fulfilled by experimental design, e.g. each sample was treated with no more than one type of siRNA.

- Normal distribution: The dependent variable has to be normally distributed in each group which was tested by visual inspection of density plots and the Shapiro-Wilk test ($p>0.05$=normal) (Royston, 1982; Shapiro & Wilk, 1965). If needed a log transformation was calculated to normalize the data for further statistical analysis (Curran-Everett, 2018).
- Homogeneity of variance: The variances of the treatment groups have to be equal which was tested using Levene's Test ($p>0.05$=equal) (Levene, 1960).

5 Materials

All chemicals and solutions had p. a. grade. General laboratory equipment and solutions are not specified. Solutions used in different experiments are only listed once.

5.1 *Hydra* materials

5.1.1 *Hydra* husbandry

Solution I (1000×): 42,18 g/l $CaCl_2 \cdot 2\,H_2O$ in MilliQ-H_2O.

Solution II (100×): 14.45 g/l $MgSO_4 \cdot 7\,H_2O$, 4.238 g/l $NaHCO_3$, 1.0985 g/l K_2CO_3 in MilliQ-H_2O.

Artificial sea water: 1000 g (Tropic MarinPro-Reef sea salt) in 30 l VE-H_2O.

Artemia salina cysts: Ocean Nutrition brine Shrimp Eggs; Erdmann, CN ON-151041.

5.1.2 *Hydra* fixation

Paraformaldehyde (PFA): Sigma-Aldrich; 4 % [w/v] in 1× PBS.

Urethan: 2 % [w/v] in *Hydra* medium, sterile filtered.

5.1.3 *Hydra* maceration

Denhardt's (1×): 0.02 % polyvinylpyrrolidone, 0.02 % ficoll, 0.02 % albumin fraction V, 3× SSC, in MilliQ-H_2O. Used for coating of slides.

Formaldehyde (37 %)

Maceration solution: 1:1:13 glycerin: glacial acetic acid: MilliQ-H_2O.

poly-L-lysine: For coating of slides. 10 µl were spread on a slide and dried.

Tween80

5.1.4 *Hydra* transplants

Insect needles: Ento Sphinx, size 000.

Paraffine

Silicone tubes

5.1.5 Pharmacological inhibition of *Hydra*

Adenosine triphosphate (ATP): Roth.

Alsterpaullone (ALP): Sigma-Aldrich; 20 mM stock solution in DMSO.

Alsterpaullone-inhibitor-solution: 5 µM ALP, 0.025 % DMSO, in *Hydra* medium.

Dimethylsulfoxid (DMSO) Roth, CN A994.1.

SU5402: $C_{17}H_{16}N_2O_3$, Calbiochem, CN D00116169, 10 mM stock solution in DMSO.

SU5402-inhibitor solution: 10 µM SU5402, 1 % DMSO, 1 mM ATP in *Hydra* medium.

5.1.6 Microinjection of *Hydra*

FemtoJet: Eppendorf.

Femtotips Microinjection Capillary Tips: Eppendorf.

Low-melt agarose: Roth, 1.6 % in *Hydra* medium + 0.4 % $MgCl_2$.

CellTracker CM-DiI: Thermo Fisher Scientific, CN C7000. 5 mM stock solution.

5.1.7 Electroporation

Dissociation medium: After Gierer et al. (1972). 3.6 mM KCl, 6 mM $CaCl_2$, 1.2 mM $MgSO_4$, 6 mM Na-Citrate, 6 mM pyruvate, 6 mM glucose, 12.5 mM $C_6H_{15}NO_6S$ (TES, pH 6.9), 0.05 g/L rifampicin, 0.10 g/L phenol-red. pH 6.9.

Easyject Plus Electroporator: Equibio, Square-pulser.

Electroporation cuvette: VWR/Peqlab, CN 732-2924, 4 mm, long electrode.

Fluorescein Isothiocyanate (FITC)-Dextran: Sigma-Aldrich, 25 mg/ml in MilliQ-H_2O.

Recovery medium: 80 % *Hydra* medium + 20 % dissociation medium.

5.2 siRNA Duplexes

Table 5.1: List of siRNA duplexes. The sequences of the used siRNA duplexes is provided and the usage indicated. The luciferase (firefly) *pGL2* duplex serves as negative control.

siRNA Duplex	sense sequence	antisense sequence	usage
siFGFRa_1	5'-CAGAGCCAGUU AAUUAUAUdTdT-3'	5'-AUAUAAUUAAC UGGCUCUGdTdT-3'	*FGFRa* knockdown; positive control
siFGFRa_2	5'-ACUGCCAGCUU CAGAAACUdTdT-3'	5'AGUUUCUGAAG CUGGCAGUdTdT-3'	*FGFRa* knockdown; positive control
siFGFRb_1	5'-GGUAGAACAUG UAAUGACUdTdT-3'	5'AGUCAUUACAU GUUCUACCdTdT-3'	*FGFRb* knockdown, extracellular domain
siFGFRb_2	5'-AGGUGAGACUC GAUGAUGdTdT-3'	5'AUCAUCGAGUC UCACCUCdTdT-3'	*FGFRb* knockdown, extracellular domain
siFGFb_1	5'-CCUAACUCAUG GUAUCUAUdTdT-3'	5'AUAGAUACCAU GAGUUAGGdTdT-3'	*FGFb* knockdown
siFGFb_2	5'-CCAACCUUGAU GCCAAGAAdTdT-3'	5'UUCUUGGCAUCA AGGUUGGdTdT-3'	*FGFb* knockdown
siFGFc_1	5'-GUUCAGAGAAC ACCUGAAAdTdT-3'	5'UUUCAGGUGUUC UCUGAACdTdT-3'	*FGFc* knockdown
siFGFc_2	5'-CCAAUAUCAAA CCGACUAUdTdT-3'	5'AUAGUCGGUUU GAUAUUGGdTdT-3'	*FGFc* knockdown
siFGFf_1	5'-GCGAUGCAAUG GAGUUAUAdTdT-3'	5'UAUAACUCCAU UGCAUCGCdTdT-3'	*FGFf* knockdown
siFGFf_2	5'-GUCGAUAUAUG AAGACCAAdTdT-3'	5'UUGGUCUUCAUA UAUCGACdTdT-3'	*FGFf* knockdown
pGL2	5'-CGUACGCGGAA UACUUCGAdTdT-3'	5'-UCGAAGUAUUC CGCGUACGdTdT-3'	negative control, sequence from Elbashir et al. (2001)

5.3 RNA materials

5.3.1 Pharmacological inhibition

10× Digoxigenin-labelling mix: 10 mM ATP, 10 mM CTP, 10 mM GTP, 6.5 mM UTP, 3.5 mM Dig-11-UTP in DEPC-H_2O.

10× Fluorescein labelling mix: 10 mM ATP, 10 mM CTP, 10 mM GTP, 6.5 mM UTP, 3.5 mM Fluo-12-UTP in DEPC-H_2O.

10× transcription buffer: Roche.

DEPC (diethylpyrocarbonate): Sigma-Aldrich.

DEPC-H_2O: 400 µl DEPC / 1 l MilliQ-H_2O, left overnight, then autoclaved.

Digoxigenin-11-UTP: Roche.

Fluorescein-12-UTP: Roche.

LiCl: 4 M.

Ribonucleoside Triphosphate Set: Roche.

SP6 RNA Polymerase: Roche 20 U/µl.

T3 RNA Polymerase: Roche 20 U/µl.

T7 RNA Polymerase: Roche 20 U/µl.

Transcription reaction: 6 µl DEPC-H_2O, 1 µl 10× transcription buffer, 1 µl 10× Digoxigenin (or fluorescein) labelling mix, 1 µl linearized DNA (Insert PCR, 1:100 dilution), 1 µl RNA polymerase.

5.3.2 Northern Blot and Dot Blot

Amersham Hybond-N+ membrane: GE Healthcare; positively charged Nylon transfer membrane.

Anti-Digoxigenin-AP Fab fragments: Roche, 1:5000 dilution in washing buffer.

Anti-Fluorescein-AP Fab fragments: Roche, 1:5000 dilution in washing buffer.

Blocking solution (Dot Blot): 1 % blocking reagent in 0.1 M maleic acid buffer + 0.15 M NaCl, pH 7.5 .

Blocking buffer (Northern blot): 0.5 % blocking reagent in washing buffer.

Blocking Reagent: Roche.

Blot staining solution: NBT/BCIP in NTM (20 µl/ml).

Marker staining solution: 0.02 % methylene blue in 0.3 M Na-acetate pH 5.5.

MOPS-buffer (10×): 20.45 g MOPS, 10 ml EDTA (0.5 M, pH 8), 2.05 g Na-acetate, ad 400 ml MilliQ-H_2O. Titrate to pH 7 with 10 N NaOH, fill up to 500 ml. Sterile filtered, kept dark.

Northern blot gel: 36.8 ml DEPC-H_2O + 0.4 g agarose, melt, cooldown to 60 °C. Add 9 ml formaldehyde (37 %) + 5 ml MOPS buffer (10×).

Northern blot running buffer: 35 ml MOPS buffer (10×), 62.5 ml formaldehyde (37 %), 252.5 ml DEPC-H_2O.

Northern blot samplesv 4.5 µl DEPC-H_2O, 1 µl MOPS buffer (10×), 3.5 µl formamide, 1 µl RNA probe (diluted 1:10).

NTM: 100 mM NaCl, 100 mM Tris-HCL pH 9.5, 50 mM MgCl2 in DEPC-H_2O.

RNA-load (10×): 50 % glycerine, 1mM EDTA (pH 8), 0.4 % bromphenolblue, 0.4 % xylencyanol. Sterile filtered.

RNA marker RiboRuler HR RNA ladder ready-to-use: Thermo Fisher Scientific.

SSC (20×)v 3 M NaCl, 0.3 M Na-Citrate, 400 µl DEPC. Left overnight, then autoclaved.

Staining solution: 20 µl/ml NBT/BCIP in NTM.

Transfer bufferv 20× SSC, reusable.

Washing buffer: 100 mM Tris (pH 7.5), 150 mM NaCl in DEPC-H_2O.

Whatman paper: 3 mm.

5.3.3 *In situ* hybridization

Albumin fraction V (BSA): Roth, protease-free, 100 %.

Acetic anhydride: Roth.

Anti-Digoxigenin-AP Fab fragments: Roche, preabsorbed, 1:2000 dilution in blocking solution, reusable.

Anti-Fluorescein-AP Fab fragments: Roche, preabsorbed, 1:2000 dilution in blocking solution, reusable.

Blocking solution: 80 % MAB-B + 20 % sheep serum.

CHAPS: $C_{32}H_{58}N_2O_7S$, 10 % in DEPC-H_2O, sterile filtered.

Denhardt's (50×): 1% polyvinylpyrrolidone, 1% ficoll, 1% BSA fraction V in DEPC-H_2O, sterile filtered.

EDTA (ISH): 0.5 M, pH 8.0.

Formamide: 100 %, deionised.

Glycin-HCL: 100 mM, pH 2.2.

Glycine stock solution: 40 mg/ml in DEPC-H_2O, sterile filtered.

Heparin: 10 mg/ml in DEPC-H_2O.

Hybridization solution: 50 % formamide (v/v), 5 × SSC, 200 µg/ml Torula RNA, 0.1 % Tween20 (v/v), 0.1 % CHAPS (w/v), 1× Denhardt's, 10 µg/ml Heparin in DEPC-H_2O.

MAB: 100 mM maleic acid buffer, 150 mM NaCl, pH 7.5 in DEPC-H_2O, autoclaved.

MAB-B: MAB + 1 % albumin fraction V (BSA).

NBT/BCIP Stock Solution: Roche, Used 20 µl /ml in NTMT + Tetramisole (end conc. 1 mM).

NTMT: NTM + 0.1 % Tween20.

PBS (10×): 1.5 M NaCl, 0.08 M $Na_2HPO_4 - 2\,H_2O$, 0.02 KH_2PO_4-H_2O, 400 µl DEPC, pH 7.4. Left overnight, then autoclaved.

PBS/Glycerin: 20 % 1× PBS + 80 % Glycerin.

PBTw (1×): 100 ml 10× PBS / 1 l DEPC-H_2O + 0.1 % Tween20.

Proteinase K: Roche, recombinant PCR Grade, stock solution 10 mg/ml in DEPC-H_2O.

Reduced hybridization solution: 50 % formamide (v/v), 5× SSC, 0.1 % Tween20 (v/v), 0.1 % CHAPS (w/v) in DEPC -H_2O.

sheep serum: 100 %, heat inactivated.

SIGMAFast TM FastRed TR/ Naphtol AS-MX tablets: Sigma-Aldrich.

Sodium-azide: 10 % stock solution in MilliQ-H_2O.

Staining solution: NTMT + Tetramisole (end conc. 1 mM) + 20 µl/ml NBT/BCIP.

Triethanolamine (TEA): 0.1 M in DEPC-H_2O, pH 7.8, sterile filtered.

Torula RNA: 10 mg/ml in DEPC-H_2O, phenol extracted.

Tween20: stock solution 10 % in DEPC-H_2O.

Tetramisole: 1 M in DEPC-H_2O.

5.4 Protein materials

5.4.1 Immunodetection

Blocking solution: 2 % Albumin fraction V (BSA) in 1× PBTx.

Na-phosphate buffer (0.1 M): 3.1 g $NaH_2PO_4 \cdot H_2O$ (MW 137,99 g/mol) + 10.9 g Na_2HPO_4 (MW 141.99 g/mol) in 1 l MilliQ-H_2O, pH 7.4, autoclaved.

PBS (10×): 1.5 M NaCl in 0.1 M Na-phosphate buffer, pH 7.4, autoclaved.

PBTx (1×): 1× PBS + 0.25 % Triton X-100.

Triton X-100: 10 % stock solution in MilliQ-H_2O.

Phalloidin-TRITC: $C_{62}H_{72}N_{12}O_{12}S_4$, Sigma-Aldrich, CN P1951. 0.5 mg/ml stock solution. 1:150 dilution in immunodetection.

DAPI, dilactate: $C_{16}H_{15}N_5 \cdot 2\,HCl$, Sigma-Aldrich. 5 mg/ml stock solution. 1:10000 dilution in immunodetection.

RotiMount FluorCare: Roth, CN HP19.1.

Anti-GFP mouse: Abcam, CN ab1218. 1:500 dilution in immunodetection.

Anti-FGFf rabbit: Davids Biotechnologie GmbH. 1:100 dilution in immunodetection. Specific for *Hydra* FGFf. epitope: EVNKLNDEIEKMKLENLKKN.

Fluorescein (FITC) AffiniPure Rabbit Anti-Mouse IgG (H+L) : Anti-rabbit FITC, JacksonImmuno Research, CN 315-095-003. Used 1:750 dilution in immunodetection.

Anti-mouse Alexa488: Abcam, 1:1000 dilution in immunodetection.

Goat Anti-Rabbit IgG H&L (Alexa Fluor 488) Abcam, CN ab150077, 1:000 dilution in immunodetection.

Goat Anti-Rabbit IgG FITC: Sigma-Aldrich, CN F9887-1ML, 1:750 dilution in immunodetection.

5.4.2 SDS-PAGE and Western Blot

Luminol sodium salt: Sigma-Aldrich, CN A4685.

Acrylamide: 30 % stock solution.

Anti-α-Tubulin Mouse: Sigma-Aldrich, 1:500 dilution, in western blot.

Anti-FGFf rabbit: Davids Biotechnologie, 1:500 dilution, in western blot. Epitope: EVNKLNDEIEKMKLENLKKN.

Ammoniumperoxodisulfat (APS): 10 % stock solution in MilliQ-H_2O.

Bjerrum buffer (10×): 48 mM TRIS, 39 mM Glycin, 0.1 % SDS.

Bjerrum transfer buffer: 20 ml 10× Bjerrum buffer, 40 ml MeOH, 140 ml MilliQ-H_2O.

Blocking buffer: 5 % casein in washing buffer.

ECL-solution: 1 ml SA + 0.3 µl H_2O_2 (30 %) + 100 µl SB.

Goat anti-Rabbit IgG (H+L) Cross-Adsorbed Sec. Antibody, HRP: Thermo Fisher Scientific, CN G-21234, 1:20000 dilution.

Goat anti-Mouse IgG (H+L) Cross-Adsorbed Sec. Antibody, HRP: Thermofisher Scientific, CN G-21040, 1:10000 dilution.

SE300 miniVE Int. Vertical Protein Electrophoresis & Blotting Unit: Hoefer Serva, CN SE300-10A-1.0.

Laemmli buffer (10×): 250 mM Tris, 1.92 M Glycine, pH 8.3–8.4.

Laemmli buffer (1×): dilute from 10× Laemmli buffer + 0.1 % SDS.

Laemmli sample buffer (2×): 2 % SDS, 20 % Glycerin, 2 % β-mercaptoethanol, 20 mM Tris-HCL (pH 6.8), 0.025 % bromphenolblue.

Odyssey Fc Imaging System: LI-COR Biotechnology.

PageRuler™ Plus Prestained Protein Ladder,10 to 250 kDa: Thermo Fisher Scientific, CN 26619.

p-Coumaric acid: Sigma-Aldrich, CN C9008.

PBS (10×): 87.7 g NaCl/ l, 0.1 M phosphate buffer, pH 7.4.

Phosphate buffer (0.1 M): 0.1 M $NaH_2PO_4 \cdot H_2O$ + 0.1 M Na_2HPO_4 in MilliQ-H_2O, mixed until pH 7.4 was reached, autoclaved.

PVDF membrane

SDS: 10 % stock solution.

Solution A (SA): 200 ml 0.1 TRIS-HCL (pH 8.6) + 50 mg Luminol.

Solution B (SB): 11 mg p-Coumaric acid in 10 ml DMSO.

Tetramethylethylenediamine (TEMED): Sigma-Aldrich.

Tris-HCL: pH 8.8 & pH 6.8.

Washing buffer: 1x PBS + 0.1 % Triton X-100.

5.5 Cloning materials

5.5.1 Oligonucleotides

All PCR oligonucleotides were purchased in HPLC-quality at Sigma-Aldrich. The primer sequence is given in 5' → 3' direction. Enzyme restriction sites are given in bold letters. Primer pairs for *FGFa*, *FGFc*, *FGFe* and *FGFf* are listed in Lange et al. (2014). T3, T7 and SP6 were standard oligonucleotides.

H6_FGFb_fw 1: **CATATG**ATATTGCTTCAAAGTTTTTTTGAG

H6_FGFb_rv 1: **GAATTC**TTATGCTTTCTGCTTTTTTCC

FGFRb_ex fw: GTCCCTGTGTAATAAGCAAAATG

FGFRb_ex rv: TGAGGGTTAGGTAGAAATGCAG

5.5.2 Enzymes

Pfu DNA Polymerase: Promega, CN M7741.

Pwo SuperYield DNA Polymerase Sigma-Aldrich, CN 4340868001.

Restriction enzymes & Buffers: Thermo Fisher Scientific.

T4 DNA-ligase: Thermofisher Scientific.

Taq-DNA-Polymerase: Axon Labortechnik, CN 22466.

5.5.3 Bacteria

XL1-blue: Agilent Technologies/Stratagene, *endA1 gyrA96(nalR) thi-1 recA1 relA1 lac glnV44 F'[::Tn10 proAB+ lacIq Δ(lacZ)M15] hsdR17(rK- mK+).*

DH5α: *fhuA2 lac(del)U169 phoA glnV44 Φ80' lacZ(del)M15 gyrA96 recA1 relA1 endA1 thi-1 hsdR17.*

5.5.4 Vectors

pBluescript SK (+): Agilent Technologies/Stratagene.

pJet1.2/blunt: Thermo Fisher Scientific.

pGEM-T Easy Vector: Promega.

LigAF: *Hydra* specific expression vector, Bosch lab, Kiel, Germany.

pQE-TriSystem: Qiagen.

5.5.5 Kits

Monarch DNA Gel Extraction Kit: New England Biolabs, CN T1020L.

NucleoSpin Gel and PCR Clean-up: Macherey-Nagel.

NucleoSpin Plasmid: Macherey-Nagel.

Qiagen Plasmid Midi Kit: Qiagen, CN 12145.

CloneJET PCR-cloning Kit: Thermo Fisher Scientfic, CN K1232.

pGEM-T easy Vector Systems: Promega, CN A1360.

5.6 Additional chemicals, substances, and reagents

Agarose-Gel: 1% Agarose in 1× TAE buffer.

DNA Gel Loading Dye (6×): Thermo Fisher Scientific, CN R0611.

GeneRuler DNA Ladder Mix, ready-to-use: Thermo Fisher Scientific, CN SM0334.

GelRed Nucleic Acid Gel Stain: Biotium.

Luria-Bertani (LB)-Medium: 1 % (w/v) Bacto-Trypton, 0.5 % (w/v) yeast extract, 1 % (w/v) NaCl, in MilliQ-H2O. pH 7.5, then autoclaved.

LB-Agar: 1.5% Agar-Agar in liquid LB-Medium.

LB-Amp plates: 100 µg/ml Ampicillin in LB-Agar.

LB-Kan plates: 50 µg/ml Kanamycin in LB-Agar.

TAE buffer (50×): 242 g Tris base (pH 8.0), 57.1 ml glacial acetic acid, 100 ml 0.5 M EDTA (pH 8), in 1 l MilliQ-H_2O.

5.7 Software and online tools

Fiji: Schindelin et al. (2012).

Image Studio 5.2: LI-COR Biotechnology.

Leica LAS AF Lite: Leica Microsystems.

Microsoft Office: Microsoft Corporation.

Oligo Analyzer Tool: https://eu.idtdna.com/pages

LaTeX: Typesetting software (Lamport, 1994).

R: Open source programming language for statistical computing (R Core Team, 2020).

ggplot2: Graphical package for R (Wickham, 2016).

Bibliography

Abraham, J. A., Mergia, A., Whang, J. L., Tumolo, A., Friedman, J., Hjerrild, K. A., Gospodarowicz, D., & Fiddes, J. C. (1986). Nucleotide sequence of a bovine clone encoding the angiogenic protein, basic fibroblast growth factor. *Science*, *233*(4763), 545–548. https://doi.org/10.1126/science.2425435

Abraham, J. A., Whang, J. L., Tumolo, A., Mergia, A., Friedman, J., Gospodarowicz, D., & Fiddes, J. C. (1986). Human basic fibroblast growth factor: nucleotide sequence and genomic organization. *The EMBO journal*, *5*(10), 2523–8.

Agata, K., Saito, Y., & Nakajima, E. (2007). Unifying principles of regeneration I: Epimorphosis versus morphallaxis. https://doi.org/10.1111/j.1440-169X.2007.00919.x

Agrawal, N., Dasaradhi, P. V. N., Mohmmed, A., Malhotra, P., Bhatnagar, R. K., & Mukherjee, S. K. (2003). RNA Interference: Biology, Mechanism, and Applications. *MICROBIOLOGY AND MOLECULAR BIOLOGY REVIEWS*, *67*(4), 657–685. https://doi.org/10.1128/MMBR.67.4.657-685.2003

Alzheimer, C., & Werner, S. (2003). Fibroblast Growth Factors and Neuroprotection. *Cell* (pp. 335–351). https://doi.org/10.1007/978-1-4615-0123-7_12

Ambrosone, A., Marchesano, V., Tino, A., Hobmayer, B., & Tortiglione, C. (2012). Hymyc1 downregulation promotes stem cell proliferation in hydra vulgaris. *PLoS One*, *7*(1). https://doi.org/10.1371/journal.pone.0030660

Armelin, H. A., & Sato, G. (1973). Pituitary Extracts and Steroid Hormones in the Control of 3T3 Cell Growth (mouse fibroblasts/growth factor). *Proceedings of the National Academy of Sciences*, *70*(9), 2702–2706.

Arvizu, F., Aguilera, A., & Salgado, L. M. (2006). Activities of the protein kinases STK, PI3K, MEK, and ERK are required for the development of the head organizer in Hydra magnipapillata. *Differentiation*, *74*(6), 305–312. https://doi.org/10.1111/j.1432-0436.2006.00078.x

Attia, L., Schneider, J., Yelin, R., & Schultheiss, T. M. (2015). Collective cell migration of the nephric duct requires FGF signaling. *Developmental Dynamics*, *244*(2), 157–167. https://doi.org/10.1002/dvdy.24241

Aufschnaiter, R., Wedlich-Söldner, R., Zhang, X., & Hobmayer, B. (2017). Apical and basal epitheliomuscular F-actin dynamics during Hydra bud evagination. *Biology Open*, *6*(8), 1137–1148. https://doi.org/10.1242/bio.022723

Aufschnaiter, R., Zamir, E. A., Little, C. D., özbek, S., Münder, S., David, C. N., Li, L., Sarras, M. P., & Zhang, X. (2011). In vivo imaging of basement membrane movement: ECM patterning shapes Hydra polyps. *Journal of Cell Science*, *124*(23), 4027–4038. https://doi.org/10.1242/jcs.087239

Babonis, L. S., & Martindale, M. Q. (2017). PaxA, but not PaxC, is required for cnidocyte development in the sea anemone Nematostella vectensis. *EvoDevo*, *8*(1), 14. https://doi.org/10.1186/s13227-017-0077-7

Bae, Y. K., Trisnadi, N., Kadam, S., & Stathopoulos, A. (2012). The role of FGF signaling in guiding coordinate movement of cell groups guidance cue and cell adhesion regulator? *Cell Adhesion and Migration*, *6*(5), 397–403. https://doi.org/10.4161/cam.21103

Balasubramanian, R., & Zhang, X. (2016). Mechanisms of FGF gradient formation during embryogenesis. https://doi.org/10.1016/j.semcdb.2015.10.004

Basilico, C., & Moscatelli, D. (1992). The fgf family of growth factors and oncogenes. *Advances in Cancer Research*, *59*(100), 115–165. https://doi.org/10.1016/S0065-230X(08)60305-X

Baulcombe, D. C. (1999). Fast forward genetics based on virus-induced gene silencing. *Current Opinion in Plant Biology*, *2*(2), 109–113. https://doi.org/10.1016/S1369-5266(99)80022-3

Beenken, A., & Mohammadi, M. (2009). The FGF family: Biology, pathophysiology and therapy. https://doi.org/10.1038/nrd2792

Beenken, A., & Mohammadi, M. (2012). The structural biology of the FGF19 subfamily. *Advances in Experimental Medicine and Biology*, *728*, 1–24. https://doi.org/10.1007/978-1-4614-0887-1_1

Belov, A. A., & Mohammadi, M. (2013). Molecular mechanisms of fibroblast growth factor signaling in physiology and pathology. *Cold Spring Harbor Perspectives in Biology*, *5*(6). https://doi.org/10.1101/cshperspect.a015958

Bergmann, A., Agapite, J., McCall, K., & Steller, H. (1998). The Drosophila gene hid is a direct molecular target of ras-dependent survival signaling. *Cell*, *95*(3), 331–341. https://doi.org/10.1016/S0092-8674(00)81765-1

Berking, S. (2003). A model for budding in hydra: pattern formation in concentric rings. *Journal of Theoretical Biology*, *222*, 37–52. https://doi.org/10.1016/S0022-5193(03)00012-2

Bernstein, E., Caudy, A. A., Hammond, S. M., & Hannon, G. J. (2001). Role for a bidentate ribonuclease in the initiation step of RNA interference. *Nature*, *409*(6818), 363–366. https://doi.org/10.1038/35053110

Bertrand, S., Iwema, T., & Escriva, H. (2014). FGF signaling emerged concomitantly with the origin of eumetazoans. *Molecular Biology and Evolution*, *31*(2), 310–318. https://doi.org/10.1093/molbev/mst222

Bibb, C., & Campbell, R. D. (1972). Tissue Healing a N D Septate. *Cell*, *5*(October).

Birge, R. B., Kalodimos, C., Inagaki, F., & Tanaka, S. (2009). Crk and CrkL adaptor proteins: Networks for physiological and pathological signaling. https://doi.org/10.1186/1478-811X-7-13

Bjerrum, O., & Schäfer-Nielsen, C. (1986). Buffer systems and transfer parameters for semidry electroblotting with a horizontal apparatus. *Analytical electrophoresis*, 315–327.

Blanca, M. J., Alarcón, R., Arnau, J., Bono, R., & Bendayan, R. (2017). Non-normal data: Is ANOVA still a valid option? *Psicothema*, *29*(4), 552–557. https://doi.org/10.7334/psicothema2016.383

Bode, H. R. (1983). Reducing Populations of Interstitial Cells and Nematoblasts with Hydroxyurea. *Hydra: Research methods* (pp. 291–294). Springer US. https://doi.org/10.1007/978-1-4757-0596-6_39

Bode, H. R. (1996). The interstitial cell lineage of hydra: a stem cell system that arose early in evolution. *Journal of cell science*, *109 (Pt 6*, 1155–1164.

Bode, H. R. (2003). Head regeneration in Hydra. *Developmental dynamics: an official publication of the American Association of Anatomists*, *226*(2), 225–236. https://doi.org/10.1002/dvdy.10225

Bode, H. R. (2009). Axial patterning in hydra. *Cold Spring Harbor perspectives in biology*, *1*(1), a000463. https://doi.org/10.1101/cshperspect.a000463

Bode, H. R. (2011). Axis Formation in Hydra. *Annual Review of Genetics*, *45*(1), 105–117. https://doi.org/10.1146/annurev-genet-102209-163540

Bode, H. R. (2012). The head organizer in Hydra. *International Journal of Developmental Biology*, *56*(6-8), 473–478. https://doi.org/10.1387/ijdb.113448hb

Bode, H. R., Heimfeld, S., Koizumi, O., Llttlefield, C. L., & Yaross, M. S. (1988). Maintenance and regeneration of the nerve net in hydra. *Integrative and Comparative Biology*, *28*(4), 1053–1063. https://doi.org/10.1093/icb/28.4.1053

Boehm, A. M., & Bosch, T. C. (2012). Migration of multipotent interstitial stem cells in Hydra. *Zoology*, *115*(5), 275–282. https://doi.org/10.1016/j.zool.2012.03.004

Boehm, A. M., Khalturin, K., Anton-Erxleben, F., Hemmrich, G., Klostermeier, U. C., Lopez-Quintero, J. A., Oberg, H. H., Puchert, M., Rosenstiel, P., Wittlieb, J., & Bosch, T. C. (2012). FoxO is a critical regulator of stem cell maintenance in immortal Hydra. *Proceedings of the National Academy of Sciences of the United States of America*, *109*(48), 19697–19702. https://doi.org/10.1073/pnas.1209714109

Boilly, B., Vercoutter-Edouart, A. S., Hondermarck, H., Nurcombe, V., & Le Bourhis, X. (2000). FGF signals for cell proliferation and migration through different pathways. *Cytokine and Growth Factor Reviews*, *11*(4), 295–302. https://doi.org/10.1016/S1359-6101(00)00014-9

Bökel, C., & Brand, M. (2013). Generation and interpretation of FGF morphogen gradients in vertebrates. *Current Opinion in Genetics and Development*, *23*(4), 415–422. https://doi.org/10.1016/j.gde.2013.03.002

Bosch, T. C. (2007). Why polyps regenerate and we don't: Towards a cellular and molecular framework for Hydra regeneration. https://doi.org/10.1016/j.ydbio.2006.12.012

Bosch, T. C., Anton-Erxleben, F., Hemmrich, G., & Khalturin, K. (2009). The Hydra polyp: Nothing but an active stem cell community. *Development, Growth and Differentiation*, *52*(1), 15–25. https://doi.org/10.1111/j.1440-169X.2009.01143.x

Bosch, T. C., & David, C. N. (1986). Male and female stem cells and sex reversal in Hydra polyps. *Proceedings of the National Academy of Sciences*, *83*(24), 9478–9482. https://doi.org/10.1073/pnas.83.24.9478

Bosch, T. C., & Fujisawa, T. (2001). Polyps, peptides and patterning. *BioEssays*, *23*(5), 420–427. https://doi.org/10.1002/bies.1060

Böttger, A., Alexandrova, O., Cikala, M., Schade, M., Herold, M., & David, C. N. (2002). GFP expression in Hydra: Lessons from the particle gun. *Development Genes and Evolution*, *212*(6), 302–305. https://doi.org/10.1007/s00427-002-0245-0

Böttger, A., Doxey, A. C., Hess, M. W., Pfaller, K., Salvenmoser, W., Deutzmann, R., Geissner, A., Pauly, B., Altstätter, J., Münder, S., Heim, A., Gabius, H. J., McConkey, B. J., & David, C. N. (2012). Horizontal Gene Transfer Contributed to the Evolution of Extracellular Surface Structures: The Freshwater Polyp Hydra Is Covered by a Complex Fibrous Cuticle Containing Glycosaminoglycans and Proteins of the

PPOD and SWT (Sweet Tooth) Families. *PLoS ONE*, *7*(12). https://doi.org/10.1371/journal.pone.0052278

Böttger, A., & Hassel, M. (2012). Hydra, a model system to trace the emergence of boundaries in developing eumetazoans. *International Journal of Developmental Biology*, *56*(6-8), 583–591. https://doi.org/10.1387/ijdb.113454ab

Brewer, J. R., Mazot, P., & Soriano, P. (2016). Genetic insights into the mechanisms of Fgf signaling. *Genes & development*, 751–771. https://doi.org/10.1101/gad.277137.115. GENES

Broun, M., & Bode, H. R. (2002). Characterization of the head organizer in hydra. *Development*, *129*(4).

Broun, M., Gee, L., Reinhardt, B., & Bode, H. R. (2005). Formation of the head organizer in hydra involves the canonical Wnt pathway. *Development*, *132*(12), 2907–2916. https://doi.org/10.1242/dev.01848

Burdine, R. D., Chen, E. B., Kwok, S. F., & Stern, M. J. (1997). egl-17 encodes an invertebrate fibroblast growth factor family member required specifically for sex myoblast migration in Caenorhabditis elegans. *Proceedings of the National Academy of Sciences of the United States of America*, *94*(6), 2433–2437. https://doi.org/10.1073/pnas.94.6.2433

Burnett, A. L. (1966). The acquisition, maintenance and lability of the differentiated state in hydra.

Campbell, R. D. (1967). Tissue dynamics of steady state growth in Hydra littoralis. II. Patterns of tissue movement. *Journal of Morphology*, *121*(1), 19–28. https://doi.org/10.1002/jmor.1051210103

Carter, J. A., Hyland, C., Steele, R. E., & Collins, E. M. S. (2016). Dynamics of Mouth Opening in Hydra. *Biophysical journal*, *110*(5), 1191–1201. https://doi.org/10.1016/j.bpj.2016.01.008

Cebrià, F., Nakazawa, M., & Mineta, K. (2002). Dissecting planarian central nervous system regeneration by the expression of neural-specific genes. *Development Growth and Differentiation*, *44*(2), 135–146. https://doi.org/10.1046/j.1440-169x.2002.00629.x

Chapman, J. A., Kirkness, E. F., Simakov, O., Hampson, S. E., Mitros, T., Weinmaier, T., Rattei, T., Balasubramanian, P. G., Borman, J., Busam, D., Disbennett, K., Pfannkoch, C., Sumin, N., Sutton, G. G., Viswanathan, L. D., Walenz, B., Goodstein, D. M., Hellsten, U., Kawashima, T., … Steele, R. E. (2010). The dynamic genome of Hydra. *Nature*, *464*, 592–596. https://doi.org/10.1038/nature08830

Clarkson, S. G., & Wolpert, L. (1967). Bud morphogenesis in hydra. *Nature*, *214*(5090), 780–783. https://doi.org/10.1038/214780a0

Cogoni, C., & Macino, G. (2000). Post-transcriptional gene silencing across kingdoms. *Current Opinion in Genetics and Development*, *10*(6), 638–643. https://doi.org/10.1016/S0959-437X(00)00134-9

Cottrell, G. A., Green, K. A., & Davies, N. W. (1990). The neuropeptide Phe-Met-Arg-Phe-NH_2 (FMRFamide) can activate a ligand-gated ion channel in Helix neurons. *Pflügers Archiv*, *416*(5), 612–614. https://doi.org/10.1007/BF00382698

Coulier, F., Pontarotti, P., Roubin, R., Hartung, H., Goldfarb, M., & Birnbaum, D. (1997). Of worms and men: An evolutionary perspective on the fibroblast growth factor (FGF) and FGF receptor families. *Journal of Molecular Evolution*, *44*(1), 43–56. https://doi.org/10.1007/PL00006120

Cristino, L., Guglielmotti, V., Musio, C., & Santillo, S. (2007). Diffuse nerve net of hydra revealed by NADPH-diaphorase histochemical labeling. *Lecture Notes in Computer Science (including subseries Lecture Notes in Artificial Intelligence and Lecture Notes in Bioinformatics)*, *4729 LNCS*, 11–20. https://doi.org/10.1007/978-3-540-75555-5_2

Cullen, B. R. (2005). RNAi the natural way. https://doi.org/10.1038/ng1105-1163

Cummings, S. G., & Bode, H. R. (1984). Head regeneration and polarity reversal in Hydra attenuata can occur in the absence of DNA synthesis. *Wilhelm Roux's Archives of Developmental Biology*, *194*(2), 79–86. https://doi.org/10.1007/BF00848347

Curran-Everett, D. (2018). Explorations in statistics: the log transformation. *Adv Physiol Educ*, *42*, 343–347. https://doi.org/10.1152/advan.00018.2018.-Learning

Dai, S., Zhou, Z., Chen, Z., Xu, G., & Chen, Y. (2019). Fibroblast Growth Factor Receptors (FGFRs): Structures and Small Molecule Inhibitors. *Cells*, *8*(6), 614. https://doi.org/10.3390/cells8060614

Dailey, L., Ambrosetti, D., Mansukhani, A., & Basilico, C. (2005). Mechanisms underlying differential responses to FGF signaling. *Cytokine and Growth Factor Reviews*, *16*(2 SPEC. ISS.), 233–247. https://doi.org/10.1016/j.cytogfr.2005.01.007

David, C. N., & Campbell, R. D. (1972). Cell cycle kinetics and development of Hydra attenuata. I. Epithelial cells. *Journal of cell science*, *11*(2), 557–68.

David, C. N., & Gierer, A. (1974). Cell cycle kinetics and development of Hydra attenuata. II. Interstitial cells. *Journal of Cell Science*, *16*(2), 349–358.

David, C. N. (1973). A quantitative method for maceration of hydra tissue. *Wilhelm Roux Archiv für Entwicklungsmechanik der Organismen*, *171*(4), 259–268. https://doi.org/10.1007/BF00577724

David, C. N. (2012). Interstitial stem cells in Hydra: Multipotency and decision-making. *International Journal of Developmental Biology*, *56*(6-8), 489–497. https://doi.org/10.1387/ijdb.113476cd

David, C. N., & Murphy, S. (1977). Characterization of interstitial stem cells in hydra by cloning. *Developmental Biology*, *58*(2), 372–383. https://doi.org/10.1016/0012-1606(77)90098-7

Davis, L. E. (1973). Histological and ultrastructural studies of the basal disk of Hydra - I. The glandulomuscular cell. *Zeitschrift für Zellforschung und Mikroskopische Anatomie*, *139*(1), 1–27. https://doi.org/10.1007/BF00307458

DeVore, D. L., Horvitz, H., & J.Stern, M. (1995). An FGF receptor signaling pathway is required for the normal cell migrations of the sex myoblasts in C. elegans hermaphrodites. *Cell*, *83*(4), 611–620. https://doi.org/10.1016/0092-8674(95)90101-9

Dono, R., Texido, G., Dussel, R., Ehmke, H., & Zeller, R. (1998). Impaired cerebral cortex development and blood pressure regulation in FGF-2-deficient mice. *EMBO Journal*, *17*(15), 4213–4225. https://doi.org/10.1093/emboj/17.15.4213

Dorey, K., & Amaya, E. (2010). FGF signalling: diverse roles during early vertebrate embryogenesis. *Development*, *137*(22), 3731–3742. https://doi.org/10.1242/dev.037689

Dübel, S., Hoffmeister, S. A., & Schaller, H. C. (1987). Differentiation pathways of ectodermal epithelial cells in hydra. *Differentiation*, *35*(3), 181–189. https://doi.org/10.1111/j.1432-0436.1987.tb00167.x

Dupre, C., & Yuste, R. (2017). Non-overlapping Neural Networks in Hydra vulgaris. *Current Biology*, *27*(8), 1085–1097. https://doi.org/10.1016/j.cub.2017.02.049

Dyer, C., Blanc, E., Hanisch, A., Roehl, H., Otto, G. W., Yu, T., Basson, M. A., & Knight, R. (2014). A bi-modal function of Wnt signalling directs an FGF activity gradient to spatially regulate neuronal differentiation in the midbrain. *Development (Cambridge)*, *141*(1), 63–72. https://doi.org/10.1242/dev.099507

Elbashir, S. M., Harborth, J., Lendeckel, W., Yalcin, A., Weber, K., & Tuschl, T. (2001). Duplexes of 21-nucleotide RNAs mediate RNA interference in cultured mammalian cells. *Nature*, *411*(6836), 494–498. https://doi.org/10.1038/35078107

Espinoza, E., Carrigan, M., Thomas, S. G., Shaw, G., & Edison, A. S. (2000). A Statistical View of FMRFamide Neuropeptide Diversity. *Molecular neurobiology*, *21*(1-2), 035–056. https://doi.org/10.1385/mn:21:1-2:035

Eswarakumar, V. P., Lax, I., & Schlessinger, J. (2005). Cellular signaling by fibroblast growth factor receptors. *Cytokine and Growth Factor Reviews*, *16*(2 SPEC. ISS.), 139–149. https://doi.org/10.1016/j.cytogfr.2005.01.001

Feinberg, E. H., & Hunter, C. P. (2003). Transport of dsRNA into cells by the transmembrane protein SID-1. *Science*, *301*(5639), 1545–1547. https://doi.org/10.1126/science.1087117

Fields, S., & Song, O. K. (1989). A novel genetic system to detect protein-protein interactions. *Nature*, *340*(6230), 245–246. https://doi.org/10.1038/340245a0

Fire, A., Xu, S., Montgomery, M. K., Kostas, S. A., Driver, S. E., & Mello, C. C. (1998). Potent and specific genetic interference by double-stranded RNA in caenorhabditis elegans. *Nature*, *391*(6669), 806–811. https://doi.org/10.1038/35888

Fisher, R. A. (1918). The correlation between relatives on the supposition of mendelian inheritance. *Philosophical Transactions of the Royal Society of Edinburgh*, *52*, 399–433.

Franzenburg, S., Fraune, S., Altrock, P. M., Künzel, S., Baines, J. F., Traulsen, A., & Bosch, T. C. (2013). Bacterial colonization of Hydra hatchlings follows a robust temporal pattern. *ISME Journal*, *7*(4), 781–790. https://doi.org/10.1038/ismej.2012.156

Fraune, S., Augustin, R., Anton-Erxleben, F., Wittlieb, J., Gelhaus, C., Klimovich, V. B., Samoilovich, M. P., & Bosch, T. C. (2010). In an early branching metazoan, bacterial colonization of the embryo is controlled by maternal antimicrobial peptides. *Proceedings of the National Academy of Sciences of the United States of America*, *107*(42), 18067–18072. https://doi.org/10.1073/pnas.1008573107

Froger, A., & Hall, J. E. (2007). Transformation of Plasmid DNA into E. Coli using the heat shock method. *Journal of Visualized Experiments*, (6). https://doi.org/10.3791/253

Fujisawa, T., David, C. N., & Bosch, T. C. (1990). Transplantation stimulates interstitial cell migration in hydra. *Developmental Biology*, *138*(2), 509–512. https://doi.org/10.1016/0012-1606(90)90216-6

Furdui, C. M., Lew, E. D., Schlessinger, J., & Anderson, K. S. (2006). Autophosphorylation of FGFR1 kinase is mediated by a sequential and precisely ordered reaction. *Molecular Cell*, *21*(5), 711–717. https://doi.org/10.1016/j.molcel.2006.01.022

Galliot, B. (2012). Hydra, a fruitful model system for 270 years. *The International Journal of Developmental Biology*, *56*(6-7-8), 411–423. https://doi.org/10.1387/ijdb.120086bg

Galliot, B. (2013). Injury-induced asymmetric cell death as a driving force for head regeneration in Hydra. https://doi.org/10.1007/s00427-012-0411-y

Galliot, B., Quiquand, M., Ghila, L., de Rosa, R., Miljkovic-Licina, M., & Chera, S. (2009). Origins of neurogenesis, a cnidarian view. https://doi.org/10.1016/j.ydbio.2009.05.563

Gavrieli, Y., Sherman, Y., & Ben-Sasson, S. A. (1992). Identification of programmed cell death in situ via specific labeling of nuclear DNA fragmentation. *Journal of cell Biology*, *119*(3), 493–501. https://doi.org/10.1083/jcb.119.3.493

Gibbs, H. C., Chang-Gonzalez, A., Hwang, W., Yeh, A. T., & Lekven, A. C. (2017). Midbrain-hindbrain boundary morphogenesis: At the intersection of wnt and Fgf signaling. https://doi.org/10.3389/fnana.2017.00064

Gierer, A., Berking, S., Bode, H. R., David, C. N., Flick, K., Hansmann, G., Schaller, H., & Trenkner, E. (1972). Regeneration of hydra from reaggregated cells. *Nature New Biology*, *239*(91), 98–101. https://doi.org/10.1038/newbio239098a0

Glass, G. V., Peckham, P. D., & Sanders, J. R. (1972). Consequences of Failure to Meet Assumptions Underlying the Fixed Effects Analyses of Variance and Covariance. *Review of Educational Research*, *42*(3), 237–288. https://doi.org/10.3102/00346543042003237

Glauber, K. M., Dana, C. E., Park, S. S., Colby, D. A., Noro, Y., Fujisawa, T., Chamberlin, A. R., & Steele, R. E. (2015). Erratum to: A small molecule screen identifies a novel compound that induces a homeotic transformation in Hydra, (Development (Cambridge), (2015) 142, 4788-4796). https://doi.org/10.1242/dev.126235

Goetz, R., Beenken, A., Ibrahimi, O. A., Kalinina, J., Olsen, S. K., Eliseenkova, A. V., Xu, C., Neubert, T. A., Zhang, F., Linhardt, R. J., Yu, X., White, K. E., Inagaki, T., Kliewer, S. A., Yamamoto, M., Kurosu, H., Ogawa, Y., Kuro-o, M., Lanske, B., … Mohammadi, M. (2007). Molecular Insights into the Klotho-Dependent, Endocrine Mode of Action of Fibroblast Growth Factor 19 Subfamily Members. *Molecular and Cellular Biology*, *27*(9), 3417–3428. https://doi.org/10.1128/mcb.02249-06

Goldfarb, M. (2005). Fibroblast growth factor homologous factors: Evolution, structure, and function. *Cytokine and Growth Factor Reviews*, *16*(2 SPEC. ISS.), 215–220. https://doi.org/10.1016/j.cytogfr.2005.02.002

Golubovic, A., Kuhn, A., Williamson, M., Kalbacher, H., Holstein, T. W., Grimmelikhuijzen, C. J., & Gründer, S. (2007). A peptide-gated ion channel from the freshwater polyp Hydra. *Journal of Biological Chemistry*, *282*(48), 35098–35103. https://doi.org/10.1074/jbc.M706849200

Goodman, S. J., Branda, C. S., Robinson, M. K., Burdine, R. D., & Stern, M. J. (2003). Alternative splicing affecting a novel domain in the C. elegans EGL-15 FGF

receptor confers functional specificity. *Development*, *130*(16), 3757–3766. https://doi.org/10.1242/dev.00604

Gospodarowicz, D. (1974). Localisation of a fibroblast growth factor and its effect alone and with hydrocortisone on 3T3 cell growth. *Nature*, *249*(5453), 123–127. https://doi.org/10.1038/249123a0

Gospodarowicz, D., & Moran, J. S. (1975). Mitogenic effect of fibroblast growth factor on early passage cultures of human and murine fibroblasts. *Journal of Cell Biology*, *66*(2), 451–457. https://doi.org/10.1083/jcb.66.2.451

Gotoh, N. (2008). Regulation of growth factor signaling by FRS2 family docking/scaffold adaptor proteins. https://doi.org/10.1111/j.1349-7006.2008.00840.x

Gregory, R. I., Chendrimada, T. P., Cooch, N., & Shiekhattar, R. (2005). Human RISC Couples MicroRNA Biogenesis and Posttranscriptional Gene Silencing. *Cell*, *123*, 631–640. https://doi.org/10.1016/j.cell.2005.10.022

Grens, A., Gee, L., Fisher, D. A., & Bode, H. R. (1996). CnNK-2, and NK-2 homeobox gene, has a role in patterning the basal end of the axis in hydra. *Developmental Biology*, *180*(2), 473–488. https://doi.org/10.1006/dbio.1996.0321

Gritti, A., Parati, E. A., Cova, L., Frolichsthal, P., Galli, R., Wanke, E., Faravelli, L., Morassutti, D. J., Roisen, F., Nickel, D. D., & Vescovi, A. L. (1996). Multipotential stem cells from the adult mouse brain proliferate and self-renew in response to basic fibroblast growth factor. *Journal of Neuroscience*, *16*(3), 1091–1100. https://doi.org/10.1523/jneurosci.16-03-01091.1996

Gründer, S., & Assmann, M. (2015). Peptide-gated ion channels and the simple nervous system of Hydra. https://doi.org/10.1242/jeb.111666

Guha, A., Lin, L., & Kornberg, T. B. (2009). Regulation of Drosophila matrix metalloprotease Mmp2 is essential for wing imaginal disc:trachea association and air sac tubulogenesis. *Developmental Biology*, *335*(2), 317–326. https://doi.org/10.1016/j.ydbio.2009.09.005

Guillemot, F., & Zimmer, C. (2011). From cradle to grave: The multiple roles of fibroblast growth factors in neural development. https://doi.org/10.1016/j.neuron.2011.08.002

Gutzman, J. H., Sahu, S. U., & Kwas, C. (2015). Non-muscle myosin IIA and IIB differentially regulate cell shape changes during zebrafish brain morphogenesis. *Developmental Biology*, *397*(1), 103–115. https://doi.org/10.1016/j.ydbio.2014.10.017

Hadari, Y. R., Kouhara, H., Lax, I., & Schlessinger, J. (1998). Binding of Shp2 Tyrosine Phosphatase to FRS2 Is Essential for Fibroblast Growth Factor-Induced PC12

Cell Differentiation. *Molecular and Cellular Biology*, *18*(7), 3966–3973. https://doi.org/10.1128/mcb.18.7.3966

Hallinan, N., Finn, S., Cuffe, S., Rafee, S., O'Byrne, K., & Gately, K. (2016). Targeting the fibroblast growth factor receptor family in cancer. https://doi.org/10.1016/j.ctrv.2016.03.015

Hamilton, A. J., & Baulcombe, D. C. (1999). A species of small antisense RNA in post-transcriptional gene silencing in plants. *Science*, *286*(5441), 950–952. https://doi.org/10.1126/science.286.5441.950

Hanneken, A. (2001). Structural characterization of the circulating soluble FGF receptors reveals multiple isoforms generated by secretion and ectodomain shedding. *FEBS Letters*, *489*(2-3), 176–181. https://doi.org/10.1016/S0014-5793(00)02409-1

Hannon, G. J. (2002). RNA interference. *nature*, *418*(July), 24–26.

Hansen, G. N., Williamson, M., & Grimmelikhuijzen, C. J. (2000). Two-color double-labeling in situ hybridization of whole-mount Hydra using RNA probes for five different Hydra neuropeptide preprohormones: Evidence for colocalization. *Cell and tissue research*, *301*(2), 245–253. https://doi.org/10.1007/s004410000240

Harada, H., Sato, T., & Nakamura, H. (2016). Fgf8 signaling for development of the midbrain and hindbrain. *Development, Growth & Differentiation*, *58*(5), 437–445. https://doi.org/10.1111/dgd.12293

Harding, M. J., & Nechiporuk, A. V. (2012). Fgfr-Ras-MAPK signaling is required for apical constriction via apical positioning of Rho-associated kinase during mechano-sensory organ formation. *Development (Cambridge)*, *139*(17), 3130–3135. https://doi.org/10.1242/dev.082271

Harwell, M. R., Rubinstein, E. N., Hayes, W. S., & Olds, C. C. (1992). Summarizing Monte Carlo Results in Methodological Research: The One- and Two-Factor Fixed Effects ANOVA Cases. *Journal of Educational Statistics*, *17*(4), 315–339. https://doi.org/10.3102/10769986017004315

Hasse, C., Holz, O., Lange, E., Pisowodzki, L., Rebscher, N., Christin Eder, M., Hobmayer, B., & Hassel, M. (2014). FGFR-ERK signaling is an essential component of tissue separation. *Developmental Biology*, *395*(1). https://doi.org/10.1016/j.ydbio.2014.08.010

Hassel, M., & Berking, S. (1988). Nerve cell and nematocyte production in Hydra is deregulated by lithium ions. *Roux's Archives of Developmental Biology*, *197*(8), 471–475. https://doi.org/10.1007/BF00385680

Hassel, M., Bridge, D. M., Stover, N. A., Kleinholz, H., & Steele, R. E. (1998). The level of expression of a protein kinase C gene may be an important component of the patterning process in Hydra. *Development Genes and Evolution*, *207*(8), 502–514. https://doi.org/10.1007/s004270050141

Hébert, J. M. (2011). FGFs: Neurodevelopment's jack-of-all-trades - How do they do it? *Frontiers in Neuroscience*, *5*(DEC), 1–10. https://doi.org/10.3389/fnins.2011.00133

Hobmayer, B., & David, C. N. (1989). Differentiation of a Nerve Cell-Battery Cell Complex in Hydra. *Evolution of the first nervous systems* (pp. 71–80). Springer US. https://doi.org/10.1007/978-1-4899-0921-3_5

Hobmayer, B., Jenewein, M., Eder, D., Eder, M.-K., Glasauer, S., Gufler, S., Hartl, M., & Salvenmoser, W. (2012). Stemness in Hydra - a current perspective. *The International Journal of Developmental Biology*, *56*(6-7-8), 509–517. https://doi.org/10.1387/ijdb.113426bh

Hobmayer, B., Rentzsch, F., Kuhn, K., Happel, C. M., von Laue, C. C., Snyder, P., Rothbächer, U., & Holstein, T. W. (2000). WNT signalling molecules act in axis formation in the diploblastic metazoan Hydra. *Nature*, *407*(6801), 186–9. https://doi.org/10.1038/35025063

Holland, P. W. (1999). The future of evolutionary developmental biology. *Nature*, *402*, C41–C44. https://doi.org/10.1038/35011536

Holstein, T. W., Hess, M. W., & Salvenmoser, W. (2010). *Preparation techniques for transmission electron microscopy of hydra* (Vol. 96). Methods Cell Biol. https://doi.org/10.1016/S0091-679X(10)96013-5

Holstein, T. W., Hobmayer, B., & David, C. N. (1991). Pattern of epithelial cell cycling in hydra. *Developmental biology*, *148*(2), 602–611. https://doi.org/10.1016/0012-1606(91)90277-A

Holz, O., Apel, D., & Hassel, M. (2020). Alternative pathways control actomyosin contractility in epitheliomuscle cells during morphogenesis and body contraction. *Developmental Biology*, *463*(1), 88–98. https://doi.org/10.1016/j.ydbio.2020.04.001

Holz, O., Apel, D., Steinmetz, P., Lange, E., Hopfenmüller, S., Ohler, K., Sudhop, S., & Hassel, M. (2017). Bud detachment in ¡i¿hydra¡/i¿ requires activation of fibroblast growth factor receptor and a Rho-ROCK-myosin II signaling pathway to ensure formation of a basal constriction. *Developmental Dynamics*, *246*(7), 502–516. https://doi.org/10.1002/dvdy.24508

Holzmann, K., Grunt, T., Heinzle, C., Sampl, S., Steinhoff, H., Reichmann, N., Kleiter, M., Hauck, M., & Marian, B. (2012). Alternative splicing of fibroblast growth factor receptor IgIII loops in cancer. https://doi.org/10.1155/2012/950508

Ibrahimi, O. A., Yeh, B. K., Eliseenkova, A. V., Zhang, F., Olsen, S. K., Igarashi, M., Aaronson, S. A., Linhardt, R. J., & Mohammadi, M. (2005). Analysis of Mutations in Fibroblast Growth Factor (FGF) and a Pathogenic Mutation in FGF Receptor (FGFR) Provides Direct Evidence for the Symmetric Two-End Model for FGFR Dimerization. *Molecular and Cellular Biology*, *25*(2), 671–684. https://doi.org/10.1128/mcb.25.2.671-684.2005

Itoh, N., & Ornitz, D. M. (2011). Fibroblast growth factors: from molecular evolution to roles in development, metabolism and disease. *Journal of Biochemistry*, *149*(2), 121–130. https://doi.org/10.1093/jb/mvq121

Itoh, N., Ohta, H., & Konishi, M. (2015). Endocrine FGFs: Evolution, Physiology, Pathophysiology, and Pharmacotherapy. *Frontiers in Endocrinology*, *6*. https://doi.org/10.3389/fendo.2015.00154

Itoh, N., Ohta, H., Nakayama, Y., & Konishi, M. (2016). Roles of FGF signals in heart development, health, and disease. *Frontiers in cell and developmental biology*, *4*(OCT), 1–11. https://doi.org/10.3389/fcell.2016.00110

Itoh, N., & Ornitz, D. M. (2004). Evolution of the Fgf and Fgfr gene families. *Trends in genetics : TIG*, *20*(11), 563–9. https://doi.org/10.1016/j.tig.2004.08.007

Johnson, D. E., Lee, P. L., Lu, J., & Williams, L. T. (1990). Diverse forms of a receptor for acidic and basic fibroblast growth factors. *Molecular and Cellular Biology*, *10*(9), 4728–4736. https://doi.org/10.1128/mcb.10.9.4728

Johnson, D. E., & Williams, L. T. (1992). Structural and functional diversity in the fgf receptor multigene family. *Advances in Cancer Research*, *60*(100), 1–41. https://doi.org/10.1016/S0065-230X(08)60821-0

Juliano, C. E., Lin, H., & Steele, R. E. (2014). Generation of transgenic Hydra by embryo microinjection. *Journal of visualized experiments : JoVE*, (91), 51888. https://doi.org/10.3791/51888

Jungnickel, J., Haase, K., Konitzer, J., Timmer, M., & Grothe, C. (2006). Faster nerve regeneration after sciatic nerve injury in mice over-expressing basic fibroblast growth factor. *Journal of Neurobiology*, *66*(9), 940–948. https://doi.org/10.1002/neu.20265

Kadam, S., McMahon, A., Tzou, P., & Stathopoulos, A. (2009). FGF ligands in Drosophila have distinct activities required to support cell migration and differentiation. *Development*, *136*(5), 739–747. https://doi.org/10.1242/dev.027904

Kadu, V., S Ghaskadbi, S., & Ghaskadbi, S. (2012). Induction of secondary axis in hydra revisited: New insights into pattern formation. *International journal of molecular and cellular medicine*, *1*(1), 11–20.

Kaliszewicz, A., & Lipińska, A. (2013). Environmental condition related reproductive strategies and sex ratio in hydras. *Acta Zoologica*, *94*(2), 177–183. https://doi.org/10.1111/j.1463-6395.2011.00536.x

Kamei, S., Yajima, I., Yamamoto, H., Kobayashi, A., Makabe, K. W., Yamazaki, H., Hayashi, S. I., & Kunisada, T. (2000). Characterization of a novel member of the FGFR family, HrFGFR, in Halocynthia roretzi. *Biochemical and Biophysical Research Communications*, *275*(2), 503–508. https://doi.org/10.1006/bbrc.2000.3334

Kaufmann, J., & Schering, A. (2014). Analysis of Variance ANOVA. *Wiley StatsRef: Statistics reference online*. John Wiley & Sons, Ltd. https://doi.org/10.1002/9781118445112.stat06938

Kawakami, Y., Capdevila, J., Büscher, D., Itoh, T., Esteban, C. R., & Belmonte, J. C. I. (2001). WNT signals control FGF-dependent limb initiation and AER induction in the chick embryo. *Cell*, *104*(6), 891–900. https://doi.org/10.1016/S0092-8674(01)00285-9

Khalturin, K., Anton-Erxleben, F., Milde, S., Plötz, C., Wittlieb, J., Hemmrich, G., & Bosch, T. C. (2007). Transgenic stem cells in Hydra reveal an early evolutionary origin for key elements controlling self-renewal and differentiation. *Developmental Biology*, *309*(1), 32–44. https://doi.org/10.1016/j.ydbio.2007.06.013

Klimovich, A., Wittlieb, J., & Bosch, T. C. (2019). Transgenesis in Hydra to characterize gene function and visualize cell behavior. *Nature Protocols*. https://doi.org/10.1038/s41596-019-0173-3

Klingseisen, A., Clark, I. B., Gryzik, T., & Müller, H. A. (2009). Differential and overlapping functions of two closely related Drosophila FGF8-like growth factors in mesoderm development. *Development*, *136*(14), 2393–2402. https://doi.org/10.1242/dev.035451

Kobayashi, H., & Tomari, Y. (2016). RISC assembly: Coordination between small RNAs and Argonaute proteins. https://doi.org/10.1016/j.bbagrm.2015.08.007

Koizumi, O. (2002). Developmental neurobiology of hydra, a model animal of cnidarians. *Canadian Journal of Zoology*, *80*(10), 1678–1689. https://doi.org/10.1139/z02-134

Kostakopoulou, K., Vogel, A., Brickell, P., & Tickle, C. (1996). 'Regeneration' of wing bud stumps of chick embryos and reactivation of Msx-1 and Shh expression in response to FGF-4 and ridge signals. *Mechanisms of Development*, *55*(2), 119–131. https://doi.org/10.1016/0925-4773(95)00492-0

Krishnapati, L.-S., & Ghaskadbi, S. (2013). Identification and characterization of VEGF and FGF from Hydra. *The International Journal of Developmental Biology*, *57*(11-12), 897–906. https://doi.org/10.1387/ijdb.130077sg

Kubota, Y., & Ito, K. (2000). Chemotactic migration of mesencephalic neural crest cells in the mouse. *Developmental Dynamics*, *217*(2), 170–179. https://doi.org/10.1002/(SICI)1097-0177(200002)217:2⟨170::AID-DVDY4⟩3.0.CO;2-9

Kupferschmidt, K. (2013). A lethal dose of RNA. https://doi.org/10.1126/science.341.6147.732

Laemmli, U. K. (1970). Cleavage of structural proteins during the assembly of the head of bacteriophage T4. *Nature*, *227*(5259), 680–685. https://doi.org/10.1038/227680a0

Lamport, L. (1994). *LaTeX: A document preparation system* (2nd ed.). Addison Wesley.

Landgren, E., Klint, P., Yokote, K., & Claesson-Welsh, L. (1998). Fibroblast growth factor receptor-1 mediates chemotaxis independently of direct SH2-domain protein binding. *Oncogene*, *17*(3), 283–291. https://doi.org/10.1038/sj.onc.1201936

Lange, E. (2016). *Identifizierung und Charakterisierung von Fibroblasten-Wachstumsfaktoren und-Rezeptoren bei Hydra* (Dissertation). Philipps-Universität Marburg. https://doi.org/10.17192/z2016.0678

Lange, E., Bertrand, S., Holz, O., Rebscher, N., & Hassel, M. (2014). Dynamic expression of a Hydra FGF at boundaries and termini. *Development Genes and Evolution*, *224*(4-6), 235–244. https://doi.org/10.1007/s00427-014-0480-1

Lax, I., Wong, A., Lamothe, B., Lee, A., Frost, A., Hawes, J., & Schlessinger, J. (2002). The docking protein FRS2α controls a MAP kinase-mediated negative feedback mechanism for signaling by FGF receptors. *Molecular Cell*, *10*(4), 709–719. https://doi.org/10.1016/S1097-2765(02)00689-5

Lecaudey, V., Cakan-Akdogan, G., Norton, W. H., & Gilmour, D. (2008). Dynamic Fgf signaling couples morphogenesis and migration in the zebrafish lateral line primordium. *Development*, *135*(16), 2695–2705. https://doi.org/10.1242/dev.025981

Leclère, L., & Röttinger, E. (2017). Diversity of cnidarian muscles: Function, anatomy, development and regeneration. https://doi.org/10.3389/fcell.2016.00157

Lee, P. L., Johnson, D. E., Cousens, L. S., Fried, V. A., & Williams, L. T. (1989). Purification and complementary DNA cloning of a receptor for basic fibroblast growth factor. *Science*, *245*(4913), 57–60. https://doi.org/10.1126/science.2544996

Lemmon, M. A., & Schlessinger, J. (2010). Cell signaling by receptor tyrosine kinases. https://doi.org/10.1016/j.cell.2010.06.011

Lengfeld, T., Watanabe, H., Simakov, O., Lindgens, D., Gee, L., Law, L., Schmidt, H. A., özbek, S., Bode, H. R., & Holstein, T. W. (2009). Multiple Wnts are involved in Hydra organizer formation and regeneration. *Developmental biology*, *330*(1), 186–199. https://doi.org/10.1016/j.ydbio.2009.02.004

Lentz, T. L. (1966). Intramitochondrial glycogen granules in digestive cells of Hydra. *The Journal of cell biology*, *29*(1), 162–167. https://doi.org/10.1083/jcb.29.1.162

Leontovich, A. A., Zhang, J., Shimokawa, K., Nagase, H., & Sarras, M. P. (2000). A novel hydra matrix metalloproteinase (HMMP) functions in extracellular matrix degradation, morphogenesis and the maintenance of differentiated cells in the foot process. *Development (Cambridge, England)*, *127*(4), 907–20.

Levene, H. (1960). Robust tests for the equality of variance. In I. Olkin (Ed.), *Contributions to probability and statistics* (pp. 278–292). Stanford Univ. Press.

Li, Z., & Rana, T. M. (2012). Molecular mechanisms of RNA-triggered gene silencing machineries. *Accounts of Chemical Research*, *45*(7), 1122–1131. https://doi.org/10.1021/ar200253u

Lim, J., Yusoff, P., Wong, E. S. M., Chandramouli, S., Lao, D.-H., Fong, C. W., & Guy, G. R. (2002). The Cysteine-Rich Sprouty Translocation Domain Targets Mitogen-Activated Protein Kinase Inhibitory Proteins to Phosphatidylinositol 4,5-Bisphosphate in Plasma Membranes. *Molecular and Cellular Biology*, *22*(22), 7953–7966. https://doi.org/10.1128/mcb.22.22.7953-7966.2002

Lin, X. (2004). Functions of heparan sulfate proteoglycans in cell signaling during development. https://doi.org/10.1242/dev.01522

Lingueglia, E., Champigny, G., Lazdunski, M., & Barbry, P. (1995). Cloning of the amiloride-sensitive FMRFamide peptide-gated sodium channel. *Nature*, *378*(6558), 730–733. https://doi.org/10.1038/378730a0

Lix, L. M., Keselman, J. C., & Keselman, H. J. (1996). Consequences of Assumption Violations Revisited: A Quantitative Review of Alternatives to the One-Way Analysis of Variance *F* Test. *Review of Educational Research*, *66*(4), 579–619. https://doi.org/10.3102/00346543066004579

Lodish, H., Berk, A., Zipursky, S. L., Matsudaira, P., Baltimore, D., & Darnell, J. (2000). *Molecular Cell Biology (4th edition)* (4th editio).

Lohmann, J. U., Endl, I., & Bosch, T. C. (1999). Silencing of developmental genes in Hydra. *Developmental biology*, *214*(1), 211–214. https://doi.org/10.1006/dbio.1999.9407

Lommel, M., Tursch, A., Rustarazo-Calvo, L., Trageser, B., & Holstein, T. (2017). Genetic knockdown and knockout approaches in Hydra. *bioRxiv*, 230300. https://doi.org/10.1101/230300

Lotz, S., Goderie, S., Tokas, N., Hirsch, S. E., Ahmad, F., Corneo, B., Le, S., Banerjee, A., Kane, R. S., Stern, J. H., Temple, S., & Fasano, C. A. (2013). Sustained Levels of FGF2 Maintain Undifferentiated Stem Cell Cultures with Biweekly Feeding. *PLoS ONE*, *8*(2), 56289. https://doi.org/10.1371/journal.pone.0056289

Lou, J. Y., Laezza, F., Gerber, B. R., Xiao, M., Yamada, K. A., Hartmann, H., Craig, A. M., Nerbonne, J. M., & Ornitz, D. M. (2005). Fibroblast growth factor 14 is an intracellular modulator of voltage-gated sodium channels. *Journal of Physiology*, *569*(1), 179–193. https://doi.org/10.1113/jphysiol.2005.097220

Lowenstein, E. J., Daly, R. J., Batzer, A. G., Li, W., Margolis, B., Lammers, R., Ullrich, A., Skolnik, E. Y., Bar-Sagi, D., & Schlessinger, J. (1992). The SH2 and SH3 domain-containing protein GRB2 links receptor tyrosine kinases to ras signaling. *Cell*, *70*(3), 431–442. https://doi.org/10.1016/0092-8674(92)90167-B

MacWilliams, H. K. (1983). Hydra transplantation phenomena and the mechanism of Hydra head regeneration. II. Properties of the head activation. *Developmental Biology*, *96*(1), 239–257. https://doi.org/10.1016/0012-1606(83)90325-1

Maddaluno, L., Urwyler, C., & Werner, S. (2017). Fibroblast growth factors: Key players in regeneration and tissue repair. *Development*, *144*(22), 4047–4060. https://doi.org/10.1242/dev.152587

Majumdar, R., Rajasekaran, K., & Cary, J. W. (2017). RNA interference (RNAi) as a potential tool for control of mycotoxin contamination in crop plants: Concepts and considerations. *Frontiers in Plant Science*, *8*. https://doi.org/10.3389/fpls.2017.00200

Makanae, A., Mitogawa, K., & Satoh, A. (2014). Co-operative Bmp- and Fgf-signaling inputs convert skin wound healing to limb formation in urodele amphibians. *Developmental Biology*, *396*(1), 57–66. https://doi.org/10.1016/j.ydbio.2014.09.021

Makanae, A., Mitogawa, K., & Satoh, A. (2016). Cooperative inputs of Bmp and Fgf signaling induce tail regeneration in urodele amphibians. *Developmental Biology*, *410*(1), 45–55. https://doi.org/10.1016/j.ydbio.2015.12.012

Marban, E., Yamagishi, T., & Tomaselli, G. F. (1998). Structure and function of voltage-gated sodium channels. https://doi.org/10.1111/j.1469-7793.1998.647bp.x

Marcum, B. A., & Campbell, R. D. (1978). Development of hydra lacking nerve and interstitial cells. *Journal of Cell Science*, *Vol. 29*, 17–33.

Martin, G. R. (1998). The roles of FGFs in the early development of vertebrate limbs. https://doi.org/10.1101/gad.12.11.1571

Martin, V., Littlefield, C., Archer, W., & Bode, H. R. (1997). Embryogenesis in hydra. *The Biological Bulletin*, *192*(3), 345–363.

Martínez, D. E., Iñiguez, A. R., Percell, K. M., Willner, J. B., Signorovitch, J., & Campbell, R. D. (2010). Phylogeny and biogeography of Hydra (Cnidaria: Hydridae) using mitochondrial and nuclear DNA sequences. *Molecular Phylogenetics and Evolution*, *57*(1), 403–410. https://doi.org/10.1016/j.ympev.2010.06.016

Martínez, D. E., & Bridge, D. (2012). Hydra, the everlasting embryo, confronts aging. *International Journal of Developmental Biology*, *56*(6-8), 479–487. https://doi.org/10.1387/ijdb.113461dm

Matus, D. Q., Thomsen, G. H., & Martindale, M. Q. (2007). FGF signaling in gastrulation and neural development in Nematostella vectensis, an anthozoan cnidarian. *Development Genes and Evolution*, *217*(2), 137–148. https://doi.org/10.1007/s00427-006-0122-3

McCoon, P. E., Angerer, R. C., & Angerer, L. M. (1996). SpFGFR, a new member of the fibroblast growth factor receptor family, is developmentally regulated during early sea urchin development. *Journal of Biological Chemistry*, *271*(33), 20119–20125. https://doi.org/10.1074/jbc.271.33.20119

Meinhardt, H. (2002). The radial-symmetric hydra and the evolution of the bilateral body plan: an old body became a young brain. *BioEssays*, *24*(2), 185–191. https://doi.org/10.1002/bies.10045

Miyagishi, M., & Taira, K. (2002). U6 promoter-driven siRNAs with four uridine 3' overhangs efficiently suppress targeted gene expression in mammalian cells. *Nature Biotechnology*, *20*(5), 497–500. https://doi.org/10.1038/nbt0502-497

Miyoshi, K., Wakioka, T., Nishinakamura, H., Kamio, M., Yang, L., Inoue, M., Hasegawa, M., Yonemitsu, Y., Komiya, S., & Yoshimura, A. (2004). The Sprouty-related protein, Spred, inhibits cell motility, metastasis, and Rho-mediated actin reorganization. *Oncogene*, *23*(33), 5567–5576. https://doi.org/10.1038/sj.onc.1207759

Mohammadi, M., Honegger, A. M., Rotin, D., Fischer, R., Bellot, F., Li, W., Dionne, C. A., Jaye, M., Rubinstein, M., & Schlessinger, J. (1991). A tyrosine-phosphorylated

carboxy-terminal peptide of the fibroblast growth factor receptor (Flg) is a binding site for the SH2 domain of phospholipase C-gamma 1. *Molecular and Cellular Biology*, *11*(10), 5068–5078. https://doi.org/10.1128/mcb.11.10.5068

Mohammadi, M., McMahon, G., Sun, L., Tang, C., Hirth, P., Yeh, B. K., Hubbard, S. R., & Schlessinger, J. (1997). Structures of the Tyrosine Kinase Domain of Fibroblast Growth Factor Receptor in Complex with Inhibitors. *Science*, *276*(5314), 955–960. https://doi.org/10.1126/science.276.5314.955

Mohammadi, M., Olsen, S. K., & Ibrahimi, O. a. (2005). Structural basis for fibroblast growth factor receptor activation. *Cytokine & growth factor reviews*, *16*(2), 107–37. https://doi.org/10.1016/j.cytogfr.2005.01.008

Mortzfeld, B. M., Taubenheim, J., Fraune, S., Klimovich, A. V., & Bosch, T. C. (2018). Stem Cell Transcription Factor FoxO Controls Microbiome Resilience in Hydra. *Frontiers in Microbiology*, *9*. https://doi.org/10.3389/fmicb.2018.00629

Mossahebi-Mohammadi, M., Quan, M., Zhang, J. S., & Li, X. (2020). FGF Signaling Pathway: A Key Regulator of Stem Cell Pluripotency. https://doi.org/10.3389/fcell.2020.00079

Muha, V., & Müller, H.-A. J. (2013). Functions and Mechanisms of Fibroblast Growth Factor (FGF) Signalling in Drosophila melanogaster. *International journal of molecular sciences*, *14*, 5920–5937. https://doi.org/10.3390/ijms14035920

Mullen, L. M., Bryant, S. V., Torok, M. A., Blumberg, B., & Gardiner, D. M. (1996). Nerve dependency of regeneration: the role of Distal-less and FGF signaling in amphibian limb regeneration. *Development (Cambridge, England)*, *122*(11), 3487–97. https://doi.org/8951064

Müller, W. A. (1989). Diacylglycerol-induced multihead formation in Hydra. *Development*, *105*(2), 309–316.

Mullis, K., Faloona, F., Scharf, S., Saiki, R., Horn, G., & Erlich, H. (1986). Specific enzymatic amplification of DNA in vitro: The polymerase chain reaction. *Cold Spring Harbor Symposia on Quantitative Biology*, *51*(1), 263–273. https://doi.org/10.1101/sqb.1986.051.01.032

Münder, S., Käsbauer, T., Prexl, A., Aufschnaiter, R., Zhang, X., Towb, P., & Böttger, A. (2010). Notch signalling defines critical boundary during budding in Hydra. *Developmental Biology*, *344*(1), 331–345. https://doi.org/10.1016/j.ydbio.2010.05.517

Münder, S., Tischer, S., Grundhuber, M., Büchels, N., Bruckmeier, N., Eckert, S., Seefeldt, C. A., Prexl, A., Käsbauer, T., & Böttger, A. (2013). Notch-signalling is required

for head regeneration and tentacle patterning in Hydra. *Developmental Biology*, *383*(1), 146–157. https://doi.org/10.1016/j.ydbio.2013.08.022

Mundie, J. R. (1926). Maceration of green Hydra. *Science*, *64*(1667), 579. https://doi.org/10.1126/science.64.1667.579

Murate, M., Kishimoto, Y., Sugiyama, T., Fujisawa, T., Takahashi-Iwanaga, H., & Iwanaga, T. (1997). Hydra regeneration from recombined ectodermal and endodermal tissue. II. Differential stability in the ectodermal and endodermal epithelial organization. *Journal of cell science*, *110 (Pt 1*, 1919–34.

Nacu, E., Gromberg, E., Oliveira, C. R., Drechsel, D., & Tanaka, E. M. (2016). FGF8 and SHH substitute for anterior-posterior tissue interactions to induce limb regeneration. *Nature*, *533*(7603), 407–410. https://doi.org/10.1038/nature17972

Naiche, L. A., Holder, N., & Lewandoski, M. (2011). FGF4 and FGF8 comprise the wavefront activity that controls somitogenesis. *Proceedings of the National Academy of Sciences of the United States of America*, *108*(10), 4018–4023. https://doi.org/10.1073/pnas.1007417108

Noda, K. (1971). Reconstitution of dissociated cells of hydra. *Zoological magazine*, *80*, 99–101.

Nunes, Q. M., Li, Y., Sun, C., Kinnunen, T. K., & Fernig, D. G. (2016). Fibroblast growth factors as tissue repair and regeneration therapeutics. *PeerJ*, *2016*(1), 1–31. https://doi.org/10.7717/peerj.1535

Obbard, D. J., Gordon, K. H., Buck, A. H., & Jiggins, F. M. (2009). The evolution of RNAi as a defence against viruses and transposable elements. *Philosophical Transactions of the Royal Society B: Biological Sciences*, *364*(1513), 99–115. https://doi.org/10.1098/rstb.2008.0168

Ogawa, K., Kobayashi, C., Hayashi, T., Orii, H., Watanabe, K., & Agata, K. (2002). Planarian fibroblast growth factor receptor homologs expressed in stem cells and cephalic ganglions. *Development, Growth and Differentiation*, *44*(3), 191–204. https://doi.org/10.1046/j.1440-169X.2002.00634.x

Ohuchi, H., Nakagawa, T., Yamamoto, A., Araga, A., Ohata, T., Ishimaru, Y., Yoshioka, H., Kuwana, T., Nohno, T., Yamasaki, M., Itoh, N., & Noji, S. (1997). The mesenchymal factor, FGF10, initiates and maintains the outgrowth of the chick limb bud through interaction with FGF8, an apical ectodermal factor. *Development*, *124*(11), 2235–2244.

Olsen, S. K., Ibrahimi, O. A., Raucci, A., Zhang, F., Eliseenkova, A. V., Yayon, A., Basilico, C., Linhardt, R. J., Schlessinger, J., & Mohammadi, M. (2004). Insights into the

molecular basis for fibroblast growth factor receptor autoinhibition and ligand-binding promiscuity. *Proceedings of the National Academy of Sciences*, *101*(4), 935–940. https://doi.org/10.1073/pnas.0307287101

Ornitz, D. M. (2000). FGFs, heparan sulfate and FGFRs: Complex interactions essential for development. *BioEssays*, *22*(2), 108–112. https://doi.org/10.1002/(SICI)1521-1878(200002)22:2⟨108::AID-BIES2⟩3.0.CO;2-M

Ornitz, D. M., & Itoh, N. (2001). Protein family review: Fibroblast growth factors. *Genome Biology*, *2*(3), reviews3005.1–3005.12. https://doi.org/10.1186/gb-2001-2-3-reviews3005

Ornitz, D. M., & Itoh, N. (2015). The fibroblast growth factor signaling pathway. *Wiley Interdisciplinary Reviews: Developmental Biology*, *4*(3), 215–266. https://doi.org/10.1002/wdev.176

Otto, J. J., & Campbell, R. D. (1977). Budding in Hydra attenuata: Bud stages and fate map. *Journal of Experimental Zoology*, *200*(3), 417–428. https://doi.org/10.1002/jez.1402000311

Oulion, S., Bertrand, S., & Escriva, H. (2012). Evolution of the FGF Gene Family. *International Journal of Evolutionary Biology*, *2012*, 1–12. https://doi.org/10.1155/2012/298147

Paddison, P. J., Caudy, A. A., Bernstein, E., Hannon, G. J., & Conklin, D. S. (2002). Short hairpin RNAs (shRNAs) induce sequence-specific silencing in mammalian cells. *Genes and Development*, *16*(8), 948–958. https://doi.org/10.1101/gad.981002

Pak, J., Maniar, J. M., Mello, C. C., & Fire, A. (2012). Protection from feed-forward amplification in an amplified RNAi mechanism. *Cell*. https://doi.org/10.1016/j.cell.2012.10.022

Pellegrini, L., Burke, D. F., Von Delft, F., Mulloy, B., & Blundell, T. L. (2000). Crystal structure of fibroblast growth factor receptor ectodomain bound to ligand and heparin. *Nature*, *407*(6807), 1029–1034. https://doi.org/10.1038/35039551

Philipp, I., Aufschnaiter, R., Ozbek, S., Pontasch, S., Jenewein, M., Watanabe, H., Rentzsch, F., Holstein, T. W., & Hobmayer, B. (2009). Wnt/β-Catenin and noncanonical Wnt signaling interact in tissue evagination in the simple eumetazoan Hydra. *Proceedings of the National Academy of Sciences of the United States of America*, *106*(11), 4290–4295.

Plotnikov, A. N., Hubbard, S. R., Schlessinger, J., & Mohammadi, M. (2000). Crystal structures of two FGF-FGFR complexes reveal the determinants of ligand-receptor specificity. *Cell*, *101*(4), 413–424. https://doi.org/10.1016/S0092-8674(00)80851-X

Popovici, C., Roubin, R., Coulier, F., & Birnbaum, D. (2005). An evolutionary history of the FGF superfamily. *BioEssays*, *27*(8), 849–857. https://doi.org/10.1002/bies.20261

Powers, C. J., McLeskey, S. W., & Wellstein, a. (2000). Fibroblast growth factors, their receptors and signaling. *Endocrine-related cancer*, *7*(3), 165–97.

Powers, N., & Srivastava, A. (2018). The Air Sac Primordium of Drosophila: A Model for Invasive Development. *International Journal of Molecular Sciences*, *19*(7), 2074. https://doi.org/10.3390/ijms19072074

Pratt, A. J., & MacRae, I. J. (2009). The RNA-induced Silencing Complex: A Versatile Gene-silencing Machine. *Journal of Biological Chemistry*, *284*(27), 17897–17901. https://doi.org/10.1074/jbc.R900012200

Prexl, A., Münder, S., Loy, B., Kremmer, E., Tischer, S., & Böttger, A. (2011). The putative Notch ligand HyJagged is a transmembrane protein present in all cell types of adult Hydra and upregulated at the boundary between bud and parent. *BMC Cell Biology*, *12*. https://doi.org/10.1186/1471-2121-12-38

R Core Team. (2020). *R: A language and environment for statistical computing*. R Foundation for Statistical Computing. Vienna, Austria.

Raballo, R., Rhee, J., Lyn-Cook, R., Leckman, J. F., Schwartz, M. L., & Vaccarino, F. M. (2000). Basic fibroblast growth factor (Fgf2) is necessary for cell proliferation and neurogenesis in the developing cerebral cortex. *Journal of Neuroscience*, *20*(13), 5012–5023. https://doi.org/10.1523/jneurosci.20-13-05012.2000

Rabinowitz, A. H., & Vokes, S. A. (2012). Integration of the transcriptional networks regulating limb morphogenesis. https://doi.org/10.1016/j.ydbio.2012.05.035

Rao, D. D., Vorhies, J. S., Senzer, N., & Nemunaitis, J. (2009). siRNA vs. shRNA: Similarities and differences. https://doi.org/10.1016/j.addr.2009.04.004

Rash, B. G., David Lim, H., Breunig, J. J., & Vaccarino, F. M. (2011). FGF signaling expands embryonic cortical surface area by regulating notch-dependent neurogenesis. *Journal of Neuroscience*, *31*(43), 15604–15617. https://doi.org/10.1523/JNEUROSCI.4439-11.2011

Rebscher, N., Deichmann, C., Sudhop, S., Fritzenwanker, J. H., Green, S., & Hassel, M. (2009). Conserved intron positions in FGFR genes reflect the modular structure of FGFR and reveal stepwise addition of domains to an already complex ancestral FGFR. *Development genes and evolution*, *219*(9-10), 455–68. https://doi.org/10.1007/s00427-009-0309-5

Reim, I., Hollfelder, D., Ismat, A., & Frasch, M. (2012). The FGF8-related signals Pyramus and Thisbe promote pathfinding, substrate adhesion, and survival of migrating

longitudinal gut muscle founder cells. *Developmental Biology*, *368*(1), 28–43. https://doi.org/10.1016/j.ydbio.2012.05.010

Reinhardt, B., Broun, M., Blitz, I. L., & Bode, H. R. (2004). HyBMP5-8b, a BMP5-8 orthologue, acts during axial patterning and tentacle formation in hydra. *Developmental Biology*, *267*(1), 43–59. https://doi.org/10.1016/j.ydbio.2003.10.031

Rentzsch, F., Fritzenwanker, J. H., Scholz, C. B., & Technau, U. (2008). FGF signalling controls formation of the apical sensory organ in the cnidarian Nematostella vectensis. *Development*, *135*(10), 1761–1769. https://doi.org/10.1242/dev.020784

Rentzsch, F., Layden, M., & Manuel, M. (2017). The cellular and molecular basis of cnidarian neurogenesis: *WIREs Dev Biol*, *6*, 257. https://doi.org/10.1002/wdev.257

Röttinger, E., Sadumenont, A., Duboc, V., Besnardeau, L., McClay, D., & Lepage, T. (2008). FGF signals guide migration of mesenchymal cells, control skeletal morphogenesis and regulate gastrulation during sea urchin development. *Development*, *135*(2), 353–365. https://doi.org/10.1242/dev.014282

Royston, J. P. (1982). Algorithm AS 181: The W Test for Normality. *Applied Statistics*, *31*(2), 176. https://doi.org/10.2307/2347986

Rudolf, A., Hübinger, C., Hüsken, K., Vogt, A., Rebscher, N., önel, S. F., Renkawitz-Pohl, R., & Hassel, M. (2013). The Hydra FGFR, Kringelchen, partially replaces the Drosophila Heartless FGFR. *Development Genes and Evolution*, *223*(3), 159–169. https://doi.org/10.1007/s00427-012-0424-6

Sacks, P. G., & Davis, L. E. (1979). Production of nerveless Hydra attenuata by hydroxyurea treatments. *Journal of Cell Science*, *37*, 189–203.

Sahu, S. U., Visetsouk, M. R., Garde, R. J., Hennes, L., Kwas, C., & Gutzman, J. H. (2017). Calcium signals drive cell shape changes during zebrafsh midbrain-hindbrain boundary formation. *Molecular Biology of the Cell*, *28*(7), 875–882. https://doi.org/10.1091/mbc.E16-08-0561

Sambrook, J., & Russell, D. W. (2006). Preparation and Transformation of Competent E. coli Using Calcium Chloride. *Cold Spring Harbor Protocols*, *2006*(1). https://doi.org/10.1101/pdb.prot3932

Sarras, M. P., Madden, M. E., Zhang, X. M., Gunwar, S., Huff, J. K., & Hudson, B. G. (1991). Extracellular matrix (mesoglea) of Hydra vulgaris. I. Isolation and characterization. *Developmental biology*, *148*(2), 481–494. https://doi.org/10.1016/0012-1606(91)90267-7

Sarras, M. P. (2012). Components, structure, biogenesis and function of the Hydra extracellular matrix in regeneration, pattern formation and cell differentiation.

The International Journal of Developmental Biology, *56*(6-7-8), 567–576. https://doi.org/10.1387/ijdb.113445ms

Sarras, M. P., Yan, L., Leontovich, A., & Zhang, J. S. (2002). Structure, expression, and developmental function of early divergent forms of metalloproteinases in Hydra. *Cell Research*, *12*(3-4), 163–176. https://doi.org/10.1038/sj.cr.7290123

Sato, M., Bode, H. R., & Sawada, Y. (1990). Patterning processes in aggregates of hydra cells visualized with the monoclonal antibody, TS19. *Developmental Biology*, *141*(2), 412–420. https://doi.org/10.1016/0012-1606(90)90395-Y

Satou, Y., Imai, K. S., & Satoh, N. (2002). Fgf genes in the basal chordate Ciona intestinalis. *Development genes and evolution*, *212*(9), 432–438. https://doi.org/10.1007/s00427-002-0266-8

Schindelin, J., Arganda-Carreras, I., Frise, E., Kaynig, V., Longair, M., Pietzsch, T., Preibisch, S., Rueden, C., Saalfeld, S., Schmid, B., Tinevez, J.-Y., White, D. J., Hartenstein, V., Eliceiri, K., Tomancak, P., & Cardona, A. (2012). Fiji: an open-source platform for biological-image analysis. *Nature methods*, *9*(7), 676–82. https://doi.org/10.1038/nmeth.2019

Schlessinger, J. (2000). Cell signaling by receptor tyrosine kinases. https://doi.org/10.1016/S0092-8674(00)00114-8

Schliermann, A., & Nickel, J. (2018). Unraveling the connection between fibroblast growth factor and bone morphogenetic protein signaling. https://doi.org/10.3390/ijms19103220

Schmider, E., Ziegler, M., Danay, E., Beyer, L., & Bühner, M. (2010). Is It Really Robust?: Reinvestigating the robustness of ANOVA against violations of the normal distribution assumption. *Methodology*, *6*(4), 147–151. https://doi.org/10.1027/1614-2241/a000016

Schröder, K., & Bosch, T. C. (2016). The origin of mucosal immunity: Lessons from the holobiont Hydra. https://doi.org/10.1128/mBio.01184-16

Schwentner, M., & Bosch, T. C. (2015). Revisiting the age, evolutionary history and species level diversity of the genus Hydra (Cnidaria: Hydrozoa). *Molecular Phylogenetics and Evolution*, *91*, 41–55. https://doi.org/10.1016/j.ympev.2015.05.013

Shapiro, S. S., & Wilk, M. B. (1965). An analysis of variance test for normality (complete samples). *Biometrika*, *52*(3-4), 591–611. https://doi.org/10.1093/biomet/52.3-4.591

Sharma, R., Beer, K., Iwanov, K., Schmöhl, F., Beckmann, P. I., & Schröder, R. (2015). The single fgf receptor gene in the beetle Tribolium castaneum codes for two

isoforms that integrate FGF8-and Branchless-dependent signals. *Developmental Biology*, *402*(2), 264–275. https://doi.org/10.1016/j.ydbio.2015.04.001

Shih, J. D., & Hunter, C. P. (2011). SID-1 is a dsRNA-selective dsRNA-gated channel. *Rna*, 1057–1065. https://doi.org/10.1261/rna.2596511.genetic

Shimizu, H. (2012). Transplantation analysis of developmental mechanisms in Hydra. *International Journal of Developmental Biology*, *56*(6-8), 463–472. https://doi.org/10.1387/ijdb.123498hs

Shimizu, H., Aufschnaiter, R., Li, L., Sarras, M. P., Borza, D. B., Abrahamson, D. R., Sado, Y., & Zhang, X. (2008). The extracellular matrix of hydra is a porous sheet and contains type IV collagen. *Zoology*, *111*(5), 410–418. https://doi.org/10.1016/j.zool.2007.11.004

Shimizu, H., & Sawada, Y. (1987). Transplantation phenomena in hydra: Cooperation of position-dependent and structure-dependent factors determines the transplantation result. *Developmental Biology*, *122*(1), 113–119. https://doi.org/10.1016/0012-1606(87)90337-X

Shimizu, H., Takaku, Y., Zhang, X., & Fujisawa, T. (2007). The aboral pore of hydra: Evidence that the digestive tract of hydra is a tube not a sac. *Development Genes and Evolution*, *217*(8), 563–568. https://doi.org/10.1007/s00427-007-0165-0

Shimizu-Nishikawa, K., Takahashi, J., & Nishikawa, A. (2003). Intercalary and supernumerary regeneration in the limbs of the frog, Xenopus laevis. *Developmental Dynamics*, *227*(4), 563–572. https://doi.org/10.1002/dvdy.10345

Shishido, E., Higashijima, S., Emori, Y., & Saigo, K. (1993). Two FGF-receptor homologues of Drosophila: one is expressed in mesodermal primordium in early embryos. *Development*, *117*(2).

Siomi, H., & Siomi, M. C. (2009). On the road to reading the RNA-interference code. https://doi.org/10.1038/nature07754

Stathopoulos, A., Tam, B., Ronshaugen, M., Frasch, M., & Levine, M. (2004). Pyramus and thisbe: FGF genes that pattern the mesoderm of Drosophila embryos. *Genes and Development*, *18*(6), 687–699. https://doi.org/10.1101/gad.1166404

Steele, R. E. (2002). REVIEW Developmental Signaling in Hydra: What Does It Take to Build a "Simple"Animal? *Developmental biology*. https://doi.org/10.1006/dbio.2002.0744

Steinberg, F., Zhuang, L., Beyeler, M., Kälin, R. E., Mullis, P. E., Brändli, A. W., & Trueb, B. (2010). The FGFRL1 receptor is shed from cell membranes, binds Fibroblast Growth Factors (FGFs), and antagonizes FGF signaling in Xenopus embryos.

Journal of Biological Chemistry, *285*(3), 2193–2202. https://doi.org/10.1074/jbc.M109.058248

Stern, C. D. (2005). Neural induction: Old problem, new findings, yet more questions. https://doi.org/10.1242/dev.01794

Storm, E. E., Rubenstein, J. L., & Martin, G. R. (2003). Dosage of Fgf8 determines whether cell survival is positively or negatively regulated in the developing forebrain. *Proceedings of the National Academy of Sciences of the United States of America*, *100*(4), 1757–1762. https://doi.org/10.1073/pnas.0337736100

Sudhop, S. (2006). *Knospung-steuernde Gene in Hydra vulgaris: Ein evolutionsgeschichtlich alter FGFR kontrolliert die Knopsenablösung* (Dissertation). Philipps-Universität Marburg. https://doi.org/https://doi.org/10.17192/z2006.0130

Sudhop, S., Coulier, F., Bieller, A., Vogt, A., Hotz, T., & Hassel, M. (2004). Signalling by the FGFR-like tyrosine kinase, Kringelchen, is essential for bud detachment in Hydra vulgaris. *Development (Cambridge, England)*, *131*(16), 4001–11. https://doi.org/10.1242/dev.01267

Sugiyama, T., & Fujisawa, T. (1978). Genetic analysis of developmental mechanisms in Hydra. II. Isolation and characterization of an interstitial cell-deficient strain. *Strain*, *52*, 175–185.

Sun, X., Meyers, E. N., Lewandoski, M., & Martin, G. R. (1999). Targeted disruption of Fgf8 causes failure of cell migration in the gastrulating mouse embryo. *Genes and Development*, *13*(14), 1834–1846. https://doi.org/10.1101/gad.13.14.1834

Suryawanshi, A. (2017). *Identification and characterization of downstream elements of Hydra FGFR signaling* (Dissertation). Philipps-Universität Marburg. https://doi.org/https://doi.org/10.17192/z2017.0122

Suryawanshi, A., Schaefer, K., Holz, O., Apel, D., Lange, E., Hayward, D. C., Miller, D. J., & Hassel, M. (2020). What lies beneath: Hydra provides cnidarian perspectives into the evolution of FGFR docking proteins. *Development Genes and Evolution*, *230*(3), 227–238. https://doi.org/10.1007/s00427-020-00659-4

Sutherland, D., Samakovlis, C., & Krasnow, M. A. (1996). branchless encodes a Drosophila FGF homolog that controls tracheal cell migration and the pattern of branching. *Cell*, *87*(6), 1091–1101. https://doi.org/10.1016/S0092-8674(00)81803-6

Takahashi, T., Muneoka, Y., Lohmann, J., Lopez de Haro, M. S., Solleder, G., Bosch, T. C., David, C. N., Bode, H. R., Koizumi, O., Shimizu, H., Hatta, M., Fujisawa, T., & Sugiyama, T. (1997). Systematic isolation of peptide signal molecules regulating

development in hydra: LWamide and PW families. *Proceedings of the National Academy of Sciences of the United States of America*, *94*(4), 1241–6.

Takahashi, T., Koizumi, O., Ariura, Y., Romanovitch, A., Bosch, T. C., Kobayakawa, Y., Mohri, S., Bode, H. R., Yum, S., Hatta, M., & Fujisawa, T. (2000). A novel neuropeptide, Hym-355, positively regulates neuron differentiation in Hydra. *Development*, *127*(5), 997–1005. https://doi.org/10.1016/s1095-6433(99)90367-7

Takahashi, T., Koizumi, O., Hayakawa, E., Minobe, S., Suetsugu, R., Kobayakawa, Y., Bosch, T. C., David, C. N., & Fujisawa, T. (2009). Further characterization of the PW peptide family that inhibits neuron differentiation in Hydra. *Development Genes and Evolution*, *219*(3), 119–129. https://doi.org/10.1007/s00427-009-0272-1

Takeo, M., Chou, W. C., Sun, Q., Lee, W., Rabbani, P., Loomis, C., Mark Taketo, M., & Ito, M. (2013). Wnt activation in nail epithelium couples nail growth to digit regeneration. *Nature*, *499*(7457), 228–232. https://doi.org/10.1038/nature12214

Tanaka, E., & Reddien, P. W. (2011). The cellular basis for animal regeneration Sources of new cells in animal regeneration. *Dev Cell*, *21*(1), 172–185. https://doi.org/10.1016/j.devcel.2011.06.016.The

Tannreuther, G. W. (1908). The development of Hydra. *The Biological Bulletin*, *14*(5), 261–[280]–1. https://doi.org/10.2307/1535623

Tardent, P. (1966). Zur Sexualbiologie von Hydra attenuata (Pall). *Revue suisse de zoologie*, *73*, 357–382. https://doi.org/10.5962/bhl.part.75824

Technau, U., Cramer Von Laue, C., Rentzsch, F., Luft, S., Hobmayer, B., Bode, H. R., & Holstein, T. W. (2000). Parameters of self-organization in Hydra aggregates. *Proceedings of the National Academy of Sciences of the United States of America*, *97*(22), 12127–12131. https://doi.org/10.1073/pnas.97.22.12127

Technau, U., & Holstein, T. W. (1992). Cell sorting during the regeneration of Hydra from reaggregated cells. *Developmental Biology*, *151*(1), 117–127. https://doi.org/10.1016/0012-1606(92)90219-7

Technau, U., Steele, R. E., Technau, U., & Steele, R. E. (2012). Erratum to Evolutionary crossroads in developmental biology: Cnidaria (Development, 138, (1447-1458)). *Development (Cambridge)*, *139*(23), 4491. https://doi.org/10.1242/dev.090472

Teven, C. M., Farina, E. M., Rivas, J., & Reid, R. R. (2014). Fibroblast growth factor (FGF) signaling in development and skeletal diseases. https://doi.org/10.1016/j.gendis.2014.09.005

Thisse, B., & Thisse, C. (2005). Functions and regulations of fibroblast growth factor signaling during embryonic development. *Developmental Biology*, *287*(2), 390–402. https://doi.org/10.1016/j.ydbio.2005.09.011

Thotakura, S., Basova, L., & Makarenkova, H. P. (2019). FGF Gradient Controls Boundary Position Between Proliferating and Differentiating Cells and Regulates Lacrimal Gland Growth Dynamics. *Frontiers in genetics*, *10*(MAY), 362. https://doi.org/10.3389/fgene.2019.00362

Tiong, K. H., Mah, L. Y., & Leong, C. O. (2013). Functional roles of fibroblast growth factor receptors (FGFRs) signaling in human cancers. *Apoptosis*, *18*(12), 1447–1468. https://doi.org/10.1007/s10495-013-0886-7

Tischer, S., Reineck, M., Söding, J., Münder, S., & Böttger, A. (2013). Eph receptors and ephrin class B ligands are expressed at tissue boundaries in Hydra vulgaris. *The International journal of developmental biology*, *57*(9-10), 759–765. https://doi.org/10.1387/ijdb.130158ab

Trueb, B. (2011). Biology of FGFRL1, the fifth fibroblast growth factor receptor. *Cellular and Molecular Life Sciences*, *68*(6), 951–964. https://doi.org/10.1007/s00018-010-0576-3

Tsang, M., & Dawid, I. B. (2004). Promotion and attenuation of FGF signaling through the Ras-MAPK pathway. https://doi.org/10.1126/stke.2282004pe17

Tukey, J. W. (1977). *Exploratory data analysis* (Vol. 2). Reading, MA.

Turwankar, A., & Ghaskadbi, S. (2019). VEGF and FGF signaling during head regeneration in hydra. *Gene*, *717*, 144047. https://doi.org/10.1016/j.gene.2019.144047

Vaccarino, F. M., Schwartz, M. L., Raballo, R., Nilsen, J., Rhee, J., Zhou, M., Doetschman, T., Coffin, J. D., Wyland, J. J., & Hung, Y. T. E. (1999). Changes in cerebral cortex size are governed by fibroblast growth factor during embryogenesis. *Nature Neuroscience*, *2*(3), 246–253. https://doi.org/10.1038/6350

Vemaraju, S., Kantarci, H., Padanad, M. S., & Riley, B. B. (2012). A Spatial and Temporal Gradient of Fgf Differentially Regulates Distinct Stages of Neural Development in the Zebrafish Inner Ear. *PLoS Genet*, *8*(11). https://doi.org/10.1371/journal.pgen.1003068

Vermeulen, A., Behlen, L., Reynolds, A., Wolfson, A., Marshall, W. S., Karpilow, J., & Khvorova, A. (2005). The contributions of dsRNA structure to Dicer specificity and efficiency. *RNA*, *11*(5), 674–682. https://doi.org/10.1261/rna.7272305

Vincent, S., Wilson, R., Coelho, C., Affolter, M., & Leptin, M. (1998). The Drosophila protein Dof is specifically required for FGF signaling. *Molecular Cell*, *2*(4), 515–525. https://doi.org/10.1016/S1097-2765(00)80151-3

Vogg, M. C., Galliot, B., & Tsiairis, C. D. (2019). Model systems for regeneration: Hydra. *Development*, *146*(21). https://doi.org/10.1242/dev.177212

Wahl, M. B., Deng, C., Lewandowski, M., & Pourquié, O. (2007). FGF signaling acts upstream of the NOTCH and WNT signaling pathways to control segmentation clock oscillations in mouse somitogenesis. *Development*, *134*(22), 4033–4041. https://doi.org/10.1242/dev.009167

Wan, J., & Goldman, D. (2017). Opposing Actions of Fgf8a on Notch Signaling Distinguish Two Muller Glial Cell Populations that Contribute to Retina Growth and Regeneration. *Cell Reports*, *19*(4), 849–862. https://doi.org/10.1016/j.celrep.2017.04.009

Wang, Q., Uhlirova, M., & Bohmann, D. (2010). Spatial Restriction of FGF Signaling by a Matrix Metalloprotease Controls Branching Morphogenesis. *Developmental Cell*, *18*(1), 157–164. https://doi.org/10.1016/j.devcel.2009.11.004

Watanabe, T., Hosoya, H., & Yonemura, S. (2007). Regulation of myosin II dynamics by phosphorylation and dephosphorylation of its light chain in epithelial cells. *Molecular Biology of the Cell*, *18*(2), 605–616. https://doi.org/10.1091/mbc.E06-07-0590

Werner, S., & Grose, R. (2003). Regulation of Wound Healing by Growth Factors and Cytokines. *Physiological Reviews*, *83*(3), 835–870. https://doi.org/10.1152/physrev.2003.83.3.835

Whitehead, G. G., Makino, S., Lien, C. L., & Keating, M. T. (2005). Developmental biology: fgf20 is essential for initiating zebrafish fin regeneration. *Science*, *310*(5756), 1957–1960. https://doi.org/10.1126/science.1117637

Wickham, H. (2016). *Ggplot2: Elegant graphics for data analysis*. Springer-Verlag.

Wiedemann, M., & Trueb, B. (2000). Characterization of a novel protein (FGFRL1) from human cartilage related to FGF receptors. *Genomics*, *69*(2), 275–279. https://doi.org/10.1006/geno.2000.6332

Wittlieb, J., Khalturin, K., Lohmann, J. U., Anton-Erxleben, F., & Bosch, T. C. (2006). Transgenic Hydra allow in vivo tracking of individual stem cells during morphogenesis. *Proceedings of the National Academy of Sciences of the United States of America*, *103*(16), 6208–6211. https://doi.org/10.1073/pnas.0510163103

Wolpert, L., Hornbruch, A., & Clarke, M. R. B. (1974). Positional Information and Positional Signalling in Hydra. *American Zoologist*, *14*, 647–663.

Wolpert, L., Beddington, R., Jessell, T., Lawrence, P., Meyerowitz, E., & Smith, J. (2002). *Principles of Development, Second Edition* (Vol. 1).

Xu, J., Nakahara, M., Crabb, J. W., Shi, E., Matuo, Y., Fraser, M., Kan, M., Hou, J., & McKeehan, W. L. (1992). Expression and immunochemical analysis of rat and human fibroblast growth factor receptor (flg) isoforms. *The Journal of biological chemistry*, *267*(25), 17792–803.

Xu, X., Weinstein, M., Li, C., Naski, M., Cohen, R. I., Ornitz, D. M., Leder, P., & Deng, C. (1998). Fibroblast growth factor receptor 2 (FGFR2)-mediated reciprocal regulation loop between FGF8 and FGF10 is essential for limb induction. *Development*, *125*(4), 753–765.

Yokoyama, H., Ide, H., & Tamura, K. (2001). FGF-10 stimulates limb regeneration ability in Xenopus laevis. *Developmental Biology*, *233*(1), 72–79. https://doi.org/10.1006/dbio.2001.0180

Yu, J. Y., DeRuiter, S. L., & Turner, D. L. (2002). RNA interference by expression of short-interfering RNAs and hairpin RNAs in mammalian cells. *Proceedings of the National Academy of Sciences of the United States of America*, *99*(9), 6047–6052. https://doi.org/10.1073/pnas.092143499

Yum, S., Takahashi, T., Hatta, M., & Fujisawa, T. (1998). The structure and expression of a preprohormone of a neuropeptide, Hym-176 in *Hydra magnipapillata*. *FEBS letters*, *439*(1-2), 31–34. https://doi.org/10.1016/S0014-5793(98)01314-3

Yun, Y.-R., Won, J. E., Jeon, E., Lee, S., Kang, W., Jo, H., Jang, J.-H., Shin, U. S., & Kim, H.-W. (2010). Fibroblast Growth Factors: Biology, Function, and Application for Tissue Regeneration (R. Day, Ed.). *Journal of tissue engineering*, *1*(1), 218142. https://doi.org/10.4061/2010/218142

Zamore, P. D., Tuschl, T., Sharp, P. A., & Bartel, D. P. (2000). RNAi: Double-stranded RNA directs the ATP-dependent cleavage of mRNA at 21 to 23 nucleotide intervals. *Cell*, *101*(1), 25–33. https://doi.org/10.1016/s0092-8674(00)80620-0

Zhang, X., Bao, L., Yang, L., Wu, Q. F., & Li, S. (2012). Roles of intracellular fibroblast growth factors in neural development and functions. *Science China Life Sciences*, *55*(12), 1038–1044. https://doi.org/10.1007/s11427-012-4412-x

Zhu, X., Komiya, H., Chirino, A., Faham, S., Fox, G. M., Arakawa, T., Hsu, B. T., & Rees, D. C. (1990). Three-dimensional structures of acidic and basic fibroblast growth factors. *Science*, *251*(4989), 90–93. https://doi.org/10.1126/science.1702556

Zwilling, E. (1956). Interaction between limb bud ectoderm and mesoderm in the chick embryo. II. Experimental limb duplication. *J. Exp. Zool.*, *132*(1), 173–187. https://doi.org/10.1002/jez.1401320111

A Supplements

Table A.1: FGFf antibody western blot data quantification analysis. ROI was analyzed using Fiji.

sample	FGFf rb1 ROI [%]	FGFf rb2 ROI [%]	rb2 : rb1 [%]
wt105 (1 & 5)	24.174	6.308	26.09
AEP (2 & 6)	21.335	5.431	25.46
1184a (3 & 7)	13.542	2.853	21.07
Zürich (4 & 8)	17.670	8.687	49.16

Table A.2: Percentage of non-detached buds after siRNA treatment in *Hydra vulgaris* Zürich. *Hydra* were collected and treated at bud stage 3. Animals with buds still attached (non-detached) were counted at the indicated points of time and the percentage of non-detached buds calculated.

	0 h	24 h	48 h	120 h	144 h	172 h
siFGFRa_1	100%	100%	100%	68.6%	53.5%	48.8%
siFGFRa_2	100%	100%	65.7%	37.1%	31.4%	31.4%
siFGFf_1	100%	100%	84.8%	26.1%	17.7%	6.3%
siFGFf_2	100%	100%	65.7%	31.4%	25.7%	11.4%
pGL2	100%	100%	100%	34.9%	9.3%	4.7%

Table A.6: Raw data of siRNA macerates. The unprocessed data of the cell counts after siRNA treatment and electroporation. Ecto- and endodermal cells are not yet summarized as epithelial cells. N=8, except *siFGFc* (n=3). The sum of total cells per counted slide is indidcated by sum.

treatment	ecto	endo	nemato-blasts	I-cells	neurons	gland cells	sum
H_2O-	55	103	158	142	49	52	559
H_2O-	31	45	148	44	44	21	333
H_2O-	25	51	108	56	35	22	297

Raw data of siRNA macerates – continued

treatment	ecto	endo	nemato-blasts	I-cells	neurons	gland cells	sum
H_2O-	34	66	212	89	39	26	466
H_2O-	19	31	152	87	20	21	330
H_2O-	32	62	184	80	48	34	440
H_2O-	42	65	302	103	52	22	586
H_2O-	73	91	370	156	88	31	809
H_2O+	75	100	112	86	58	32	463
H_2O+	24	37	96	51	26	14	248
H_2O+	55	87	236	76	58	24	536
H_2O+	38	68	232	80	40	24	482
H_2O+	48	69	310	81	54	24	586
H_2O+	45	92	232	38	42	23	472
H_2O+	53	100	268	81	62	27	591
H_2O+	58	114	320	99	68	29	688
pGL2	44	65	168	80	40	35	432
pGL2	34	47	84	48	34	14	261
pGL2	45	71	192	61	49	36	454
pGL2	69	105	292	92	82	48	688
pGL2	94	133	334	103	84	59	807
pGL2	66	131	296	88	75	46	702
pGL2	93	154	316	113	115	52	843
pGL2	83	95	322	97	81	52	730
siFGFb_1	55	97	198	92	85	32	559
siFGFb_1	21	37	114	63	51	26	312
siFGFb_1	56	98	228	145	77	27	631
siFGFb_1	44	67	284	159	67	32	653
siFGFb_1	82	104	336	143	85	56	806
siFGFb_1	67	77	214	99	48	31	536
siFGFb_1	37	70	160	109	44	34	454
siFGFb_1	57	83	230	127	71	45	613
siFGFb_2	57	107	234	102	80	27	607
siFGFb_2	25	63	152	65	44	34	383

Raw data of siRNA macerates – continued

treatment	ecto	endo	nemato-blasts	I-cells	neurons	gland cells	sum
siFGFb_2	36	85	134	103	72	34	464
siFGFb_2	40	73	224	107	45	26	515
siFGFb_2	58	103	254	157	83	60	715
siFGFb_2	64	144	332	177	69	54	840
siFGFb_2	55	92	224	147	75	35	628
siFGFb_2	44	82	264	134	62	34	620
siFGFRa_1	60	75	168	77	62	22	464
siFGFRa_1	27	58	112	85	112	30	424
siFGFRa_1	71	80	272	135	171	50	779
siFGFRa_1	73	134	368	166	178	46	965
siFGFRa_1	47	78	204	76	101	35	541
siFGFRa_1	54	90	228	95	93	55	615
siFGFRa_1	122	200	369	175	232	78	1176
siFGFRa_1	84	138	332	124	190	67	935
siFGFRa_2	30	29	52	39	32	10	192
siFGFRa_2	23	62	140	67	84	20	396
siFGFRa_2	70	115	260	128	137	39	749
siFGFRa_2	49	77	276	115	132	54	703
siFGFRa_2	45	60	138	85	45	14	387
siFGFRa_2	41	76	230	81	102	30	560
siFGFRa_2	57	72	306	113	100	46	694
siFGFRa_2	38	47	210	85	80	35	495
siFGFf_1	59	105	264	74	57	27	586
siFGFf_1	30	61	98	68	61	30	348
siFGFf_1	44	110	202	160	50	50	616
siFGFf_1	69	131	224	145	75	46	690
siFGFf_1	57	141	306	192	92	52	840
siFGFf_1	81	164	382	186	74	50	937
siFGFf_1	73	127	284	159	83	55	781
siFGFf_1	62	144	298	192	122	74	892
siFGFf_2	22	59	108	59	31	12	291

Raw data of siRNA macerates – continued

treatment	ecto	endo	nemato-blasts	I-cells	neurons	gland cells	sum
siFGFf_2	23	53	76	44	56	20	272
siFGFf_2	64	118	308	147	71	53	761
siFGFf_2	42	97	340	97	59	55	690
siFGFf_2	86	141	258	78	84	40	687
siFGFf_2	59	107	262	92	83	62	665
siFGFf_2	62	127	350	95	87	41	762
siFGFf_2	102	158	358	143	90	62	913
siFGFRb_1	55	120	312	109	143	55	794
siFGFRb_1	52	91	264	94	119	59	679
siFGFRb_1	37	62	264	94	57	12	526
siFGFRb_1	38	51	272	80	50	28	519
siFGFRb_1	57	36	320	141	102	36	692
siFGFRb_1	58	77	412	144	104	62	857
siFGFRb_1	48	80	404	93	68	33	726
siFGFRb_1	56	105	336	146	83	46	772
siFGFRb_2	36	55	176	90	53	20	430
siFGFRb_2	37	66	214	86	71	42	516
siFGFRb_2	32	47	276	77	47	10	489
siFGFRb_2	37	80	276	92	65	33	583
siFGFRb_2	20	33	80	35	23	10	201
siFGFRb_2	22	39	152	59	35	16	323
siFGFRb_2	47	139	372	126	72	49	805
siFGFRb_2	45	103	300	128	38	45	659
siFGFc_1	58	24	294	188	62	76	702
siFGFc_1	59	47	184	196	39	29	554
siFGFc_1	141	68	342	263	58	82	954
siFGFc_2	106	40	264	195	69	88	762
siFGFc_2	115	59	217	251	47	59	748
siFGFc_2	97	73	394	214	40	39	857

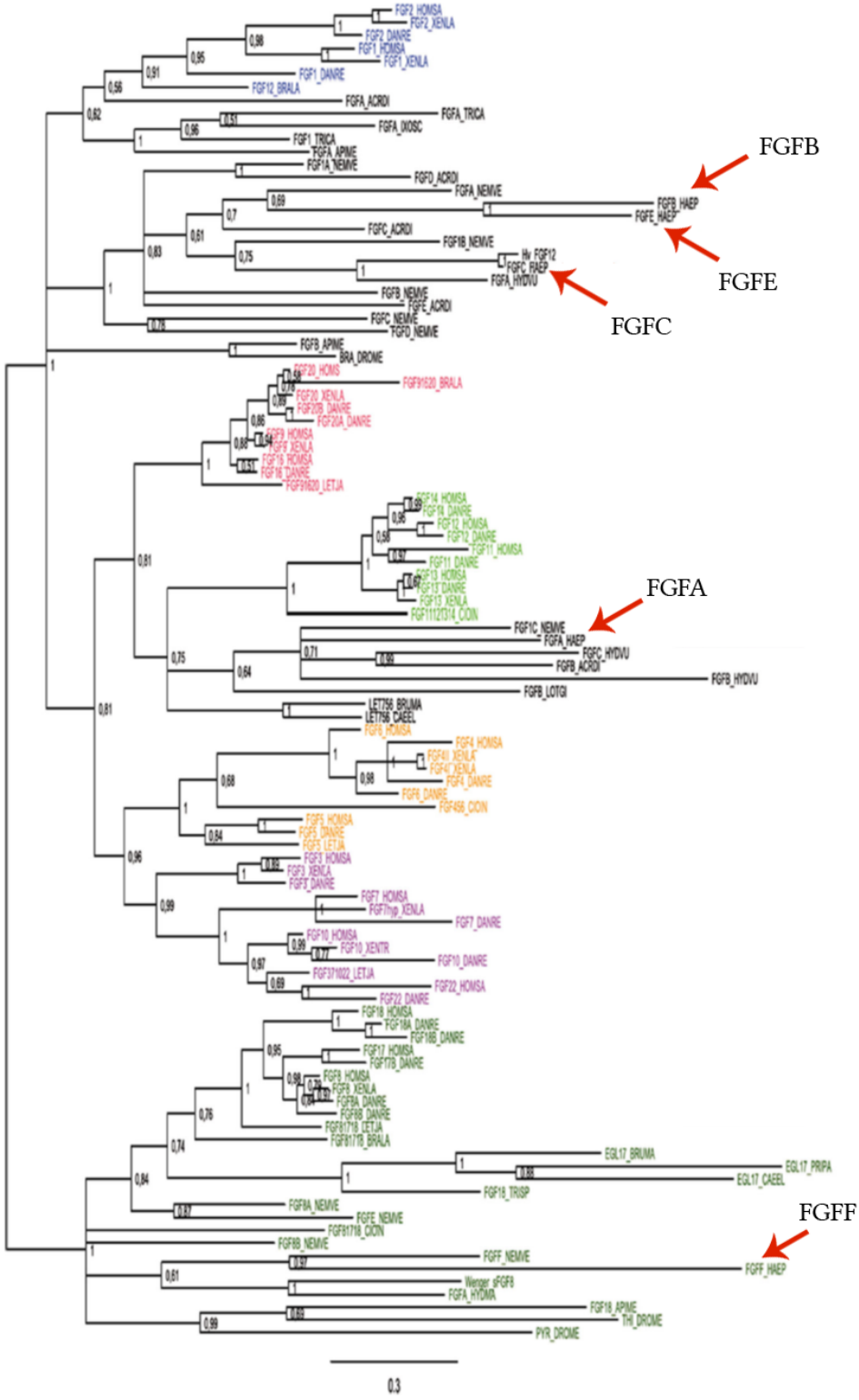

Figure A.1: Phylogenetic tree of FGFs using the FGF core sequence. The positions of the FGFs used in this study are marked with a red arrow. Modified after Lange et al. (2014).

Table A.3: Raw data of bud detachment after siRNA treatment. The counted non-detached buds after the siRNA treatment in bud stage 3 are listed for each observation point.

treatment	0 h	24 h	48 h	120 h	144 h	172 h
siFGFRa_1	16	16	16	16	11	11
siFGFRa_1	26	26	26	20	18	18
siFGFRa_1	25	25	25	10	9	9
siFGFRa_1	19	19	19	13	8	8
siFGFRa_2	35	35	23	13	11	11
siFGFf_1	25	25	25	2	2	0
siFGFf_1	19	19	19	5	0	0
siFGFf_1	35	35	23	14	12	5
siFGFf_2	35	35	23	11	9	4
pGL2	16	16	16	14	2	1
pGL2	26	26	26	3	2	2
pGL2	25	25	25	4	3	1
pGL2	19	19	19	9	1	0

Table A.4: FGFf antibody western blot data quantification analysis after siRNA treatment. ROI was analyzed using Fiji.

samples	tubulin ROI [%]	FGFf ROI [%]	FGFf : tubulin [%]
control	31.349	25.329	80.80
pGL2	26.483	26.631	100.55
siFGFRa_1	14.274	25.097	175.82
siFGFf_1	27.894	22.943	82.25

TTTTTAGTCCCTGTGTAATAAGATTTTATTGTTTATAAAAAAAAAAAATTGTTGGATTTAATGCTGTGTATTTATAAATACAAATGT
TGTATATAGCAAAATGATATCAGATTGGTGTGTTGTTTTGGTTTTATTAATGTCAAGATTAGTTTTTGGGCTGAATTTTACAGAGCC
AGTTAATTATATATTGAAATTAGGAGAAGATAGTTCATCTAGACTATTAGATTGTTCAGTTAATCTTCCTGTTGAATTAATCAAAAA
AATTGATTGGACACACAATGATATTGTTATCAATAATAAACCTAATATAACATTATCTGAAAATGGTCAAAAACTTGTTATTGCTCA
TTACCAATCCCATAATTCTGGTCGTTATGGGTGCAAAGTAACAGCTATGAATGAAGAATCTGTTCAAAGGGTATTTGATCTACTGCC
AGCTTCAGAAACTGAGGGAAACCAAACCATTGAAATGATGCTGAGAATAAAAAATGACATATCGTTACTTGTTGAGTTAGTGATGAA
TAAATTAGATTTAGATTGTACCGCTGTAGGTGCTTCACCTATTAATATTACATGGATAAAAAATGATCGGCTGATAGAAGCAAGGTC
CAACTTGTCTAATTTTCGTTATTCTTTCTCACCAAATTTTTTGAAATTAAGTATAAAAGAATTGCGACTTGATGATGCTGGTATTTA
CAAATGTATTTTGGAAAATAAATATGGCAAGATAGAACATATAATGACTGTTGAAATATATGAGAAAATGTTCTCTAAACCAATAGT
ATCTTCTACAGACAAACATAAAGTTTTTTATGTCAACTATGGTCAGAATTTAACTGTCCCTATATATGTTACTGCATTTCTACCCCA
CCCTCACTTTCAAATGTTATACGTTTACAGCATGACAAGTCCAAATACAAATGAAACTAAATTGGCACTTAGGGTATTACCAACAAT
GAGAGAACTAACTGTCTTGGAGAAAGGCCAGAGAAGAGGCAATTCAATTTCTCATATCAAGCTAGATTATTTTTTCAATAATATATC
AGAGCAAGATTTTGGTAATTATACCTTTATGGCTGGAAATAAGTATGGTTTTGATATATACCCGTTTCAAATATTGCATACAAAATA
TATGCAAACAACTGTCTTCCCGCCAATGAAATCAAGTATTAATAAAATCTACAAAGAGGAATCCGTAGAAAAAACAGTTATTTTTAT
TGTCATAACTTCAATGCTTGCTGGGCTAATTTTTGTTGCATTTGTTATTTTTTTTATTTGTCGTGTTCGTAGCAAAGACAAATTTAA
AAACAGTAACATCAACTACATCAAACCTTTAGAAACTGTGATTCTTAATCTTGGGGATAATAACACTAGTGGTGTTACCATGGTTAC
TTCTGTCTCTGCTTCCTATGCCAGTCGGCGTTTCAGACATTCACTTAATAATAATTTAATAAATGATAAGCAAAAATTGAATTTAAA
AATAGCTCCAGATCCTGCTTGGGAGATAAAACTTGAACAATTAGAAACAGATTGTTTATTGGGAGAGGGAGCTTTTGGTAGAGTTTT
TCGTGCAACAGCAAGAGATTTACCAAATCACACTGGAGTTCAAACAGTTGCTGTCAAAATGCTGAAAGAAGATTGTTGTGAACAAGA
TTTAAAAGATTTTATATCTGAAATAGAAGTAATGAAATCTATAGGAAAACATATCAATATTCTGAATTTACTTGCAGTGTCATCTCA
GCAAGGAAAGTTATATATAGTGGTTGAATATTGTCGTCATGGTAATTTGCGCTCTTTTCTGAAAGACAATCGACCTGTTATGCAAGC
TAATTCTGTGATAACAAAAAAAATAACATTGTACGATTTAACGTCGTTTTGCTTACAAGTTGCAAGAGGAATGAATTTTTTAGCTTC
AAAAAAGTGCATCCATCGAGACATAGCTGCTCGAAATGTTCTTGTTGGTGAAGGTTATTTAATGAAAATTGCTGATTTTGGACTTGC
ACGTGATATTCATGAACAAGATTATTATAGAAAATGCACAGATGGGCGATTACCCGTCAAATGGATGGCAATTGAAGCTTTGTTCGA
TCGTGTTTATACTACTCAAAGTGATATATGGTCATTTGGAATTTTGGCATGGGAAATTGTAACATTTGGTGGATCGCCTTACCCTGG
AATTGCATTAGAAAAATTGTTTGATTTATTAAAGCAAGGCTATCGAATGGAAAGACCACTTAATTGTACTGATGATATGTATACACT
TATGCTGAATTGTTGGAAAGAAATCCCATCAAAACGTCCGACATTTTCACAACTAATTGAAGATCTAGAAAGAATGCTATTGGATGC
AAGTTCTACAGAATATATAGATCTTCAACCAATTCAACCAGAACGCACAGAGTCATTTTCAACATCATTACACACTTCTGCAAGCAT
GTTGAATACAGATTTGCACGAGAAAAATAAATGTGATCATGACGAAATATCCTTCACTCATGAAGATGGTTTATCAGAAGCAGATAT
TCTTCTTAGTCACTATGCAGTTTCTTAATTACTTCAACTGCTTGTGACGTTTTTAGATGTAAACTTGATTTATCAGTTTCTCTAAAT
GATTGCCTTGTCATTAACGTGTATTGCATTTGACTTTCATCATGAAGAATCTAGAGATCTATCCGATTCTTCTCTATTAATAAACAC
TGTCATGAAGATTGTTTATATATGAATCATTGGATCAGGAACTTCTTGAGGATCATAATAAAAGTAATACTAAATATGAAATTGCCA
GCTAAAACCAAAGGTTCGTAATTTTCGATGCGAATAAATGAGCTTTTCAAAAAAAAAAAAAAA

Figure A.2: Sequence of *FGFRa*. Indicated in red is the sequence for the siRNA *siFGFRa_1*, in blue for *siFGFRa_2*. Green indicated is the predicted start codon; pink indicated is the predicted stop codon. Sequences for Ig loops are underlined. Accession number: NM_001309765.1 *Hydra vulgaris* fibroblast growth factor receptor (LOC100206525), mRNA (kringelchen).

ACGGAAAAAAACACATACTGAAACTTTTTAGTCCCTGTGTAATAAGCAAAATGATATCAGATTGGTGTGTTATTTTGGTTCTATCAA
TTTCAAGATTAGTTTTTGGGATAAATTTTACAGAGCCAGTTAATTATATATTGAAAGTAGGAGAAAATAATTCATCTAGACTATTAG
ATTGTTCAGTTGATCTTTCTGTTGAATTAATTAAAAGAATTGATTGGACATACAATGGTATTGTTATTAATAAAAAACCTAATGTAA
CATTCACTGACAAAGGTCAAAAACTTATTATTGGTCATTATAAATCCCAAAATTCTGGTCGCTATGGGTGTAAAGTTACAGCTGTAA
GTGAAGAATCTGTTGAAAGGATATTTGATCTACTGCCCACATCAGATCTGATGCCAAGAATAAAAAATGATATTTCATTGCTTGTTG
AGTTAGTGATGAATAAATTAGATTTGGATTGTACTGCTGTAGGTGCTTCACCTATTAGTATCATGTGGTTAAAAAATGATAAACTGA
TTGAAGCAAGATCTAACTTACGTTATTATTTCTCACCAAATTTTTTAAAACTAAGTATAAAAGAGGTGAGACTCGATGATGCTGGTA
TTTACAAATGCATCTTGGAAAATAAATATGGCAAGGTAGAACATGTAATGACTGTTGAAATATATGAGAAAATGTTCGCTAAACCAA
TAGTATCATCTACAGACAAACATAAAGTTTTTTTATGTCGACTATGGTCAGAATTTAACTGTCCCTATATATGTTACTGCATTTCTA
CCTAACCCTCACTTTTCAAATGTTTATACGTTTACAGCATGACAAATCCAAATACAAATGAAACTAAATTGGCCCTAAGAGTATTAC
CAACAATGAGAGAACTAACTGTCTTGGAGAAAGGCCAGAGAAGAGGCAATTCAATTTCTCATATCAAGCTAGATTATTTTTTCAATA
ATATATCAGAGCAAGATTTTGGTAATTATACCTTAATGGCTGGAAATAAGTATGGTTTTGATATATACCCCTTTCAAATATTGCATA
CAAAATATATGCAAACGACTGTCCTCCCGCCGATGAAATCAAGCATTAATAAAATCTACAAGGAGGAATCCGTAGAAAAAACAGTTA
TTTTTATTGTCATAACCTCAATGCTTGCTGGGTTAATTTTTGTTGCATTTGTTATTTTTTTTATTTGTCGTGTTCGTAGTAAAGACA
AATTTAAAAACAGTAACATCTACTACATCAAACCTTCACAACCTGTGATTCTTAATCTTGGGGATAACAACACTAGTGGTGTTACCA
TGGTTACTTCTGTCTCTGCTTCCTATGCCAGTCGACGTTTCAGACATTCACTCAATAATAATTTAATAAATGATAAGCAAAAATGCA
ATTTAAAAATAGCTCCAGATCCTGCTTGGGAGATTAAGCTTGAACAGTTAGAAACAGATTGTTTATTGGGAGAGGGAGCTTTTGGTA
GAGTTTTTCGTGCAACAGCAAAAGATTTACCAAATCACACTGGAGTTCAAACAGTTGCTGTCAAAATGTTGAAAGAAGATTGTTGTG
AACAAGATTTAAAAGATTTTATATCTGAAATAGAAGTAATGAAATCTATAGGAAAACACATCAATATTCTGAATTTACTTGCAGTGT
CATCACAGCAAGGAAAGTTATATATAGTGGTTGAATATTGTCGTCATGGTAATTTGCGCTCCTTTCTGAAAGACAATCGACCTGTTA
TGCAAGCTAATTCTGTGATAATCAAGAAAATAACATTGTATGATTTAACATCGTTTTGCTTACAAGTTGCAAGAGGAATGAATTTTT
TAGCTTCAGAAAAGTGCATCCATCGAGACATAGCTGCTCGAAATGTTCTTGTTGGTGAAGGTTATTTAATGAAAATTGCTGATTTTG
GACTTGCACGTGATATTCATGAACAAGATTATTATAGAAAATGCACAGATGGGCGTTTACCTGTCAAATGGGTGGCAATTGAAGCTT
TGTTTGATCGTGTTTACACTACTCGAAGTGATATATGGTCATTTGGAATTTTGGCATGGGAAATTGTAACATTTGGTGGATCACCCT
ACCCTGGAATTGCATTGGAAAAAATGTTTGATTTATTAAAGCAAGGCTATCGAATGGAAAAACCACTTAATTGTACTGATGATATGT
ATGCACTTATGCTAAATTGCTGGAAAGAAATCCCATTAAAACGTCCGACATTTTCACAACTAATTGAAGATCTAGAAAAAATGCTAT
TGGATGCAAGTTCTACAGAATATATAGATCTTCAACCAATCCAACCAGAGTGCGCAGAGTTACTTTCAACCTCAATACACACTTCTG
CAAGCATGTTGAATACAGATTTGTTTAACAAACATAAATATGATCACGATGAAGTGTCCTTTACTCATAAAAATGGTTTATCAGAAG
CAGATGTTCTTCTTAATTACCAAGTAGTTTCTTGA

Figure A.3: Sequence of *FGFRb*. Indicated in red is the sequence for the siRNA *siFGFRb_ex1*, in blue for *siFGFRb_ex2*. Indicated in orange is the sequence binding site for the siRNA *siFGFRa_1*. Green indicated is the predicted start codon; pink indicated is the predicted stop codon. Sequences for Ig loops are underlined.

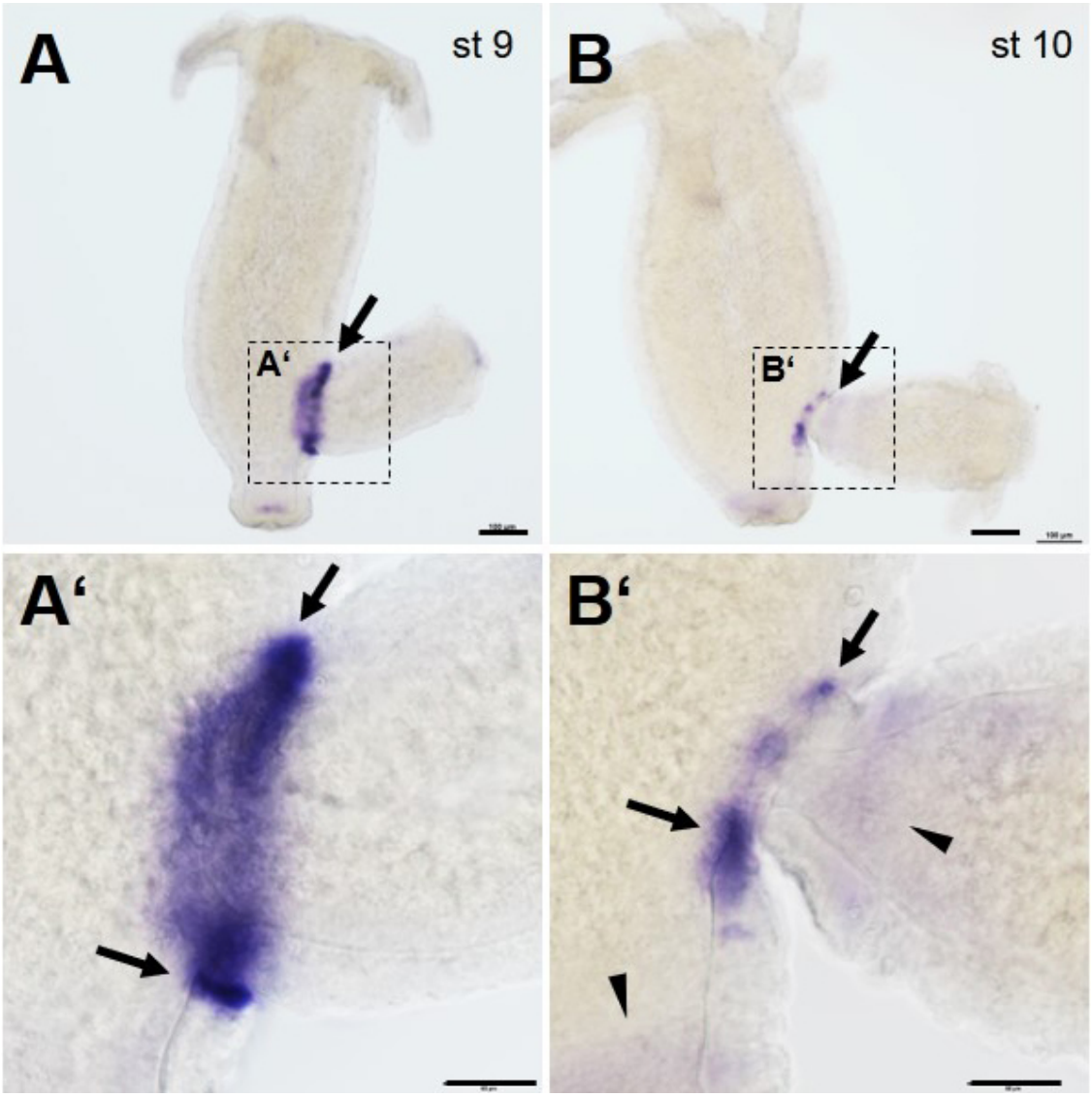

Figure A.4: Transcription of *FGFRa* in *Hydra vulgaris* Zürich. (A, B) In the detachment phase *FGFRa* is transcribed in ectodermal cells at the bud base (black arrows). (B) When the bud's basal disc has formed, *FGFRa* is restricted to ectodermal cells of the adult tissue. A weak endodermal transcription in the peduncle is indicated by black arrowheads. Scale bar 100 µm.

CGGTAGAGTACGCGGGGACGGAAAAAAACACATACTGAAACTTTTTAGTCCCTGTGTAATAAGTGAACACTAGTTTTAAAAATGATA
TTGCTTCAAAGTTTTTTTGAGAAGACAATTTTTATTTTTGTTGTGGTTAAACTATCGCAACCAGTACCAACCTTGATGCCAAGAAAT
GTAAAACTGTCTTTAATTAAAGATGAAATGGTAAAATACCTAAAACATCCTTCTTATAAAAAAAGCGTATTGCTCTATTCAAAGCAA
GGTTATTTTTTATCGATTGCAGACGACGGGAAAATATATGGAACTCATGATGGATTTTCACCTGATGCTCAGCTAGAAGTACAGTCA
TTTGGAGTGAACTATAAACGTATAAGAAAACCTAACTCATGGTATCTATCAATTGATAAAAACGGCGCAGTAAAAGCTGAGAATGAT
CCAAAAAACGAAACTTTATTCCAAGAAGTAATCGATAAAGAAGGTTGGGCAATATACCGTAATGATTTAACTGGATATCTACTTGCG
TTCAATAAAAATGGAAAATTACAACAAAACTTGAAGAGCTCTAAAGTAAAAAATAAAGCAAAGTTTCTACTTCTTTCTTCTTTTTCT
AGTGGTGGAAAAAAGCAGAAAGCATAAAAAAAACTTTGAAAAGATTCTTTAAATATGATAGGTGTAAATAATGTAAAATAAAAAGA
CAAAAATTAATTTTATTACCAACCGCTCCGCTTTATATTTTATAGTTCAAAAGCTTTAAGAATTTATATGTCAATAAATTATAATAA
TTTATGTAAATATTTAAA

Figure A.5: Sequence of *FGFb*. Indicated in red is the sequence for the siRNA *siFGFb_1*, in blue for *siFGFb_2*. The core sequence is underlined. Green indicated is the predicted start codon, pink indicated is the predicted stop codon. Accession number: HAEP_T-CDS_v02_10362.

CTTTTAGAATAAAAACTTAGTTTTTGCTAACATGAAGTTCTACTTTTTAGTGTTTCTGACTTACATTGATAATGGTAATAGCCAACT
ATCGGAATATCCGCACAAAAAAGAAGAGTTAAATGATTTTACGTTGCAAAAGGAATGGAGCGCAGTTCAGAGAACACCTGAAAAAAA
TGAAAAACATCATAAACCTATCCTCACAAAAGAAGTTAATCTTATTTTTGATAAATGGGGAAACTGCAAGCTAGCATTGTTGTATTG
TCGAAATGGATTTTACATTGATATTACAAATAACAACGTGGTTGGGGTTTCTTATAAAAGTTTCATAACAAATGAAACAGGTTTATT
TCAAATAGAAACGTATGGTAAAAGTTTCGTTATGTTAAAGCATGTAAAAACAAATAACTATATTGCAATGAATAATGAAGGAAAACT
GCACTCGTCGGAAACAAAGACGGACGAATGTTTATTCTATTATTATTTGGAGAAAGGAGAATACGCAACTTTTTCTTCTGCAAAATA
TTTTGTTAACGATTATTACGATTTGTACATAAGTTTAAGAAAAACTGGAAAATTACGTAAGGCCAATCATTCAACACCATTTCAACG
CTCATCTCAGTTTGAAATAATTCCAAAGATATCTGAAAAAGATCAACTGTGCATCCGAAGATGAAGTAGTACCAATATCAAACCGA
CTATAAATGGCTTGTGGTTTTATGGCAATAAAAAAAAAAGTTTTTACTCAGCATACAAAACTTTGGCATTAATAAATTCTGCAATCA
TTCTAGGACAGTAGTTACTCGAGTCAGCTCCTCTTTAATTAATGCTTTTTAAAAAACATCTTTTTAGCAATATGCAGCAATATAAAG
TTCAAGCTTTTGTATATACTTATTTATGTATATAAAGATATATTTGACCT

Figure A.6: Sequence of *FGFc*. Indicated in red is the sequence for the siRNA *siFGFc_1*, in blue for *siFGFc_2*. The core sequence is underlined. Green indicated is the predicted start codon, pink indicated is the predicted stop codon. Accession number: HAEP_T-CDS_v02_11252.

GATATTTAAAAACATAGGAGGTGGCAATACTCAAACTGATAAGGTGCAATCAATTTTTGGTGACCATTATTTAATACACATAACCAC
ATCCGAAAACCCTTATTTTTCATCGTTATTCTTTGTAGTAGGTTCTCGGCAAAAACTTTTTGCGTTACTTGTTGTTTATCGTTAGCA
CTTATTCAAAAAAAATAACTTTGCGATAAAATATTTTTAAACAGAAAAGGATTTAAAATGATTCGAATGAATGGTTTAAAACGAGTC
ACATTTATTACTTTGAGCATGGTTTTTATTTCTTTATCGATCCAATCATCTCCTCCTGTTACTACTTCAAAAGTCCATGGAGGAACT
ACGAAGTCGATATATGAAGACCAATTTGAAGGTTCGCTTGCAGAACCGACTCATGATCAACAAAATTTTTACGACGCTACAGTAAGC
GATGCAATGGAGTTATATTCTATATCAGCAAAACGTCTTGTTATTGTTCAAGACAAACCTGGAACCAAACCTTGGGATCATGAATCA
GAATTAATAATTAACAAAAAACAGAGAATATACGGAAGAGAAAATCAGTTTGTTACTGAGACAGTTTCGTACGGGCGATTAAAGATC
AAGTCAGAATACGCCAAGCAATATTTGTGTGTGAAAAATGACGGTGTTATTTCTTTAAAGCAAAATGCTGATAGTAGCAAAAACCAC
CGTTCACGAAAGCGATGTCTTTTCAATATGAATCTTACTCAACTCATGCATATTACATTATCCGTCTATATCGGTAAAACAACCTGG
TATTTAACTGTAAAAGATGATGTTATTTCTATGACTGACAATCTTCGAAGTAATGAACTAGAACGATCGTTCATGTGGCTTCCAACG
ATGAGTGGCACTAGCCTAGCACCATCAAGACTGAGAAGTTTTGATGATAAATCTCGGACTGTTTGTGATTCTTCCAATAAAAGAATA
ACCAATCAAATAAAAAAAATTAAAGAACTTCAAAACGAAGTAAATAAATTAAATGATGAAATTGAAAAGATGAAATTGGAAAATTTA
AAAAAAAATTAGTTGACTAATTTGAAAAAAATGCAAAAATAAAGGTTGTAAATTTTCATAGGGTGTATCTTGTGGATTGATACGCCC
ACTATGAATGTCATAAGTCAATAACGACGTCGTCATTCAGCGCAACAAAGTCCACATTGTGGGTTTCAATCATTGTAGAAACTACAA
AAATTATTTAAAACGCATTTTAAAAACAGTATTGTATCATAGTTTTTATGTTTATTTTATTATGACTAGGCGTTATTTTTGACTGCG
ACGTTAAGTAAACGTCGTGTAGACGATTAATGAGCAGACTACGAAAAAGGAAGATCAAACTGTAATACGAAACTCTTGCATAATAGC
TTAAAAAGTTCTTTCTTTTAACCTTTTTTTCCTTTTAT

Figure A.7: Sequence of *FGFf*. Indicated in red is the sequence for the siRNA *siFGFf_1*, in blue for *siFGFf_2*. The core sequence is underlined. Green indicated is the predicted start codon, pink indicated is the predicted stop codon. Accession number: HAEP_T-CDS_v02_48314.

Table A.5: Percentual distribution of cell types in *Hydra* after siRNA knockdown. Cell types were set in proportion to the number of total cells per treatment and are given as percentage. Total cell counts: H_2O- (n=3820); H_2O+ (n=4097); *pGL2* (n4917); siFGFRa_1 (n=5899); *siFGFRa_2* (n=4176); *siFGFRb_1* (n=5565); *siFGFRb_2* (n=4006); *siFGFb_1* (n=4564); *siFGFb_2* (n=4772); *siFGFc_1* (n=2210); *siFGFc_2* (n=2367); *siFGFf_1* (n=5690); *siFGFf_2* (n=5041). Epithelial cells include ecto- and endodermal epithelial cells. Outlieres are indidcated in bold.

treatment	epithelial cells	I-cells	neurons	nemato-blasts	gland cells
H_2O-	21.6	19.8	9.8	42.8	6.0
H_2O+	25.9	15.2	10.0	44.1	4.8
pGL2	27.0	13.9	11.4	40.8	7.0
siFGFRa_1	23.6	15.8	19.3	34.8	6.5
siFGFRa_2	21.3	17.1	**17.0**	38.6	5.9
siFGFRb_1	**19.5**	17.2	**13.8**	**49.2**	6.3
siFGFRb_2	20.5	**8.9**	9.9	45.2	5.5
siFGFb_1	23.0	20.5	11.6	38.7	6.2
siFGFb_2	23.6	20.8	11.1	38.1	6.4
siFGFc_1	**18.0**	**29.3**	**7.2**	**37.1**	**8.5**
siFGFc_2	20.7	**27.9**	**6.6**	**37.0**	**7.9**
siFGFf_1	**25.6**	20.7	10.8	**36.2**	6.7
siFGFf_2	**26.2**	15.0	11.1	40.9	6.8

Table A.8: Summary statistics for siRNA macerates. The arithmetic mean (mean), standard deviation (sd) and standard error (se) for each cell type in the maceration are depicted.

treatment	cell type	n	mean	sd	se
siFGFb_1	ecto	8	52.38	18.61	6.58
siFGFb_1	endo	8	79.12	21.77	7.70
siFGFb_1	nematoblasts	8	220.50	68.73	24.30
siFGFb_1	I-cells	8	117.12	32.19	11.38
siFGFb_1	neurons	8	66.00	16.48	5.83
siFGFb_1	gland cells	8	35.38	10.14	3.59
siFGFb_2	ecto	8	47.38	13.29	4.70
siFGFb_2	endo	8	93.62	25.01	8.84
siFGFb_2	nematoblasts	8	227.25	62.64	22.15
siFGFb_2	I-cells	8	124.00	36.30	12.83
siFGFb_2	neurons	8	66.25	14.89	5.26
siFGFb_2	gland cells	8	38.00	12.32	4.35
siFGFc_1	ecto	3	86.00	47.63	27.50
siFGFc_1	endo	3	46.33	22.01	12.71
siFGFc_1	nematoblasts	3	273.33	81.00	46.77
siFGFc_1	I-cells	3	215.67	41.19	23.78
siFGFc_1	neurons	3	53.00	12.29	7.09
siFGFc_1	gland cells	3	62.33	29.02	16.76
siFGFc_2	ecto	3	106.00	9.00	5.20
siFGFc_2	endo	3	57.33	16.56	9.56
siFGFc_2	nematoblasts	3	291.67	91.69	52.93
siFGFc_2	I-cells	3	220.00	28.48	16.44
siFGFc_2	neurons	3	52.00	15.13	8.74
siFGFc_2	gland cells	3	62.00	24.64	14.22
siFGFf_1	ecto	8	59.38	16.29	5.76
siFGFf_1	endo	8	122.88	31.31	11.07
siFGFf_1	nematoblasts	8	257.25	84.41	29.84
siFGFf_1	I-cells	8	147.00	49.94	17.66
siFGFf_1	neurons	8	76.75	22.94	8.11
siFGFf_1	gland cells	8	48.00	14.73	5.21
siFGFf_2	ecto	8	57.50	28.15	9.95

Summary statistics for siRNA macerates – continued

treatment	cell type	n	mean	sd	se
siFGFf_2	endo	8	107.50	37.03	13.09
siFGFf_2	nematoblasts	8	257.50	109.10	38.57
siFGFf_2	I-cells	8	94.38	36.26	12.82
siFGFf_2	neurons	8	70.12	20.33	7.19
siFGFf_2	gland cells	8	43.12	18.78	6.64
siFGFRa_1	ecto	8	67.25	28.24	9.99
siFGFRa_1	endo	8	106.62	47.24	16.70
siFGFRa_1	nematoblasts	8	256.62	95.10	33.62
siFGFRa_1	I-cells	8	116.62	39.51	13.97
siFGFRa_1	neurons	8	142.38	58.46	20.67
siFGFRa_1	gland cells	8	47.88	18.85	6.66
siFGFRa_2	ecto	8	44.12	14.89	5.27
siFGFRa_2	endo	8	67.25	25.15	8.89
siFGFRa_2	nematoblasts	8	201.50	85.31	30.16
siFGFRa_2	I-cells	8	89.12	28.92	10.22
siFGFRa_2	neurons	8	89.00	37.29	13.18
siFGFRa_2	gland cells	8	31.00	15.52	5.49
siFGFRb_1	ecto	8	50.12	8.41	2.97
siFGFRb_1	endo	8	77.75	27.81	9.83
siFGFRb_1	nematoblasts	8	323.00	58.97	20.85
siFGFRb_1	I-cells	8	112.62	26.89	9.51
siFGFRb_1	neurons	8	90.75	32.09	11.34
siFGFRb_1	gland cells	8	41.38	17.25	6.10
siFGFRb_2	ecto	8	34.50	9.67	3.42
siFGFRb_2	endo	8	70.25	35.96	12.71
siFGFRb_2	nematoblasts	8	230.75	93.39	33.02
siFGFRb_2	I-cells	8	86.62	31.22	11.04
siFGFRb_2	neurons	8	50.50	17.98	6.36
siFGFRb_2	gland cells	8	28.12	16.07	5.68
H_2O-	ecto	8	38.88	17.55	6.20
H_2O-	endo	8	64.25	23.54	8.32
H_2O-	nematoblasts	8	204.25	88.48	31.28

Summary statistics for siRNA macerates – continued

treatment	cell type	n	mean	sd	se
H_2O-	I-cells	8	94.62	38.62	13.65
H_2O-	neurons	8	46.88	19.48	6.89
H_2O-	gland cells	8	28.62	10.64	3.76
H_2O+	ecto	8	49.50	14.98	5.29
H_2O+	endo	8	83.38	24.41	8.63
H_2O+	nematoblasts	8	225.75	82.57	29.19
H_2O+	I-cells	8	74.00	19.76	6.98
H_2O+	neurons	8	51.00	13.86	4.90
H_2O+	gland cells	8	24.62	5.29	1.87
pGL2	ecto	8	66.00	23.18	8.19
pGL2	endo	8	100.12	37.59	13.29
pGL2	nematoblasts	8	250.50	91.12	32.22
pGL2	I-cells	8	85.25	21.64	7.65
pGL2	neurons	8	70.00	27.12	9.59
pGL2	gland cells	8	42.75	14.17	5.01

Table A.10: Tukey's HSD for siRNA maceration. The full list of Tukey's HSD calculation for each siRNA treatment and cell type.

comparison	ecto	endo	gland cells	I-cells	nemato-blasts	neurons
siFGFb_2–siFGFb_1	1.000	0.999	1.000	1.000	1.000	1.000
siFGFc_1–siFGFb_1	0.826	0.571	0.332	0.274	0.999	1.000
siFGFc_2–siFGFb_1	0.144	0.992	0.352	0.220	0.989	0.999
siFGFf_1–siFGFb_1	1.000	0.503	0.910	0.995	1.000	1.000
siFGFf_2–siFGFb_1	1.000	0.953	0.998	0.968	1.000	1.000
H_2O-–*siFGFb_1*	0.908	0.993	1.000	0.963	1.000	0.671
H_2O+–*siFGFb_1*	1.000	1.000	0.971	0.305	1.000	0.963
pGL2–siFGFb_1	0.988	0.997	0.999	0.847	1.000	1.000
siFGFRa_1–siFGFb_1	0.989	0.975	0.916	1.000	1.000	0.013
siFGFRa_2–siFGFb_1	1.000	0.999	1.000	0.900	1.000	0.989

Tukey's HSD for siRNA maceration – continued

comparison	ecto	endo	gland cells	I-cells	nemato-blasts	neurons
siFGFRb_1–siFGFb_1	1.000	1.000	1.000	1.000	0.445	0.935
siFGFRb_2–siFGFb_1	0.697	0.999	0.999	0.786	1.000	0.913
siFGFc_1–siFGFb_2	0.651	0.168	0.496	0.407	1.000	1.000
siFGFc_2–siFGFb_2	0.071	0.795	0.519	0.339	0.996	0.999
siFGFf_1–siFGFb_2	0.992	0.974	0.984	1.000	1.000	1.000
siFGFf_2–siFGFb_2	1.000	1.000	1.000	0.879	1.000	1.000
H_2O-–*siFGFb_2*	0.987	0.640	0.991	0.868	1.000	0.642
H_2O+–*siFGFb_2*	1.000	1.000	0.872	0.164	1.000	0.954
pGL2–siFGFb_2	0.911	1.000	1.000	0.665	1.000	1.000
siFGFRa_1–siFGFb_2	0.915	1.000	0.986	1.000	1.000	0.015
siFGFRa_2–siFGFb_2	1.000	0.778	0.999	0.746	1.000	0.992
siFGFRb_1–siFGFb_2	1.000	0.995	1.000	1.000	0.555	0.946
siFGFRb_2–siFGFb_2	0.902	0.787	0.986	0.586	1.000	0.898
siFGFc_2–siFGFc_1	0.999	1.000	1.000	1.000	1.000	1.000
siFGFf_1–siFGFc_1	0.989	0.010	0.975	0.813	1.000	0.970
siFGFf_2–siFGFc_1	0.889	0.062	0.820	0.019	1.000	0.998
H_2O-–*siFGFc_1*	0.127	0.978	0.080	0.018	0.992	1.000
H_2O+–*siFGFc_1*	0.748	0.448	0.027	0.001	1.000	1.000
pGL2–siFGFc_1	0.999	0.132	0.800	0.008	1.000	0.999
siFGFRa_1–siFGFc_1	0.999	0.078	0.973	0.240	1.000	0.022
siFGFRa_2–siFGFc_1	0.426	0.949	0.140	0.011	0.989	0.866
siFGFRb_1–siFGFc_1	0.846	0.675	0.720	0.220	1.000	0.733
siFGFRb_2–siFGFc_1	0.060	0.946	0.070	0.006	1.000	1.000
siFGFf_1–siFGFc_2	0.453	0.175	0.979	0.750	1.000	0.949
siFGFf_2–siFGFc_2	0.195	0.526	0.837	0.013	1.000	0.996
H_2O-–*siFGFc_2*	0.004	1.000	0.086	0.013	0.947	1.000
H_2O+–*siFGFc_2*	0.104	0.976	0.030	0.001	0.995	1.000
pGL2–siFGFc_2	0.684	0.732	0.818	0.005	1.000	0.998
siFGFRa_1–siFGFc_2	0.678	0.587	0.977	0.190	1.000	0.016
siFGFRa_2–siFGFc_2	0.029	1.000	0.150	0.007	0.934	0.815
siFGFRb_1–siFGFc_2	0.158	0.998	0.741	0.174	1.000	0.664

Tukey's HSD for siRNA maceration – continued

comparison	ecto	endo	gland cells	I-cells	nemato-blasts	neurons
siFGFRb_2–*siFGFc_2*	0.001	1.000	0.076	0.004	0.997	1.000
siFGFf_2–*siFGFf_1*	1.000	1.000	1.000	0.356	1.000	1.000
H_2O-–*siFGFf_1*	0.417	0.037	0.375	0.340	0.989	0.195
H_2O+–*siFGFf_1*	0.999	0.671	0.130	0.017	1.000	0.579
pGL2–*siFGFf_1*	1.000	0.989	1.000	0.170	1.000	1.000
siFGFRa_1–*siFGFf_1*	1.000	0.999	1.000	0.990	1.000	0.116
siFGFRa_2–*siFGFf_1*	0.915	0.067	0.585	0.221	0.983	1.000
siFGFRb_1–*siFGFf_1*	1.000	0.369	1.000	0.986	0.940	1.000
siFGFRb_2–*siFGFf_1*	0.197	0.070	0.335	0.131	1.000	0.448
H_2O-–*siFGFf_2*	0.827	0.282	0.798	1.000	0.988	0.515
H_2O+–*siFGFf_2*	1.000	0.988	0.449	0.991	1.000	0.901
pGL2–*siFGFf_2*	0.997	1.000	1.000	1.000	1.000	1.000
siFGFRa_1–*siFGFf_2*	0.997	1.000	1.000	0.981	1.000	0.026
siFGFRa_2–*siFGFf_2*	0.998	0.409	0.932	1.000	0.982	0.998
siFGFRb_1–*siFGFf_2*	1.000	0.891	1.000	0.987	0.941	0.979
siFGFRb_2–*siFGFf_2*	0.569	0.419	0.759	1.000	1.000	0.814
H_2O+–H_2O-	0.959	0.967	1.000	0.992	1.000	1.000
pGL2–H_2O-	0.177	0.542	0.824	1.000	0.997	0.616
siFGFRa_1–H_2O-	0.182	0.350	0.385	0.978	0.990	0.000
siFGFRa_2–H_2O-	1.000	1.000	1.000	1.000	1.000	0.063
siFGFRb_1–H_2O-	0.888	0.999	0.905	0.985	0.224	0.025
siFGFRb_2–H_2O-	1.000	1.000	1.000	1.000	1.000	1.000
pGL2–H_2O+	0.964	1.000	0.483	1.000	1.000	0.946
siFGFRa_1–H_2O+	0.967	0.995	0.135	0.360	1.000	0.000
siFGFRa_2–H_2O+	1.000	0.991	1.000	0.999	1.000	0.280
siFGFRb_1–H_2O+	1.000	1.000	0.608	0.396	0.530	0.139
siFGFRb_2–H_2O+	0.808	0.992	1.000	1.000	1.000	1.000
siFGFRa_1–*pGL2*	1.000	1.000	1.000	0.889	1.000	0.017
siFGFRa_2–*pGL2*	0.676	0.689	0.945	1.000	0.994	0.994
siFGFRb_1–*pGL2*	0.992	0.985	1.000	0.910	0.886	0.955
siFGFRb_2–*pGL2*	0.066	0.699	0.788	1.000	1.000	0.883

Tukey's HSD for siRNA maceration – continued

comparison	ecto	endo	gland cells	I-cells	nemato-blasts	neurons
siFGFRa_2–siFGFRa_1	0.685	0.489	0.597	0.932	0.984	0.311
siFGFRb_1–siFGFRa_1	0.992	0.932	1.000	1.000	0.936	0.524
siFGFRb_2–siFGFRa_1	0.069	0.499	0.345	0.837	1.000	0.000
siFGFRb_1–siFGFRa_2	1.000	1.000	0.978	0.947	0.196	1.000
siFGFRb_2–siFGFRa_2	0.990	1.000	1.000	1.000	1.000	0.191
siFGFRb_2–siFGFRb_1	0.661	1.000	0.879	0.864	0.613	0.088

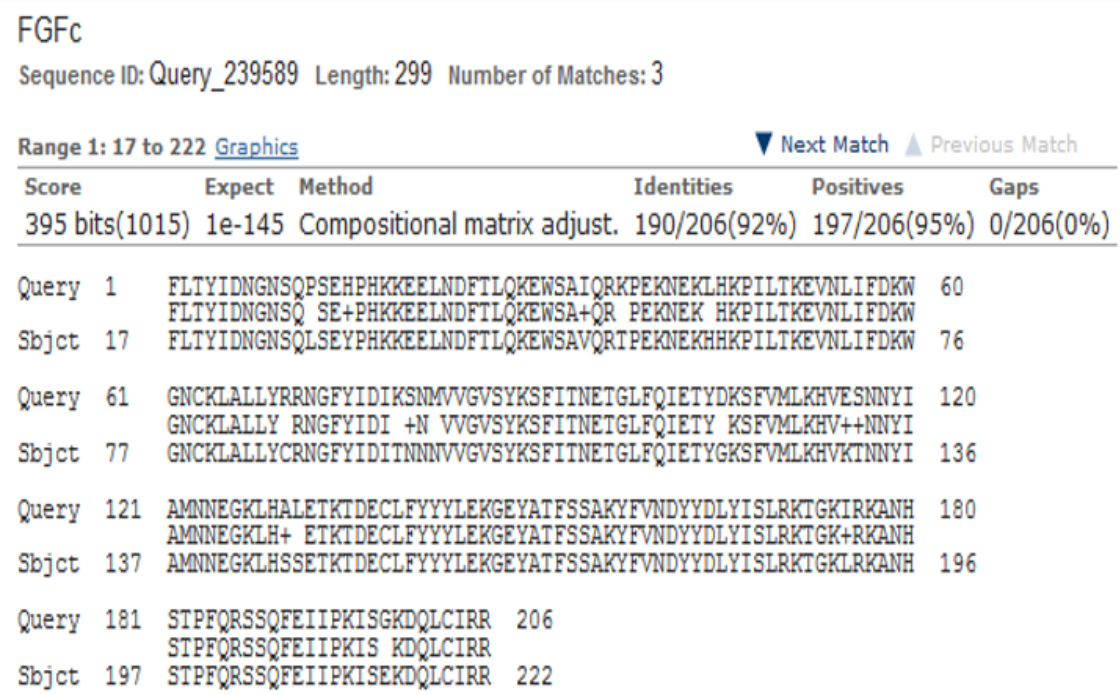

Figure A.8: Protein sequence alignment of FGFc and another *Hydra* FGF. Both sequences share an identity of 92 %. Sequence of the *Hydra* FGF taken from Krishnapati and Ghaskadbi (2013).

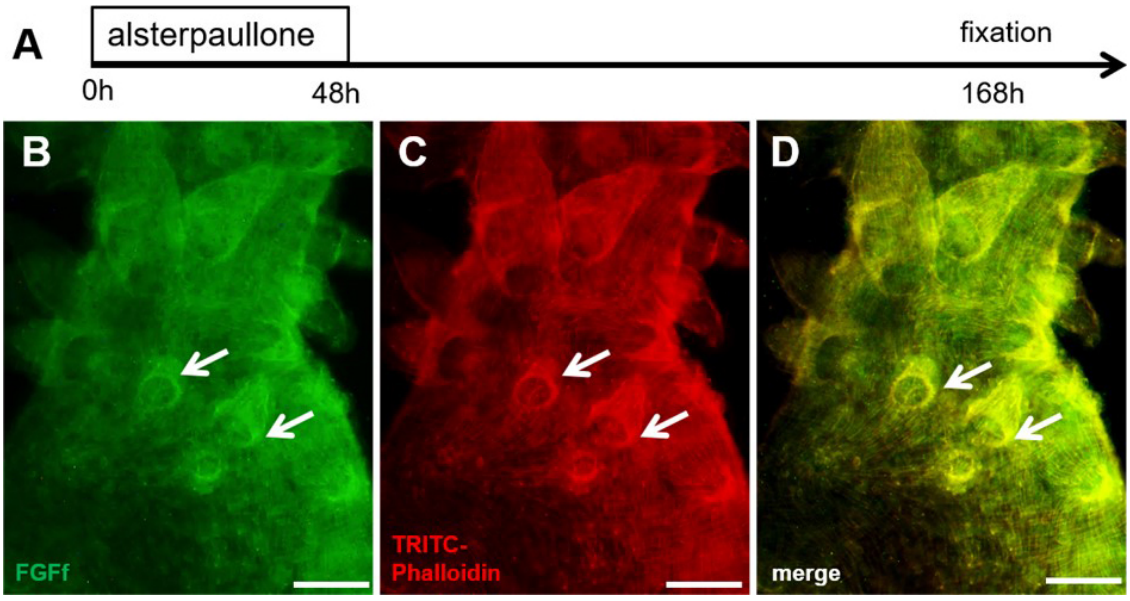

Figure A.9: Immunodetection of FGFf after treatment with alsterpaullone. (A) Scheme of the treatment with alsterpaullone (ALP). Animals were treated with 5 µM ALP for 48 hours. Fixation occurred seven days after the beginning of the treatment. (B) The FGFf protein accumulated in newly developing tentacle bases (white arrows). (C) The actin fibers arranged towards newly developing tentacles (white arrows). (D) Overlay of (B) and (C). Scale bars 100 µm.

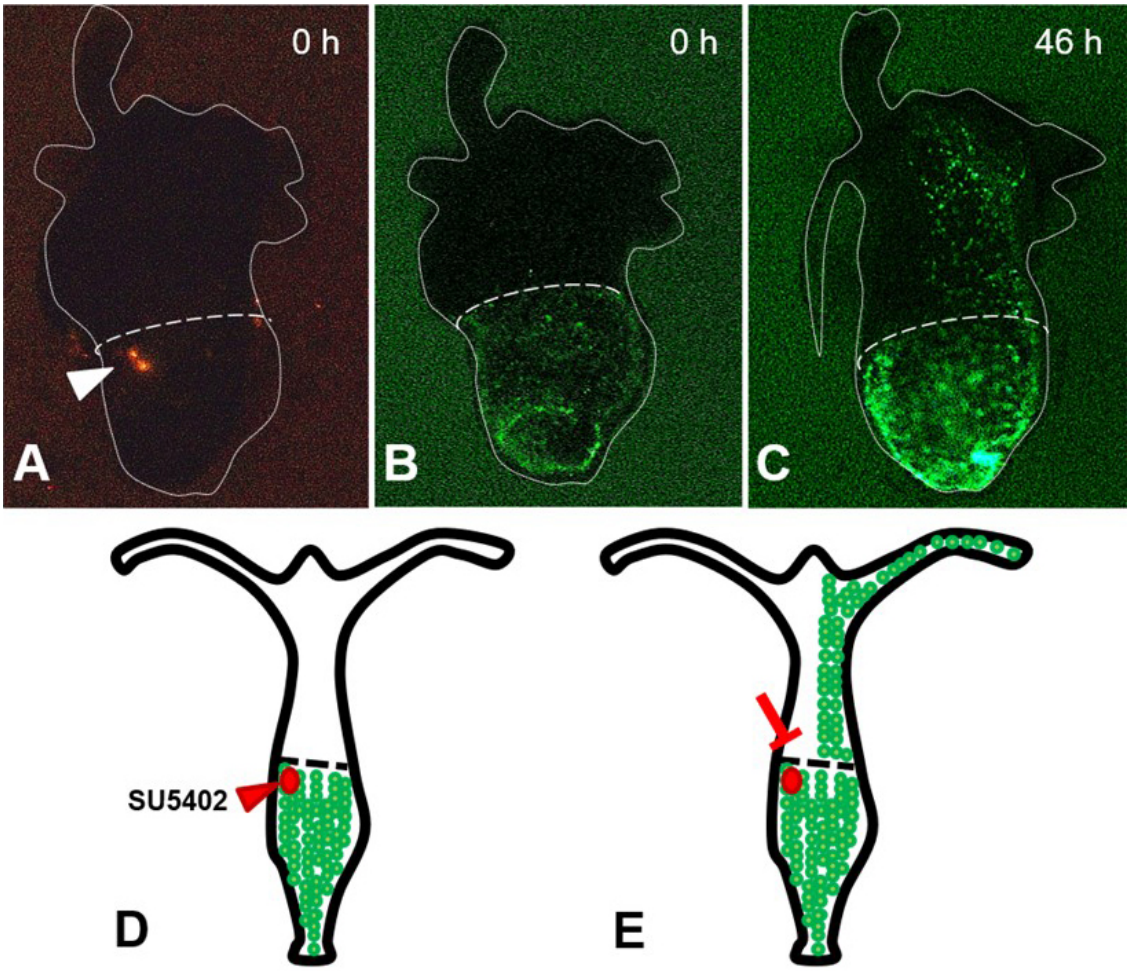

Figure A.10: Local injection of SU5402 inhibits i-cell migration. Transgenic Icy foot tissue and non-transgenic *Hydra vulgaris* AEP tissue was transplanted. (A) Red dots (fluorescent DiI marker) indicate the injection site (white arrowhead). (B) Directly after injection, i-cells were localized in the transgenic lower transplant half, but not the upper half. (C) After 46 hours, i-cells had migrated unilaterally: At the SU5402 injection site i-cell migration was stalled. (D) Scheme of i-cell migration directly after inhibitor injection and (E) 46 hours after injection. The transplantation site is indicated by a dashed with line. The shapes of the animal was outlined. Experimental part and imaging were performed by Annegret Rittershaus, B.Sc.

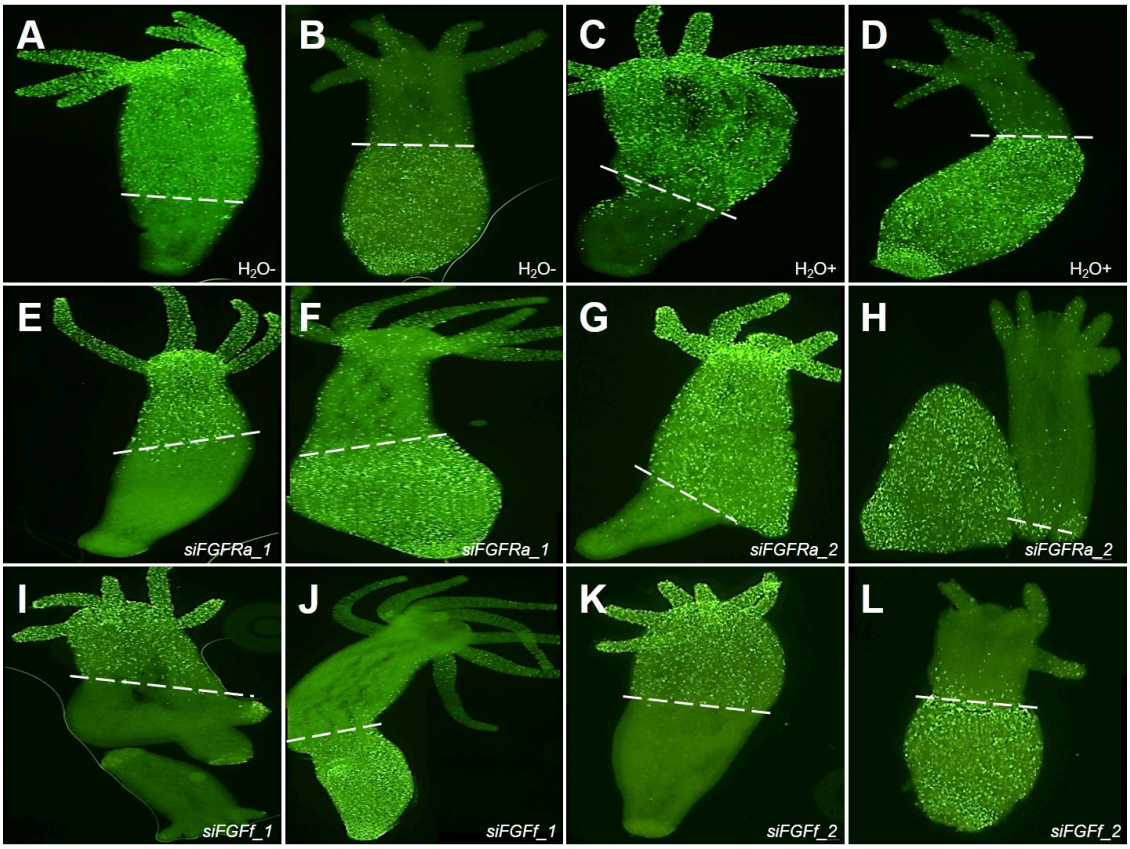

Figure A.11: Migration of i-cells after siRNA knockdown. Electroporated transgenic animals were transplanted on non-transgenic animals. Fixation occurred two to three days after the transplantation. (A–D) Control groups. (A, C) i-cells migrated towards the foot. (B, D) i-cells migrated towards head and tentacles. (E, F) *siFGFRa_1* knockdown. (E) Few i-cells migrated towards the foot. (F) Transgenic i-cells populate head and foot. (G, H) *siFGFRa_2* knockdown. (G) Few i-cells migrated towards the foot. (H) i-cells migrated towards the head. Animal was disrupted at the transplantation site during the experiment. (I, J) *siFGFf_1* knockdown. (I) No i-cell migration towards the foot. (J) Unilateral migration towards the upper body half. (K, L) *siFGFf_2* knockdown. (K) No migration towards the foot. (L) i-cells migrated towards the upper body part. Transplantation site is indicated by a dashed with line. Experimental part and images were made by Madeleine Thamm, B.Sc.

B Danksagung

Zuerst möchte ich mich bei Prof. Dr. Monika Hassel bedanken, für die Aufnahme in der Arbeitsgruppe, für die Möglichkeit an diesem Projekt zu arbeiten und vor allem auch für die Betreuung, Unterstützung und die Anregungen.

Ebenfalls möchte ich mich bedanken bei Prof. Dr. Christian Helker für die Übernahme des Zweitgutachtens sowie Prof. Dr. Uwe Homberg und Prof. Dr. Annette Borchers für die Einwilligung Mitglieder meiner Prüfungskommission zu sein.

Ein großes Danke auch an alle ehemaligen und aktuellen Mitglieder der AG. Ihr alle habt dazu beigetragen, dass eine schöne Atmosphäre herrschte, in der man sich fachlich und persönlich jederzeit austauschen konnte. Einen ganz lieben Dank auch an Heide, die mir immer mit Rat und Tat zur Seite stand und ein offenes Ohr für alles hatte. Ein großes Dankeschön an die besten Kollegen der Welt: Anne, David, Karo und Oli! Die regelmäßigen Besuche auf dem Sonnendeck habe ich sehr genossen, und sie haben uns zu einem super Team werden lassen, das sich auch in den Pausen gerne über die Projekte und anderes ausgetauscht hat. Danke, dass ihr meine Arbeitsfamilie wart!

Danke auch an alle Studierenden, die ich während ihrer Abschlussarbeiten begleiten durfte und mit denen ich zusammen an meinem Projekt gewachsen bin. Hierbei möchte ich vor allem Gretel, Anne, Kevin, Dominic, Madeleine und Lars danken, die sich tapfer mit mir zusammen durch die Höhen und Tiefen dieses Projekts gekämpft haben. Danke für euren Einsatz und das gemeinsame Werkeln an den FGFs! Ich habe mich gefreut, jeden einzelnen von euch begleiten zu dürfen.

Danke an meine Familie, die mir in allen Phasen dieser Arbeit eine große Unterstützung war. Vor allem danke ich meinem Mann Thomas: Danke, dass du mich beim Erklimmen dieses Berges unterstützt hast, mich motiviert hast, wenn die Steigung zu steil wurde und mir immer wieder hochgeholfen hast, wenn ich gefallen bin. Dass du vor allem auch bei den letzten anstrengenden Metern immer für mich da warst und mir Mut zugesprochen hast. Mit dir konnte ich jede Freude und jeden Frust teilen, da du dir immer Zeit für mich genommen hast. Danke auch an meinen wundervollen Sohn Valentin: Du bist mein Glück und hast immer dafür gesorgt, dass ich allen Stress vergessen konnte.

C Wissenschaftlicher Lebenslauf

Diese Seite enthält persönliche Daten. Sie ist deshalb nicht Bestandteil der Online-Veröffentlichung.

D Eidesstattliche Erklärung

Ich versichere hiermit, dass ich die vorliegende Dissertation "Functional analysis of siRNA mediated knockdowns of fibroblast growth factors in *Hydra vulgaris*" selbstständig verfasst und nur die angegebenen Quellen und Hilfsmittel verwendet habe. Wörtlich oder sinngemäß anderen Werken entnommene Stellen sind unter Angabe der Quelle als Entlehnung kenntlich gemacht.

Die Dissertation wurde in der jetzigen oder einer ähnlichen Form noch bei keiner anderen Hochschule eingereicht und hat noch keinen sonstigen Prüfungszwecken gedient.

Ort, Datum	Unterschrift